Thermodynamic modeling of martensitic transformations in shape memory alloys

A DISSERTATION
SUBMITTED TO THE FACULTY OF THE GRADUATE SCHOOL
OF THE UNIVERSITY OF MINNESOTA
BY

Venkata Suresh Reddy Guthikonda

IN PARTIAL FULFILLMENT OF THE REQUIREMENTS
FOR THE DEGREE OF
Doctor of Philosophy

July, 2010

Acknowledgements

I would like to take this opportunity to thank everybody who have helped and inspired me during my doctoral study.

I especially want to deeply appreciate my advisor, Assistant Professor Ryan S. Elliott, for his guidance and patience through the many years of my apprenticeship. Your perpetual energy and enthusiasm in research have motivated me in research. Your exceptional organizational skills have inspired me to get more organized which indirectly resulted into smooth and rewarding graduate student experience. In addition, your accessibility and willingness to guide me in my research with patience is really applaudable.

I thank my dissertation committee: Professor Ellad Tadmor, Professor Perry Leo, and Nelson Assistant Professor Traian Dumitrica for their insight and advice.

I thank my family for their love, encouragement, and friendship without which I would not be the person I am today.

During these five years of my stay at The University of Minnesota, I have encountered great friends and colleagues without whom my life at university would rather be dull. I have learned many valuable things from each of you and I am thankful for that. I especially would like to thank Nikhil Admal, Vincent Jusuf, Dr. Vijay Srivastava, Udaya Kiran Kalluri, Harris Ismail, Amith Singh, Narina Jung, Shankar Krishnan, and Amartya Banerjee.

This work has been supported by The University of Minnesota Grant-in-Aid of Research, Artistry and Scholarship Program (GIA), The University of Minnesota Supercomputing Institute, and National Science Foundation (NSF) CAREER grant (CMMI-0746628).

Dedication

To my loving family.

Abstract

The unusual properties of shape memory alloys (SMAs) are due to solid-to-solid martensitic transformations (MTs) which correspond to a lattice level instability of the crystal structure. Currently, there exists a shortage of material models that can capture the details of lattice level MTs occurring in SMAs.

In the first part of this work, an effective interaction potential (EIP) model is developed for the SMA AuCd. EIPs are atomic interaction potentials that are explicit functions of temperature. In particular, the Morse pair potential is used and its adjustable coefficients are taken to be temperature dependent. A hysteretic temperature-induced MT between the B2 cubic and B19 orthorhombic crystal structures is predicted. This is the behavior that is observed in the real material. The model predicts, to reasonable accuracy, the transformation strain tensor and captures the latent heat and thermal hysteresis to within an order of magnitude.

The second part of this work consists of developing a lattice dynamics model to simulate the MTs. The atomic interactions are modeled using temperature independent Morse pair potentials. The effects of atomic vibrations on the material properties are captured using the first-order self-consistent approach which consists of renormalizing the frequencies of atomic vibration using self-consistent equations. These renormalized frequencies are dependent on both configuration and temperature. The model is applied for the case of a one-dimensional bi-atomic chain. The constant Morse pair potential parameters are chosen to demonstrate the usefulness of the current model. The resulting model is evaluated by generating equilibrium paths with temperature and mechanical load as the loading parameters. In both types of loading, a first-order MT is predicted indicating that the current model is able to capture the first-order MTs that occur in SMAs.

This qualitative prediction of a first-order MT indicates the likely-hood that the current model can be used for the computational design and discovery of SMAs with better properties. Such an undertaking would involve, first, determining the potential parameters of new alloys from first-principles calculations and, second, using these parameter values with the current self-consistent model to evaluate the shape memory

behavior of the new previously unstudied materials.

Contents

List of Tables

List of Figures

Chapter 1

Introduction

1.1 Shape memory alloy background

Shape memory alloys (SMA's), such as NiTi, AuCd, CuAlNi, AgCd, and TiPd, are special materials that exhibit an unusual set of properties such as the *shape memory effect* and *pseudo-elasticity*. The shape memory effect refers to the material's ability to fully recover apparently permanent deformation of up to 10% strain upon a modest increase in material temperature. At higher temperatures these materials are pseudo-elastic which means they may be subjected to large deformations and completely recover, via a hysteric process, upon removal of applied loads. These peculiar properties are due to the existence of solid-to-solid diffusionless phase transformations (PT's). The *diffusionless* PT's (also called *displacive* or *martensitic*) involve the coordinated motion of the atoms in the crystal as the material structure transforms from one lattice type to another. The high temperature lattice or phase is usually a high symmetry structure and is called the *austenite* phase. The low temperature lattice structure has a lower symmetry and is called the *martensite* phase.

The first SMA discovered was AuCd. *Olander* (1932) used electrochemical techniques to identify the B2 cubic (austenite) phase and the B19 orthorhombic (martensite) phase of AuCd. Further, he was the first to recognize its peculiar (i.e., SMA) behavior. Later, *Bystrom and Almin* (1947) performed an X-ray investigation and found the different phases of the AuCd alloy for different compositions. The SMA properties of Au-47.5at%Cd were identified by *Chang and Read* (1951) by studying the movement of

boundaries between the two phases during phase transformation using an X-ray analysis of the orientation relationships, electrical resistivity measurements, and motion picture studies. From the observations of this experiment, it was concluded that Au-47.5at%Cd undergoes a diffusionless transformation from a high symmetry B2 cubic structure to a low symmetry B19 orthorhombic structure when it is cooled to its austenite finish temperature (A_f) at about 60 °C. The reverse transformation occurs from the B19 structure to the B2 structure at 80 °C (the martensite finish temperature, M_f) as the alloy is heated (*Chang and Read*, 1951). The same researchers found the lattice parameters of Au-47.5at%Cd to be: $a = 3.3165$ Å for the B2 cubic structure and $a = 3.1476$ Å, $b = 4.7549$ Å, and $c = 4.8546$ Å for the B19 orthorhombic structure.

The martensitic transformations (MT's) found in SMA's are reversible in the sense that as the temperature is lowered the material experiences the "forward" transformation (from austenite to martensite) and a subsequent increase in temperature results in the "reverse" transformation (from martensite back to austenite). This temperature-induced MT cycle is illustrated in Fig. 1.1 (from *Shaw and Kyriakides*, 1995) which shows a differential scanning calorimetry (DSC) thermogram for a NiTi thin wire. The supplied power $\dot{Q}$ versus temperature T is plotted for the forward and reverse MT's. The experiment starts with cooling of the NiTi thin wire from a starting temperature of 100 °C with the material in the austenite phase (right side of lower curve). As the temperature is decreased the wire first experiences an exothermic MT and transforms into an intermediate rhombohedral martensite phase (first valley from right side in the DSC thermogram, labeled R-phase) that starts at the temperature $R_s = 54$ °C and finishes at temperature $R_f = 32$ °C. As the temperature is further decreased the wire starts its transformation to the monoclinic martensite phase (second valley from right side in the DSC thermogram) at the "martensite start" temperature $M_s = -1$ °C and completes its transformation at the "martensite finish" temperature $M_f = -70$ °C. The upper curve shows the reverse transformation from monoclinic martensite to cubic austenite. This transformation is an endothermic MT (hill in the DSC thermogram). The monoclinic martensite phase starts transforming into the cubic austenite phase at the "austenite start" temperature $A_s = 29.5$ °C and finishes its transformation at the "austenite finish" temperature $A_f = 62$ °C. This shows that the NiTi thin wire exists in only the austenite phase at temperatures above A_f and only in the martensite phase at

temperatures below M_f. Both austenite and martensite phases exist as a combination for temperatures between M_f and A_f.

In addition to temperature-induced MT's, SMA's also exhibit stress-induced MT's. Together, these two types of MT's can give rise to the shape memory effect and pseudo-elasticity, which are illustrated in Fig. 1.2 (from *Shaw*, 1997). This figure shows the temperature-load-deformation behavior for a polycrystalline NiTi thin wire, where δ/L is the elongation of the wire from its original length L, T is the temperature in degrees Celcius, and P/A_0 is the reaction load of the wire normalized by its original cross-sectional area A_0. From Fig. 1.2, the shape memory effect is depicted by the segments (0)–(2) and (2)–(4) in which the material is "permanently" deformed by the application on removal of load (segment (0)–(2)) and subsequently the material is able to recover from this deformation with a modest increase in temperature (segment (2)–(4)). The experiment starts at point (0) where the alloy exists in the martensite phase and corresponds to a *twinned* configuration of the B19′ monoclinic structure. Upon loading, the twinned structure is converted into a *detwinned* configuration resulting in a change of the length of the NiTi wire. This configuration remains after the load is removed at point (2). As the temperature is raised, the low symmetry (B19′ monoclinic) martensite phase becomes unstable and transforms to the high symmetry (B2 cubic) austenite phase (segment (2)–(4)). As a result, the wire recovers its original length at point (4). Completion of a shape memory cycle requires cooling of the specimen from point (4) which makes the austenite cubic phase unstable and results in transformation back to the martensite (twinned B19′ monoclinic) phase at point (0). Instead, in this experiment, the NiTi wire is further heated to point (5) and then subjected to isothermal loading near 70 °C. Pseudo-elastic behavior of the alloy is illustrated by segment (5)–(10) in which the material recovers from a strain of almost 7% immediately upon removal of the load. The term pseudo-elastic refers to the fact that dissipation of energy occurs via a hysteresis loop as shown in the figure. The material behaves as a linear elastic material until it reaches a critical stress at point (6) where the austenite phase becomes unstable and starts the stress-induced phase transformation to stable martensite. From point (6) to (7), the wire elongates substantially, without any additional applied load, by transforming from unstable austenite to stable martensite. Lüders-like transformation fronts, separating austenite from martensite, travel along the length of the wire during

this transformation (see *Shaw and Kyriakides*, 1995; *Shaw*, 1997). Further loading from point (7) will eventually cause plastic deformation. However in this experiment, the material is unloaded from point (7) until the critical stress, point (8), is encountered. Here, the martensite becomes unstable and begins to transform back to austenite. From point (8) to (9), the material transforms from unstable martensite to stable austenite with a slight decrease in load. Finally, the material recovers its original length in a linearly elastic fashion between points (9) and (10) as the remaining load is removed. A more detailed discussion of the shape memory effect and pseudo-elasticity are presented in the excellent books available on SMA's, including for example, *Duerig et al.* (1990), *Otsuka and Wayman* (1998), and *Bhattacharya* (2003).

Due to their unique properties, discussed above, SMA's are used in a number of special-purpose industrial applications and more are being developed everyday. SMA's were first applied commercially for the repair of leaking titanium hydraulic pipes in the wing box of A-10 Thunderbolt aircraft during the 1960's. A SMA of NiTi is used to make flexible eyeglass frames under the trademark Flexon. The range of applications for SMA's has been increasing in recent years, with one major area of expansion being medical device industry: for example, the development of dental braces that exert a constant force on the teeth. Also, NiTi's excellent shape memory properties has led to the development of SMA vascular stents which are used during angioplasty procedures to prevent the blood vessel from returning to its constricted state after the procedure. SMA vascular stents are now a multi-million dollar industry (Johnson & Johnson, Medtronics, Boston Scientific, Gore, etc.) that continues to grow each year.

Although SMA's are very attractive for certain commercial applications, as mentioned above, they offer some serious challenges in terms of energy inefficiency, slow response times, fatigue, corrosion, bio-compatibility, and amount of hysteresis. One of the main challenges comes from the manufacturing of the SMA's. For instance, SMA material properties can change dramatically in response to a slight change in composition or processing. Contaminants such as oxygen, carbon, and nitrogen can cause changes in the material's transformation temperature and can also change the material's durability etc. Recently, it has been shown that NiTi (one of the most widely used SMA's) has issues with bio-compatibility due to toxicity of nickel, long-term corrosion resistance, and fatigue life (*Laing et al.*, 1967; *Putters et al.*, 1992; *Watah et al.*, 2001;

Hoh et al., 2009). Developing models to understand how the material's composition affects its properties is critical in design and discovery of better SMA's with improved properties such that the above mentioned difficulties can be avoided.

1.2 Review of SMA modeling

Various models have been presented in the literature to simulate the behavior of SMAs. These models can be broadly categorized as continuum mechanics based models, quantum mechanics based Density Functional Theory (DFT) models, and phenomenological atomistic models.

Continuum mechanics based models can be divided into phenomenological and micromechanical type models. Phenomenological models usually consist of a mechanical law to govern the stress-strain behavior and a kinetic law to govern the crystallographic transformation (*Tanaka and Nagaki*, 1982; *Liang and Rogers*, 1990; *Brinson*, 1993; *Ivshin and Pence*, 1994). The mechanical part of the model plays a less significant role and the particular kinetic law distinguishes these models (*Brinson and Huang*, 1996). Micromechanics based models take account of varying amounts of the crystallographic symmetry of SMAs and use the laws of thermodynamics to describe the transformation behavior (*Patoor et al.*, 1988, 1993; *Sun and Hwang*, 1993a,b; *Leo et al.*, 1993; *Shield*, 1995; *James et al.*, 1995; *Goo and Lexcellent*, 1997; *Lu and Weng*, 1997; *Huang and Brinson*, 1998; *Vivet and Lexcellent*, 1998; *James and Hane*, 2000; *Shaw*, 2002; *Guthikonda et al.*, 2008). These models use the geometric properties of martensitic variants that make up a transforming inclusion and apply micromechanics calculations to obtain the interaction energy of phase transformation in the material. Stresses and strains are obtained as averages over a volume in which many inclusions may exist. The major shortcoming of these continuum models are that á priori knowledge of the martensite structure must be known. Most of the models rely on the availability of experimentally obtained phase diagrams and other physical properties for both the austenite and martensite phases. In other words, these models cannot be used if the nature of the material's MTs are not known. Thus, they are not helpful in the search for new shape memory materials.

Quantum mechanics based first-principles DFT methods are valuable for investigating the energy differences between many phases of a material, and for studying the stability of these phases all at 0 K (*Ye et al.*, 1997; *Huang et al.*, 2001; *Parlinski and Parlinska-Wojtan*, 2002; *Huang et al.*, 2003; *Parlinski et al.*, 2003). These methods are capable of calculating atomic-level information regarding energies, forces, and stresses independent of any empirical fitting. DFT calculations such as those of *Huang et al.* (2001, 2003) performed at 0 K show that the B2 cubic austenite crystal structure of NiTi is unstable. That is, NiTi has imaginary phonon frequencies at 0 K. This indicates that temperature effects are responsible for the existence of a stable austenite phase in NiTi at high temperature. However, extensive direct DFT based studies of temperature effects on the microstructural behavior of MTs in NiTi and other SMAs are prohibitive due to the computationally intensive nature of DFT calculations.

In contrast, atomistic models based on Molecular Dynamics (MD) or Monté Carlo (MC) simulations are capable of capturing temperature effects and are invaluable for studying the behavior of homogeneous MTs. In particular, MD simulations based on different phenomenological atomic interaction potentials have been useful for exploring the dependence of a MT on properties such as temperature, composition, concentration of defects, etc. (*Rubini and Ballone*, 1995; *Grujicic and Dang*, 1995; *Shao et al.*, 1996; *Meyer and Entel*, 1998; *Entel et al.*, 1999, 2000; *Ozgen and Adiguzel*, 2003; *Wang et al.*, 2006; *Ishida and Hiwatari*, 2007). However, the extension of MD and MC simulations to larger length- and time-scales in order to study the formation and evolution of microstructures in SMAs is impractical except on the largest of currently available parallel-computing systems. Even on these systems, the size of the simulations of interest would require considerable computation time. Thus, alternative methods need to be developed. These methods must provide accurate predictions of material behavior and be easily incorporated into large scale simulation techniques such as the finite element method (FEM), the quasicontinuum (QC) method, and the peridynamic (PD) method.

1.3 Outline

In this work, two models are developed to address the above mentioned shortcomings of currently available modeling techniques to accurately predict the behavior of SMAs

and be easily incorporated into the large scale simulation techniques such as the FEM, QC method, and the PD method.

The first model is based on the recent studies of *Elliott et al.* (2006a,b) and *Guthikonda and Elliott* (2008a). In these studies, Effective Interaction Potentials (EIPs) are used to model the behavior of SMAs. That is, atomic interactions are modeled with empirical atomic "free energy" potentials that are explicit functions of temperature. The EIPs are computationally efficient and capable of capturing a wide range of material behavior. Thus, the EIP methodology appears to be a promising tool for capturing the real atomic-scale behavior of materials that exhibit MTs while also allowing for the efficient simulation of large-scale phenomena, for example, the formation of complex microstructures. In a best case scenario, EIPs should recover the DFT potential energy of the material as the temperature goes to zero. However, this may not be practical and in many cases an EIP model must be restricted to a range of temperatures for which it gives good predictions. An interesting application of EIPs would be to employ them in the development of a new continuum level polycrystalline constitutive model similar to those discussed above. Such a model would automatically inherit the thermodynamic properties associated with the EIP instead of postulating a phenomenological kinetic law. In *Guthikonda and Elliott* (2008a) it is observed that an EIP model based on the Morse pair potential is appropriate for capturing a transformation between the B2 cubic structure and the B19 orthorhombic structure. Thus, in Chapter 2 (which is based on *Guthikonda and Elliott*, 2009) an EIP model is developed to study the B2 to B19 transformation observed in Au-47.5at%Cd.

Chapter 2 is organized as follows. Section 2.1 introduces the EIP model, Cauchy-Born kinematics, the free energy density, equilibrium equations, and the stability criteria. Thermo-elastic crystal properties of interest are defined in Section 2.2. Section 2.3 gives a description of the Morse EIPs with temperature dependent potential parameters along with a general approach used to fit the EIP model parameters to experimental data for a binary alloy. Finally, Section 2.4 discusses the behavior of the final EIP model which has temperature-dependent bond-stiffness, bond-strength, and pair equilibrium-spacing parameters.

EIPs are capable of capturing the temperature effects and are essential for studying the behavior of homogeneous MTs. This approach is computationally efficient and can

be easily incorporated into large scale simulation techniques such as the FEM, the QC method, and the PD method. However, models based on EIPs require fitting of a large number of potential parameters by matching the various properties of austenite phase of the SMA at multiple temperatures as shown in Section 2.3. Though various material properties of well known SMAs are available from experiments, it is not possible to know them in design and discovery of SMAs with better properties. Thus, it is useful to have a computational model that requires minimum fitting by matching only a few material properties from experiments or first-principles calculations. Atomistic models based on MD or MC simulations require minimum fitting. This is due to the modeling of atomic interactions by temperature independent interatomic potentials. The temperature effects on the material properties are modeled by studying the dynamics of atomic vibrations. However, the computational design and discovery of new SMAs involves parametric studies based on the atomic composition of the material. The usefulness of the MD and MC simulations in these types of studies is limited due to thermodynamic integration required in order to calculate the material's free energy.

The second part of this work aims to develop a lattice dynamics model with all the advantages of MD and MC techniques that can also be parametrically explored in a computationally efficient way using Branch-following and bifurcation (BFB) methods (*Elliott*, 2007; *Jusuf*, 2010). In particular, a lattice dynamics model based on the self-consistent approach (SCA) (*Hooton*, 1955a,b; *Boccara and Sarma*, 1965; *Huang and Born*, 1962; *Choquard*, 1967; *Gillis et al.*, 1968; *Shukla*, 1998; *Wallace*, 1998) is developed to study the MTs that occur in SMAs. The SCA method requires minimum fitting due to modeling of atomic interactions by temperature independent interatomic potentials. The temperature dependence of material properties are modeled by considering the atomic vibrations. The effects of atomic vibrations are captured by renormalizing the frequencies of atomic vibration using self-consistent equations. These renormalized frequencies of atomic vibration are not only dependent on the configuration but also temperature. This explicit dependence of renormalized frequencies of atomic vibration on both configuration and temperature enables the SCA method to capture the entropic stabilization and simulate the MTs that occur in SMAs. The theoretical picture is that at temperatures above the transition temperature, certain harmonic frequencies are imaginary but all the renormalized phonon frequencies are real. This implies that

although the material is unstable according to the harmonic approximation it becomes stable due to the anharmonic effects which are considered in calculating the renormalized phonon frequencies. As the temperature is decreased the magnitude of renormalized phonon frequencies decreases which leads to the material becoming unstable at the transition temperature.

In this work, the SCA method is developed using a classical mechanics approach and for the first time integrated into computational BFB methods (*Elliott*, 2007) which enables a systematic investigation of the materials behavior by following the "equilibrium paths" of a materials energy landscape to obtain the accurate predictions for SMA behavior. The rest of this work is organized as follows. Chapter 3 explains the concept of entropic stabilization that is observed during MTs. A generalized lattice dynamics problem is formulated for the case of a one-dimensional bi-atomic chain in Chapter 4. The SCA model is developed using a classical mechanics approach for the one dimensional case in Chapter 5. Chapter 6 explains the critical aspects involved in numerical implementation of the SCA model developed in Chapter 5 such that the BFB methods (*Elliott*, 2007) can be exploited to systematically investigate the SMA behavior. The SCA model is evaluated in Chapter 7 by simulating the MT that is observed in SMAs for the case of one-dimensional chain. Finally, Chapter 8 summarizes the results of EIP model for shape memory alloy AuCd and SCA model for a one-dimensional bi-atomic chain.

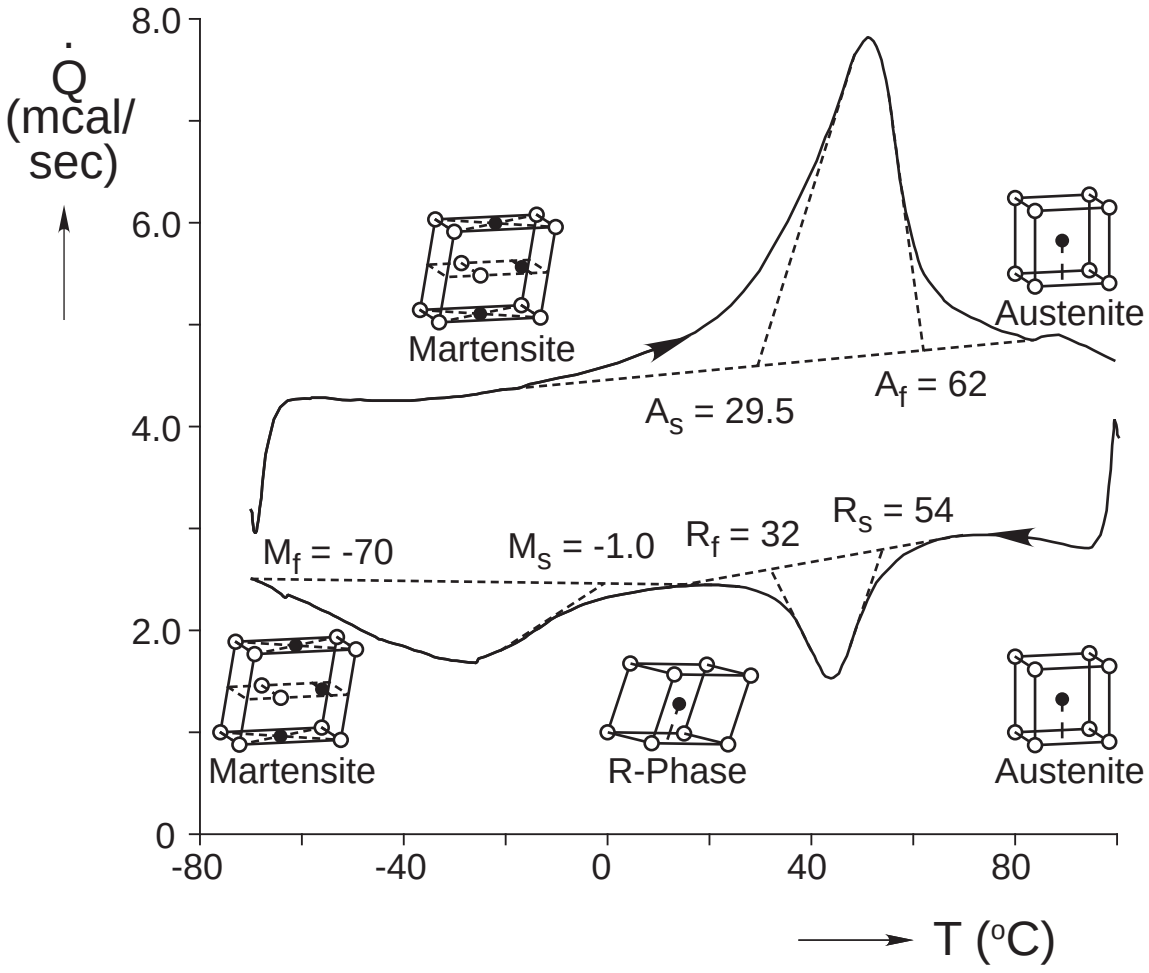

Figure 1.1: Differential scanning calorimetry thermogram showing the supplied power versus the specimen temperature (from *Shaw and Kyriakides*, 1995).

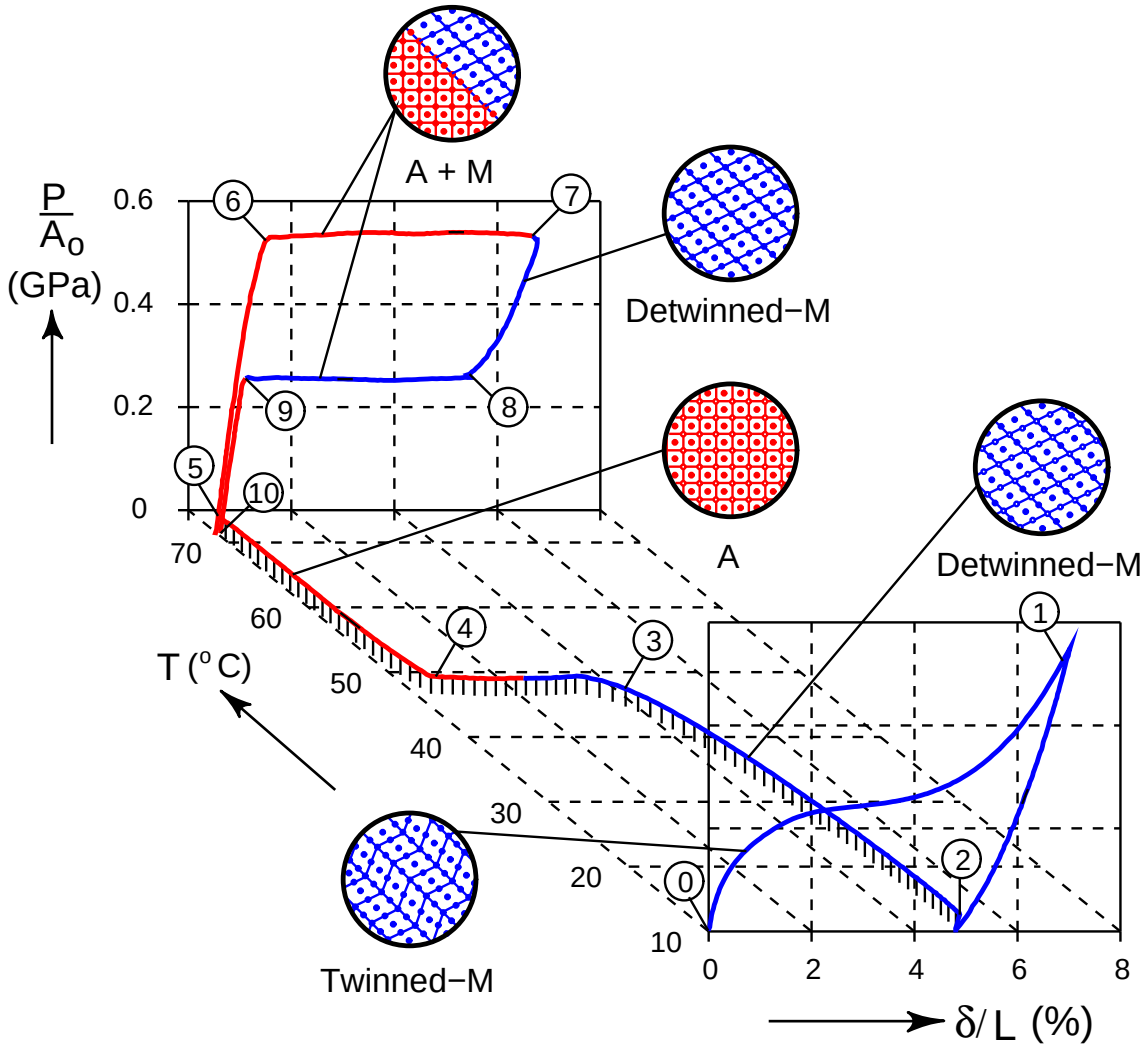

Figure 1.2: Experiment on NiTi thin wire showing the properties of shape memory and pseudo-elasticity (from *Shaw*, 1997).

Chapter 2

An effective interaction potential model for the shape memory alloy AuCd

2.1 Effective interaction potential model

The motivation and justification for phenomenological thermomechanical continuum materials modeling theory is based on macroscopic testing and observation of the relationship between the continuum concepts of stress, strain, and temperature. In an analogous way, we are motivated to consider a phenomenological thermomechanical discrete materials modeling theory based on the experimental observations of finite-temperature x-ray and high-resolution microscopy. This theory describes the thermodynamic equilibrium (time-averaged) atomic structure of a material and how it depends on applied mechanical loads and temperature applied in the experiment. For example, this theory would aim to be able to describe the thermal expansion behavior of a perfect or defected crystal, the existence of structural phase transitions between different bulk crystalline structures, and the temperature-dependent behavior of crystalline surface reconstructions. Such a theory is, thus, intermediate between the usual continuum and atomistic materials viewpoints. Again, the ability of today's sophisticated microscopy techniques to accurately measure the time average atomic configuration of solid state

materials indicates that such a phenomenological theory is reasonable under appropriate conditions.

EIPs are simply one approach to the construction of a constitutive model for this discrete materials modeling theory. They are based on the hypothesis that the free energy of the system may be partitioned into individual atom contributions dependent only on the relative distances between the atomic nuclei and, of course, the temperature.[1]

This hypothesis, of course, requires testing. Thus, the goal of our previous work (*Elliott et al.*, 2002b; *Elliott*, 2004; *Elliott et al.*, 2006b; *Elliott*, 2007; *Guthikonda and Elliott*, 2008a) and the current investigation is to explore the ability of EIPs to capture the free energy landscape of SMAs. One significant advantage of the EIP approach is that it provides a natural mechanism for capturing all the correct nonlinear geometric symmetries of the constitutive model. (This advantage is also exploited by more standard empirical atomic interaction potentials.)

With this theory in mind, this section presents a model of a perfect, infinite, biatomic crystal. First, Section 2.1.1 discusses the use of an effective pair potential to model the atomic interactions. Second, the kinematics used to describe crystalline deformation are presented in Section 2.1.2. The focus of this work is to develop a model for the SMA AuCd. This will involve fitting effective interaction potentials to experimentally obtained values for not only the B2 cubic AuCd crystal, but also for pure face-centered cubic (FCC) Au and pure hexagonal-close packed (HCP) Cd crystals. Thus, details of the kinematics for each of these crystal structures are presented. Finally, Section 2.1.3 defines the crystal's free energy density, its equilibrium equations, and the appropriate stability criteria.

2.1.1 Effective pair potentials

In the current work a pair potential $\phi(r;\theta)$ is used, where ϕ is the free energy associated with an interaction between two atoms, r is the distance between two atoms, and $\theta = \frac{T}{T_{\text{ref}}}$ is the non-dimensional temperature with T the absolute temperature and T_{ref} a suitable (but arbitrary) reference temperature. To model a particular material, first a functional form for the pair potential is chosen, such as the well known Lennard-Jones or

[1] This is similar, in many respects, to the hypothesis (used by most empirical interatomic potentials) that the potential energy of an atomistic system may be partitioned into individual atom contributions.

Morse potential. Next, the interactions between atoms are made temperature-dependent by letting the parameters of the potential be functions of temperature. Finally, any adjustable potential parameters are determined by a fitting procedure in order to match certain experimental values of a material's properties.

Multiple types of atoms in a material give rise to multiple types of atomic interactions. For example, a binary alloy such as AuCd is made up of two types of atoms denoted here by "a" (Au) and "b" (Cd) which results in the need for three types of atomic pair interactions a − a, b − b, and a − b. In this case, each of these interactions is modeled with a separate free energy potential denoted by $\phi^{\mathrm{aa}}(r;\theta)$, $\phi^{\mathrm{bb}}(r;\theta)$, and $\phi^{\mathrm{ab}}(r;\theta)$ respectively.

2.1.2 Cauchy-Born kinematics

In order to describe a perfect infinite crystalline material, a representative translational unit cell is chosen and its associated lattice vectors, $\mathbf{G}_1, \mathbf{G}_2$, and $\mathbf{G}_3$ are identified. The chosen unit cell will contain some number of atoms, N, and the crystal structure is constructed by using the lattice vectors to generate the infinite number of translationally periodic images of the representative unit cell. This is called a "multilattice" description of the crystal structure (*Pitteri and Zanzotto*, 2002).

Deformations of the crystal are described using Cauchy-Born (CB) kinematics (*Huang and Born*, 1962; *Elliott et al.*, 2006a,b). Each unit cell in the crystal is labeled by a set of three integers $\ell = (\ell^1, \ell^2, \ell^3)$ and each atom in a given unit cell is labeled by an integer α. Thus, the reference position of atom α in unit cell ℓ is given by

$$\begin{aligned} \mathbf{X}\begin{bmatrix}\ell\\ \alpha\end{bmatrix} &= \mathbf{X}[\ell] + \mathbf{P}[\alpha], \\ \mathbf{X}[\ell] &= \ell^1\mathbf{G}_1 + \ell^2\mathbf{G}_2 + \ell^3\mathbf{G}_3, \end{aligned} \tag{2.1}$$

where $\mathbf{X}[\ell]$ is the position vector locating unit cell ℓ in space and $\mathbf{P}[\alpha]$ is the relative position vector locating atom α within this unit cell.

As described in *Elliott et al.* (2006b), CB kinematics describe the crystal's deformation in terms of "internal atomic shift vectors" $\mathbf{S}[\alpha]$ and a uniform deformation characterized by a 3×3 symmetric right-stretch tensor $\mathbf{U}$. Thus, the current position

of atom α in unit cell ℓ is[2]

$$\mathbf{x}\begin{bmatrix}\ell\\ \alpha\end{bmatrix} = \mathbf{U}\cdot(\mathbf{X}\begin{bmatrix}\ell\\ \alpha\end{bmatrix} + \mathbf{S}[\alpha]). \tag{2.2}$$

To eliminate rigid-body translations, $\mathbf{S}[0]$ is set to zero. Rigid-body rotations have already been eliminated by the use of the symmetric right-stretch tensor $\mathbf{U}$, instead of the general 3×3 deformation gradient tensor $\mathbf{F}$.

CB kinematics of the face-centered cubic crystal structure

The face-centered cubic (FCC) crystal has an essential unit cell that contains one atom ($\alpha \in \{0\}$) as shown in Fig. 2.1. The lattice basis vectors of this unit cell are given by

$$\mathbf{G}_1 = \frac{a_0}{2}(\mathbf{e}_2+\mathbf{e}_3), \quad \mathbf{G}_2 = \frac{a_0}{2}(\mathbf{e}_3+\mathbf{e}_1), \quad \mathbf{G}_3 = \frac{a_0}{2}(\mathbf{e}_1+\mathbf{e}_2), \tag{2.3}$$

where a_0 is the lattice parameter of the conventional FCC unit cell and $\{\mathbf{e}_1,\mathbf{e}_2,\mathbf{e}_3\}$ is a reference orthonormal basis aligned with the FCC cubic axes. The relative reference position vector locating atom $\alpha = 0$ within the one atom unit cell of the FCC crystal structure is, trivially, taken to be

$$\mathbf{P}[0] = \mathbf{0}. \tag{2.4}$$

The FCC structure is a Bravais lattice for which the CB kinematics of Eq. (2.2) simplify to give the current position of each atom in terms of its reference position as

$$\mathbf{x}\begin{bmatrix}\ell\\ 0\end{bmatrix} = \mathbf{U}\cdot\mathbf{X}\begin{bmatrix}\ell\\ 0\end{bmatrix}. \tag{2.5}$$

CB kinematics of the hexagonal close-packed crystal structure

The hexagonal close-packed (HCP) crystal structure has an essential unit cell that contains two atoms ($\alpha \in \{0,1\}$) as shown in Fig. 2.2. The lattice basis vectors of this

[2] Here the "Lagrangian" form of CB kinematics is used. Alternative forms are available, however we find this to be the most intuitive representation.

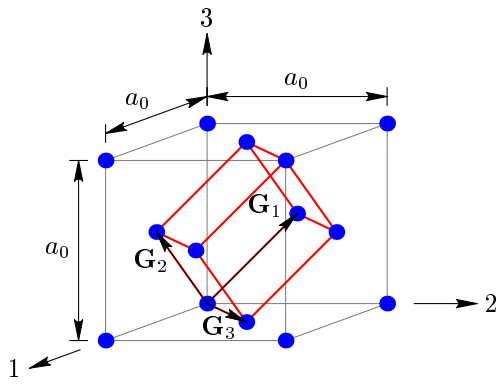

Figure 2.1: Conventional unit cell, with four atoms, and essential unit cell, with one atom, of the FCC crystal structure.

unit cell are given by

$$\mathbf{G}_1 = \frac{a_0}{2}(-\mathbf{e}_2 + \sqrt{3}\mathbf{e}_1), \quad \mathbf{G}_2 = a_0\mathbf{e}_2, \quad \mathbf{G}_3 = c_0\mathbf{e}_3, \tag{2.6}$$

where a_0 and c_0 are the lattice parameters of the HCP crystal and $\{\mathbf{e}_1, \mathbf{e}_2, \mathbf{e}_3\}$ is a reference orthonormal basis as indicated in Fig. 2.2. The relative reference position vectors locating atoms $\alpha \in \{0, 1\}$ within the two atom unit cell of the HCP crystal structure are taken to be

$$\mathbf{P}[0] = \mathbf{0}, \quad \mathbf{P}[1] = \frac{1}{3}\mathbf{G}_1 + \frac{2}{3}\mathbf{G}_2 + \frac{1}{2}\mathbf{G}_3. \tag{2.7}$$

CB kinematics of the B2 cubic crystal structure

The B2 cubic crystal structure has an essential unit cell that contains two atoms as shown on the left side of Fig. 2.3. The works of *Zener* (1947); *Zirinsky* (1956) and *Ren et al.* (2001) have shown that the geometry of the B2 crystal results in an inherent soft response to shear deformations along the $< 110 >$ directions. Further, *Elliott et al.* (2006b) and *Guthikonda and Elliott* (2008a) have shown that although the elastic shear modulus is soft, the first instability to occur in many B2 materials is associated with

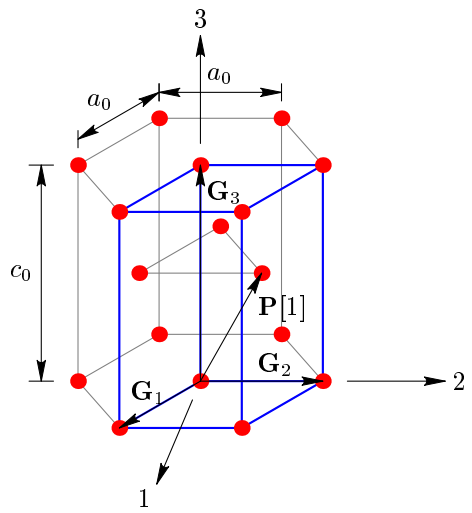

Figure 2.2: Conventional unit cell, with six atoms, and essential unit cell, with two atoms, of the HCP crystal structure.

the non-essential unit cell containing four atoms (4-lattice) as shown on the right side of Fig. 2.3. Thus, it is important to use the 4-lattice unit cell of B2 cubic crystal because it will allow for the identification of the onset of instability using the CB kinematics. This also allows for post-bifurcation behavior associated with this initial instability of the B2 phase.

The non-essential lattice vectors, $\mathbf{G}_x, \mathbf{G}_y$, and $\mathbf{G}_z$ are the three non-coplanar vectors for the 4-lattice unit cell. These vectors are related to the essential cubic basis vectors $\mathbf{G}_1 = a_0\mathbf{e}_1, \mathbf{G}_2 = a_0\mathbf{e}_2$, and $\mathbf{G}_3 = a_0\mathbf{e}_3$ (defining the essential unit cell shown on the left side of Fig. 2.3) by

$$\mathbf{G}_x = \mathbf{G}_1 + \mathbf{G}_2, \quad \mathbf{G}_y = \mathbf{G}_2 - \mathbf{G}_1, \quad \mathbf{G}_z = \mathbf{G}_3. \tag{2.8}$$

The reference relative position vectors of the four atoms $\alpha \in \{0, 1, 2, 3\}$ for the B2 cubic crystal structure are

$$\begin{aligned} \mathbf{P}[0] &= \mathbf{0}, & \mathbf{P}[1] &= \frac{1}{2}\mathbf{G}_x + \frac{1}{2}\mathbf{G}_z, \\ \mathbf{P}[2] &= \frac{1}{2}\mathbf{G}_x + \frac{1}{2}\mathbf{G}_y, & \mathbf{P}[3] &= \frac{1}{2}\mathbf{G}_y + \frac{1}{2}\mathbf{G}_z, \end{aligned} \tag{2.9}$$

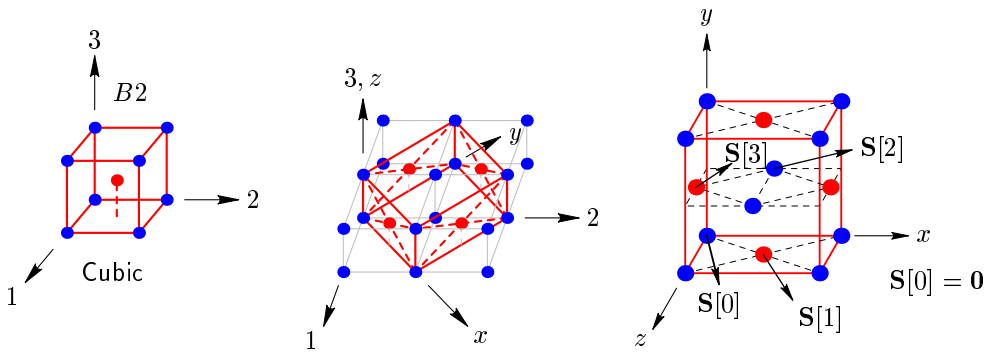

Figure 2.3: Essential unit cell (left), with two atoms, and the 4-lattice unit cell used in this work (right), with four atoms, of the B2 cubic crystal structure.

where $\alpha = 0$ and $\alpha = 2$ correspond to "a" (Au) atoms and $\alpha = 1$ and $\alpha = 3$ correspond to "b" (Cd) atoms as shown in Fig. 2.3.

2.1.3 Free energy density, equilibrium equations, and stability criteria

The EIP model gives the crystal's bulk free energy density as half the sum of all effective pair-interactions between atoms in one unit cell, say $\ell = (0, 0, 0)$, and all other atoms in the crystal, normalized by the reference unit cell volume. Thus, the free energy density per unit reference volume of a crystal is given by

$$\widetilde{W}(\mathbf{u};\theta) = \frac{1}{2V} \sum_{\alpha} \sum_{\begin{bmatrix}\ell' \\ \alpha'\end{bmatrix}} \phi^{\eta(\alpha)\eta(\alpha')} \left(r \begin{bmatrix} 0 & \ell' \\ \alpha & \alpha' \end{bmatrix}; \theta \right), \tag{2.10}$$

where $\mathbf{u} = (\mathbf{U}; \mathbf{S}[1], \mathbf{S}[2], \cdots, \mathbf{S}[N-1])$ represents the chosen set of independent degrees of freedom (DOFs) that describe the deformation of the crystal, θ is the non-dimensional temperature, V is the reference unit cell volume, $\eta(\alpha)$ represents the type of atom α ("a", "b", "c", etc.), and $r \begin{bmatrix} 0 & \ell' \\ \alpha & \alpha' \end{bmatrix} \equiv ||\mathbf{x} \begin{bmatrix} \ell' \\ \alpha' \end{bmatrix} - \mathbf{x} \begin{bmatrix} 0 \\ \alpha \end{bmatrix}||$ is the current distance between atom α' in unit cell ℓ' and atom α in the unit cell located at the origin. The factor of $1/2$ in Eq. (2.10) arises from the fact that the pair interaction energy is equally shared by the two involved atoms. Technically, the summation over $\begin{bmatrix} \ell' \\ \alpha' \end{bmatrix}$ in Eq. (2.10) extends to all atoms in the infinite crystal, but such a summation is computationally impossible. Due to the rapid decay of most commonly used pair potentials, it is acceptable to employ

a cutoff distance r_{cut}. Thus, the summation in Eq. (2.10) extends to all atoms in an Eulerian sphere of influence, that is, all atoms such that $r\begin{bmatrix}0\,\ell'\\ \alpha\,\alpha'\end{bmatrix} \leq r_{\text{cut}}$.

The equilibrium equations for the infinite perfect multilattice crystal with zero-stress conditions at infinity are given by the derivatives of $\widetilde{W}$,

$$\frac{\partial \widetilde{W}}{\partial \mathbf{u}} = \mathbf{0} \begin{cases} \frac{\partial \widetilde{W}}{\partial \mathbf{U}} = \mathbf{0}, & \\ \frac{\partial \widetilde{W}}{\partial \mathbf{S}[\alpha]} = \mathbf{0}, & \alpha = 1, 2, ..., N-1. \end{cases} \tag{2.11}$$

As shown in *Elliott et al.* (2006a) the translational periodicity of the crystal structure and the use of multilattice CB kinematics ensures that solutions of Eqs. (2.11) also correspond to true equilibrium configurations for the crystal. That is, if Eqs. (2.11) are satisfied, then the sum of forces acting on each atom in the crystal is zero.

Due to the "microscopic" nature of the CB shift DOFs, their direct control is difficult if not impossible. Therefore, most available experimental data corresponds to a state of the material in which the shifts are in equilibrium. That is, they satisfy Eq. $(2.11)_2$ for any given value of the deformation $\mathbf{U}$. Thus, the form of the material's free energy density that is most appropriate for comparison to macroscopic experimental data is the "Homogenized Continuum (HC) free energy density" (*Elliott et al.*, 2006a). To obtain the HC free energy density, Eq. $(2.11)_2$ is used to implicitly define the shifts $\mathbf{S}[\alpha]$ as functions of the uniform deformation $\mathbf{U}$ and temperature θ, i.e., $\mathbf{S}[\alpha] = \mathbf{S}[\alpha](\mathbf{U};\theta)$. The HC free energy density is then defined by

$$\widetilde{\widetilde{W}}(\mathbf{U};\theta) \equiv \widetilde{W}(\mathbf{U};\mathbf{S}[\alpha](\mathbf{U};\theta);\theta). \tag{2.12}$$

It should be noted that this does not imply that the shifts are unimportant. In fact, instabilities associated with the shifts are usually responsible for the existence of phase transformations and, indeed, are required to capture the critical deformation modes at the onset of instability (*Guthikonda and Elliott*, 2008a).

It is especially important to use the HC free energy density when calculating properties associated with non-centrosymmetric crystals, such as the HCP lattice and the αIrV and B19 orthorhombic structures encountered in Section 2.4. For these crystals the shifts couple directly to the uniform deformation of the crystal. Ignoring this coupling will result in significant errors in the computation of many thermo-elastic material

properties (see for example *Tadmor et al.*, 1999). It should be noted that the HC free energy as defined here may not be single valued. That is, for any given deformation $\mathbf{U}$ there may be multiple solutions to Eq. $(2.11)_2$. These will lead to a multi-valued HC free energy. Which of these multiple values $\overset{\approx}{W}(\mathbf{U};\theta)$ takes on at any given time will then depend on the deformation history.

The infinitesimal stability of an equilibrium configuration, i.e., a solution to Eqs. (2.11), is defined in terms of the "material" stability criterion of *Elliott et al.* (2006b). This requires the crystal to satisfy both the "Cauchy-Born (CB) stability criterion" and the "phonon stability criterion."

The CB stability criterion defines the stability of crystal structure by considering the quasi-uniform perturbations that conform to the Cauchy-Born kinematics of Eq. (2.2). An equilibrium crystal structure is considered CB stable if it is a local minimum of the free energy density Eq. (2.10), that is, the CB stability criterion requires that

$$[\delta\mathbf{U} \quad \delta\mathbf{S}[\alpha]] \begin{bmatrix} \frac{\partial^2\tilde{W}}{\partial\mathbf{U}\partial\mathbf{U}} & \frac{\partial^2\tilde{W}}{\partial\mathbf{U}\partial\mathbf{S}[\alpha']} \\ \frac{\partial^2\tilde{W}}{\partial\mathbf{S}[\alpha]\partial\mathbf{U}} & \frac{\partial^2\tilde{W}}{\partial\mathbf{S}[\alpha]\partial\mathbf{S}[\alpha']} \end{bmatrix} \begin{bmatrix} \delta\mathbf{U} \\ \delta\mathbf{S}[\alpha'] \end{bmatrix} > 0 \tag{2.13}$$

is satisfied at equilibrium for all non-zero $(\delta\mathbf{U};\delta\mathbf{S}[\alpha])$ with $\delta\mathbf{U} = \delta\mathbf{U}^T$ and $\alpha = 1, 2, ..., N-1$. Here, both uniform deformation $\delta\mathbf{U}$ and internal atomic shift $\delta\mathbf{S}[\alpha]$ perturbations are allowed to vary independently. At the macroscopic scale, uniform deformation perturbations $\delta\mathbf{U}$ (with $\delta\mathbf{S}[\alpha]$ following Eq. $(2.11)_2$) explore the crystal's response to slowly varying, strain-like, deformations. At the microscopic scale, internal shift perturbations $\delta\mathbf{S}[\alpha]$ (with $\delta\mathbf{U} = 0$) explore the crystal's response to perturbations that conform to the periodicity of the Cauchy-Born kinematics, Eq. (2.2).

The phonon stability criterion defines the stability of the crystal structure by considering all small atomic displacement perturbations of the crystal irrespective of the Cauchy-Born kinematics enforced by Eq. (2.2) for equilibrium configuration. However, this criterion is not complete in the sense that it does not consider uniform perturbations or the more general quasi-uniform perturbations, which are addressed by the CB stability criterion as explained above. An analysis that takes advantage of the translational symmetry of an equilibrium configuration reveals the eigen-modes of the stability operator for phonon stability to be plane wave displacements of the atoms in the crystal

that can be parameterized by a wave vector $\mathbf{k}$ (see *Elliott et al.*, 2006b),

$$\delta\mathbf{u}\begin{bmatrix}\ell\\ \alpha\end{bmatrix}^{(q)}(\mathbf{k}) = \Delta\hat{\mathbf{v}}^{(q)}[\alpha]\exp\left\{-i\mathbf{k}\cdot\mathbf{X}\begin{bmatrix}\ell\\ \alpha\end{bmatrix}\right\}, \tag{2.14}$$

where $\Delta\hat{\mathbf{v}}^{(q)}[\alpha]$ is the amplitude vector that describes the relative displacements of the atoms. The index $q = 1, 2, ..., 3N$ serves to distinguish these individual eigen-modes. The wave vector provides the orientation (direction of $\mathbf{k}$) and the spatial wavelength (proportional to the reciprocal of the length of $\mathbf{k}$) of a particular plane wave perturbation.

The phonon frequencies $\omega^{(q)}(\mathbf{k})$ and their associated phonon eigen-modes $\delta\mathbf{u}\begin{bmatrix}\ell\\ \alpha\end{bmatrix}^{(q)}(\mathbf{k})$ of Eq. (2.14) are found from the *dynamical matrix* $\mathbb{K}^{j}{}_{k}\begin{bmatrix}\mathbf{k}\\ \alpha\ \alpha'\end{bmatrix}$ for each wave vector $\mathbf{k}$ obtained from a second-order expansion of the energy density of Eq. (2.10) in the phonon-modes of Eq. (2.14), and is given by

$$\mathbb{K}^{j}{}_{k}\begin{bmatrix}\mathbf{k}\\ \alpha\ \alpha'\end{bmatrix} = (m_\alpha m_{\alpha'})^{-1/2}\sum_{l'\in\mathbb{Z}^3} G^{jp}\overset{\circ}{\Phi}_{pk}\begin{bmatrix}0\ l'\\ \alpha\ \alpha'\end{bmatrix}\exp\left\{-i\mathbf{k}\cdot\left(\mathbf{X}\begin{bmatrix}l'\\ \alpha'\end{bmatrix} - \mathbf{X}\begin{bmatrix}0\\ \alpha\end{bmatrix}\right)\right\}, \tag{2.15}$$

where m_α is the mass of atom α, $\mathbb{Z}^3$ is the set of all lattice points, G^{jp} is the metric of the reciprocal lattice basis vectors $\{\mathbf{G}^x, \mathbf{G}^y, \mathbf{G}^z\}$, and $\overset{\circ}{\Phi}_{pk}\begin{bmatrix}0\ l'\\ \alpha\ \alpha'\end{bmatrix} \equiv \frac{\partial^2 W}{\partial\mathbf{u}\begin{bmatrix}0\\ \alpha\end{bmatrix}\partial\mathbf{u}\begin{bmatrix}\ell'\\ \alpha'\end{bmatrix}}$ is the stiffness coefficient between atoms $\begin{bmatrix}0\\ \alpha\end{bmatrix}$ and $\begin{bmatrix}l'\\ \alpha'\end{bmatrix}$ evaluated at the equilibrium configuration (*Elliott et al.*, 2006a). The wave vector $\mathbf{k}$ ranges over values in the unit cell of the reciprocal reference lattice (multiplied by a factor 2π) $\mathbf{k} \in \{k_i\mathbf{G}^i | -\pi \leq k_i < \pi\}$. The phonon stability criterion requires the eigenvalues of the dynamical matrix, which are the squared phonon frequencies $(\omega^{(q)}(\mathbf{k}))^2$, to all be positive. That is,

$$(\omega^{(q)}(\mathbf{k}))^2 > 0, \quad q = 1, 2, ..., 3N \tag{2.16}$$

for all $\mathbf{k}$. See *Elliott et al.* (2006a,b); *Elliott* (2007) for further details on the phonon stability criterion.

Since neither of the stability criteria (CB or phonon) examine the stability of the crystal for all types of perturbations, both criteria must be satisfied for an equilibrium state of a crystal to be stable.

The above described "material" stability criterion ensures that the corresponding

equilibrium configuration is *observable*. Thus, if a material phase becomes unstable (in the "material" sense as defined above) as the temperature crosses a critical value, then a phase transition must occur. This is because once the phase is unstable, any perturbation (no matter how small) will cause the system to diverge from the equilibrium configuration. Thus, this criterion identifies the limits of temperature for which it is possible to observe a particular material phase.

In addition to the material stability criterion there is also the "equilibrium thermodynamics" stability criterion. This criterion states that the material phase (equilibrium configuration) with the *lowest* free energy corresponds to the *observed* phase of the material. This criterion chooses one phase, from all of the observable ("material" stable) phases that coexist at any given temperature, as the phase that is *most likely* to be observed. Thus, equilibrium thermodynamics predicts that a phase transformation will occur at the exact temperature where the minimum free energy value changes from one observable phase to a different observable phase.

In reality, the temperature at which transformation occurs will be somewhere in between the "material" transformation temperatures of each phase. These temperatures define a coexistence temperature range. The equilibrium thermodynamic transformation temperature will fall somewhere inside this range and represents the temperature at which transformation is most likely to occur. Generally, this temperature will depend on whether the material is being heated or cooled. Thus, there will be some "inherent" hysteresis associated with the transformation. The recent work of *James and Zhang* (2006); *Cui et al.* (2006); *Delville et al.* (2008) indicates that the majority of hysteresis in SMAs is a result of the process of microstructure evolution. Thus, it is likely that in most materials the amount of "inherent" hysteresis is quite small.

It is clear then that both stability criteria, material and equilibrium thermodynamic, are important concepts. Therefore, in this work we will identify both the phase coexistence range(s) and the most likely transition temperature(s) for the predicted material behavior.

2.2 Thermo-elastic properties of crystals

In this section, the thermal and elastic material properties that are used in this work for fitting to and comparison with available experimental data are presented.

The entropy per mole S is given by

$$S = -\frac{1}{T_{\text{ref}}} \frac{\partial \overset{\approx}{W}}{\partial \theta}\bigg|_{(\mathbf{U}_0;\theta_0)} \frac{V N_A}{N}, \tag{2.17}$$

where $\overset{\approx}{W}(\mathbf{U}_0;\theta_0)$ is the HC free energy density, $\mathbf{U}_0$ is the CB deformation corresponding to the stress-free configuration at the non-dimensional temperature θ_0, V is the reference unit cell volume, N is the number of atoms in the unit cell, and N_A is Avogadro's constant (6.023×10^{23}).

The cohesive energy E_{c} is the energy (per atom) released by the formation of the crystal from a set of dissociated atoms that are initially infinitely far apart. In other words it is the enthalpy of formation ΔH which is related to the change in free energy density $\Delta \overset{\approx}{W}$ and change in entropy ΔS given by $\Delta H = \Delta \overset{\approx}{W} + T\Delta S$. Taking the energy of infinitely far apart atoms as the energy datum, the cohesive energy is given by

$$E_{\text{c}} = -\left(\overset{\approx}{W}(\mathbf{U}_0;\theta_0) - \theta_0 \frac{\partial \overset{\approx}{W}}{\partial \theta}\bigg|_{(\mathbf{U}_0;\theta_0)} \right) \frac{V}{N}. \tag{2.18}$$

Here, the minus sign is required to obtain the energy *released* during the crystal's formation.

The instantaneous thermal expansion tensor $\boldsymbol{\alpha}$ is obtained by taking a total temperature derivative of the stress-free equilibrium equation $\frac{\partial \overset{\approx}{W}}{\partial \mathbf{U}} = \mathbf{0}$, solving for $\frac{d\mathbf{U}}{d\theta}\big|_{(\mathbf{U}_0;\theta_0)}$, and defining the instantaneous thermal expansion as $\boldsymbol{\alpha} \equiv \frac{1}{T_{\text{ref}}} \mathbf{U}_0^{-1} \frac{d\mathbf{U}}{d\theta}\big|_{(\mathbf{U}_0;\theta_0)}$ results in[3]

$$\boldsymbol{\alpha} = -\frac{1}{T_{\text{ref}}} \mathbf{U}_0^{-1} \cdot \left[\left(\frac{\partial^2 \overset{\approx}{W}}{\partial \mathbf{U}^2} \right)^{-1} : \left(\frac{\partial^2 \overset{\approx}{W}}{\partial \mathbf{U} \partial \theta} \right) \right]_{(\mathbf{U}_0;\theta_0)}. \tag{2.19}$$

[3] The double tensor contraction $\mathbf{A} : \mathbf{B}$ is defined in cartesian tensor component form by $A_{ij} B_{ijkl}$.

For cubic crystals (or isotropic materials), $\boldsymbol{\alpha}$ is an isotropic second-order tensor and one may speak of the "linear thermal expansion coefficient." However, for non-cubic (non-isotropic) materials, the directional dependence of thermal expansion must be specified and, therefore, one speaks of the "thermal expansion tensor."

The heat capacity per mole at constant volume C_{v} is defined as

$$C_{\mathrm{v}} = -\left(\frac{\theta}{T_{\mathrm{ref}}}\frac{\partial^2 \overset{\approx}{W}}{\partial \theta^2}\right)_{(\mathbf{U}_0;\theta_0)} \frac{VN_A}{N}. \tag{2.20}$$

The definition of heat capacity per mole at constant pressure is $C_{\mathrm{p}} = T\left(\frac{\partial S}{\partial T}\right)_{\mathrm{p}}$. An expression for C_{p} may be obtained by taking the total temperature derivative of Eq. (2.17), multiplying by $T(=\theta\, T_{\mathrm{ref}})$, solving Eq. (2.19) for $\frac{\partial^2 \overset{\approx}{W}}{\partial \mathbf{U} \partial \theta}$ and substituting the resulting expression. The result is

$$C_{\mathrm{p}} = -\frac{\theta}{T_{\mathrm{ref}}}\left[\frac{\partial^2 \overset{\approx}{W}}{\partial \theta^2} + \frac{\partial \mathbf{U}}{\partial \theta} : \frac{\partial^2 \overset{\approx}{W}}{\partial \mathbf{U}^2} : \frac{\partial \mathbf{U}}{\partial \theta}\right]_{(\mathbf{U}_0;\theta_0)} \frac{VN_A}{N}. \tag{2.21}$$

The instantaneous bulk modulus K for the material relates a change in volume to an increment in an applied hydrostatic pressure. In terms of the instantaneous elastic moduli $\boldsymbol{\mathcal{L}}$ (see Appendix A), the instantaneous bulk modulus is given by,

$$K = \frac{1}{\left[\mathbf{I} : \boldsymbol{\mathcal{L}}^{-1} : \mathbf{I}\right]}, \tag{2.22}$$

where $\mathbf{I}$ is the identity tensor. It is worth noting that some authors define the instantaneous bulk modulus as the proportionality constant relating a change in the spherical part of the stress to an increment of an applied pure dilatation. This results in an instantaneous bulk modulus defined as

$$K = \frac{1}{9}\left[\mathbf{I} : \boldsymbol{\mathcal{L}} : \mathbf{I}\right]. \tag{2.23}$$

The two definitions, Eq. (2.22) and Eq. (2.23), are in general, different (see Appendix A for a detailed derivation). In the special case of a cubic crystal or an isotropic

material they agree but otherwise significant discrepancies occur[4] . Therefore, one must use special care to determine which definition has been used when experimental data is reported in the literature. We feel that Eq. (2.22) more accurately represents the common interpretation of the instantaneous bulk modulus. Therefore, Eq. (2.22) will be used exclusively in the remainder of this work.

2.3 Morse EIPs with temperature dependent potential parameters

The Morse pair potential is used exclusively in this work to model the atomic pair-interactions present in the binary alloy Au-47.5at%Cd. The general form of the Morse pair potential is

$$\phi(r) \quad = A\left\{\exp\left[-2B\left(\tfrac{r}{\hat{r}}-1\right)\right]-2\exp\left[-B\left(\tfrac{r}{\hat{r}}-1\right)\right]\right\}, \tag{2.24}$$

where r is the distance between two interacting atoms, $\hat{r}$ is the zero force distance, A is related to the bond strength, and B is related to the bond stiffness. A cutoff distance (r_{cut}) of 20 $\mathring{\text{A}}$ is found to provide converged results for the summations associated with Eq. (2.10). Our investigations indicate that the EIP model developed in this work is relatively sensitive to smaller r_{cut} values, which do not provide converged results. However, a systematic exploration of this issue has not been performed. In this work, the temperature dependence of the material properties is captured by making the free potential parameters $\hat{r}$, B, and A temperature dependent.

2.3.1 Choosing temperature dependent potential parameters

Experimental observations of pure Au, pure Cd, and B2 AuCd show that as the temperature is increased the equilibrium spacing increases, free energy decreases, bulk modulus decreases, thermal expansion increases, entropy increases, and heat capacity increases. The temperature dependence of $\hat{r}$, B, and A should be selected such that they reproduce

[4] For example, the instantaneous bulk modulus of HCP Cd (*Chang and Himmel*, 1966a) is $K = 58.13$ GPa when Eq. (2.23) is used. However, a value 16.77% smaller, $K = 48.38$ GPa, is found when Eq. (2.22) is used.

these experimental trends. Thus, a simple analysis is used to understand the dependence of properties of the material on the potential parameters. This is done by plotting Eq. (2.24) for different values of each parameter and keeping all other parameters constant.

Figure 2.4(a) shows the Morse pair potential as $\hat{r}$ is increased while B and A are kept constant. As $\hat{r}$ increases the bond equilibrium distance increases, stiffness (curvature at equilibrium spacing) decreases, and equilibrium energy remains constant when only nearest neighbor interactions are considered. However, for a crystal with r_{cut} greater than the nearest neighbor distance this implies that if $\hat{r}$ is the only temperature dependent parameter and its value increases with temperature, the model will exhibit an increase in equilibrium spacing and decrease in stiffness which are in agreement with the experimental observations. It also results in an increase in free energy which in turn produces negative entropy as temperature increases at constant configuration. This violates the basic principles of equilibrium thermodynamics. Thus, $\hat{r}$ alone is not sufficient for the temperature dependence of the model.

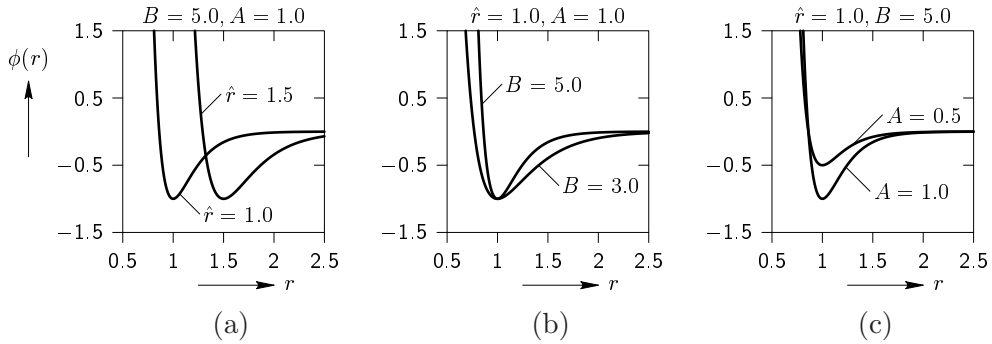

Figure 2.4: Morse pair potential when only parameter (a) $\hat{r}$ is changed, (b) B is changed, and (c) A is changed.

Figure 2.4(b) plots the Morse pair potential as B is decreased keeping all other parameters fixed. Here, a decrease in the value of B decreases the stiffness whereas bond equilibrium distance and energy remain constant when only nearest neighbor interactions are considered. For a crystal with r_{cut} greater than nearest neighbor distance the model exhibits a decrease in stiffness and free energy at constant configuration which are in agreement with experimental observations. However, it also exhibits a decrease

in equilibrium spacing which is in contradiction with experimental observations. Thus, B alone is not sufficient for the temperature dependence of the model.

Figure 2.4(c) shows the Morse pair potential as A is increased keeping all other parameters fixed. As parameter A increases there is no change in the bond equilibrium spacing but stiffness increases and energy decreases when only nearest neighbor interactions are considered. For a crystal with r_{cut} greater than the nearest neighbor distance the model exhibits no change in equilibrium spacing, but it exhibits a decrease in free energy which is in agreement with experimental observations and an increase in stiffness which opposes the experimental observations. Thus, A alone is not sufficient for the temperature dependence of the model.

Table 2.1 summarizes the qualitative behavior of crystalline equilibrium properties (r_{cut} greater than first nearest neighbor distance) with respect to the change in parameter values when temperature θ is increased. The first column in the table shows the property of the material under consideration, the second column gives the experimentally observed behavior of the property as temperature is increased, the remaining columns show how the property varies for an EIP when only the indicated parameter is temperature dependent. From this table it is observed that no single temperature dependent parameter can model all of the experimentally observed behavior. However, it seems that some combination might be able to simulate the experimental behavior. Thus, various combinations are selected based on the information in Table 2.1 and each of these combinations is studied to determine if it is able to capture the qualitative behavior indicated in the second column of Table 2.1.

2.3.2 General fitting procedure for model parameters

Before discussing any particular EIP model we describe the general fitting procedure that is used to fit the particular EIP model parameters. The fitting procedure for a generalized EIP model for AuCd is explained here. The fitting of model parameters is done using a MATLAB executable file (generally called as MEX file) which dynamically links the BFBSymPac (*Elliott*, 2010) software package which is written in C++ with MATLAB. Optimization is done using MATLAB's *lsqnonlin* function (*Mathworks*, 2009) which solves nonlinear least-square problems. *lsqnonlin* takes a vector values function $\mathbf{f}(\mathbf{q})$ and determines the values of $\mathbf{q}$ that minimizes the L^2-norm of $\mathbf{f}$. In the present

situation, $\mathbf{q}$ is the vector of EIP parameters and $\mathbf{f}(\mathbf{q})$ corresponds to the difference between the experimental data and the model's calculated material parameters. A tolerance of $\epsilon = 1.0 \times 10^{-3}$ is used here.

The approach used in this work to determine the free potential parameters starts by choosing a reference temperature for which significant experimental data is available for the alloy of interest. Here, a reference temperature of $T_{\text{ref}} = 333.15$ K is chosen, which is also the transformation temperature (A_f) of Au-47.5at%Cd.

The generalized EIP model based on the Morse pair potential is selected such that the model will capture all the combinations considered later. The EIP Morse pair potential is given by

$$\begin{aligned} \phi(r;\theta) &= A(\theta)\left\{\exp\left[-2B(\theta)\left(\frac{r}{\hat{r}(\theta)}-1\right)\right]-2\exp\left[-B(\theta)\left(\frac{r}{\hat{r}(\theta)}-1\right)\right]\right\}, \\ \hat{r}(\theta) &= r_1 + r_2 f_r(\theta), \\ B(\theta) &= B_1 + B_2 f_B(\theta), \\ A(\theta) &= A_1 + A_2 f_A(\theta), \end{aligned} \tag{2.25}$$

where $f_r(\theta)$, $f_B(\theta)$, and $f_A(\theta)$ are some chosen nonlinear functions. These functions are

	(i)	(ii)	(iii)	(iv)
Property	Experimental	$\hat{r}(\theta)\uparrow$	B$(\theta)\downarrow$	A$(\theta)\uparrow$
Lattice parameter (a)	Increases	Increases	Decreases	Constant
Linear thermal expansion (α)	Increases	Increases	Decreases	0
Bulk modulus (K)	Decreases	Decreases	Decreases	Increases
Cohesive energy (E_{c})	Increases	Increases	Increases	Increases
Entropy (S)	Increases	Decreases	Increases	Increases
Heat capacity (C_{v})	Increases	Decreases	Increases	Increases

Table 2.1: Qualitative behavior of lattice parameter a, coefficient of linear thermal expansion α, instantaneous bulk modulus K, cohesive energy E_{c}, entropy S, and heat capacity C_{v} for the Morse EIP as non-dimensional temperature θ is increased: (i) experimental observations, (ii) when only $\hat{r}$ is dependent on θ such that its value increases as θ increases, (iii) when only B is dependent on θ such that its value decreases as θ increases, and (iv) when only A is dependent on θ such that its value increases as θ increases.

constructed such that their value is zero at the reference temperature ($\theta = 1$). In this work several distinct EIP models corresponding to different choices for f_r, f_B, and f_A are explored. For each of these models, the fitting of parameters is divided into two stages. First, all the parameters from Eq. (2.25) are determined for the Au-Au, Cd-Cd, and Au-Cd bonds by matching different material properties of pure Au, pure Cd, and B2 AuCd at different temperatures respectively. Finally the determined parameters from the first stage are used as the starting point in the MATLAB optimization problem to fit all the material properties simultaneously as an unconstrained optimization problem. Note that properties of the martensite phase of the material are not used for fitting. This means that any MT and its associated properties indicated by the model will be pure predictions.

Stage 1: Fitting of individual bond parameters

In this stage the potential parameters corresponding to each type of bond present in the binary alloy AuCd are determined by matching, at the reference temperature $T_{\text{ref}} = 333.15$ K ($\theta = 1$), the stress-free equilibrium lattice spacing a, instantaneous bulk modulus K, cohesive energy E_{c}, linear thermal expansion α, and heat capacity at constant pressure C_{p}. Additionally, a and E_{c} are matched at multiple temperatures.

It is found that the resulting set of fitted parameters does not capture the B2 to B19 type of MT that occurs in AuCd whose transformation temperature is also the reference temperature ($\theta = 1$). To address this short coming, the fitting procedure for the Au-Cd bond is slightly modified. Since the lattice parameter and elastic constants play an important role in MT, the fitting of these properties of B2 AuCd at reference temperature is retained. The fitting of cohesive energy of B2 AuCd at the reference temperature is replaced by requiring that the B2 AuCd be at its stability transition point at the reference temperature. This is appropriate because the reference temperature is chosen as the experimentally observed transformation temperature (A_f) of Au-47.5at%Cd (*Chang and Read*, 1951).

Thus all the potential parameters from Eq. (2.25) for the Au-Au and Cd-Cd bonds are determined by fitting a, K, E_{c}, α, and C_{p} at the reference temperature for pure Au and pure Cd respectively. Additionally, a and E_{c} are fit at multiple temperatures. The potential parameters for the Au-Cd bond are determined by fitting a, K, the stability

transition point of B2 AuCd, α, and C_{p} at the reference temperature. Additionally, a is fit at multiple temperatures.

Stage 2: Fitting of all model parameters simultaneously

Many possible solutions are found for the fitted values of parameters from Section 2.3.2 by varying the initial conditions that are given to the MATLAB optimization program. This implies that the EIP model's predictions of the fitted properties are insensitive to small choices in the parameters. This type of model behavior is the essence of the "Sloppy model" concept introduced by *Brown and Sethna* (2003); *Daniels et al.* (2008), who have also developed methods to evaluate a model's degree of sloppiness.

In this stage, the different sets of fitted parameters obtained in Section 2.3.2 are provided as initial conditions to the MATLAB optimization program in which all model parameters are determined simultaneously as an unconstrained optimization problem. It is observed that the solutions obtained in this stage do not deviate significantly from the starting point. This indicates that the different solutions that are observed in Section 2.3.2 are likely to be local minima of the optimization problem. From these different sets of solutions the solution that corresponds most closely to the qualitative experimental behavior of pure Au, pure Cd, and B2 AuCd upon variation of temperature is selected.

2.3.3 Temperature dependence of parameters $\hat{r}$, B, and A

Returning now to the discussion of the possible types of Morse EIP temperature dependence, various combinations of temperature dependent parameters are analyzed. The fitting procedure explained in Section 2.3.2 is used and the final form of the temperature dependent parameters is selected such that the model exhibits the most accurate qualitative and quantitative behavior of material properties as temperature is varied.

Case 1: Linear temperature dependence of parameters $\hat{r}$ and B

Based on the observations from Figure 2.4 and Table 2.1, parameters $\hat{r}$ and B are taken to be temperature dependent such that $\hat{r}$ will increase and B will decrease with

temperature. Here the parameter A is kept constant. When $\hat{r}$ increases the stress-free equilibrium distance and free energy increase. When B decreases, the equilibrium spacing and free energy decrease. The temperature dependence of both parameters $\hat{r}$ and B should be such that the net stress-free equilibrium spacing increases and free energy decreases as temperature increases. As a first choice the parameters $\hat{r}$ and B are selected to be linear functions of temperature. In this case the Morse pair potential is given by

$$\begin{aligned}
\phi(r;\theta) &= A\left\{\exp\left[-2B(\theta)\left(\frac{r}{\hat{r}(\theta)}-1\right)\right]-2\exp\left[-B(\theta)\left(\frac{r}{\hat{r}(\theta)}-1\right)\right]\right\},\\
\hat{r}(\theta) &= r_1 + r_2(\theta-1),\\
B(\theta) &= B_1 + B_2(\theta-1),\\
A(\theta) &= A_1,
\end{aligned} \tag{2.26}$$

where r_1, r_2, B_1, B_2, and A_1 are constant parameters. Recall that for a binary alloy, there are three distinct types of pair interactions (a – a, b – b, and a – b) which lead to the need for three sets of these parameters.

The potential parameters in this model are determined by the procedure of Section 2.3.2. The results of this model have been reported in *Guthikonda and Elliott* (2008c). The model was able to predict the $B2 \leftrightarrow B19$ MT that occurs in Au-47.5at%Cd and it also seems to capture some other important properties of MT such as the volume preserving nature and transformation stretch tensor of the MT. However, this model predicted a negative thermal expansion for B2 AuCd at higher temperatures. This is contrary to the experimental behavior of B2 AuCd.

In order to understand the reasons for the negative thermal expansion in the EIP model of Eq. (2.26), the dependence of the Au FCC lattice parameter on the parameters $\hat{r}$ and B is considered. Figure 2.5 plots the variation of lattice parameter a for the fitted parameters of Model 2 from *Guthikonda and Elliott* (2008c) when only $\hat{r}$ is varied with respect to temperature (dashed line), when only B is varied (dotted line), and when both $\hat{r}$ and B are varied (solid line). From the dashed line in the figure it is observed that a linear variation of $\hat{r}$ with temperature causes a linear increase of the lattice parameter. From the dotted line it is observed that a linear variation of B with temperature causes a strong non-linear decrease of the lattice parameter. When both $\hat{r}$ and B vary linearly

the solid line is obtained. From this it is understood that in order to have an increasing lattice parameter for the temperature range of interest $\hat{r}$ should increase at a superlinear rate as compared to the decrease of B.

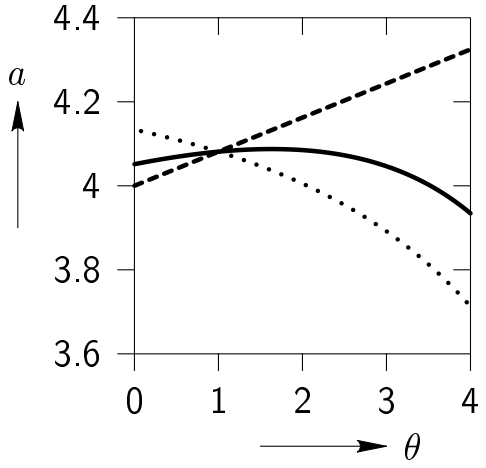

Figure 2.5: Variation of lattice parameter a of FCC Au for the fitted parameters of Model 2 from (*Guthikonda and Elliott*, 2008c) when only $\hat{r}$ is varied with non-dimensional temperature θ (dashed line), when only B is varied with non-dimensional temperature θ (dotted line), and when both $\hat{r}$ and B are varied with non-dimensional temperature θ (solid line).

Case 2: Polynomial temperature dependence of parameters $\hat{r}$ and B

Based on the results of Section 2.3.3, an extension to the EIP model of Eq. (2.26) is performed by taking the parameters $\hat{r}$ and B as power law functions of temperature. In this case the EIP Morse pair potential is given by

$$\begin{aligned}
\phi(r;\theta) &= A\left\{\exp\left[-2B(\theta)\left(\frac{r}{\hat{r}(\theta)}-1\right)\right]-2\exp\left[-B(\theta)\left(\frac{r}{\hat{r}(\theta)}-1\right)\right]\right\},\\
\hat{r}(\theta) &= r_1 + r_2(\theta^{r_3}-1),\\
B(\theta) &= B_1 + B_2(\theta^{B_3}-1),\\
A(\theta) &= A_1,
\end{aligned} \tag{2.27}$$

where r_1, r_2, r_3, B_1, B_2, B_3, and A_1 are constant parameters.

It turns out that if these parameters are fitted according to Section 2.3.2 the problem of negative thermal expansion is corrected but the heat capacity at constant pressure C_{p} decreases at higher temperatures. This is undesirable. If A is taken as a power law function in addition to $\hat{r}$ and B one finds the opposite situation where C_{p} behaves acceptably but a negative thermal expansion is found at low temperatures.

Case 3: Exponential temperature dependence of parameters $\hat{r}$, B, and A

In order to address the short coming of decreasing lattice parameter at lower temperatures in the EIP model, the temperature dependence of the parameters $\hat{r}$, B, and A is taken to be exponential instead of power law. In this case the Morse potential is given by

$$\begin{aligned}
\phi(r;\theta) &= A(\theta)\left\{\exp\left[-2B(\theta)\left(\frac{r}{\hat{r}(\theta)}-1\right)\right]-2\exp\left[-B(\theta)\left(\frac{r}{\hat{r}(\theta)}-1\right)\right]\right\},\\
\hat{r}(\theta) &= r_1 + r_2(\exp(r_3(\theta-1))-1),\\
B(\theta) &= B_1 + B_2(\exp(B_3(\theta-1))-1),\\
A(\theta) &= A_1 + A_2(\exp(A_3(\theta-1))-1),
\end{aligned} \tag{2.28}$$

where r_1, r_2, r_3, B_1, B_2, B_3, A_1, A_2, and A_3 are constant parameters.

The fitting procedure is unsuccessful with this model because of a rapid increase of lattice parameter and heat capacity with increasing temperature that is inherent to the exponential temperature dependence of all the potential parameters used in this case. However, it seems that a combination of exponential and power law temperature dependence might produce the desired qualitative and quantitative behavior of material properties as temperature is varied.

Case 4: Polynomial and exponential temperature dependence of the Morse parameters

From Case 2 and Case 3 it is observed that polynomial temperature dependence of all three parameters results in negative thermal expansion at low temperatures and exponential temperature dependence of all three parameters makes the fitting procedure unsuccessful. With this in mind the temperature dependence of $\hat{r}$ is selected to be

exponential and that of B and A are selected to be power law. This combination of exponential and power law temperature dependence seems to eliminate the problems that are observed in Case 2 and Case 3. Thus, the final form of the Morse pair potential is taken as

$$\begin{aligned}
\phi(r;\theta) &= A\left\{\exp\left[-2B(\theta)\left(\frac{r}{\hat{r}(\theta)}-1\right)\right]-2\exp\left[-B(\theta)\left(\frac{r}{\hat{r}(\theta)}-1\right)\right]\right\},\\
\hat{r}(\theta) &= r_1 + r_2(\exp(r_3(\theta-1.0))-1.0),\\
B(\theta) &= B_1 + B_2(\theta^{B_3}-1.0),\\
A(\theta) &= A_1 + A_2(\theta^{A_3}-1.0),
\end{aligned} \tag{2.29}$$

where r_1, r_2, r_3, B_1, B_2, B_3, A_1, A_2, and A_3 are constant parameters.

For a temperature range of $\theta = 0.0$ to 3.0, this model seems to capture the qualitative material behavior shown in the second column of Table 2.1. Thus, the EIP model of Eq. (2.29) is taken as the final EIP model form.

2.4 Final EIP model

2.4.1 Model parameters and property predictions

The complete set of 27 parameters of the final EIP model of Eq. (2.29) are determined by applying the fitting procedure described in Section 2.3.2 for pure Au, pure Cd, and B2 AuCd. The material properties and their fitted values for pure Au, pure Cd, and B2 AuCd are given in Tables 2.2, 2.3, and 2.4 respectively. The corresponding model parameters are reported in Table 2.5. Note that a set of eleven experimental values (Table 2.2) are used to fit the nine parameters for the a − a bond. Additional experimental values are used to ensure that the resulting potential accurately reproduces the experimentally observed lattice parameter a and cohesive energy E_c values (*Villars et al.*, 1985; *Hultgren et al.*, 1963) over the temperature range $0 \leq \theta \leq 3$. Also, since B2 AuCd is unstable at low temperatures it is not possible to obtain experimental values for the lattice parameter a at 0 K and 150 K. Thus, the values given in Table 2.4 are determined by linear interpolation from the values near $\theta = 1.0$ (*Zirinsky*, 1956).

Figure 2.6 shows the variation of lattice parameter, cohesive energy, linear thermal expansion coefficient, entropy per mole, instantaneous bulk modulus, and heat capacity

FCC Au

Property	Unit	Temperature K	Experimental Value	Fitted Value
Lattice parameter (a)	Å	700.00	4.1054	4.1126
Lattice parameter (a)	Å	550.00	4.0962	4.0946
Lattice parameter (a)	Å	333.15	4.0819	4.0786
Lattice parameter (a)	Å	150.00	4.0701	4.0688
Lattice parameter (a)	Å	0.00	4.0604	4.0605
Cohesive energy (E_c)	$\frac{\mathrm{eV}}{\mathrm{atom}}$	700.00	-3.7069	-3.7053
Cohesive energy (E_c)	$\frac{\mathrm{eV}}{\mathrm{atom}}$	550.00	-3.7485	-3.7555
Cohesive energy (E_c)	$\frac{\mathrm{eV}}{\mathrm{atom}}$	333.15	-3.8248	-3.8192
Bulk modulus (K)	GPa	333.15	171.8388	171.8400
Thermal expansion coefficient (α)	10^{-6} K^{-1}	333.15	14.2846	14.2847
Heat capacity (C_p)	$\frac{\mathrm{J}}{\mathrm{mol\ K}}$	333.15	25.4698	25.4700

Table 2.2: Experimental values and corresponding fitted values of lattice parameter a at 700 K, 550 K, 333.15 K, 150 K, and 0 K; cohesive energy E_c at 700 K, 550 K, and 333.15 K; bulk modulus K, thermal expansion coefficient α, and heat capacity at constant pressure C_p at reference temperature 333.15 K ($\theta = 1$) of pure Au (*Villars et al.*, 1985; *Chang and Himmel*, 1966b; *Hultgren et al.*, 1963).

HCP Cd

Property	Unit	Temperature K	Experimental Value	Fitted Value
Lattice parameter (a)	Å	550.00	2.9935	2.9924
Lattice parameter (a)	Å	333.15	2.9758	2.9764
Lattice parameter (a)	Å	150.00	2.9631	2.9660
Lattice parameter (a)	Å	0.00	2.9526	2.9583
Cohesive energy (E_c)	$\frac{\mathrm{eV}}{\mathrm{atom}}$	550.00	-1.0869	-1.0837
Cohesive energy (E_c)	$\frac{\mathrm{eV}}{\mathrm{atom}}$	333.15	-1.1682	-1.1718
Bulk modulus (K)	GPa	333.15	47.9209	47.9213
Thermal expansion coefficient (α)	10^{-6} K^{-1}	333.15	20.8744	20.8749
Heat capacity (C_p)	$\frac{\mathrm{J}}{\mathrm{mol\ K}}$	333.15	26.3578	26.3520

Table 2.3: Experimental values and corresponding fitted values of lattice parameter a at 550 K, 333.15 K, 150 K, and 0 K; cohesive energy E_c at 550 K and 333.15 K; bulk modulus K, thermal expansion coefficient α, and heat capacity at constant pressure C_p at reference temperature 333.15 K ($\theta = 1$) of pure Cd (*Edwards et al.*, 1952; *Chang and Himmel*, 1966a; *Hultgren et al.*, 1963).

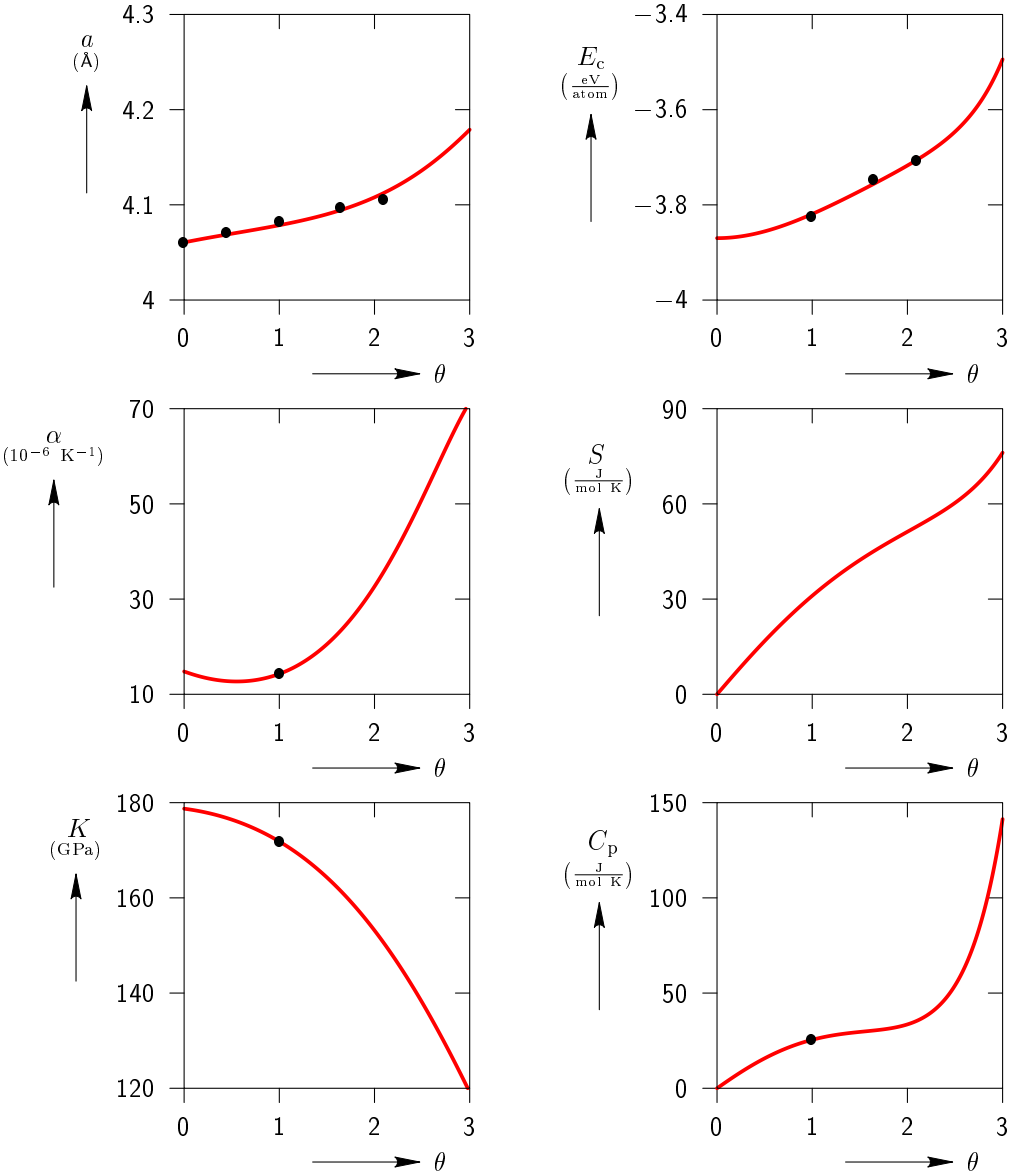

Figure 2.6: Variation of lattice parameter a, cohesive energy E_c, linear thermal expansion coefficient α, entropy per mole S, instantaneous bulk modulus K, and heat capacity per mole at constant pressure C_p of FCC Au vs. non-dimensional temperature θ for the parameters in Table 2.5. Solid circles in each plot identify the corresponding experimental values.

per mole at constant pressure for FCC Au with respect to non-dimensional temperature θ where only the a − a pair interaction is required for the monoatomic crystal. Solid circles show the experimental values given in Table 2.2. The lattice parameter and cohesive energy increase as θ increases. The linear thermal expansion coefficient decreases for very low θ which contradicts the experimental observations (*Villars et al.*, 1985) but remains positive and starts increasing around $\theta = 0.45$. The instantaneous bulk modulus decreases as θ increases. The entropy per mole and heat capacity per mole at constant pressure increases as θ increases. Thus, the qualitative behavior of all these properties, except the linear thermal expansion at very low temperatures, is in agreement with the general experimental observations of properties of pure Au (*Villars et al.*, 1985; *Chang and Himmel*, 1966b; *Hultgren et al.*, 1963). The crystal structure of pure Au is stable over the entire temperature range as indicated by the solid lines in Figure 2.6.

Figure 2.7 shows values for HCP Cd of the close-packed plane lattice parameter, cohesive energy, in-plane linear thermal expansion coefficient, entropy per mole, instantaneous bulk modulus, and heat capacity per mole at constant pressure, where only the b − b pair interaction is required for the monoatomic crystal. The symmetry of the HCP structure dictates that the internal atomic shift vector remains zero as the

B2 AuCd

Property	Unit	Temperature K	Experimental Value	Fitted Value
Lattice parameter (a)	Å	700.00	3.3420	3.3492
Lattice parameter (a)	Å	550.00	3.3316	3.3295
Lattice parameter (a)	Å	333.15	3.3165	3.3105
Lattice parameter (a)	Å	150.00	3.3038	3.2999
Lattice parameter (a)	Å	0.00	3.2935	3.2940
Cohesive energy (E_c)	$\frac{eV}{atom}$	333.15	−2.6936	−1.8318*
Bulk modulus (K)	GPa	333.15	99.5103	99.4973
Thermal expansion coefficient (α)	10^{-6} K^{-1}	333.15	20.9000	20.8990
Heat capacity (C_p)	$\frac{J}{mol\ K}$	333.15	26.1093	26.1079

Table 2.4: Experimental values and corresponding fitted values of lattice parameter a at 700 K, 550 K, 333.15 K, 150 K, and 0 K; cohesive energy E_c, bulk modulus K, thermal expansion coefficient α, and heat capacity at constant pressure C_p at reference temperature 333.15 K ($\theta = 1$) of B2 AuCd (*Chang and Read*, 1951; *Zirinsky*, 1956; *Hultgren et al.*, 1963, 1973). *E_c at 333.15 K is not actually fitted. See Section 2.3.2 for more details.

Final EIP parameters

Potential	parameter	Value
Au-Au	A_1^{aa}	0.482917351030788 eV
	A_2^{aa}	−0.000855192503400 eV
	A_3^{aa}	3.625177992551010
	B_1^{aa}	4.708238552507823
	B_2^{aa}	−0.083925503055104
	B_3^{aa}	2.005750046077795
	r_1^{aa}	3.035902348167637 Å
	r_2^{aa}	0.040386678684356 Å
	r_3^{aa}	0.951807321991185
Cd-Cd	A_1^{bb}	0.151331888205594 eV
	A_2^{bb}	0.002988464666570 eV
	A_3^{bb}	2.080803415890498
	B_1^{bb}	4.631077953243956
	B_2^{bb}	−0.048032181489227
	B_3^{bb}	2.117843852765962
	r_1^{bb}	3.144811091489227 Å
	r_2^{bb}	0.048803776186845 Å
	r_3^{bb}	0.784063749845215
Au-Cd	A_1^{ab}	0.198800688293818 eV
	A_2^{ab}	0.002241110733955 eV
	A_3^{ab}	2.000000020369559
	B_1^{ab}	5.452742482206239
	B_2^{ab}	−0.007514062001064
	B_3^{ab}	3.298115567103574
	r_1^{ab}	3.081961402980163 Å
	r_2^{ab}	0.028018026615333 Å
	r_3^{ab}	0.842955022337628

Table 2.5: Fitted parameters for the Au-47.5at%Cd Morse EIP model of Eq. (2.29).

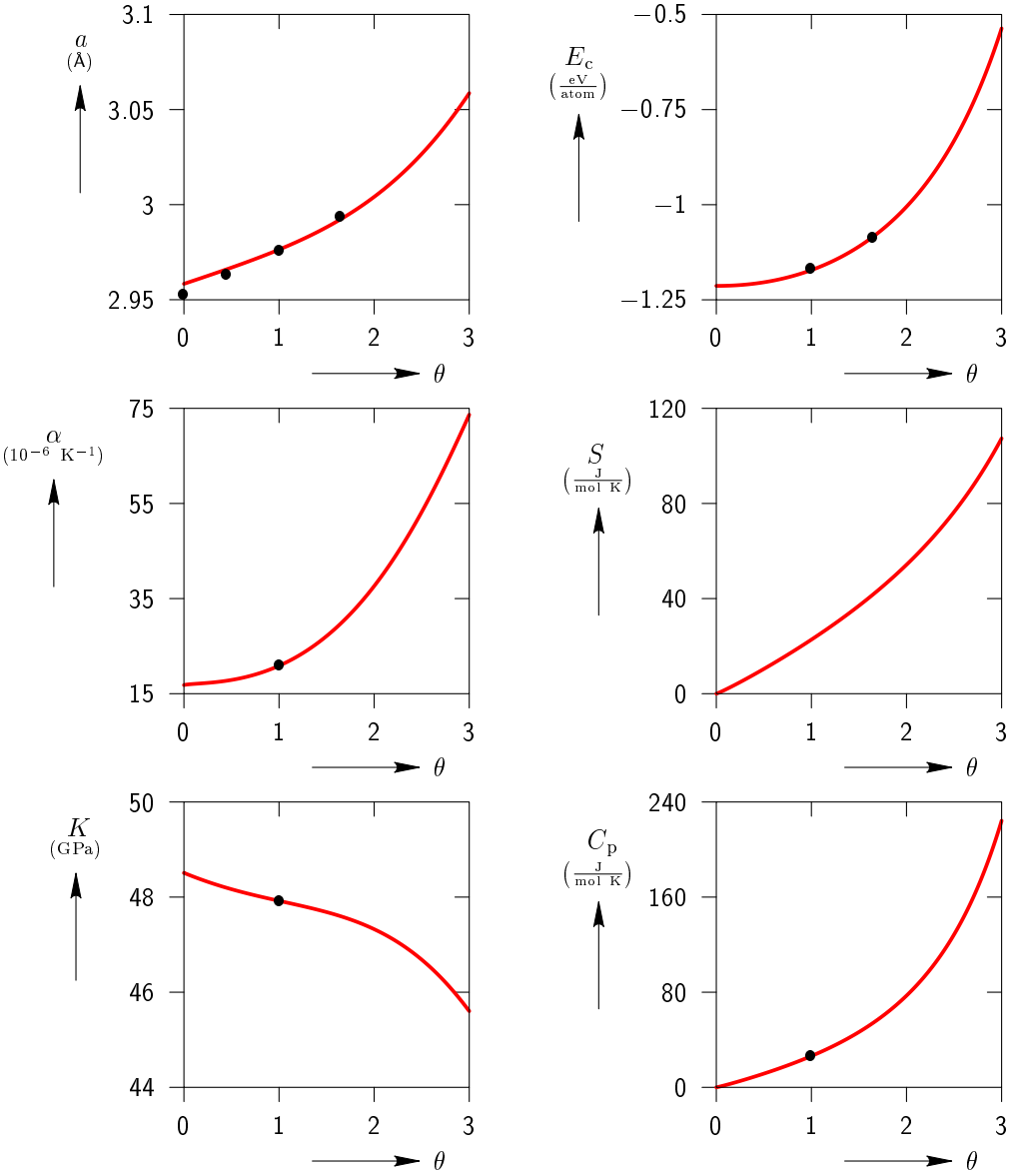

Figure 2.7: Variation of close-packed plane lattice parameter a, cohesive energy E_c, in-plane linear thermal expansion coefficient α, entropy per mole S, instantaneous bulk modulus K, and heat capacity per mole at constant pressure C_p of HCP Cd vs. non-dimensional temperature θ for the parameters in Table 2.5. Solid circles in each plot identify the corresponding experimental values.

temperature is varied. Solid circles in each plot correspond to the experimental values given in Table 2.3. In this case, the lattice parameter, cohesive energy, and in-plane linear thermal expansion coefficient increases as θ increases. The bulk modulus decreases as θ increases. The entropy per mole and heat capacity per mole at constant pressure increase as θ increases. Again, the qualitative behavior of these properties is in agreement with experimental observations (*Edwards et al.*, 1952; *Chang and Himmel*, 1966a; *Hultgren et al.*, 1963). The crystal structure of pure Cd is stable over the entire temperature range as shown by the solid lines in Figure 2.7.

Figure 2.8 shows the variation of lattice parameter, cohesive energy, linear thermal expansion coefficient, entropy per mole, instantaneous bulk modulus, and heat capacity per mole at constant pressure of B2 AuCd, where all three pair interactions (a$-$a, b$-$b, and a$-$b) are required for the biatomic crystal. As in the HCP Cd case, the symmetry of the B2 structure dictates that the internal atomic shifts remain zero as the temperature is varied. Solid circles in each plot show the experimental values given in Table 2.4. Note that the cohesive energy of B2 AuCd is not fitted at the reference temperature, Instead, the B2 AuCd is made to change stability at the reference temperature. The qualitative behavior of all the properties is in agreement with experimental observations of B2 AuCd (*Chang and Read*, 1951; *Zirinsky*, 1956; *Hultgren et al.*, 1963, 1973). The B2 AuCd crystal structure is stable at high temperatures (denoted by the solid line segments) and becomes unstable (denoted by the dotted line segments) at $\theta = 1$ as temperature is decreased.

2.4.2 Temperature-induced MTs associated with the EIP model

A stress-free bifurcation diagram (*Elliott et al.*, 2002b, 2006b) is generated for the EIP model of Eq. (2.29) in order to evaluate its ability to correctly predict the B2 to B19 phase transformation found in Au-47.5at%Cd. Figure 2.9 displays the results by plotting the maximum principal stretch λ_3 vs. non-dimensional temperature θ. Here, the maximum principal stretch λ_3 is calculated as the (algebraically) largest eigenvalue of the symmetric right stretch tensor $\mathbf{U}$. Figure 2.9 also shows the crystal structures of the different phases that are found. Here, solid lines represent stable (CB and phonon) equilibrium configurations and dashed lines represent unstable configurations. Bifurcation points are represented by hollow circles whereas turning points are represented

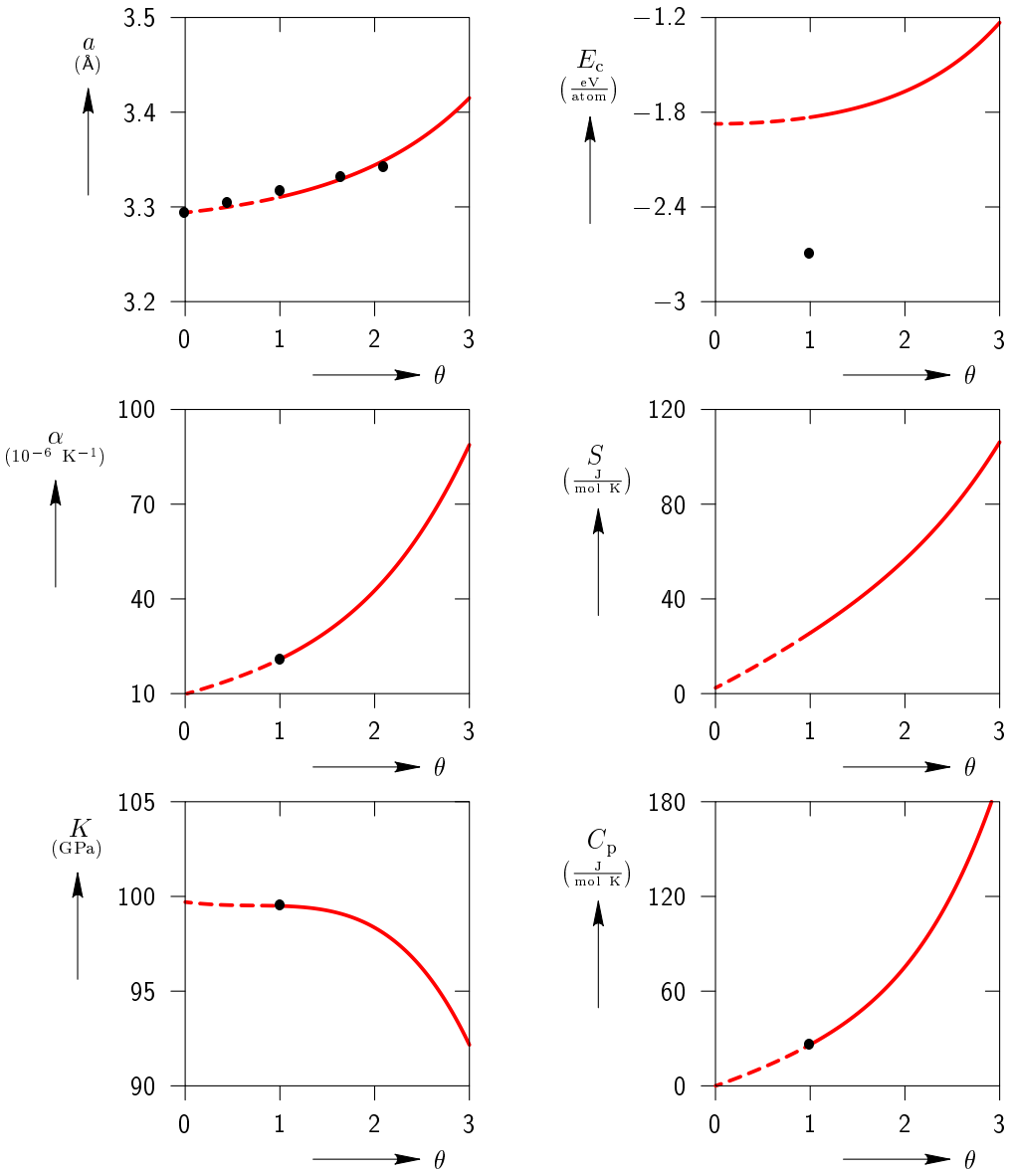

Figure 2.8: Variation of lattice parameter a, cohesive energy E_c, linear thermal expansion coefficient α, entropy per mole S, instantaneous bulk modulus K, and heat capacity per mole at constant pressure C_p of B2 Au-47.5at%Cd vs. non-dimensional temperature θ for the parameters in Table 2.5. Solid circles in each plot identify the corresponding experimental values. Solid (dashed) lines indicate stable (unstable) equilibrium configurations.

by solid circles. The behavior is qualitatively similar to the results reported in *Elliott et al.* (2006b). Thus, for a more detailed description of the various crystal structures indicated in Figure 2.9, see *Elliott et al.* (2006b). The B2 austenite phase (red line) is stable at higher temperatures and becomes unstable as the temperature is decreased with bifurcation at $\theta = 1$ (T_{ref}=333.15 K) which is in correspondence with experimental observations (*Chang and Read*, 1951). The onset of instability is associated with a deformation mode where the shifts become non-zero as discussed in *Guthikonda and Elliott* (2008a). A set of B19 and αIrV orthorhombic equilibrium paths emerge from the bifurcation point at $\theta = 1$. The B19 equilibrium path (green line) is initially unstable as it emerges from the bifurcation point, but becomes stable at a turning point near $\theta = 2.61$. It continues to be stable as temperature is decreased to 0 K. It is also observed that an initially unstable path of a monoclinic structure with space group P2/m (yellow line) originates from the secondary bifurcation point on the B19 path at around $\theta = 2.52$ and it continues to be unstable as temperature decreases to 0 K. The αIrV equilibrium path (purple line) is initially unstable as it emerges from the B2 bifurcation point, but becomes stable at a turning point near $\theta = 2.44$. It continues to be stable until $\theta = 1.47$ where it encounters another turning point. The αIrV path eventually reaches a point where it intersects an $L1_0$ equilibrium path at around $\theta = 2.41$. Starting from this point the $L1_0$ equilibrium path is found to be stable as λ_3 is increased until temperature reaches 0 K. It becomes unstable as λ_3 is decreased and continues to be unstable through 0 K. From our experience (see, for example *Elliott*, 2007; *Guthikonda and Elliott*, 2008c) we believe that this unstable path would eventually meet another bifurcation point on the B2 path at some negative temperature. An additional unstable path of αIrV is also found originating from the bifurcation point on the unstable $L1_0$ path at $\theta = 0.80$.

The variation of the HC (Gibbs) free energy density $\overset{\approx}{W}$ with respect to the non-dimensional temperature θ is plotted in Fig. 2.4.2. The slope and curvature of all stress-free equilibrium paths are found to be negative for all temperatures. This indicates that the entropy and heat capacity at constant pressure are positive, as required by equilibrium thermodynamics.

At this point, we restrict our attention to the stable path segments for B2, $L1_0$, B19, and αIrV predicted by the EIP model. Figure 2.4.2 displays the variation of $\overset{\approx}{W}$ of these

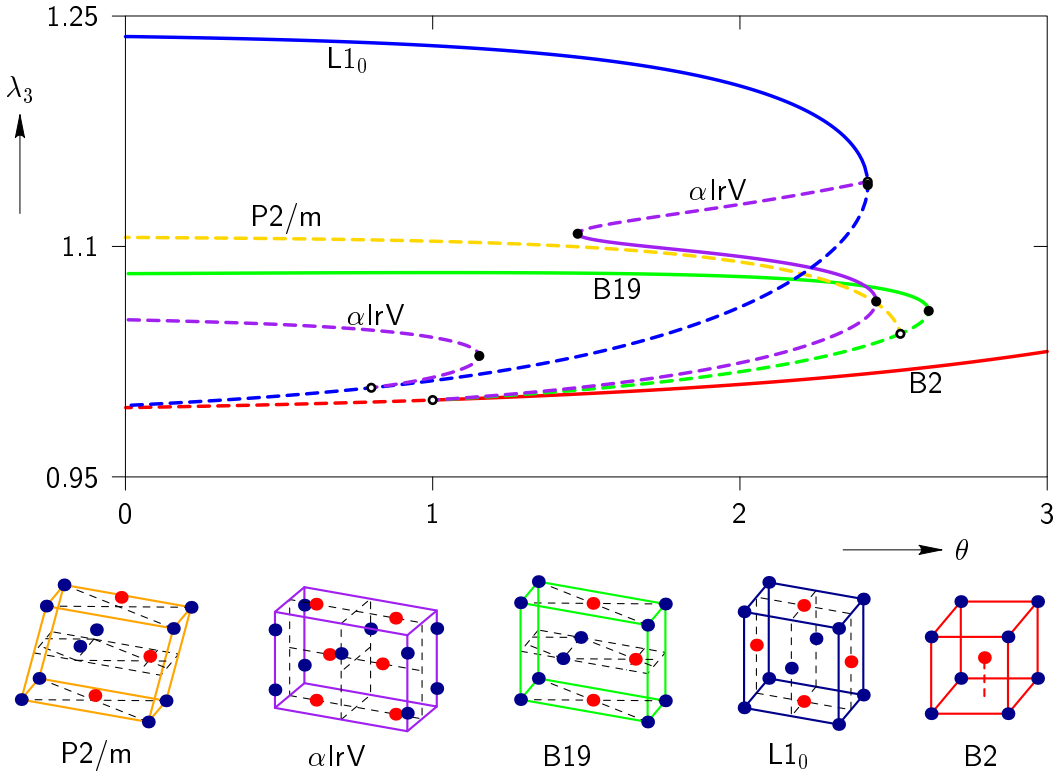

Figure 2.9: Variation of λ_3 (largest eigenvalue of $\mathbf{U}$) of B2, $L1_0$, B19, αIrV, and P2/m crystal structures of Au-47.5at%Cd with respect to non-dimensional temperature θ.

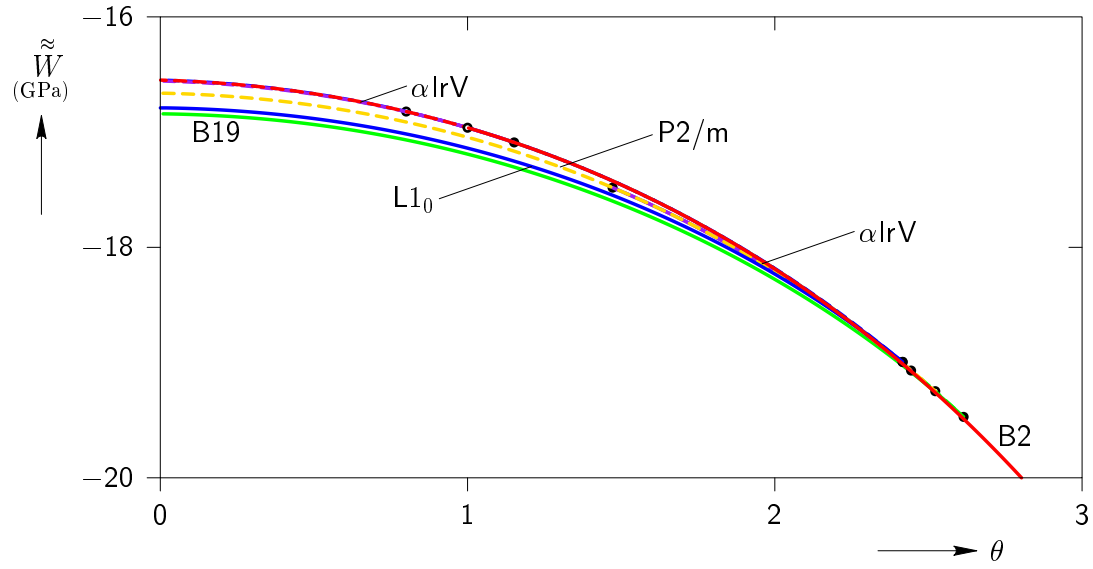

Figure 2.10: Variation of (Gibbs) free energy density of B2, $L1_0$, B19, αIrV, and P2/m crystal structures of Au-47.5at%Cd with respect to non-dimensional temperature θ.

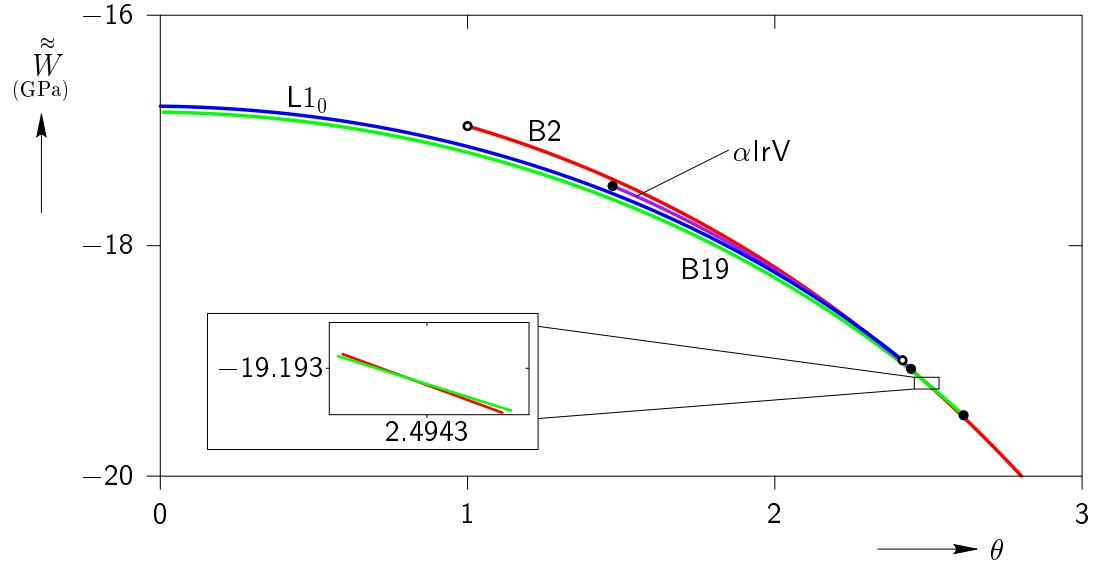

Figure 2.11: Variation of (Gibbs) free energy density of stable path segments for the B2, $L1_0$, B19, and αIrV crystal structures of Au-47.5at%Cd with respect to non-dimensional temperature θ.

phases with respect to θ. At high temperatures the B2 crystal is the only stable phase, at intermediate temperatures four phases are stable, and at low temperatures two phases are stable. Figure 2.12 displays the variation of unit cell volume with respect to non-

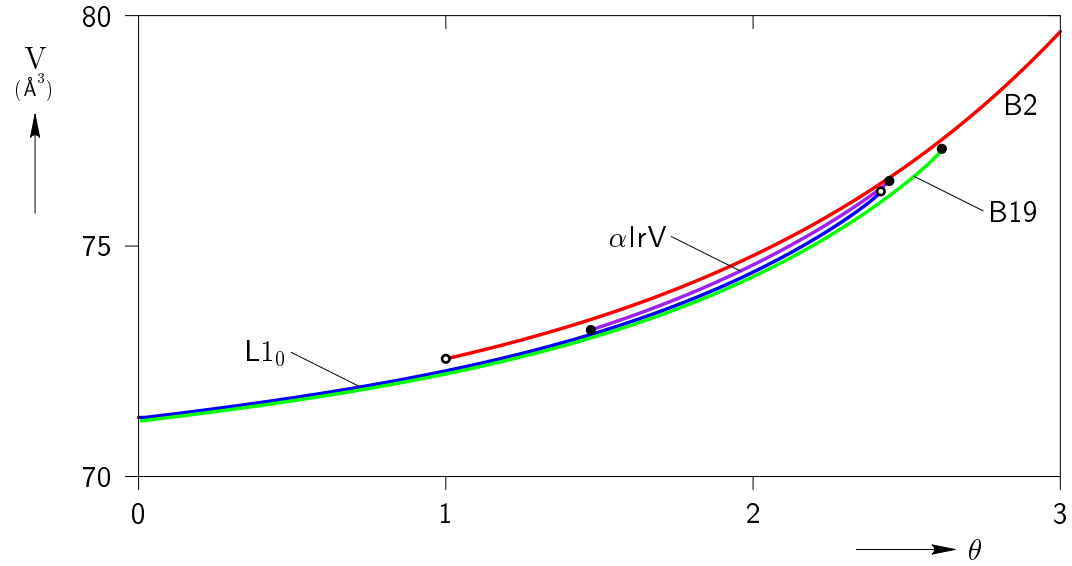

Figure 2.12: Variation of unit cell volume of the B2, $L1_0$, B19, and αIrV crystal structures for Au-47.5at%Cd with respect to non-dimensional temperature θ.

dimensional temperature θ. The unit cell volume of all stable phases are nearly equal which shows that any MTs predicted by this model will result in a volume change of less than 0.1%. The unit cell volume of different phases increase as temperature is increased which is in coincidence with general experimental observations. Figure 2.13 displays the variation of instantaneous bulk modulus K with respect to non-dimensional temperature θ. For αIrV and B19, $K \rightarrow 0$ as a turning point is approached on the respective equilibrium paths. Figures 2.14 and 2.15 display the variation of entropy and heat capacity at constant pressure, respectively, with respect to non-dimensional temperature θ. In general, entropy and heat capacity are found to increase with temperature. This is in general agreement with thermodynamic theory. For the $L1_0$, B19, and αIrV phases C_{p} diverges to infinity as a turning point is approached on the respective equilibrium paths. This is a result of the fact that the bulk modulus goes to zero at these points.

Returning to Fig. 2.4.2, it is observed that upon decreasing temperature the B2

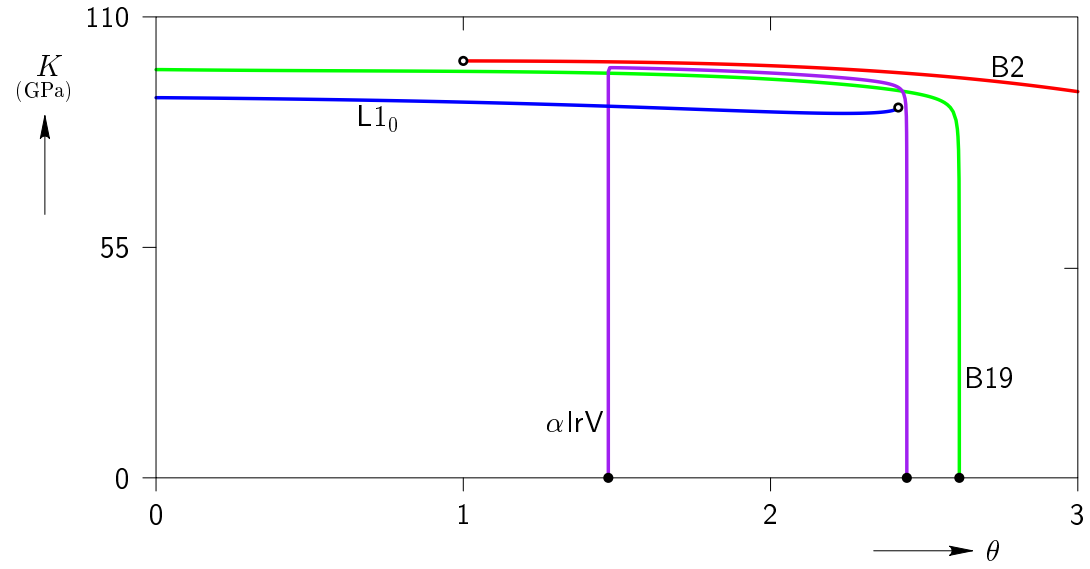

Figure 2.13: Variation of instantaneous bulk modulus K of the B2, $L1_0$, B19, and αIrV crystal structures for Au-47.5at%Cd with respect to non-dimensional temperature θ.

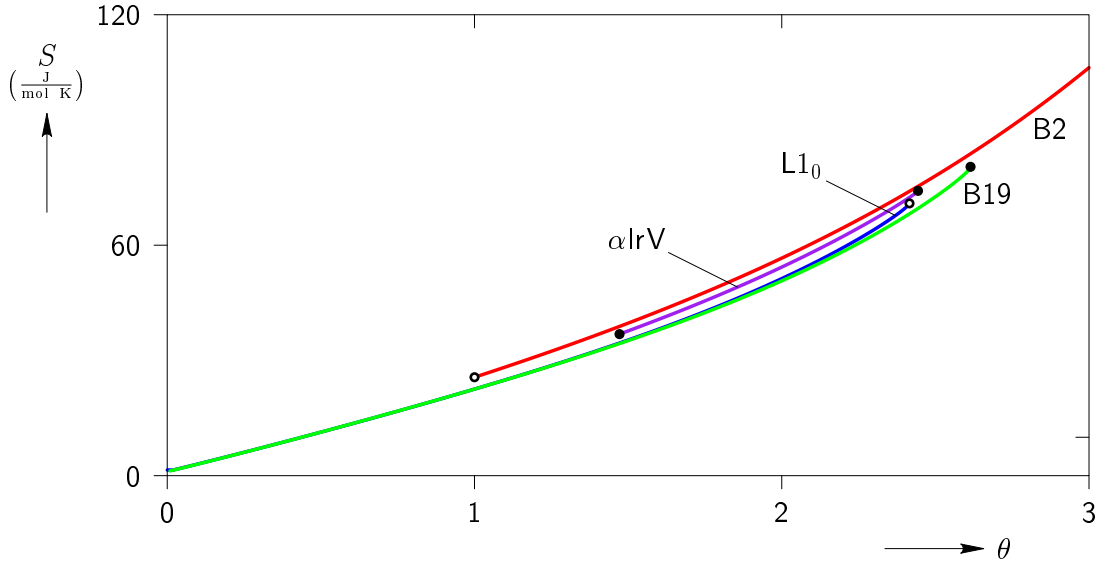

Figure 2.14: Variation of entropy S of the B2, $L1_0$, B19, and αIrV crystal structures for Au-47.5at%Cd with respect to non-dimensional temperature θ.

phase becomes metastable at the "equilibrium thermodynamics" transition temperature $\theta = 2.49$ (with the B19 phase having lower free energy for lower temperatures) and finally loses material stability at $\theta = 1$ which is the models value for A_f. At this temperature the only stable phases are B19 and $L1_0$. However, B19 is the stable phase with minimum free energy. Thus, a transformation from B2 to B19 can be expected. For lower temperatures the B19 phase continues to be the stable phase with minimum free energy. In the case of increasing temperature, the orthorhombic B19 structure has the global minimum free energy until $\theta = 2.49$ where it becomes metastable with respect to the B2 phase. It loses material stability soon afterward at $\theta = 2.55$ which is the models prediction for M_f where it ceases to exist for higher temperatures. Ideally, one should verify that no other equilibrium crystal structures exist with lower energy. This would ensure that the minimum energy phases shown in Fig. 2.4.2 capture the model's ground state phase at any given temperature. However, this theoretically infinite investigation is not pursued in this work.

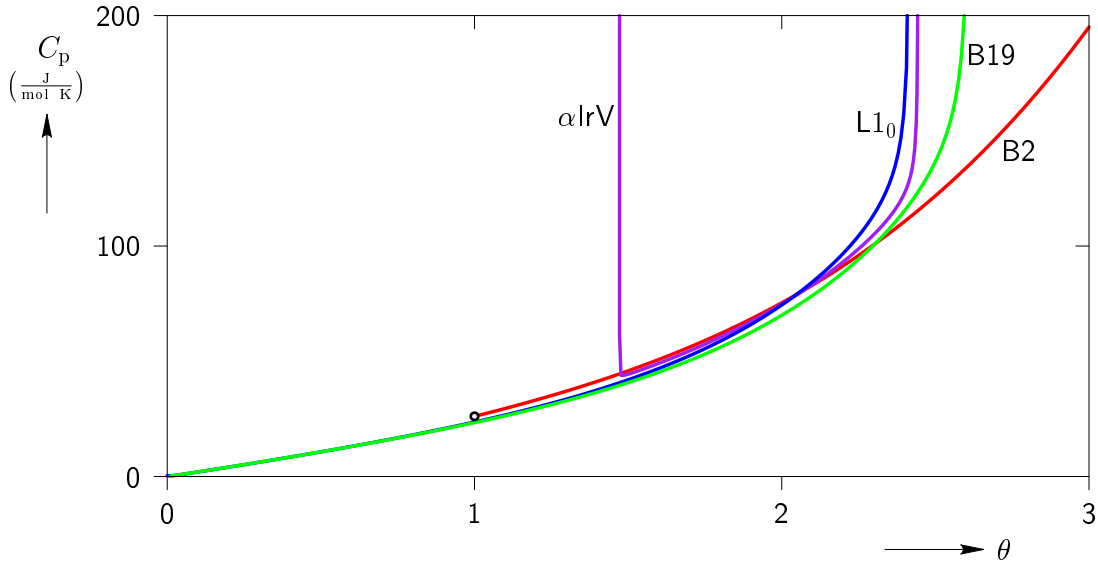

Figure 2.15: Variation of heat capacity at constant pressure C_p of the B2, $L1_0$, B19, and αIrV crystal structures for Au-47.5at%Cd with respect to non-dimensional temperature θ.

The above discussion show that the model predicts a hysteretic martensitic transformation between experimentally observed austenite (B2) and martensite (B19) phases for AuCd. Upon cooling the austenite to martensite transition begins at $\theta = 2.49$ and would complete at $\theta = 1.0$. The reverse transformation, upon heating, would begin at $\theta = 2.49$ and complete at $\theta = 2.55$. Therefore, the predicted maximum possible temperature hysteresis is $\theta_{M_f} - \theta_{A_f} = 1.55$ (516.38 K). This is within an order of magnitude of the experimental value 30 K (*Chang and Read*, 1951).

At the transformation temperature (A_f), 333.15 K (*Chang and Read*, 1951), the transformation stretch associated with the B2 to B19 MT is found to be

$$\mathbf{U}^* = \begin{pmatrix} 1.05388872 & 0.02908900 & 0 \\ 0.02908900 & 1.05388872 & 0 \\ 0 & 0 & 0.89693725 \end{pmatrix}, \tag{2.30}$$

where $\mathbf{U}_{\mathrm{B19}} = \mathbf{U}^* \cdot \mathbf{U}_{\mathrm{B2}}$. Here, $\mathbf{U}_{\mathrm{B19}}$ is the right stretch tensor for the stress-free configuration of the B19 orthorhombic structure at the reference temperature ($\theta = 1$), and $\mathbf{U}_{\mathrm{B2}}$ ($= \mathbf{I}$) is the Right Stretch tensor of the stress-free B2 cubic structure at $\theta = 1$. The components of $\mathbf{U}^*$ are given in an ortho-normal basis aligned with the reference B2 cubic axes. The corresponding experimental value (*Ohba et al.*, 1990) is

$$\mathbf{U}^*_{\mathrm{exp}} = \begin{pmatrix} 1.0260 & 0.0100 & 0 \\ 0.0100 & 1.0260 & 0 \\ 0 & 0 & 0.9501 \end{pmatrix}. \tag{2.31}$$

There is reasonable agreement between the EIP model's prediction and the experimentally observed value of the transformation stretch tensor.

The latent heat ($\Delta\overset{\approx}{W} + T\Delta S$) associated with the B2 to B19 transformation at $\theta = 1$ is calculated as -844.51 $\frac{\mathrm{cal}}{\mathrm{mol}}$ (negative values correspond to exothermic transition) which is within a factor of 10 of the experimental value for the latent heat of transformation from B2 to B19 which is -88 $\frac{\mathrm{cal}}{\mathrm{mol}}$ (*Nakanishi et al.*, 1973).

Thus, it is found that the current Morse EIP model for Au-47.5at%Cd is able to match (by construction) the lattice parameter, instantaneous bulk modulus, and stability range of the B2 austenite phase as well as the austenite's linear thermal expansion

coefficient, its heat capacity at constant pressure at $\theta = 1$ and its lattice parameter at $T = 550\ K, 700\ K$. Further, the model *predicts* the existence of a temperature-induced hysteretic B2 to B19 martensitic phase transformation, and the transformation stretch tensor is predicted with reasonable accuracy. Finally, the latent heat of transformation and the size of the temperature hysteresis are predicted to be within an order of magnitude.

Chapter 3

Entropic stabilization in shape memory alloys

3.1 Introduction

Entropic stabilization is an important thermodynamic phenomenon that plays a critical role during MTs that occur in SMAs. It is the transition of a dynamically unstable crystal structure at low temperatures into a stable crystal structure at high temperatures. A crystal structure is considered to be dynamical unstable when at least one normal mode of atomic vibration is unstable. This normal mode of atomic vibration is also called a *phonon*. A wide range of materials including SMAs exhibit this phenomenon. For example, the body-centered-cubic (bcc) phase of group IIIB and IVB metals (*Persson et al.*, 2000), cubic zirconia (*Sternik and Parlinski*, 2005), the high-pressure bcc phase of Fe (*Belonoshko et al.*, 2008; *Vocadlo et al.*, 2003), and the B2 cubic phase of the SMA NiTi (*Huang et al.*, 2001) exhibit one or several dynamically unstable phonon modes, i.e., modes of atomic vibration with imaginary harmonic frequencies (*Huang and Born*, 1962).

Figure 3.1 shows the phonon dispersion for the B2 cubic austenite phase of NiTi at 0 K obtained from DFT calculations of *Huang et al.* (2001).[1] The imaginary phonon frequencies of the unstable modes plotted as negative values in Fig. 3.1 indicate that

[1] Reprinted Fig. 3.1 with permission from *Huang et al.* (2001). Copyright (2001) by the American Physical Society.

the B2 cubic austenite phase of NiTi is a saddle point (not a local minimum) of the free energy at 0 K. This implies that entropic stabilization is responsible for the existence of a stable (local minimum of free energy) B2 cubic austenite phase of NiTi at high temperatures.

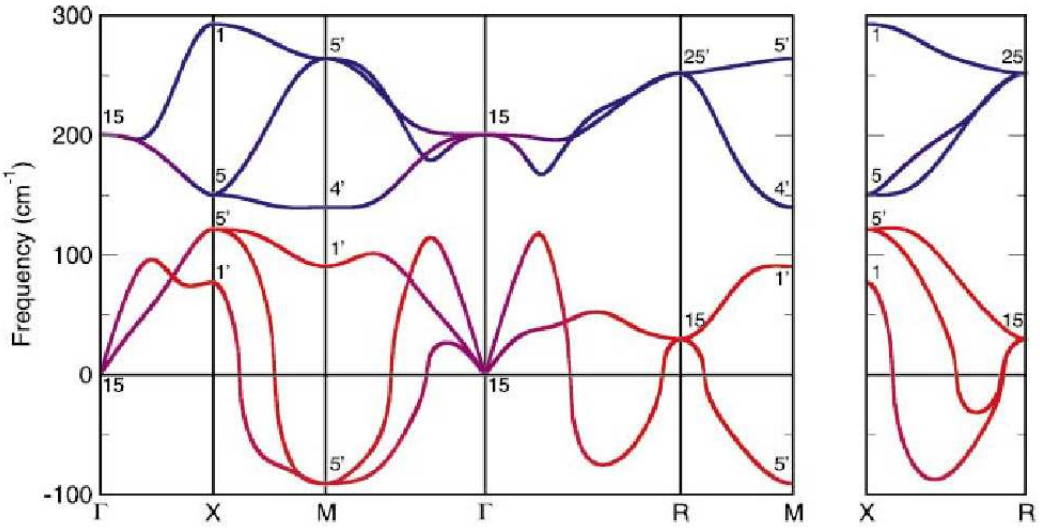

Figure 3.1: Phonon dispersion for NiTi in the B2 structure with $a_0 = 5.594$ Å along symmetry lines in the simple cubic Brillouin Zone. The imaginary frequencies of the unstable modes are plotted as negative values. (from *Huang et al.*, 2001).

The importance of entropic stabilization during MTs that occur in SMAs is schematically explained by *Elliott and Karls* (2010) using Fig. 3.2 where free energy ϕ is plotted with respect to variation of the phases δ when temperature T is varied. Here, M denotes the martensite phase, A denotes the austenite phase, T_A is the austenite start temperature, T_e is the equilibrium temperature, and T_M is the martensite start temperature. At $T = 0$ K, the austenite phase is a saddle point whereas the martensite phase is the global minimum of free energy. The austenite phase transitions from being a saddle point to a local minimum of the free energy when temperature is increased to T_A, indicating an entropic stabilization phenomenon. When the temperature is further increased to T_e, both austenite and martensite phases become global minima of the free energy. This indicates a transition from the martensite phase to the austenite phase when the temperature is increased further. Finally, the martensite phase transitions

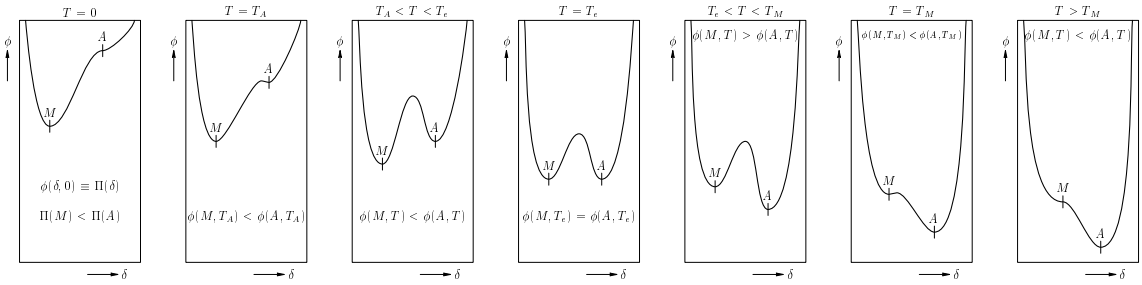

Figure 3.2: Schematic representation of entropic stabilization. Free energy ϕ is plotted with respect to variation of the phases δ when temperature T is varied.

from being a local minimum to a saddle point of the free energy when the temperature is increased such that $T > T_M$. It is critical for any atomistic model that tries to simulate the thermal behavior of martensitic phase transformations in SMAs to successfully capture the phenomena of entropic stabilization.

3.2 Density functional theory

Density functional theory (*Hohenberg*, 1964) based studies are valuable, in principle, to determine the properties of materials independent of any empirical fitting. Many of these methods depend on the quasiharmonic approximation for describing the effects of atomic vibrations on the material properties (*Wallace*, 2002). This approximation considers the atomic vibrations to be harmonic and the corresponding frequencies of atomic vibrations to be dependent on the configuration. However, the phonon spectra of Fig. 3.1 reveal that the harmonic frequencies are imaginary for some wave vectors, which shows that the B2 cubic austenite phase of NiTi is dynamically unstable. This implies that DFT based studies that depend on the quasiharmonic approximation will not be able to capture the entropic stabilization phenomena described in Section 3.1. The DFT MD (*Car and Parrinello*, 1985) method should be able to simulate the entropic stabilization of this phase, since MD explicitly models the temperature as atomic vibrations. However, DFT MD studies of the microstructural behavior of MTs in NiTi and other SMAs are prohibitive due to the computationally intensive nature of DFT MD calculations.

Recently *Souvatzis et al.* (2008); *Souvatzis and Rudin* (2008); *Souvatzis et al.* (2009,

2010) developed a self-consistent *ab initio* lattice dynamics (SCAILD) model based on first-principles theory that captures the entropic stabilization of unstable crystal structures. The SCAILD method combines concepts from the SCA method (*Hooton*, 1955a,b; *Huang and Born*, 1962; *Choquard*, 1967; *Wallace*, 1998) with *ab initio* calculations of accurate interatomic forces in a crystal supercell. In this method, entropic stabilization during solid-to-solid phase transition is simulated by treating the unstable phonon modes to be coupled to other stable phonon modes. This allows the phonon-phonon interactions which stabilize unstable phonon modes such that the effective potential experienced by these unstable phonon modes takes on a quadratic form to leading order. The additional physical content of this method which allows it to capture the entropic

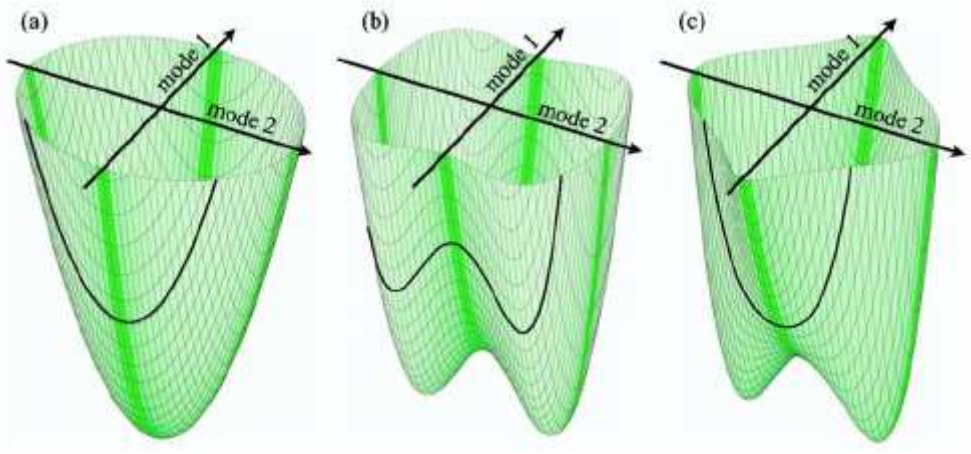

Figure 3.3: Schematic representation of potential energy of a system with two vibrational modes such that (a) both modes are independent and stable. (b) mode 2 is unstable and independent of mode 1. (c) mode 2 is not independent of mode 1. The solid black curve indicates the potential with respect to mode 2 at a high temperature. (from *Souvatzis and Rudin*, 2008).

stabilization phenomenon is beautifully explained using Fig. 3.3 in *Souvatzis and Rudin* (2008).[2]

[2] Reprinted Fig. 3.3 with permission from *Souvatzis and Rudin* (2008). Copyright (2008) by the American Physical Society.

Figure 3.3(a) illustrates the quasiharmonic approximation (*Wallace*, 2002) by considering a potential energy of a system with two vibrational modes in which both phonon-phonon interactions and dynamic instabilities are absent. Figure 3.3(b) schematically demonstrates the recent studies of *Smirnov* (1999); *Drummond and Ackland* (2002) who try to deal with dynamic instabilities while retaining the convenience of keeping the phonon modes independent of one another. Here two phonon modes are considered to be independent while mode 1 is stable and mode 2 is unstable. The unstable phonon mode (mode 2) potential energy is approximated as either a parabola combined with a Gaussian or as a quartic function which leads to an analytical solution for the independent anharmonic oscillator (mode 2). The resulting analytical solution makes the imaginary phonon frequency of mode 2 to be real above a critical temperature T_c. The main assumption behind these methods is that interactions between phonons remain weak at temperatures up to the critical temperature. This implies that unstable mode 2 is stabilized due to large fluctuations about the stabilized phase. However, the entropic stabilization that is responsible for the dynamic stabilization of B2 cubic austenite of NiTi is due to strong phonon-phonon interactions (*Huang et al.*, 2001; *Souvatzis et al.*, 2010) which lead to small fluctuations about the stabilized phase. Figure 3.3(c) demonstrates the physics behind the SCAILD method. Here, the two phonon modes are coupled. Mode 2 is unstable at low temperatures. However, it becomes stable at high temperatures due to the interactions between mode 1 and mode 2. The stabilization of mode 2 at high temperatures is denoted by the black curve in Fig. 3.3(c). Thus, SCAILD captures the entropic stabilization by modeling the phonon-phonon interactions.

The advantage of the SCAILD method is that it considers the effect of electrons due to the nature of DFT calculations involved. However, in practice, the SCAILD method (*Souvatzis et al.*, 2008, 2010) neglects thermal expansion effects by performing all calculations at a fixed experimental lattice constant value. Furthermore, the thermal excitations of the electronic subsystem are not considered in calculating the phonon frequencies. This is to be expected since it is impractical to consider the thermal expansion effects and the thermal excitations of the electronic subsystems in the SCAILD method due to the intensive computational cost involved in DFT calculations. This is a significant limitation of the SCAILD method and makes it unsuitable for use in the

computational design and discovery of SMAs with better properties.

3.3 Motivation for the classical SCA method

From Section 3.2, it is understood that first principles based methods such as DFT MD and SCAILD can model the phenomena of entropic stabilization that occur during MTs in SMAs. However, it is impractical to use these models for the design and discovery of SMAs with better properties due to their extreme computational cost.

One way to address this limitation is by modeling the potential energy with empirical interatomic potentials. This removes the expensive computational cost involved in modeling the potential energy from first-principle calculations. These empirical atomistic models consider the phonon-phonon interactions and neglect the electron-electron and electron-phonon interactions on the material properties. This implies that these models neglect the electronic effects such as the contribution of electronic excitations on the entropic stabilization of dynamically unstable phases. It is interesting to consider the possibility of modeling these electronic effects with temperature dependent interatomic potentials.

The studies of *Eriksson et al.* (1992); *Moroni et al.* (1996); *Nishitani et al.* (2001) indicated that the harmonic and quasiharmonic approximations give rise to the entropic stabilization of the bcc phase in transition metals such as Ti, indicating a transition from hcp to bcc phase as the temperature is increased. From these studies, it is calculated that the electronic entropy plays a dominating role when compared to thermal lattice vibrations. However, the studies of *May et al.* (1998); *Masuda-Jindo et al.* (2004) indicated that when anharmonic effects are considered instead of simple harmonic or quasiharmonic approximations the opposite is true. The thermal lattice vibrations play a dominating role in the entropic stabilization of the Ti bcc phase when compared to the contribution from electronic entropy. Based on these observations it is safe to assume that similar contributions of thermal lattice vibrations and electronic entropy exist for entropic stabilization during the MTs that occurs in SMAs. This indicates that an empirical atomistic model should be able to model the MTs that occur in SMAs.

The usefulness of atomistic models using empirical interaction potentials based on MD or MC simulations in the design and discovery of better SMAs is limited due

to the time consuming thermodynamic integration required in order to calculate the material's free energy. The present work aims to develop a lattice dynamics model with all the advantages of MD and MC techniques that can also be parametrically explored in a computationally efficient way using BFB methods (*Elliott*, 2007; *Jusuf*, 2010). The remainder of this work is organized as follows. Chapter 4 introduces the case of a one-dimensional multi-atom chain of vibrating atoms using the classical mechanics approach. Chapter 5 explains the self-consistent approach (SCA) based on statistical perturbation theory along with the equilibrium conditions and stability criteria to be used. Chapter 6 explains the critical aspects involved in the numerical implementation of the SCA model developed in Chapter 5 such that BFB methods can be exploited to investigate the model's behavior. Chapter 7 discusses the results of a particular bi-atomic chain model by mapping out all connected stress-free equilibrium paths and their stability as a function of temperature, and Chapter 8 summarizes the thermodynamic model developed in this work and discusses how this model can likely be extended for use as a computational technique to discover new SMAs.

Chapter 4

Lattice dynamics model

4.1 Introduction

A multi-atom chain is defined as a periodic one-dimensional chain of atoms where each atom is replaced by a cluster of atoms (see *Pitteri and Zanzotto*, 2002). Figure 4.1 shows the reference configuration of a 2-chain. Here clusters of two atoms separated by a distance of $P\,(= a/2)$ are associated with each lattice point of a *skeletal lattice* of spacing a. The *unit cell* can be considered as the periodic segment shown by the gray rectangle in Fig. 4.1. Each unit cell in the chain is labeled by an integer ℓ and each atom in a given unit cell is labeled by an integer α (with $\alpha \in \{0, 1\}$ for the case of the 2-chain of Fig. 4.1). Note that all atoms of fixed type α form as *sub chain* (1-chain) of the multi-atom chain.

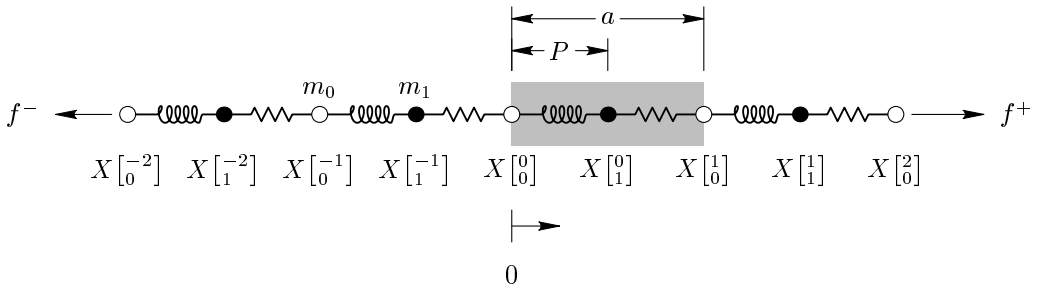

Figure 4.1: One-dimensional bi-atomic chain: 2-chain reference configuration.

The notation $X\left[\begin{smallmatrix}\ell\\ \alpha\end{smallmatrix}\right]$ is used for the referential coordinate of a unique atom within the chain. Thus, the reference position of atom α in unit cell ℓ is given by

$$X\begin{bmatrix}\ell\\ \alpha\end{bmatrix} = X[\ell] + P[\alpha],$$

$$\begin{aligned} X[\ell] &\equiv a\ell, \qquad -N \leq \ell \leq N, \\ P[\alpha] &\equiv \begin{cases} 0, & \alpha = 0, \\ a/2, & \alpha = 1, \end{cases} \end{aligned} \tag{4.1}$$

where $X[\ell]$ is the position locating unit cell ℓ and $P[\alpha]$ is the relative position locating atom α within this unit cell. The origin of the coordinate system is arbitrarily placed at the center atom of the chain $X\left[\begin{smallmatrix}0\\ 0\end{smallmatrix}\right] = 0$ and the total number of unit cells is $n \equiv 2N$ ($n = 4$ in Fig. 4.1). Here, an infinite bi-atomic chain ($N \to \infty$) is considered.

In this chapter a general multi-atom chain subjected to external loading as shown in Fig. 4.1 is investigated. The potential energy of the chain is derived in Section 4.2. Section 4.3 describes the translation invariance and periodicity relations. The Helmholtz free energy is calculated using the classical partition function in Section 4.5. Finally, Section 4.6 describes the limitations of the lattice dynamics model described in the preceding sections along with the limitations of conventional approximation methods such as the harmonic and quasiharmonic approximation for modeling the MTs that occur in SMAs.

4.2 Potential energy density

Atomic interactions are the key to understanding how a large number of atoms come together to form a multi-atom chain. In this work, these atomic interactions are modeled using pair potentials. The potential energy density due to atomic interactions is half the sum of all pair interaction energies between atoms in the chain, normalized by the reference length. Thus, the potential energy density due to atomic interactions is given

by

$$W(\mathbf{u}) = \frac{1}{2na} \sum_{\left[\begin{smallmatrix}\ell\\ \alpha\end{smallmatrix}\right]} \sum_{\left[\begin{smallmatrix}\ell'\\ \alpha'\end{smallmatrix}\right]} \phi^{\eta(\alpha)\eta(\alpha')} \left(r\left[\begin{smallmatrix}\ell\ \ell'\\ \alpha\alpha'\end{smallmatrix}\right] \right), \tag{4.2}$$

where n is the total number of unit cells in the chain, a is the reference unit cell length, and $\mathbf{u} \equiv \left(u\left[\begin{smallmatrix}\ell\\ \alpha\end{smallmatrix}\right] = x\left[\begin{smallmatrix}\ell\\ \alpha\end{smallmatrix}\right] - X\left[\begin{smallmatrix}\ell\\ \alpha\end{smallmatrix}\right] \right)$ is the set of displacements from the reference configuration $X\left[\begin{smallmatrix}\ell\\ \alpha\end{smallmatrix}\right]$ to the current configuration $x\left[\begin{smallmatrix}\ell\\ \alpha\end{smallmatrix}\right]$. $\phi^{\eta(\alpha)\eta(\alpha')}$ is the interatomic potential where $\eta(\alpha)$ represents the type of atom α and $r\left[\begin{smallmatrix}\ell\ \ell'\\ \alpha\alpha'\end{smallmatrix}\right] \equiv ||x\left[\begin{smallmatrix}\ell'\\ \alpha'\end{smallmatrix}\right] - x\left[\begin{smallmatrix}\ell\\ \alpha\end{smallmatrix}\right]||$ is the current distance between atom $\left[\begin{smallmatrix}\ell'\\ \alpha'\end{smallmatrix}\right]$ and $\left[\begin{smallmatrix}\ell\\ \alpha\end{smallmatrix}\right]$. For practical reasons, the sum of all pair interactions in Eq. (4.2) is limited to those interactions that are within a cutoff distance r_{cut}, such that $r\left[\begin{smallmatrix}\ell\ \ell'\\ \alpha\alpha'\end{smallmatrix}\right] \leq r_{\text{cut}}$. r_{cut} is chosen such that the summation in Eq. (4.2) always converges.

In order to get the total potential energy density of the chain, the potential energy density due to the external forces needs to be added. Hence, the total potential energy density $\mathcal{E}$ of a general multi-atom chain subjected to dead-loads as shown in Fig. 4.1 is given by

$$\mathcal{E}(\mathbf{u}) \equiv W(\mathbf{u}) - \frac{1}{na} \left(f^{+} u\left[\begin{smallmatrix}N\\ 0\end{smallmatrix}\right] - f^{-} u\left[\begin{smallmatrix}-N\\ 0\end{smallmatrix}\right] \right). \tag{4.3}$$

The derivatives of potential energy ($naW(\mathbf{u})$) due to atomic interactions at a given configuration $\overset{o}{\mathbf{u}}$ are often required. It is convenient, then, to introduce the following notation for derivatives of ($naW(\mathbf{u})$)

$$\overset{o}{\Phi}\left[\begin{smallmatrix}\ell\\ \alpha\end{smallmatrix}\right] \equiv \left(\frac{\partial (naW)}{\partial u\left[\begin{smallmatrix}\ell\\ \alpha\end{smallmatrix}\right]} \bigg|_{\overset{o}{\mathbf{u}}} \right), \quad \overset{o}{\Phi}\left[\begin{smallmatrix}\ell\ \ell'\\ \alpha\alpha'\end{smallmatrix}\right] \equiv \left(\frac{\partial^2 (naW)}{\partial u\left[\begin{smallmatrix}\ell\\ \alpha\end{smallmatrix}\right] \partial u\left[\begin{smallmatrix}\ell'\\ \alpha'\end{smallmatrix}\right]} \bigg|_{\overset{o}{\mathbf{u}}} \right), \quad \ldots, \tag{4.4}$$

where the superscript "o" indicates that the corresponding quantity is evaluated at a configuration $\overset{o}{\mathbf{u}}$. Note that $\overset{o}{\Phi}\left[\begin{smallmatrix}\ell\\ \alpha\end{smallmatrix}\right]$ represents the total sum of force on an atom $\left[\begin{smallmatrix}\ell\\ \alpha\end{smallmatrix}\right]$ at the configuration $\overset{o}{\mathbf{u}}$.

Using the definitions in Eq. (4.4), the potential energy is expanded in powers of the

perturbation $\delta u\left[\begin{smallmatrix}\ell\\ \alpha\end{smallmatrix}\right]$ about the configuration $\overset{o}{\mathbf{u}}$ as

$$\begin{aligned} na\mathcal{E}(\overset{o}{\mathbf{u}}+\delta\mathbf{u}) = na\mathcal{E}(\overset{o}{\mathbf{u}}) + \sum_{\left[\begin{smallmatrix}\ell\\ \alpha\end{smallmatrix}\right]} \overset{o}{\Phi}\left[\begin{smallmatrix}\ell\\ \alpha\end{smallmatrix}\right] \delta u\left[\begin{smallmatrix}\ell\\ \alpha\end{smallmatrix}\right] + \frac{1}{2!}\sum_{\left[\begin{smallmatrix}\ell\\ \alpha\end{smallmatrix}\right]}\sum_{\left[\begin{smallmatrix}\ell'\\ \alpha'\end{smallmatrix}\right]} \overset{o}{\Phi}\left[\begin{smallmatrix}\ell\,\ell'\\ \alpha\alpha'\end{smallmatrix}\right] \delta u\left[\begin{smallmatrix}\ell\\ \alpha\end{smallmatrix}\right] \delta u\left[\begin{smallmatrix}\ell'\\ \alpha'\end{smallmatrix}\right] + \dots \\ - \left(f^{+}\delta u\left[\begin{smallmatrix}N\\ 0\end{smallmatrix}\right] - f^{-}\delta u\left[\begin{smallmatrix}-N\\ 0\end{smallmatrix}\right]\right). \end{aligned} \tag{4.5}$$

4.3 Translational invariance and periodicity relations

The potential energy density due to atomic interactions $W(\mathbf{u})$ for the chain must be independent of rigid-body translation $d = u\left[\begin{smallmatrix}\ell\\ \alpha\end{smallmatrix}\right] - \overset{o}{u}\left[\begin{smallmatrix}\ell\\ \alpha\end{smallmatrix}\right]$ (constant). This imposes some restrictions on the form of $W(\mathbf{u})$. These restrictions result in useful relations that $\overset{o}{\Phi}\left[\begin{smallmatrix}\ell\\ \alpha\end{smallmatrix}\right]$, $\overset{o}{\Phi}\left[\begin{smallmatrix}\ell\,\ell'\\ \alpha\alpha'\end{smallmatrix}\right]$, …, must satisfy. The condition that the derivative of $W(\mathbf{u})$ with respect to d must be zero gives

$$\left.\frac{\partial W}{\partial d}\right|_{d=0} = \sum_{\left[\begin{smallmatrix}\ell\\ \alpha\end{smallmatrix}\right]} \frac{\partial \overset{o}{W}}{\partial u\left[\begin{smallmatrix}\ell\\ \alpha\end{smallmatrix}\right]} \frac{\partial u\left[\begin{smallmatrix}\ell\\ \alpha\end{smallmatrix}\right]}{\partial d} = \frac{1}{na}\sum_{\left[\begin{smallmatrix}\ell\\ \alpha\end{smallmatrix}\right]} \overset{o}{\Phi}\left[\begin{smallmatrix}\ell\\ \alpha\end{smallmatrix}\right] = 0. \tag{4.6}$$

Additionally, higher order derivatives of W must also be invariant with respect to rigid-body translations, giving in particular

$$\left.\frac{\partial^2 W}{\partial u\left[\begin{smallmatrix}\ell\\ \alpha\end{smallmatrix}\right]\partial d}\right|_{d=0} = \frac{1}{na}\sum_{\left[\begin{smallmatrix}\ell'\\ \alpha'\end{smallmatrix}\right]} \overset{o}{\Phi}\left[\begin{smallmatrix}\ell\,\ell'\\ \alpha\alpha'\end{smallmatrix}\right] = \frac{1}{na}\sum_{\left[\begin{smallmatrix}\ell\\ \alpha\end{smallmatrix}\right]} \overset{o}{\Phi}\left[\begin{smallmatrix}\ell\,\ell'\\ \alpha\alpha'\end{smallmatrix}\right] = 0, \tag{4.7}$$

and so on. Here, the symmetry of the coefficients $\overset{o}{\Phi}\left[\begin{smallmatrix}\ell\,\ell'\\ \alpha\alpha'\end{smallmatrix}\right]$ (due to their definition as second-order derivatives of the potential energy),

$$\overset{o}{\Phi}\left[\begin{smallmatrix}\ell\,\ell'\\ \alpha\alpha'\end{smallmatrix}\right] = \overset{o}{\Phi}\left[\begin{smallmatrix}\ell'\,\ell\\ \alpha'\alpha\end{smallmatrix}\right], \tag{4.8}$$

has been used in Eq. (4.7).

The Cauchy-Born (CB) stability criterion discussed later (Eq. (5.35)) relates to deformed configurations that retain the periodicity of the referential multi-atom chain.

The current positions of atoms are written using CB kinematics given by

$$x\begin{bmatrix}\ell\\ \alpha\end{bmatrix} = \mathrm{U}(X\begin{bmatrix}\ell\\ \alpha\end{bmatrix} + S[\alpha]), \tag{4.9}$$

where U is the deformation gradient and $S[\alpha]$ are the "*internal shifts*". For these configurations, with $\overset{o}{u}\begin{bmatrix}\ell\\ \alpha\end{bmatrix} = \overset{o}{\mathrm{U}}(X\begin{bmatrix}\ell\\ \alpha\end{bmatrix} + \overset{o}{S}[\alpha]) - X\begin{bmatrix}\ell\\ \alpha\end{bmatrix}$, the coefficients $\overset{o}{\Phi}\begin{bmatrix}\ell\\ \alpha\end{bmatrix}$, $\overset{o}{\Phi}\begin{bmatrix}\ell\ \ell'\\ \alpha\alpha'\end{bmatrix}$, ..., must also satisfy the periodicity conditions for the atoms away from the boundaries

$$\overset{o}{\Phi}\begin{bmatrix}\ell\\ \alpha\end{bmatrix} = \overset{o}{\Phi}\begin{bmatrix}\ell+l\\ \alpha\end{bmatrix}, \tag{4.10}$$

$$\overset{o}{\Phi}\begin{bmatrix}\ell\ \ell'\\ \alpha\alpha'\end{bmatrix} = \overset{o}{\Phi}\begin{bmatrix}\ell+l\ \ \ell'+l\\ \alpha\ \ \ \alpha'\end{bmatrix}, \tag{4.11}$$

and so on. Here $l \in \mathbb{Z}$ where $\mathbb{Z}$ is the set of all (positive and negative) integers. For a more complete discussion of these ideas and their generalization to three dimensional materials see *Elliott et al.* (2006a,b) and *Wallace* (1998).

4.4 Mechanical equilibrium and stability conditions

The configuration $\overset{o}{\mathbf{u}}$ is considered to be in equilibrium provided

$$\left.\frac{\partial \mathcal{E}}{\partial u\begin{bmatrix}\ell\\ \alpha\end{bmatrix}}\right|_{\overset{o}{\mathbf{u}}} = 0. \tag{4.12}$$

Using Eqs. (4.3) and (4.4), the equilibrium condition Eq. (4.12) for the multi-atom chain subjected to external loading as shown in Fig. 4.1 is given by

$$\overset{o}{\Phi}\begin{bmatrix}\ell\\ \alpha\end{bmatrix} = \begin{cases} 0, & -N < \ell < N, \alpha = 0; \\ 0, & -N \le \ell < N, \alpha = 1; \\ f^+, & \ell = N, \alpha = 0; \\ -f^-, & \ell = -N, \alpha = 0. \end{cases} \tag{4.13}$$

These relations correspond to the *mechanical* equilibrium of each atom which implies that the total force acting on each atom must vanish when all atoms are located at their equilibrium configuration $\overset{o}{\mathbf{u}}$. Application of the translational invariance relation

Eq. (4.6) results in an expression of macroscopic force balance for the chain given by

$$f^+ - f^- = 0. \tag{4.14}$$

The infinitesimal mechanical stability of the chain is evaluated by considering the dynamical behavior of the system about its equilibrium configuration. Using Eq. (4.13), the equation of motion of an atom $\begin{bmatrix}\ell\\ \alpha\end{bmatrix}$ is given by

$$\begin{aligned} m_\alpha \delta\ddot{u}\begin{bmatrix}\ell\\ \alpha\end{bmatrix} &= -\left.\frac{\partial(na\mathcal{E})}{\partial u\begin{bmatrix}\ell\\ \alpha\end{bmatrix}}\right|_{\overset{o}{\mathbf{u}}+\delta\mathbf{u}} \\ &= -\left[\sum_{\begin{bmatrix}\ell'\\ \alpha'\end{bmatrix}} \overset{o}{\Phi}\begin{bmatrix}\ell\ \ell'\\ \alpha\alpha'\end{bmatrix} \delta u\begin{bmatrix}\ell'\\ \alpha'\end{bmatrix} + \frac{1}{2!}\sum_{\begin{bmatrix}\ell'\\ \alpha'\end{bmatrix}}\sum_{\begin{bmatrix}\ell''\\ \alpha''\end{bmatrix}} \overset{o}{\Phi}\begin{bmatrix}\ell\ \ell'\ \ell''\\ \alpha\alpha'\alpha''\end{bmatrix} \delta u\begin{bmatrix}\ell'\\ \alpha'\end{bmatrix} \delta u\begin{bmatrix}\ell''\\ \alpha''\end{bmatrix} + \dots\right], \\ \delta u\begin{bmatrix}N\\ 0\end{bmatrix} &= \delta u\begin{bmatrix}-N\\ 0\end{bmatrix}, \end{aligned} \tag{4.15}$$

where $(\ddot{}) \equiv \partial^2(\ )/\partial t^2$ (t is time), and m_α is the mass of atom α.

The application of periodic boundary conditions as in Eq. (4.15) helps to eliminate boundary effects and restricts the set of allowed perturbations to those with wavelengths equal to or less than the length of the specimen (*Huang and Born*, 1962). It is important to note that the rigid-body translation mode for the chain is included in Eq. (4.15) and must be eliminated before any stability criterion is applied.

The chain is considered infinitesimally stable if there exists a $\delta(\epsilon) > 0$ such that for any small (infinitesimal) given $\epsilon > 0$ the solutions to the equations of motion (4.15) satisfy:

$$\|\delta\mathbf{u}(0)\|, \|\delta\dot{\mathbf{u}}(0)\| < \epsilon, \quad \Rightarrow \ \|\delta\mathbf{u}(t)\|, \|\delta\dot{\mathbf{u}}(t)\| < \delta(\epsilon) \quad \forall\ t, \tag{4.16}$$

where $\delta\mathbf{u}(0)$ and $\delta\dot{\mathbf{u}}(0)$ are the respective initial displacements and velocities at time $t = 0$, and $\|\cdot\|$ is any norm for $\delta\mathbf{u}$. See *Elliott* (2004) for more details.

4.5 Helmholtz free energy

For any non-zero temperature the atoms in the chain are not stationary. They are always in a state of motion such that their average positions are given by a configuration

$\overset{o}{\mathbf{u}}$. From this point onwards a configuration $\overset{o}{\mathbf{u}}$ represents the average positions of vibrating atoms in a chain. The amplitude of these vibrations about the average position (fluctuations) increases as temperature increases and approaches zero as temperature approaches 0 K. These atomic vibrations give rise to the concept of temperature and contribute to the thermal properties of all solids. Studying these atomic vibrations is of vital importance to understand the material's macroscopic thermo-mechanical properties.

The Helmholtz free energy $\mathcal{F}$ of a configuration $\overset{o}{\mathbf{u}}$ is an important macroscopic thermodynamic quantity that needs to be analyzed in order to study many material properties. According to the theory of statistical equilibrium thermodynamics (*Weiner*, 2002), any thermodynamic quantity can be calculated from the partition function Z which can be obtained from the hamiltonian $\mathcal{H}$ of the material.

The Hamiltonian of a chain of atoms vibrating about the configuration $\overset{o}{\mathbf{u}}$ is the sum of kinetic energy and internal potential energy given by

$$
\begin{aligned}
\mathcal{H} &= KE + naW(\overset{o}{\mathbf{u}} + \delta\mathbf{u}) = KE + \Phi_0 + \Phi_1 + \Phi_2 + \Phi_3 + \Phi_4 + \ldots, \\
KE &\equiv \frac{1}{2}\sum_{\left[\substack{\ell \\ \alpha}\right]} m_\alpha \left(\delta\dot{u}\left[\substack{\ell \\ \alpha}\right]\right)^2, \\
\Phi_0 &\equiv naW(\overset{o}{\mathbf{u}}), \\
\Phi_1 &\equiv \sum_{\left[\substack{\ell \\ \alpha}\right]} \overset{o}{\Phi}\left[\substack{\ell \\ \alpha}\right] \delta u\left[\substack{\ell \\ \alpha}\right], \\
\Phi_2 &\equiv \frac{1}{2!}\sum_{\left[\substack{\ell \\ \alpha}\right]}\sum_{\left[\substack{\ell' \\ \alpha'}\right]} \overset{o}{\Phi}\left[\substack{\ell\,\ell' \\ \alpha\alpha'}\right] \delta u\left[\substack{\ell \\ \alpha}\right] \delta u\left[\substack{\ell' \\ \alpha'}\right], \\
&\vdots
\end{aligned}
\tag{4.17}
$$

Here m_α is the mass of an atom $\left[\substack{\ell \\ \alpha}\right]$, $\delta\dot{u}\left[\substack{\ell \\ \alpha}\right]$ is the instantaneous velocity of atom $\left[\substack{\ell \\ \alpha}\right]$, n is the total number of unit cells that are considered in the chain, a is the reference unit cell length, $W(\overset{o}{\mathbf{u}})$ is the static potential energy density due to atomic interactions of the chain, and $\delta u\left[\substack{\ell \\ \alpha}\right]$ is the perturbation from configuration $\overset{o}{\mathbf{u}}$.

It is convenient to introduce normal mode coordinates (*Wallace*, 1998) for the velocity $\delta\dot{u}\left[\begin{smallmatrix}\ell\\ \alpha\end{smallmatrix}\right]$ and displacement $\delta u\left[\begin{smallmatrix}\ell\\ \alpha\end{smallmatrix}\right]$ such that

$$\begin{aligned}\delta u\left[\begin{smallmatrix}\ell\\ \alpha\end{smallmatrix}\right] &= (nm_\alpha)^{-1/2}\sum_{\left[\begin{smallmatrix}k\\ \nu\end{smallmatrix}\right]} q\left[\begin{smallmatrix}k\\ \nu\end{smallmatrix}\right] \mathrm{e}\left[\begin{smallmatrix}k\\ \nu\alpha\end{smallmatrix}\right] \exp\{ikX[\ell]\},\\ \delta\dot{u}\left[\begin{smallmatrix}\ell\\ \alpha\end{smallmatrix}\right] &= (nm_\alpha)^{-1/2}\sum_{\left[\begin{smallmatrix}k\\ \nu\end{smallmatrix}\right]} p^*\left[\begin{smallmatrix}k\\ \nu\end{smallmatrix}\right] \mathrm{e}\left[\begin{smallmatrix}k\\ \nu\alpha\end{smallmatrix}\right] \exp\{ikX[\ell]\},\end{aligned} \tag{4.18}$$

where $k \in \left[-\frac{\pi}{a}, \frac{\pi}{a}\right)$ is the wave number, ν labels the modes for each wave number, $q\left[\begin{smallmatrix}k\\ \nu\end{smallmatrix}\right]$ is a complex scalar amplitude and $p^*\left[\begin{smallmatrix}k\\ \nu\end{smallmatrix}\right]$ is a complex conjugate of momentum corresponding to vibrational mode $\left[\begin{smallmatrix}k\\ \nu\end{smallmatrix}\right]$. The net atomic displacement is always a real quantity which imposes the following constraint

$$q^*\left[\begin{smallmatrix}k\\ \nu\end{smallmatrix}\right] = q\left[\begin{smallmatrix}-k\\ \nu\end{smallmatrix}\right], \tag{4.19}$$

where $q^*\left[\begin{smallmatrix}k\\ \nu\end{smallmatrix}\right]$ is the complex conjugate of $q\left[\begin{smallmatrix}k\\ \nu\end{smallmatrix}\right]$. The complex quantity $\mathrm{e}\left[\begin{smallmatrix}k\\ \nu\alpha\end{smallmatrix}\right]$ is the α^{th} component of the normalized eigenvector $\mathbf{e}\left[\begin{smallmatrix}k\\ \nu\end{smallmatrix}\right]$ of the *dynamical matrix* (*Wallace*, 1998) defined by

$$\mathbb{K}\left[\begin{smallmatrix}k\\ \alpha\alpha'\end{smallmatrix}\right] = (m_\alpha m_{\alpha'})^{-1/2}\sum_{\ell'} \overset{o}{\Phi}\left[\begin{smallmatrix}0\,\ell'\\ \alpha\alpha'\end{smallmatrix}\right] \exp\left\{ikX[\ell']\right\}. \tag{4.20}$$

Thus, the diagonalization of the dynamical matrix Eq. (4.20) is given by

$$\sum_{\alpha,\alpha'} \mathrm{e}^*\left[\begin{smallmatrix}k\\ \nu\alpha\end{smallmatrix}\right] \mathbb{K}\left[\begin{smallmatrix}k\\ \alpha\alpha'\end{smallmatrix}\right] \mathrm{e}\left[\begin{smallmatrix}k\\ \nu'\alpha'\end{smallmatrix}\right] = \omega^2\left[\begin{smallmatrix}k\\ \nu\end{smallmatrix}\right]\delta_{\nu\nu'}, \tag{4.21}$$

where $\omega^2\left[\begin{smallmatrix}k\\ \nu\end{smallmatrix}\right]$ are the eigenvalues of dynamical matrix. The orthonormality and completeness of eigenvectors are respectively given by

$$\begin{aligned}\sum_{\alpha} \mathrm{e}^*\left[\begin{smallmatrix}k\\ \nu\alpha\end{smallmatrix}\right] \mathrm{e}\left[\begin{smallmatrix}k'\\ \nu'\alpha\end{smallmatrix}\right] &= \delta_{kk'}\delta_{\nu\nu'},\\ \sum_{\nu} \mathrm{e}^*\left[\begin{smallmatrix}k\\ \nu\alpha\end{smallmatrix}\right] \mathrm{e}\left[\begin{smallmatrix}k'\\ \nu\ \alpha'\end{smallmatrix}\right] &= \delta_{kk'}\delta_{\alpha\alpha'}.\end{aligned} \tag{4.22}$$

The total Hamiltonian Eq. (4.17) rewritten in terms of normal mode coordinates

Eq. (4.18) is given by

$$\mathcal{H} = \widetilde{KE} + \Phi_0 + \widetilde{\Phi}_1 + \widetilde{\Phi}_2 + \widetilde{\Phi}_3 + \widetilde{\Phi}_4 + \ldots, \tag{4.23}$$

where

$$\begin{aligned}
\widetilde{KE} &= \frac{1}{2}\sum_{\left[\substack{k\\ \nu}\right]} p^* \left[\substack{k\\ \nu}\right] p\left[\substack{k\\ \nu}\right], \\
\Phi_0 &= naW(\overset{o}{\mathbf{u}}), \\
\widetilde{\Phi}_1 &= \sum_{\left[\substack{k\\ \nu}\right]} V_1\left[\substack{k\\ \nu}\right] q\left[\substack{k\\ \nu}\right], \\
\widetilde{\Phi}_2 &= \frac{1}{2}\sum_{\left[\substack{k\\ \nu}\right]} \omega^2\left[\substack{k\\ \nu}\right] q^*\left[\substack{k\\ \nu}\right] q\left[\substack{k\\ \nu}\right], \\
\widetilde{\Phi}_3 &= \frac{1}{3!}\sum_{\left[\substack{k\\ \nu}\right]}\sum_{\left[\substack{k'\\ \nu'}\right]}\sum_{\left[\substack{k''\\ \nu''}\right]} V_3\left[\substack{kk'k''\\ \nu\nu'\nu''}\right] q\left[\substack{k\\ \nu}\right] q\left[\substack{k'\\ \nu'}\right] q\left[\substack{k''\\ \nu''}\right] \Delta(k+k'+k''), \\
\widetilde{\Phi}_4 &= \frac{1}{4!}\sum_{\left[\substack{k\\ \nu}\right]}\sum_{\left[\substack{k'\\ \nu'}\right]}\sum_{\left[\substack{k''\\ \nu''}\right]}\sum_{\left[\substack{k'''\\ \nu'''}\right]} V_4\left[\substack{kk'k''k'''\\ \nu\nu'\nu''\nu'''}\right] q\left[\substack{k\\ \nu}\right] q\left[\substack{k'\\ \nu'}\right] q\left[\substack{k''\\ \nu''}\right] q\left[\substack{k'''\\ \nu'''}\right] \Delta(k+k'+k''+k''').
\end{aligned} \tag{4.24}$$

Here V_1, V_3, and V_4 are the first, third, and fourth order terms respectively (*Wallace*, 1998) given by

$$V_1\left[\substack{k\\ \nu}\right] \equiv\ n^{-1/2}\sum_{\left[\substack{\ell\\ \alpha}\right]} (m_\alpha)^{-1/2}\, \overset{o}{\Phi}\left[\substack{\ell\\ \alpha}\right] \mathrm{e}\left[\substack{k\\ \nu\alpha}\right] \exp\{ikX[\ell]\}, \tag{4.25}$$

$$\begin{aligned}
V_3\left[\substack{kk'k''\\ \nu\nu'\nu''}\right] \equiv n^{-1/2}\sum_{\alpha}\sum_{\left[\substack{\ell'\\ \alpha'}\right]}\sum_{\left[\substack{\ell''\\ \alpha''}\right]} (m_\alpha m_{\alpha'} m_{\alpha''})^{-1/2}\, \overset{o}{\Phi}\left[\substack{0\,\ell'\,\ell''\\ \alpha\alpha'\alpha''}\right] \mathrm{e}\left[\substack{k\\ \nu\alpha}\right] \mathrm{e}\left[\substack{k'\\ \nu'\alpha'}\right] \mathrm{e}\left[\substack{k''\\ \nu''\alpha''}\right] \\
\times \exp\left\{i\left(k'X[\ell'] + k''X[\ell'']\right)\right\},
\end{aligned} \tag{4.26}$$

$$V_4\begin{bmatrix} k k' k'' k''' \\ \nu \nu' \nu'' \nu''' \end{bmatrix} \equiv n^{-1} \sum_{\alpha} \sum_{\begin{bmatrix} \ell' \\ \alpha' \end{bmatrix}} \sum_{\begin{bmatrix} \ell'' \\ \alpha'' \end{bmatrix}} \sum_{\begin{bmatrix} \ell''' \\ \alpha''' \end{bmatrix}} (m_\alpha m_{\alpha'} m_{\alpha''} m_{\alpha'''})^{-1/2} \overset{o}{\Phi}\begin{bmatrix} 0\, \ell' \ell'' \ell''' \\ \alpha \alpha' \alpha'' \alpha''' \end{bmatrix} \mathrm{e}\begin{bmatrix} k \\ \nu \alpha \end{bmatrix} \mathrm{e}\begin{bmatrix} k' \\ \nu' \alpha' \end{bmatrix} \times \mathrm{e}\begin{bmatrix} k'' \\ \nu'' \alpha'' \end{bmatrix} \mathrm{e}\begin{bmatrix} k''' \\ \nu''' \alpha''' \end{bmatrix} \exp\left\{ i \left(k' X[\ell'] + k'' X[\ell''] + k''' X[\ell'''] \right) \right\}, \tag{4.27}$$

and the function $\Delta(K)$ is defined such that $\Delta(K) = 1$ if K is a reciprocal lattice point and zero otherwise.

The classical partition function Z of a chain of vibrating atoms is given by

$$Z(\overset{o}{\mathbf{u}}; T) = \frac{1}{h^{\mathcal{N}}} \int \exp\left\{ -\frac{\mathcal{H}}{k_B T} \right\} d\mathbf{p}\; d\mathbf{q}, \tag{4.28}$$

where h is Planck's constant, $\mathcal{N}$ is the total number of atoms in the chain, $\mathbf{p} = \left\{ p\begin{bmatrix} k \\ \nu \end{bmatrix} \right\}$ and $\mathbf{q} = \left\{ q\begin{bmatrix} k \\ \nu \end{bmatrix} \right\}$ indicates the momenta and coordinates corresponding to all modes of vibrations, $\mathcal{H}$ is the hamiltonian of the chain corresponding to a configuration $\overset{o}{\mathbf{u}}$ given by Eq. (4.23), k_B is the Boltzmann constant, and T is the thermodynamic temperature.

Using the partition function Eq. (4.28), the Helmholtz free energy $\mathcal{F}$ of a chain of vibrating atoms corresponding to a configuration $\overset{o}{\mathbf{u}}$ is given by

$$\mathcal{F}(\overset{o}{\mathbf{u}}; T) = -k_B T\, \ln Z. \tag{4.29}$$

4.6 Limitations of conventional lattice dynamics models

The limitation in implementing the generalized lattice dynamics model described in Section 4.5 is due to the difficulty in analytical evaluation of the partition function. This is due to the highly nonlinear nature of the total Hamiltonian. Though the partition function can be calculated using numerical integration, this is computationally expensive and subdues the main advantage of using the lattice dynamics approach which is to have an analytical expression for the partition function. Hence, approximate methods needs to be implemented in order to evaluate the total partition function Eq. (4.28).

The harmonic approximation (see for example *Wallace*, 1998) is one such method in which the atomic vibrations are assumed to be very small when compared to the interatomic distance. This assumption simplifies the Hamiltonian significantly and results in a partition function for which the free energy can be calculated analytically. From

this analytical form of the free energy, all other thermo-mechanical properties of the material are obtained. However, the harmonic approximation considers the frequencies of atomic vibrations (phonon frequencies) to be constant for all temperatures and equal to the square roots of the eigenvalues of the dynamical matrix corresponding to the static equilibrium configuration $\overset{o}{\mathbf{u}}$. This results in a constant heat capacity (*Petit and Dulong*, 1819) and a coefficient of linear thermal expansion equal to zero for all temperatures. This is in contradiction with experimental observations. The detailed mathematical derivations of the linear thermal expansion and heat capacity at constant volume for the case of harmonic approximation are provided in Appendix B.

The quasi-harmonic approximation (QHA) (see for example *Seitz and Turnbull*, 1961) method is an improvement over the harmonic approximation method. In this method, the frequencies of atomic vibrations are calculated using the harmonic approximation but these frequencies are considered to be dependent on the configuration $\overset{o}{\mathbf{u}}$. The detailed mathematical derivation of the linear thermal expansion and heat capacity at constant volume are provided in Appendix C. Although the QHA method is able to capture realistic behavior for the coefficient of linear thermal expansion and heat capacity (at least at higher temperatures), it has limitations in predicting MTs that are exhibited by SMAs. Experimental evidence indicates that the phonon frequencies are intrinsically dependent on temperature (*Zheludev et al.*, 1995; *Mehaddene et al.*, 2008). Hence, any approximate method to model the MTs should be able to model the phonon frequencies such that they are not only functions of the configuration but also temperature.

Chapter 5

Self-consistent approach

5.1 Introduction

The SCA method (*Hooton*, 1955a,b; *Huang and Born*, 1962; *Choquard*, 1967; *Wallace*, 1998) is an approximate method of computing the free energy in which phonon frequencies are renormalized using self-consistent equations. The SCAILD method discussed in Section 3.2 is conceptually similar to the SCA method when potential energy is calculated from first principles. However, considering the potential energy from first principles in the SCA method is computationally prohibitive. In order to address this limitation the SCA method is considered by modeling the potential energy with empirical interatomic potentials. Due to the conceptual similarity between SCA method with empirical interatomic potentials and the SCAILD method, a schematic description of the SCA method is the same as the schematic description of SCAILD method given in Section 3.2 using Fig. 3.3(c).

Figure 3.3(c) considers two phonon modes that are not independent. At low temperatures, mode 1 is stable whereas mode 2 is unstable. However, the unstable mode 2 at low temperatures becomes stable at high temperatures due to the interaction with mode 1. The stabilization of mode 2 at high temperatures is denoted by the black curve in Fig. 3.3(c). The theoretical picture is that at low temperatures some of the renormalized phonon frequencies are imaginary indicating that the crystal structure is unstable at these temperatures. As the temperature increases, the contribution of anharmonic effects due to $\widetilde{\Phi}_3, \widetilde{\Phi}_4, \ldots$ terms of Eq. (4.23) to the magnitude of renormalized phonon

frequencies increases and finally at some high temperature all the renormalized phonon frequencies become real. This indicates that although the crystal structure is dynamically unstable according to the harmonic approximation it becomes dynamically stable at higher temperature due to the anharmonic effects that are considered in calculating the renormalized phonon frequencies. These renormalized phonon frequencies are not only dependent on the configuration but also temperature. This inherent dependence of the renormalized phonon frequencies on temperature enables the SCA method to model entropically stabilized MTs.

The derivation of the SCA method is presented by various authors using different mathematical techniques. This is due to the advantages of different techniques in deriving the SCA method with different order of approximation. The first-order SCA method was initially developed using the variational approach (*Hooton*, 1958; *Boccara and Sarma*, 1965; *Gillis et al.*, 1968). In this approach, the total Hamiltonian is approximated by a fictitious effective harmonic Hamiltonian such that the coefficients of the effective harmonic Hamiltonian are considered to be variational parameters and are determined by minimizing the free energy. Though this approach is elegant for the first-order SCA method, it is difficult to generalize this approach to higher order SCA methods. The diagrammatic perturbation theory applied by *Choquard* (1967) uses the well-known diagrammatic development (*Hove et al.*, 1961) in deriving SCA method. In this approach, a simple selection of graphs involving all orders of derivatives of the potential can be summed into closed form yielding equations equivalent to those of *Boccara and Sarma* (1965). This is a more fundamental approach and can be easily extended to higher order SCA methods.

Here, the first-order SCA method is formulated within classical mechanics (non quantum) for the case of a one-dimensional chain. This is based on the statistical perturbation method (*Wallace*, 1966) and first-order SCA method developed in *Wallace* (1998) which uses the operator-renormalization technique of quantum mechanical theory. The rest of this chapter is organized as follows. Section 5.2 discusses the formulation of the SCA method for a classical one-dimensional chain of atoms. The equilibrium and stability conditions of the chain are discussed in Section 5.3. Finally, the thermo-elastic properties of interest are defined in Section 5.4.

5.2 Self-consistent approach

The main idea of the SCA method involves approximating the potential energy with an effective harmonic potential energy such that the resultant effective harmonic Hamiltonian can be used to obtain the total partition function and free energy approximately.

The total Hamiltonian of the chain is given by

$$\mathcal{H}(\overset{o}{\mathbf{u}}) = KE + \Phi_0 + \Phi_1 + \Phi_2 + \Phi_3 + \Phi_4 + \dots, \tag{5.1}$$

where KE, Φ_0, Φ_1, Φ_2, ... are defined in Eq. (4.17). Introducing an effective harmonic potential Φ_{eff} defined by

$$\Phi_{\text{eff}}(\overset{o}{\mathbf{u}}) \equiv \frac{1}{2}\sum_{\left[\substack{\ell\\ \alpha}\right]}\sum_{\left[\substack{\ell'\\ \alpha'}\right]} \overset{o}{\Phi}_{\text{eff}}\begin{bmatrix}\ell\ \ell'\\ \alpha\alpha'\end{bmatrix} \delta u\begin{bmatrix}\ell\\ \alpha\end{bmatrix} \delta u\begin{bmatrix}\ell'\\ \alpha'\end{bmatrix}, \tag{5.2}$$

such that

$$\begin{aligned}\mathcal{H} &= \mathcal{H} + \Phi_{\text{eff}} - \Phi_{\text{eff}},\\ &= (KE + \Phi_0 + \Phi_{\text{eff}}) + (-\Phi_{\text{eff}} + \Phi_1 + \Phi_2 + \Phi_3 + \Phi_4 + \dots),\\ &= \mathcal{H}_{\text{eff}} + \mathcal{PT},\end{aligned} \tag{5.3}$$

where $\mathcal{H}_{\text{eff}}$ is the effective harmonic Hamiltonian such that $\mathcal{H}_{\text{eff}} = (\Phi_0 + KE + \Phi_{\text{eff}})$ and $\mathcal{PT}$ is the perturbation term such that $\mathcal{PT} = (-\Phi_{\text{eff}} + \Phi_1 + \Phi_2 + \dots)$. The effective harmonic potential Φ_{eff} is to be determined such that the perturbation term $\mathcal{PT}$ is small in the sense that it gives rise to small contributions to statistical averages such as the partition function of Eq. (4.28).

The normal mode coordinates corresponding to the effective harmonic potential Eq. (5.2) are given by

$$\begin{aligned}\delta u\begin{bmatrix}\ell\\ \alpha\end{bmatrix} &= (nm_\alpha)^{-1/2}\sum_{\left[\substack{k\\ \nu}\right]} q\begin{bmatrix}k\\ \nu\end{bmatrix} \mathrm{e}_{\text{eff}}\begin{bmatrix}k\\ \nu\alpha\end{bmatrix} \exp\{ikX[\ell]\},\\ \delta \dot{u}\begin{bmatrix}\ell\\ \alpha\end{bmatrix} &= (nm_\alpha)^{-1/2}\sum_{\left[\substack{k\\ \nu}\right]} p^*\begin{bmatrix}k\\ \nu\end{bmatrix} \mathrm{e}_{\text{eff}}\begin{bmatrix}k\\ \nu\alpha\end{bmatrix} \exp\{ikX[\ell]\},\end{aligned} \tag{5.4}$$

where $\mathrm{e}_{\text{eff}}\begin{bmatrix}k\\ \nu\alpha\end{bmatrix}$ is the α^{th} component of the normalized effective eigenvector $\mathbf{e}_{\text{eff}}\begin{bmatrix}k\\ \nu\end{bmatrix}$ of the

effective dynamical matrix given by

$$\mathbb{K}_{\text{eff}}\begin{bmatrix}k\\ \alpha\alpha'\end{bmatrix} = (m_\alpha m_{\alpha'})^{-1/2}\sum_{\ell'}\overset{o}{\Phi}_{\text{eff}}\begin{bmatrix}0\,\ell'\\ \alpha\alpha'\end{bmatrix}\exp\left\{ikX[\ell']\right\}. \tag{5.5}$$

The diagonalization of the effective dynamical matrix is given by

$$\sum_{\alpha,\alpha'}\mathrm{e}^*_{\text{eff}}\begin{bmatrix}k\\ \nu\alpha\end{bmatrix}\mathbb{K}_{\text{eff}}\begin{bmatrix}k\\ \alpha\alpha'\end{bmatrix}\mathrm{e}_{\text{eff}}\begin{bmatrix}k\\ \nu'\alpha'\end{bmatrix} = \omega^2_{\text{eff}}\begin{bmatrix}k\\ \nu\end{bmatrix}\delta_{\nu\nu'}, \tag{5.6}$$

where $\omega^2_{\text{eff}}\begin{bmatrix}k\\ \nu\end{bmatrix}$ are the eigenvalues of effective dynamical matrix Eq. (5.5).

At this point, the atoms are assumed to undergo small oscillations such that the anharmonic terms given by $\Phi_3, \Phi_4, \ldots$ in Eq. (4.17) are small in comparison to the harmonic term given by Φ_2 in Eq. (4.17) which implies that the character of phonons does not change significantly in the presence of anharmonic interactions. This implies that the value of an effective phonon frequency $\omega_{\text{eff}}\begin{bmatrix}k\\ \nu\end{bmatrix}$ changes with respect to harmonic phonon frequency $\omega\begin{bmatrix}k\\ \nu\end{bmatrix}$ due to anharmonic terms whereas the effective eigenvector $\mathbf{e}_{\text{eff}}\begin{bmatrix}k\\ \nu\end{bmatrix}$ remains approximately the same as the harmonic eigenvector $\mathbf{e}\begin{bmatrix}k\\ \nu\end{bmatrix}$. Thus, the normalization conditions corresponding to the harmonic potential Eq. (4.18) can be used instead of effective harmonic potential Eq. (5.4). The resultant diagonalization of the effective dynamical matrix corresponding to Eq. (5.6) is then given by

$$\sum_{\alpha,\alpha'}\mathrm{e}^*\begin{bmatrix}k\\ \nu\alpha\end{bmatrix}\mathbb{K}_{\text{eff}}\begin{bmatrix}k\\ \alpha\alpha'\end{bmatrix}\mathrm{e}\begin{bmatrix}k\\ \nu'\alpha'\end{bmatrix} \approx \omega^2_{\text{eff}}\begin{bmatrix}k\\ \nu\end{bmatrix}\delta_{\nu\nu'}. \tag{5.7}$$

The total Hamiltonian Eq. (5.3) rewritten in terms of normal mode coordinates of Eq. (4.18) is

$$\mathcal{H} = \mathcal{H}_{\text{eff}} + \widetilde{\mathcal{PT}}, \tag{5.8}$$

where $\mathcal{H}_{\text{eff}}$ is the effective harmonic Hamiltonian given by

$$\mathcal{H}_{\text{eff}} = \Phi_0 + \frac{1}{2}\sum_{\begin{bmatrix}k\\ \nu\end{bmatrix}} p^*\begin{bmatrix}k\\ \nu\end{bmatrix} p\begin{bmatrix}k\\ \nu\end{bmatrix} + \frac{1}{2}\sum_{\begin{bmatrix}k\\ \nu\end{bmatrix}}\omega^2_{\text{eff}}\begin{bmatrix}k\\ \nu\end{bmatrix} q^*\begin{bmatrix}k\\ \nu\end{bmatrix} q\begin{bmatrix}k\\ \nu\end{bmatrix}, \tag{5.9}$$

and $\widetilde{\mathcal{PT}}$ is the perturbation term rewritten in terms of normal mode coordinates such that $\widetilde{\mathcal{PT}} = \left(-\widetilde{\Phi}_{\text{eff}} + \widetilde{\Phi}_1 + \widetilde{\Phi}_2 + \ldots\right)$. Here, $\widetilde{\Phi}_1, \widetilde{\Phi}_2, \ldots$ are defined in Eq. (4.24) and

$\widetilde{\Phi}_{\text{eff}}$ is the normalized effective harmonic potential

$$\widetilde{\Phi}_{\text{eff}} = \frac{1}{2} \sum_{\left[\substack{k \\ \nu}\right]} \omega_{\text{eff}}^2 \left[\substack{k \\ \nu}\right] q^* \left[\substack{k \\ \nu}\right] q \left[\substack{k \\ \nu}\right]. \tag{5.10}$$

Using Eq. (5.8), the total partition function Z of a chain of vibrating atoms is rewritten as

$$\begin{aligned} Z(\overset{o}{\mathbf{u}}; T) &= \frac{1}{h^{\mathcal{N}}} \int \exp\left\{-\frac{\mathcal{H}}{k_B T}\right\} d\mathbf{p}\ d\mathbf{q}, \\ &= \frac{1}{h^{\mathcal{N}}} \int \exp\left\{-\frac{\left(\mathcal{H}_{\text{eff}} + \widetilde{\mathcal{PT}}\right)}{k_B T}\right\} d\mathbf{p}\ d\mathbf{q}, \\ &= \frac{1}{h^{\mathcal{N}}} \int \exp\left\{-\frac{\mathcal{H}_{\text{eff}}}{k_B T}\right\} \exp\left\{-\frac{\widetilde{\mathcal{PT}}}{k_B T}\right\} d\mathbf{p}\ d\mathbf{q}. \end{aligned} \tag{5.11}$$

Expanding the exponential term in $\widetilde{\mathcal{PT}}$ and rearranging results in

$$\begin{aligned} Z(\overset{o}{\mathbf{u}}; T) &= \frac{1}{h^{\mathcal{N}}} \int \exp\left\{-\frac{\mathcal{H}_{\text{eff}}}{k_B T}\right\} \exp\left\{-\frac{\widetilde{\mathcal{PT}}}{k_B T}\right\} d\mathbf{p}\ d\mathbf{q}, \\ &= \frac{1}{h^{\mathcal{N}}} \int \exp\left\{-\frac{\mathcal{H}_{\text{eff}}}{k_B T}\right\} \left(1 - \frac{\widetilde{\mathcal{PT}}}{k_B T} + \frac{1}{2!}\left(\frac{\widetilde{\mathcal{PT}}}{k_B T}\right)^2 - \dots\right) d\mathbf{p}\ d\mathbf{q}, \\ &= Z_{\text{eff}}(\overset{o}{\mathbf{u}}; T) - \frac{1}{h^{\mathcal{N}}} \int \exp\left\{-\frac{\mathcal{H}_{\text{eff}}}{k_B T}\right\} \left(\frac{\widetilde{\mathcal{PT}}}{k_B T}\right) d\mathbf{p}\ d\mathbf{q} + O\left(\widetilde{\mathcal{PT}}^2\right), \\ &= Z_{\text{eff}}(\overset{o}{\mathbf{u}}; T) + Z_1 + O\left(\widetilde{\mathcal{PT}}^2\right). \end{aligned} \tag{5.12}$$

Here, Z_{eff} is the effective harmonic partition function that can be evaluated analytically in terms of effective harmonic frequencies $\omega_{\text{eff}}\left[\substack{k \\ \nu}\right]$ and Z_1 is the first-order contribution of $\widetilde{\mathcal{PT}}$ to the total partition function Z. Conceptually the derivation of Z in terms of Z_{eff} and Z_1 as shown in Eqs. (5.11) and (5.12) is similar to the statistical perturbation method of *Wallace* (1966, 1998) which is a general method for approximating the statistical averages in a many-body problem.

The objective of the SCA method is to choose the effective harmonic potential Φ_{eff} such that the contribution of the perturbation term $\widetilde{\mathcal{PT}}$ in calculating the total

partition function Eq. (5.12) is minimized. In particular, this implies that the first-order contribution of $\widetilde{\mathcal{PT}}$ to the total partition function Z be zero

$$Z_1 = -\frac{1}{h^{\mathcal{N}}} \int \exp\left\{-\frac{\mathcal{H}_{\text{eff}}}{k_B T}\right\} \left(\frac{\widetilde{\mathcal{PT}}}{k_B T}\right) \, d\mathbf{p} \, d\mathbf{q} = 0. \tag{5.13}$$

The analytical evaluation of Eq. (5.13) involves extensive use of the following integral relations

$$\int_{-\infty}^{\infty} \exp\left\{-ax^2\right\} \, dx = \left(\frac{\pi}{a}\right)^{1/2}, \tag{5.14}$$

$$\int_{-\infty}^{\infty} \exp\left\{-ax^2\right\} x^2 \, dx = \frac{1}{2}\left(\frac{\pi}{a^3}\right)^{1/2}, \tag{5.15}$$

$$\int_{-\infty}^{\infty} \exp\left\{-ax^2\right\} x^4 \, dx = \frac{3}{4}\left(\frac{\pi}{a^5}\right)^{1/2}, \tag{5.16}$$

$$\int_{-\infty}^{\infty} \exp\left\{-ax^2\right\} x^{2s-1} \, dx = 0 \quad \text{for s} \in \mathbb{Z}. \tag{5.17}$$

The detailed mathematical derivation provided in Appendix D evaluates the analytical expression for Eq. (5.13) using Eqs. (5.14)–(5.17). This results in the set of self-consistent equations for determining the effective harmonic frequencies $\omega^2_{\text{eff}}\left[\begin{smallmatrix} k \\ \nu \end{smallmatrix}\right]$ given by

$$\omega^2_{\text{eff}}\begin{bmatrix} k \\ \nu \end{bmatrix} = \omega^2\begin{bmatrix} k \\ \nu \end{bmatrix} + \frac{k_B T}{2} \sum_{\begin{bmatrix} k' \\ \nu' \end{bmatrix}} V_4\begin{bmatrix} k & -k & k' & -k' \\ \nu & \nu & \nu' & \nu' \end{bmatrix} \frac{1}{\omega^2_{\text{eff}}\begin{bmatrix} k' \\ \nu' \end{bmatrix}} + \cdots. \tag{5.18}$$

Here, $\omega^2\left[\begin{smallmatrix} k \\ \nu \end{smallmatrix}\right]$ are the eigenvalues corresponding to the harmonic dynamical matrix Eq. (4.20) and V_4 is the fourth order term defined by Eq. (4.27). Though Eq. (5.18) provides a simple set of self-consistent equations, it is difficult to solve them in practice due to the infinite expansion on the right hand side of Eq. (5.18). However, the atoms are considered to undergo small oscillations such that the anharmonic terms given by $\Phi_3, \Phi_4, \ldots$ in Eq. (4.17) are small in comparison to the harmonic term given by Φ_2 in Eq. (4.17). This implies that the right hand side of the self-consistent Eq. (5.18) converges rapidly such that it can be truncated as follows

$$\omega^2_{\text{eff}}\begin{bmatrix} k \\ \nu \end{bmatrix} = \omega^2\begin{bmatrix} k \\ \nu \end{bmatrix} + \frac{k_B T}{2} \sum_{\begin{bmatrix} k' \\ \nu' \end{bmatrix}} V_4\begin{bmatrix} k & -k & k' & -k' \\ \nu & \nu & \nu' & \nu' \end{bmatrix} \frac{1}{\omega^2_{\text{eff}}\begin{bmatrix} k' \\ \nu' \end{bmatrix}}. \tag{5.19}$$

In this work, the Newton-Raphson algorithm (*Press et al.*, 1992) is used to solve Eq. (5.19). Due to the nonlinear nature of Eq. (5.19) there will generally be multiple solutions. The particular solution obtained will depend on the initial value given to the Newton-Raphson algorithm. Among these different solutions the one that minimizes the free energy of the material is chosen.

Thus, the total partition function Eq. (5.11) correct to first-order in the perturbation term $\widetilde{\mathcal{PT}}$ is given by

$$\begin{aligned} Z(\overset{o}{\mathbf{u}};T) &= Z_{\text{eff}}(\overset{o}{\mathbf{u}};T) + Z_1 + O\left(\widetilde{\mathcal{PT}}^2\right), \\ &= \frac{1}{h^{\mathcal{N}}} \int \exp\left\{-\frac{\mathcal{H}_{\text{eff}}}{k_B T}\right\} d\mathbf{p}\; d\mathbf{q} + Z_1 + O\left(\widetilde{\mathcal{PT}}^2\right), \\ &= \exp\left\{-\frac{\Phi_0(\overset{o}{\mathbf{u}})}{k_B T}\right\} \prod_{\left[\substack{k \\ \nu}\right]} \left[\frac{k_B T}{\hbar \omega_{\text{eff}}\left[\substack{k \\ \nu}\right]}\right] + Z_1 + O\left(\widetilde{\mathcal{PT}}^2\right), \end{aligned} \tag{5.20}$$

where $\hbar = \frac{h}{2\pi}$ is the reduced Planck constant, sometimes called the Dirac constant.

The Helmholtz free energy is given by

$$\begin{aligned} \mathcal{F}(\overset{o}{\mathbf{u}};T) &= -k_B T\, \ln Z, \\ &= -k_B T\, \ln\left[Z_{\text{eff}} + Z_1 + O\left(\widetilde{\mathcal{PT}}^2\right)\right], \\ &= -k_B T\, \ln\left[Z_{\text{eff}}\left(1 + \frac{Z_1}{Z_{\text{eff}}} + O\left(\widetilde{\mathcal{PT}}^2\right)\right)\right], \\ &= -k_B T\, \ln\left(Z_{\text{eff}}\right) - k_B T\, \ln\left[1 + \frac{Z_1}{Z_{\text{eff}}} + O\left(\widetilde{\mathcal{PT}}^2\right)\right]. \end{aligned} \tag{5.21}$$

Expanding the logarithm in Eq. (5.21) results in

$$\begin{aligned} \mathcal{F}(\overset{o}{\mathbf{u}};T) &= -k_B T\, \ln\left(Z_{\text{eff}}\right) - k_B T\left[\frac{Z_1}{Z_{\text{eff}}} + O\left(\widetilde{\mathcal{PT}}^2\right)\right], \\ &= \mathcal{F}_{\text{eff}}(\overset{o}{\mathbf{u}};T) - k_B T\left[\frac{Z_1}{Z_{\text{eff}}} + O\left(\widetilde{\mathcal{PT}}^2\right)\right]. \end{aligned} \tag{5.22}$$

Once the $\omega_{\text{eff}}\left[\substack{k \\ \nu}\right]$ are chosen to satisfy Eq. (5.19), Z_1 becomes zero and the free energy

of Eq. (5.22) becomes

$$\mathcal{F}(\overset{o}{\mathbf{u}};T) = \Phi_0(\overset{o}{\mathbf{u}}) - k_B T \sum_{\left[\substack{k\\ \nu}\right]} \ln\left[\frac{k_B T}{\hbar\omega_{\text{eff}}\left[\substack{k\\ \nu}\right]}\right] + O\left(\widetilde{\mathcal{P}\mathcal{T}}^2\right), \tag{5.23}$$

where $\omega_{\text{eff}}\left[\substack{k\\ \nu}\right]$ is an explicit function of $\overset{o}{\mathbf{u}}$ and T.

Here, the self-consistent Eq. (5.19) and the Helmholtz free energy Eq. (5.23) are obtained from the formulation of the SCA method within classical mechanics. At high temperatures, these results match with the corresponding results, Eqs. (E.124) and (E.126), from the formulation of the SCA method using quantum mechanics discussed in Appendix E.

The Helmholtz free energy Eq. (5.23) is derived within classical mechanics. This implies that at low temperatures the Helmholtz free energy given by Eq. (5.23) will not be able to capture the material properties. From our experience, the SCA model implemented with the Helmholtz free energy Eq. (5.23) and the self-consistent Eq. (5.19) results in negative entropy and abnormally high heat capacity at constant volume for low temperatures ($T < 30$ K). In order to address this limitation, the Helmholtz free energy Eq. (E.122) obtained from SCA method formulated using quantum mechanics

$$\mathcal{F}(\overset{o}{\mathbf{u}};T) = \Phi_0(\overset{o}{\mathbf{u}}) + \frac{1}{2}\sum_{\left[\substack{k\\ \nu}\right]} \hbar\omega_{\text{eff}}\left[\substack{k\\ \nu}\right] + k_B T \sum_{\left[\substack{k\\ \nu}\right]} \ln\left[1 - \exp\left\{-\frac{\hbar\omega_{\text{eff}}\left[\substack{k\\ \nu}\right]}{k_B T}\right\}\right], \tag{5.24}$$

is considered for the implementation of the SCA method. However, the self-consistent Eq. (5.19) is retained due to its simplicity in numerical implementation. It is to be noted that this modification does not change any material properties at high temperatures ($T > 30$ K) where most SMAs undergo MTs.

5.3 Equilibrium and stability

The free energy Eq. (5.24) is a function of configuration $\overset{o}{\mathbf{u}}$ and temperature T. The configuration $\overset{o}{\mathbf{u}}$ is considered to be in thermodynamic stress-free equilibrium at temperature T provided

$$\left.\frac{\partial \mathcal{F}}{\partial u\left[\substack{\ell\\ \alpha}\right]}\right|_{\overset{o}{\mathbf{u}}} = 0, \tag{5.25}$$

where each atomic degree of freedom (DOF) $\overset{o}{u}\left[\begin{smallmatrix}\ell\\ \alpha\end{smallmatrix}\right]$ is explicitly considered. Here, $u\left[\begin{smallmatrix}\ell\\ \alpha\end{smallmatrix}\right]$ in Eq. (5.25) is the average position of a vibrating atom $\left[\begin{smallmatrix}\ell\\ \alpha\end{smallmatrix}\right]$. Eq. (5.25) corresponds to the *microscopic* equilibrium which describes the thermodynamic equilibrium condition of each atom in the chain.

However, it is impractical to explicitly consider each atomic DOF $\overset{o}{u}\left[\begin{smallmatrix}\ell\\ \alpha\end{smallmatrix}\right]$ for studying any problem whose length-scale is much larger than the atomic length-scale. Thus, a reduced set of DOF's based on a continuum model is useful in these types of problems. Of course, such a model with reduced set of DOF's inherently contains less information than the corresponding model with full set of atomic DOF's.

The atomistic model is homogenized into a continuum model using CB kinematics. CB kinematics describe the crystal's deformation in terms of "internal atomic shifts" $S[\alpha]$ and uniform deformation characterized by a uniform deformation gradient U. Thus, the current position of an atom $\left[\begin{smallmatrix}\ell\\ \alpha\end{smallmatrix}\right]$ is given by

$$x\left[\begin{smallmatrix}\ell\\ \alpha\end{smallmatrix}\right] = \mathrm{U}\left(X\left[\begin{smallmatrix}\ell\\ \alpha\end{smallmatrix}\right] + S[\alpha]\right). \tag{5.26}$$

The rigid-body translation ($\mathrm{U} = 1, S[\alpha] = \text{constant}$) is eliminated by setting $S[0] = 0$. As a result of the CB kinematics assumption an M-chain transforms into another M-chain, i.e., the periodicity of the original chain is retained.

Substituting Eq. (5.26) into Eq. (5.24) results in the CB Helmholtz free energy $\tilde{\mathcal{F}}$ of a general M-chain as a function of uniform deformation gradient U and internal atomic shifts $\mathbf{S} = \{S[\alpha],\ \alpha = 1, 2, \ldots, M-1\}$ given by

$$\tilde{\mathcal{F}}(\mathrm{U}, \mathbf{S}; T) \equiv \mathcal{F}(\mathbf{u}(\mathrm{U}, \mathbf{S}); T), \tag{5.27}$$

where $\mathcal{F}(\mathbf{u}(\mathrm{U}, \mathbf{S}); T)$ is the free energy such that the atomic DOF's are restricted by CB kinematics. Corresponding to Eq. (5.24), the CB Helmholtz free energy $\tilde{\mathcal{F}}$ based on Eq. (5.27) is given by

$$\tilde{\mathcal{F}}(\mathrm{U}, \mathbf{S}; T) = \Phi_0(\mathrm{U}, \mathbf{S}) + \frac{1}{2}\sum_{\left[\begin{smallmatrix}k\\ \nu\end{smallmatrix}\right]} \hbar\omega_{\mathrm{eff}}\left[\begin{smallmatrix}k\\ \nu\end{smallmatrix}\right] + k_B T \sum_{\left[\begin{smallmatrix}k\\ \nu\end{smallmatrix}\right]} \ln\left[1 - \exp\left\{-\frac{\hbar\omega_{\mathrm{eff}}\left[\begin{smallmatrix}k\\ \nu\end{smallmatrix}\right]}{k_B T}\right\}\right], \tag{5.28}$$

where $\omega_{\mathrm{eff}}\left[\begin{smallmatrix}k\\ \nu\end{smallmatrix}\right] \equiv \omega_{\mathrm{eff}}\left[\begin{smallmatrix}k\\ \nu\end{smallmatrix}\right](\mathrm{U}, \mathbf{S}; T)$. In theory, the number of k points corresponding to

the summation in Eq. (5.28) is infinite but in practice it is taken to be a finite number n such that the corresponding results are converged with reasonable accuracy. In this work, 50 uniformly distributed k points are considered.

The equilibrium conditions corresponding to the CB free energy are given by

$$\left.\frac{\partial \tilde{\mathcal{F}}}{\partial \mathrm{U}}\right|_{(\overset{o}{\mathrm{U}},\overset{o}{\mathbf{S}})} = 0, \tag{5.29}$$

$$\left.\frac{\partial \tilde{\mathcal{F}}}{\partial S[\alpha]}\right|_{(\overset{o}{\mathrm{U}},\overset{o}{\mathbf{S}})} = 0, \quad \alpha = 1, 2, \ldots, M-1. \tag{5.30}$$

Here, Eq. (5.29) represents the *macroscopic* thermodynamic equilibrium which indicates that the average tension in the chain is equal to the applied load (zero in this case) and Eq. (5.30) expresses the sub-chain thermodynamic equilibrium condition that ensures that the corresponding sub-chain is in force equilibrium.

Together Eqs. (5.29) and (5.30) imply that the microscopic equilibrium Eq. (5.25) is satisfied. This can be seen by starting with Eq. (5.30) and using Eq. (5.26) such that

$$\left.\frac{\partial \tilde{\mathcal{F}}}{\partial S[\alpha]}\right|_{(\overset{o}{\mathrm{U}},\overset{o}{\mathbf{S}})} = \sum_{\left[\substack{\ell' \\ \alpha'}\right]} \left.\frac{\partial \mathcal{F}}{\partial u\left[\substack{\ell' \\ \alpha'}\right]}\right|_{\overset{o}{\mathbf{u}}} \frac{\partial u\left[\substack{\ell' \\ \alpha'}\right]}{\partial S[\alpha]} = \sum_{\ell} \left.\frac{\partial \mathcal{F}}{\partial u\left[\substack{\ell \\ \alpha}\right]}\right|_{\overset{o}{\mathbf{u}}} \overset{o}{\mathrm{U}} = 0, \quad \alpha = 1, 2, \ldots, M-1. \tag{5.31}$$

Using a periodicity relation, similar to Eq. (4.10), Eq. (5.31) gives

$$\left.\frac{\partial \mathcal{F}}{\partial u\left[\substack{\ell \\ \alpha}\right]}\right|_{\overset{o}{\mathbf{u}}} = 0, \quad \alpha \neq 0. \tag{5.32}$$

This implies that each atom of type $\alpha \neq 0$ is in microscopic thermodynamic equilibrium. Similarly, starting with Eq. (5.29) and using Eq. (5.26) such that

$$\left.\frac{\partial \tilde{\mathcal{F}}}{\partial \mathrm{U}}\right|_{(\overset{o}{\mathrm{U}},\overset{o}{\mathbf{S}})} = \sum_{\left[\substack{\ell' \\ \alpha'}\right]} \left.\frac{\partial \mathcal{F}}{\partial u\left[\substack{\ell' \\ \alpha'}\right]}\right|_{\overset{o}{\mathbf{u}}} \frac{\partial u\left[\substack{\ell' \\ \alpha'}\right]}{\partial \mathrm{U}} = \sum_{\ell} \left.\frac{\partial \mathcal{F}}{\partial u\left[\substack{\ell \\ \alpha}\right]}\right|_{\overset{o}{\mathbf{u}}} X\left[\substack{\ell \\ \alpha}\right] = 0. \tag{5.33}$$

Using a periodicity relation, similar to Eqs. (4.10) and (5.32), Eq. (5.31) gives

$$\left.\frac{\partial \mathcal{F}}{\partial u\left[\begin{smallmatrix}\ell\\ \alpha\end{smallmatrix}\right]}\right|_{\overset{o}{\mathbf{u}}} = 0, \quad \alpha = 0. \tag{5.34}$$

This implies that each atom of type $\alpha = 0$ is in microscopic thermodynamic equilibrium. Thus, Eqs. (5.32) and (5.34) indicate that macroscopic equilibrium conditions of CB free energy given by Eqs. (5.29) and (5.30) imply that the microscopic equilibrium condition of free energy Eq. (5.25) is also satisfied.

An equilibrium configuration, i.e., a solution to Eqs. (5.29) and (5.30), is considered to be stable if it satisfies both the "macroscopic" stability (CB stability) criterion and the "microscopic" stability criterion (*Elliott et al.*, 2006a,b) applied to the free energy.

The CB stability criterion defines the stability of the chain by considering the "quasi-uniform" perturbations that conform to the CB kinematics of Eq. (5.26). An equilibrium configuration is considered CB stable if it is a local minimum of the free energy Eq. (5.27), i.e., the CB stability criterion requires that $\tilde{\mathcal{F}}(\overset{o}{\mathrm{U}}, \overset{o}{\mathbf{S}}) < \tilde{\mathcal{F}}(\mathrm{U}, \mathbf{S})$ for all $(\mathrm{U}, \mathbf{S})$ in the neighborhood of $(\overset{o}{\mathrm{U}}, \overset{o}{\mathbf{S}})$ or equivalently that

$$[\delta \mathrm{U} \quad \delta S[\alpha]] \begin{bmatrix} \frac{\partial^2 \tilde{\mathcal{F}}}{\partial \mathrm{U} \partial U} & \frac{\partial^2 \tilde{\mathcal{F}}}{\partial \mathrm{U} \partial S[\alpha']} \\ \frac{\partial^2 \tilde{\mathcal{F}}}{\partial S[\alpha] \partial \mathrm{U}} & \frac{\partial^2 \tilde{\mathcal{F}}}{\partial S[\alpha] \partial S[\alpha']} \end{bmatrix} \begin{bmatrix} \delta \mathrm{U} \\ \delta S[\alpha'] \end{bmatrix} > 0 \tag{5.35}$$

is satisfied at equilibrium for all non-zero $(\delta \mathrm{U}; \delta S[\alpha])$ with $\alpha = 1, 2, ..., M-1$. Here, both uniform deformation $\delta \mathrm{U}$ and internal atomic shift $\delta S[\alpha]$ perturbations are allowed to vary independently.

The chain is considered to be microscopically stable at an equilibrium configuration $\overset{o}{\mathbf{u}} \equiv \left(\overset{o}{u}\left[\begin{smallmatrix}\ell\\ \alpha\end{smallmatrix}\right] = \overset{o}{\mathrm{U}} \left(X\left[\begin{smallmatrix}\ell\\ \alpha\end{smallmatrix}\right] + \overset{o}{S}[\alpha] \right) - X\left[\begin{smallmatrix}\ell\\ \alpha\end{smallmatrix}\right] \right)$ if $\overset{o}{\mathbf{u}}$ corresponds to a local minimum of the free energy Eq. (5.24), that is, $\mathcal{F}(\overset{o}{\mathbf{u}}) < \mathcal{F}(\mathbf{u})$ for all $\mathbf{u}$ in the neighborhood of $\overset{o}{\mathbf{u}}$. This criterion can be verified by increasing the size of the CB unit cell. However, this requires a large computational time. Thus, for this work an alternative stability criterion is considered which requires, as a necessary condition for microscopic stability, that all the $\omega^2_{\mathrm{eff}}\left[\begin{smallmatrix}k\\ \nu\end{smallmatrix}\right]$ be positive. That is, it is necessary that the eigenvalues of the effective

dynamical matrix Eq. (5.5) satisfy

$$\omega_{\text{eff}}^2 \begin{bmatrix} k \\ \nu \end{bmatrix} > 0, \text{ for all } \begin{bmatrix} k \\ \nu \end{bmatrix} \neq \begin{bmatrix} 0 \\ 0 \end{bmatrix}, \tag{5.36}$$

where $\begin{bmatrix} k \\ \nu \end{bmatrix} = \begin{bmatrix} 0 \\ 0 \end{bmatrix}$ has been excluded in order to eliminate consideration of the rigid-body translation mode of the chain. Thus, both criteria Eqs. (5.35) and (5.36) must be satisfied for an equilibrium state of a chain to be considered stable.

5.4 Thermo-elastic properties

Based on Section 2.2, the thermo-elastic properties of interest are defined in this section.

Most available experimental data of macroscopic thermo-elastic properties corresponds to a state of the material in which the shifts are in equilibrium. This is due to the "microscopic" nature of CB shifts $S[\alpha]$ which are difficult to control. Thus, the form of the material's free energy density that is most appropriate for comparison to macroscopic thermo-elastic experimental data is the "Homogenized Continuum (HC) free energy density" (*Elliott et al.*, 2006a). This is obtained by using Eq. (5.30) to implicitly define the shifts $S[\alpha]$ as functions of the deformation gradient U and temperature T, i.e., $S[\alpha] \equiv S[\alpha](\mathrm{U}; T)$. The HC free energy density is then defined by

$$\overset{\approx}{\mathcal{F}}(\mathrm{U}; T) \equiv \frac{1}{na} \tilde{\mathcal{F}}(\mathrm{U}, \mathbf{S}(\mathrm{U}; T); T). \tag{5.37}$$

This does not imply that the shifts are unimportant. In fact, instabilities associated with the shifts are usually responsible for the existence of phase transformations and, indeed, are required to capture the critical deformation modes at the onset of instability (*Guthikonda and Elliott*, 2008a).

It should be noted that the HC free energy density as defined in Eq. (5.37) may not be single valued. That is, for any given deformation gradient U there may be multiple solutions to Eq. (5.30). These will lead to a multi-valued HC free energy density. Which of these multiple values $\overset{\approx}{\mathcal{F}}(\mathrm{U}; T)$ takes on at any given time will then depend on the deformation history.

The thermal and elastic properties of a stress-free chain are derived from the HC

free energy density Eq. (5.37). The entropy per mole S is given by

$$S = -\frac{\partial \overset{\approx}{\mathcal{F}}}{\partial T}\bigg|_{(\overset{o}{\mathrm{U}};T)} \frac{aN_A}{M}, \tag{5.38}$$

where $\overset{o}{\mathrm{U}}$ is the CB deformation corresponding to the stress-free configuration at temperature T, M is the number of atoms in the unit cell, and N_A is the Avogadro's constant (6.023×10^{23}).

The cohesive energy E_c is the energy (per atom) released by the formation of the chain from a set of dissociated atoms that are initially infinitely far apart. In other words it is the enthalpy of formation ΔH which is related to the change in free energy $\Delta \overset{\approx}{\mathcal{F}}$ and change in entropy ΔS given by $\Delta H = \Delta \overset{\approx}{\mathcal{F}} + T\Delta S$. Taking the energy of infinitely far apart atoms as the energy datum, the cohesive energy is given by

$$E_\mathrm{c} = -\left(\overset{\approx}{\mathcal{F}}(\overset{o}{\mathrm{U}};T) - T\frac{\partial \overset{\approx}{\mathcal{F}}}{\partial T}\bigg|_{(\overset{o}{\mathrm{U}};T)} \right) \frac{a}{M}. \tag{5.39}$$

Here, the minus sign is required to obtain the energy *released* during the chain's formation.

The instantaneous linear thermal expansion α at zero load is obtained by taking a total temperature derivative of the stress-free equilibrium equation $\frac{\partial \overset{\approx}{\mathcal{F}}}{\partial \mathrm{U}} = 0$, solving for $\frac{d\overset{o}{\mathrm{U}}}{dT}\Big|_T$, and defining the instantaneous linear thermal expansion as $\alpha \equiv \overset{o}{\mathrm{U}}^{-1} \frac{d\overset{o}{\mathrm{U}}}{dT}\Big|_T$ results in

$$\alpha = -\overset{o}{\mathrm{U}}^{-1} \left[\left(\frac{\partial^2 \overset{\approx}{\mathcal{F}}}{\partial \mathrm{U}^2} \right)^{-1} \left(\frac{\partial^2 \overset{\approx}{\mathcal{F}}}{\partial \mathrm{U} \partial T} \right) \right]_{(\overset{o}{\mathrm{U}},T)}. \tag{5.40}$$

The heat capacity per mole at constant volume C_v is defined as

$$C_\mathrm{v} = -\left(T\frac{\partial^2 \overset{\approx}{\mathcal{F}}}{\partial T^2} \right)_{(\overset{o}{\mathrm{U}};T)} \frac{aN_A}{M}. \tag{5.41}$$

The definition of heat capacity per mole at constant pressure is $C_\mathrm{p} = T\left(\frac{\partial S}{\partial T}\right)_\mathrm{p}$. An expression for C_p may be obtained by taking the total temperature derivative of

Eq. (5.38), multiplying by T, solving Eq. (5.40) for $\frac{\partial^2 \overset{\approx}{\mathcal{F}}}{\partial \mathrm{U} \partial T}$ and substituting the resulting expression. The result is

$$C_{\mathrm{p}} = -T \left[\frac{\partial^2 \overset{\approx}{\mathcal{F}}}{\partial T^2} + \frac{\partial \mathrm{U}}{\partial T} \frac{\partial^2 \overset{\approx}{\mathcal{F}}}{\partial \mathrm{U}^2} \frac{\partial \mathrm{U}}{\partial T} \right]_{\overset{o}{(\mathrm{U};T)}} \frac{aN_A}{M}. \tag{5.42}$$

The instantaneous bulk modulus K for the chain relates a change in length to an increment in an applied load. The instantaneous bulk modulus is given by,

$$K = \left. \frac{\partial^2 \overset{\approx}{\mathcal{F}}}{\partial^2 \mathrm{U}} \right|_{\overset{o}{(\mathrm{U};T)}}. \tag{5.43}$$

Chapter 6

Numerical implementation

6.1 Introduction

Although the theoretical formulation of the SCA method is well established (*Hooton*, 1955a; *Huang and Born*, 1962; *Choquard*, 1967; *Gillis et al.*, 1968; *Shukla and Cowley*, 2000; *Wallace*, 1998), the method has always, to this author's knowledge, been implemented with additional simplifying assumptions. For example, the SCAILD method (*Souvatzis et al.*, 2008; *Souvatzis and Rudin*, 2008; *Souvatzis et al.*, 2009, 2010) described in Section 3.2 neglects thermal expansion effects by fixing the lattice parameters. *Gillis et al.* (1968) applied the SCA method to study the properties of neon and argon at low temperatures only. However, it is not clear or if how the derivatives of free energy and corresponding derivatives of harmonic eigenvalues and eigenvectors were calculated by *Gillis et al.* (1968).

The difficulty in fully implementing the SCA method to model the MTs that occur in SMAs is not due to any constraints imposed by available computing capacity but to the considerable number of meticulous analytical derivations involved in the numerical implementation of the method. To this author's knowledge, the SCA method is implemented completely for the first time in this work. The complete implementation is necessary for the model to be fully integrated into the BFB methods of *Elliott* (2007); *Jusuf* (2010). This integration of the SCA method into a BFB framework allows the model to be useful in parametrically exploring the configuration space of the

material in a computationally efficient way. This involves careful evaluation of the analytical expressions for derivatives of the CB free energy $\tilde{\mathcal{F}}$, effective harmonic frequencies $\omega^2_{\text{eff}}\left[{}^{k}_{\nu}\right]$, harmonic eigenvalues $\omega^2\left[{}^{k}_{\nu}\right]$ and eigenvectors $\mathbf{e}\left[{}^{k}_{\nu}\right]$, and the interatomic potential $\phi^{\eta(\alpha)\eta(\alpha')}(r)$ of Eq. (4.2) all with respect to $\mathbf{v} \equiv (\mathrm{U}, S[1], S[2], \ldots, S[M-1])$ (where $\mathbf{v}$ is a vector containing the macroscopic DOFs) and temperature T such that the equilibrium conditions of Eqs. (5.29) and (5.30), stability conditions of Eqs. (5.35) and (5.36), and all the thermo-elastic properties defined in Section 5.4 can be evaluated. The derived analytical expressions are then implemented into the BFBSymPac (*Elliott*, 2010) software package.

The rest of this chapter is organized as follows. The analytical expressions for the derivatives of the CB free energy $\tilde{\mathcal{F}}$ are given in Section 6.2. Section 6.3 discusses the analytical expressions and the numerical evaluation of the derivatives of effective harmonic frequencies $\omega^2_{\text{eff}}\left[{}^{k}_{\nu}\right]$. Section 6.4 discusses the derivatives of the harmonic eigenvalues $\omega^2\left[{}^{k}_{\nu}\right]$ and eigenvectors $\mathbf{e}\left[{}^{k}_{\nu}\right]$ that are evaluated based on Nelson's algorithm (*Nelson*, 1976) explained in Appendix F. Derivatives of the interatomic potential $\phi^{\eta(\alpha)\eta(\alpha')}(r)$ of Eq. 4.2 are described in Section 6.5. Finally, Section 6.6 discusses the verifications used to check the SCA model as implemented in the BFBSymPac (*Elliott*, 2010) software package.

6.2 Derivatives of free energy

The SCA method formulated in Chapter 5 requires the knowledge of various derivatives of the CB free energy $\tilde{\mathcal{F}}$. For example, the first- and second-order derivatives of $\tilde{\mathcal{F}}$ with respect to $\mathbf{v}$ are required to evaluate the equilibrium and stability conditions discussed in Section 5.3. In addition, the first- and second-order derivatives of $\tilde{\mathcal{F}}(\mathbf{v}; T)$ with respect to T and the second-order derivatives of $\tilde{\mathcal{F}}$ with respect to $\mathbf{v}$ and T are required to evaluate the thermo-elastic properties of interest discussed in Section 5.4. In this section, the analytical expressions of the required derivatives of the CB free energy $\tilde{\mathcal{F}}$ are provided.

The first-order derivatives of the CB free energy $\tilde{\mathcal{F}}$ with respect to the macroscopic DOFs $\mathbf{v} \equiv (\mathrm{U}, S[1], S[2], \ldots, S[M-1])$ are required to solve the equilibrium conditions of Eqs. (5.29) and (5.30). Differentiating Eq. (5.28) with respect to v_i (i^{th} element of

$\mathbf{v}$) results in

$$\frac{\partial\tilde{\mathcal{F}}(\mathbf{v};T)}{\partial \mathrm{v}_i} = \frac{\partial\Phi_0(\mathbf{v})}{\partial \mathrm{v}_i} + \hbar\sum_{\begin{bmatrix}k\\ \nu\end{bmatrix}} \frac{\partial\omega_{\mathrm{eff}}\begin{bmatrix}k\\ \nu\end{bmatrix}}{\partial \mathrm{v}_i}\left[\frac{1}{2} + \left(\exp\left\{\frac{\hbar\omega_{\mathrm{eff}}\begin{bmatrix}k\\ \nu\end{bmatrix}}{k_BT}\right\} - 1\right)^{-1}\right]. \tag{6.1}$$

The second-order derivatives of the CB free energy $\tilde{\mathcal{F}}$ with respect to $\mathbf{v}$ are required to evaluate the CB stability criterion Eq. (5.35). These second-order derivatives can be obtained by differentiating Eq. (6.1) with respect to v_j resulting in

$$\begin{aligned}\frac{\partial^2\tilde{\mathcal{F}}(\mathbf{v};T)}{\partial \mathrm{v}_i\partial \mathrm{v}_j} = \frac{\partial^2\Phi_0(\mathbf{v})}{\partial \mathrm{v}_i\partial \mathrm{v}_j} + \hbar\sum_{\begin{bmatrix}k\\ \nu\end{bmatrix}} \frac{\partial^2\omega_{\mathrm{eff}}\begin{bmatrix}k\\ \nu\end{bmatrix}}{\partial \mathrm{v}_i\partial \mathrm{v}_j}\left[\frac{1}{2} + \left(\exp\left\{\frac{\hbar\omega_{\mathrm{eff}}\begin{bmatrix}k\\ \nu\end{bmatrix}}{k_BT}\right\} - 1\right)^{-1}\right] \\ - \frac{\hbar^2}{k_BT}\sum_{\begin{bmatrix}k\\ \nu\end{bmatrix}} \frac{\partial\omega_{\mathrm{eff}}\begin{bmatrix}k\\ \nu\end{bmatrix}}{\partial \mathrm{v}_i}\frac{\partial\omega_{\mathrm{eff}}\begin{bmatrix}k\\ \nu\end{bmatrix}}{\partial \mathrm{v}_j}\exp\left\{\frac{\hbar\omega_{\mathrm{eff}}\begin{bmatrix}k\\ \nu\end{bmatrix}}{k_BT}\right\}\left(\exp\left\{\frac{\hbar\omega_{\mathrm{eff}}\begin{bmatrix}k\\ \nu\end{bmatrix}}{k_BT}\right\} - 1\right)^{-2}.\end{aligned} \tag{6.2}$$

The first-order derivative of the CB free energy $\tilde{\mathcal{F}}$ with respect to temperature T is required to evaluate the entropy S of Eq. (5.38). This is obtained by differentiating Eq. (5.28) with respect to temperature T resulting in

$$\begin{aligned}\frac{\partial\tilde{\mathcal{F}}(\mathbf{v};T)}{\partial T} = \frac{\hbar}{2}\sum_{\begin{bmatrix}k\\ \nu\end{bmatrix}} \frac{\partial\omega_{\mathrm{eff}}\begin{bmatrix}k\\ \nu\end{bmatrix}}{\partial T} + k_B\sum_{\begin{bmatrix}k\\ \nu\end{bmatrix}} \ln\left[1 - \exp\left\{-\frac{\hbar\omega_{\mathrm{eff}}\begin{bmatrix}k\\ \nu\end{bmatrix}}{k_BT}\right\}\right] \\ + \hbar\sum_{\begin{bmatrix}k\\ \nu\end{bmatrix}}\left(\frac{\partial\omega_{\mathrm{eff}}\begin{bmatrix}k\\ \nu\end{bmatrix}}{\partial T} - \frac{\omega_{\mathrm{eff}}\begin{bmatrix}k\\ \nu\end{bmatrix}}{T}\right)\left(\exp\left\{\frac{\hbar\omega_{\mathrm{eff}}\begin{bmatrix}k\\ \nu\end{bmatrix}}{k_BT}\right\} - 1\right)^{-1}.\end{aligned} \tag{6.3}$$

The second-order derivative of the CB free energy $\tilde{\mathcal{F}}$ with respect to temperature T is required to evaluate the heat capacity at constant volume C_{v} of Eq. (5.41). This is

obtained by differentiating Eq. (6.3) with respect to temperature T resulting in

$$\begin{aligned}
&\frac{\partial^2 \tilde{\mathcal{F}}(\mathbf{v};T)}{\partial T^2} \\
&= \frac{\hbar}{2}\sum_{\left[\substack{k\\ \nu}\right]} \frac{\partial^2 \omega_{\text{eff}}\left[\substack{k\\ \nu}\right]}{\partial T^2} + \hbar \sum_{\left[\substack{k\\ \nu}\right]} \frac{\partial^2 \omega_{\text{eff}}\left[\substack{k\\ \nu}\right]}{\partial T^2} \left(\exp\left\{\frac{\hbar\omega_{\text{eff}}\left[\substack{k\\ \nu}\right]}{k_B T}\right\} - 1\right)^{-1} \\
&- \frac{\hbar^2}{k_B T}\sum_{\left[\substack{k\\ \nu}\right]} \left(\frac{\partial \omega_{\text{eff}}\left[\substack{k\\ \nu}\right]}{\partial T} - \frac{\omega_{\text{eff}}\left[\substack{k\\ \nu}\right]}{T}\right)^2 \exp\left\{\frac{\hbar\omega_{\text{eff}}\left[\substack{k\\ \nu}\right]}{k_B T}\right\} \left(\exp\left\{\frac{\hbar\omega_{\text{eff}}\left[\substack{k\\ \nu}\right]}{k_B T}\right\} - 1\right)^{-2}.
\end{aligned} \tag{6.4}$$

The second-order derivative of the CB free energy $\tilde{\mathcal{F}}$ with respect to temperature T and v_i is required to evaluate the linear thermal expansion coefficient α given by Eq. (5.40). This is obtained by differentiating Eq. (6.3) with respect to v_i resulting in

$$\begin{aligned}
\frac{\partial^2 \tilde{\mathcal{F}}(\mathbf{v};T)}{\partial \mathrm{v}_i \partial T} &= \hbar \sum_{\left[\substack{k\\ \nu}\right]} \frac{\partial^2 \omega_{\text{eff}}\left[\substack{k\\ \nu}\right]}{\partial \mathrm{v}_i \partial T} \left[\frac{1}{2} + \left(\exp\left\{\frac{\hbar\omega_{\text{eff}}\left[\substack{k\\ \nu}\right]}{k_B T}\right\} - 1\right)^{-1}\right] \\
&- \frac{\hbar^2}{k_B T}\sum_{\left[\substack{k\\ \nu}\right]} \frac{\partial \omega_{\text{eff}}\left[\substack{k\\ \nu}\right]}{\partial \mathrm{v}_i} \left(\frac{\partial \omega_{\text{eff}}\left[\substack{k\\ \nu}\right]}{\partial T} - \frac{\omega_{\text{eff}}\left[\substack{k\\ \nu}\right]}{T}\right) \exp\left\{\frac{\hbar\omega_{\text{eff}}\left[\substack{k\\ \nu}\right]}{k_B T}\right\} \left(\exp\left\{\frac{\hbar\omega_{\text{eff}}\left[\substack{k\\ \nu}\right]}{k_B T}\right\} - 1\right)^{-2}.
\end{aligned} \tag{6.5}$$

6.3 Derivatives of effective harmonic frequencies

The analytical expressions for derivatives of free energy given in Section 6.2 require the corresponding derivatives of effective harmonic frequencies $\omega^2_{\text{eff}}\left[\substack{k\\ \nu}\right]$. These derivatives are obtained by differentiating the self-consistent equation Eq. (5.19). The first-order derivative of $\omega^2_{\text{eff}}\left[\substack{k\\ \nu}\right]$ with respect to a macroscopic DOF v_i is given by

$$\begin{aligned}
\frac{\partial \omega^2_{\text{eff}}\left[\substack{k\\ \nu}\right]}{\partial \mathrm{v}_i} &= \frac{\partial \omega^2\left[\substack{k\\ \nu}\right]}{\partial \mathrm{v}_i} + \frac{k_B T}{2}\sum_{\left[\substack{k'\\ \nu'}\right]} \frac{\partial V_4\left[\substack{k-k\,k'-k'\\ \nu\nu\quad \nu'\nu'}\right]}{\partial \mathrm{v}_i} \left(\omega^2_{\text{eff}}\left[\substack{k'\\ \nu'}\right]\right)^{-1} \\
&- \frac{k_B T}{2}\sum_{\left[\substack{k'\\ \nu'}\right]} V_4\left[\substack{k-k\,k'-k'\\ \nu\nu\quad \nu'\nu'}\right] \frac{\partial \omega^2_{\text{eff}}\left[\substack{k'\\ \nu'}\right]}{\partial \mathrm{v}_i} \left(\omega^2_{\text{eff}}\left[\substack{k'\\ \nu'}\right]\right)^{-2}.
\end{aligned} \tag{6.6}$$

Rearranging the terms in Eq. (6.6) results in

$$\begin{aligned}&\frac{\partial \omega_{\text{eff}}^2\left[\begin{smallmatrix}k\\ \nu\end{smallmatrix}\right]}{\partial \mathrm{v}_i}+\frac{k_BT}{2}\sum_{\left[\begin{smallmatrix}k'\\ \nu'\end{smallmatrix}\right]}V_4\left[\begin{smallmatrix}k-kk'-k'\\ \nu\nu\ \ \nu'\nu'\end{smallmatrix}\right]\left(\omega_{\text{eff}}^2\left[\begin{smallmatrix}k'\\ \nu'\end{smallmatrix}\right]\right)^{-2}\frac{\partial \omega_{\text{eff}}^2\left[\begin{smallmatrix}k'\\ \nu'\end{smallmatrix}\right]}{\partial \mathrm{v}_i}\\ &=\frac{\partial \omega^2\left[\begin{smallmatrix}k\\ \nu\end{smallmatrix}\right]}{\partial \mathrm{v}_i}+\frac{k_BT}{2}\sum_{\left[\begin{smallmatrix}k'\\ \nu'\end{smallmatrix}\right]}\frac{\partial V_4\left[\begin{smallmatrix}k-kk'-k'\\ \nu\nu\ \ \nu'\nu'\end{smallmatrix}\right]}{\partial \mathrm{v}_i}\left(\omega_{\text{eff}}^2\left[\begin{smallmatrix}k'\\ \nu'\end{smallmatrix}\right]\right)^{-1}.\end{aligned} \tag{6.7}$$

The above equation when considered for all $\left[\begin{smallmatrix}k\\ \nu\end{smallmatrix}\right]$ is revealed to be a system of linear equations that can be written in matrix form as

$$\mathbf{A}\frac{\partial \mathbf{X}}{\partial \mathrm{v}_i}=\mathbf{B}_i, \tag{6.8}$$

where $\frac{\partial \mathbf{X}}{\partial \mathrm{v}_i}$ is a vector containing $\frac{\partial \omega_{\text{eff}}^2\left[\begin{smallmatrix}k\\ \nu\end{smallmatrix}\right]}{\partial \mathrm{v}_i}$ for all $\left[\begin{smallmatrix}k\\ \nu\end{smallmatrix}\right]$ and $\mathbf{B}_i$ is a vector containing the right hand side of Eq. (6.7) for all $\left[\begin{smallmatrix}k\\ \nu\end{smallmatrix}\right]$. From the left hand side of Eq. (6.7) the matrix $\mathbf{A}$ is given by

$$A\left[\begin{smallmatrix}kk'\\ \nu\nu'\end{smallmatrix}\right]=\delta_{\left[\begin{smallmatrix}k\\ \nu\end{smallmatrix}\right],\left[\begin{smallmatrix}k'\\ \nu'\end{smallmatrix}\right]}+\frac{k_BT}{2}V_4\left[\begin{smallmatrix}k-kk'-k'\\ \nu\nu\ \ \nu'\nu'\end{smallmatrix}\right]\left(\omega_{\text{eff}}^2\left[\begin{smallmatrix}k'\\ \nu'\end{smallmatrix}\right]\right)^{-2}, \tag{6.9}$$

where $A\left[\begin{smallmatrix}kk'\\ \nu\nu'\end{smallmatrix}\right]$ is the element of matrix $\mathbf{A}$ corresponding to the $\left[\begin{smallmatrix}k\\ \nu\end{smallmatrix}\right]^{th}$ row and $\left[\begin{smallmatrix}k'\\ \nu'\end{smallmatrix}\right]^{th}$ column. The right hand side of Eq. (6.7) requires the knowledge of first-order derivatives of both $\omega^2\left[\begin{smallmatrix}k\\ \nu\end{smallmatrix}\right]$ and $V_4\left[\begin{smallmatrix}k-kk'-k'\\ \nu\nu\ \ \nu'\nu'\end{smallmatrix}\right]$ with respect to v_i. The details of the evaluation of these derivatives are discussed in Sections 6.4 and 6.5. In this work, the system of linear equations given by Eq. (6.8) is evaluated using the LU decomposition algorithm (*Press et al.*, 1992) which is available in the BFBSymPac (*Elliott*, 2010) software package.

The second-order derivatives of $\omega_{\text{eff}}^2\left[\begin{smallmatrix}k\\ \nu\end{smallmatrix}\right]$ are obtained by differentiating Eq. (6.7) with

respect to v_j resulting in

$$\begin{aligned}
\frac{\partial^2\omega^2_{\text{eff}}\left[\substack{k\\\nu}\right]}{\partial \mathrm{v}_i\partial \mathrm{v}_j} &= \frac{\partial^2\omega^2\left[\substack{k\\\nu}\right]}{\partial \mathrm{v}_i\partial \mathrm{v}_j} + \frac{k_BT}{2}\sum_{\left[\substack{k'\\\nu'}\right]}\frac{\partial^2 V_4\left[\substack{k-kk'-k'\\\nu\nu\ \ \nu'\nu'}\right]}{\partial \mathrm{v}_i\partial \mathrm{v}_j}\left(\omega^2_{\text{eff}}\left[\substack{k'\\\nu'}\right]\right)^{-1}\\
&\quad - \frac{k_BT}{2}\sum_{\left[\substack{k'\\\nu'}\right]}\left[\frac{\partial V_4\left[\substack{k-kk'-k'\\\nu\nu\ \ \nu'\nu'}\right]}{\partial \mathrm{v}_i}\frac{\partial\omega^2_{\text{eff}}\left[\substack{k'\\\nu'}\right]}{\partial \mathrm{v}_j} + \frac{\partial V_4\left[\substack{k-kk'-k'\\\nu\nu\ \ \nu'\nu'}\right]}{\partial \mathrm{v}_j}\frac{\partial\omega^2_{\text{eff}}\left[\substack{k'\\\nu'}\right]}{\partial \mathrm{v}_i}\right]\left(\omega^2_{\text{eff}}\left[\substack{k'\\\nu'}\right]\right)^{-2}\\
&\quad + k_BT\sum_{\left[\substack{k'\\\nu'}\right]}V_4\left[\substack{k-kk'-k'\\\nu\nu\ \ \nu'\nu'}\right]\frac{\partial\omega^2_{\text{eff}}\left[\substack{k'\\\nu'}\right]}{\partial \mathrm{v}_i}\frac{\partial\omega^2_{\text{eff}}\left[\substack{k'\\\nu'}\right]}{\partial \mathrm{v}_j}\left(\omega^2_{\text{eff}}\left[\substack{k'\\\nu'}\right]\right)^{-3}\\
&\quad + \frac{k_BT}{2}\sum_{\left[\substack{k'\\\nu'}\right]}V_4\left[\substack{k-kk'-k'\\\nu\nu\ \ \nu'\nu'}\right]\frac{\partial^2\omega^2_{\text{eff}}\left[\substack{k'\\\nu'}\right]}{\partial \mathrm{v}_i\partial \mathrm{v}_j}\left(\omega^2_{\text{eff}}\left[\substack{k'\\\nu'}\right]\right)^{-2}.
\end{aligned} \tag{6.10}$$

Rearranging the terms in Eq. (6.10) results in

$$\begin{aligned}
&\frac{\partial^2\omega^2_{\text{eff}}\left[\substack{k\\\nu}\right]}{\partial \mathrm{v}_i\partial \mathrm{v}_j} + \frac{k_BT}{2}\sum_{\left[\substack{k'\\\nu'}\right]}V_4\left[\substack{k-kk'-k'\\\nu\nu\ \ \nu'\nu'}\right]\left(\omega^2_{\text{eff}}\left[\substack{k'\\\nu'}\right]\right)^{-2}\frac{\partial^2\omega^2_{\text{eff}}\left[\substack{k'\\\nu'}\right]}{\partial \mathrm{v}_i\partial \mathrm{v}_j}\\
&= \frac{\partial^2\omega^2\left[\substack{k\\\nu}\right]}{\partial \mathrm{v}_i\partial \mathrm{v}_j} + \frac{k_BT}{2}\sum_{\left[\substack{k'\\\nu'}\right]}\frac{\partial^2 V_4\left[\substack{k-kk'-k'\\\nu\nu\ \ \nu'\nu'}\right]}{\partial \mathrm{v}_i\partial \mathrm{v}_j}\left(\omega^2_{\text{eff}}\left[\substack{k'\\\nu'}\right]\right)^{-1}\\
&- \frac{k_BT}{2}\sum_{\left[\substack{k'\\\nu'}\right]}\left[\frac{\partial V_4\left[\substack{k-kk'-k'\\\nu\nu\ \ \nu'\nu'}\right]}{\partial \mathrm{v}_i}\frac{\partial\omega^2_{\text{eff}}\left[\substack{k'\\\nu'}\right]}{\partial \mathrm{v}_j} + \frac{\partial V_4\left[\substack{k-kk'-k'\\\nu\nu\ \ \nu'\nu'}\right]}{\partial \mathrm{v}_j}\frac{\partial\omega^2_{\text{eff}}\left[\substack{k'\\\nu'}\right]}{\partial \mathrm{v}_i}\right]\left(\omega^2_{\text{eff}}\left[\substack{k'\\\nu'}\right]\right)^{-2}\\
&+ k_BT\sum_{\left[\substack{k'\\\nu'}\right]}V_4\left[\substack{k-kk'-k'\\\nu\nu\ \ \nu'\nu'}\right]\frac{\partial\omega^2_{\text{eff}}\left[\substack{k'\\\nu'}\right]}{\partial \mathrm{v}_i}\frac{\partial\omega^2_{\text{eff}}\left[\substack{k'\\\nu'}\right]}{\partial \mathrm{v}_j}\left(\omega^2_{\text{eff}}\left[\substack{k'\\\nu'}\right]\right)^{-3}.
\end{aligned} \tag{6.11}$$

Similar to Eq. (6.7), the above equation when considered for all $\left[\substack{k\\\nu}\right]$ is a system of linear equations that can be written in matrix form as

$$\mathbf{A}\frac{\partial^2\mathbf{X}}{\partial \mathrm{v}_i\partial \mathrm{v}_j} = \mathbf{B}_{ij}, \tag{6.12}$$

where $\frac{\partial^2 \mathbf{X}}{\partial \mathrm{v}_i \partial \mathrm{v}_j}$ is a vector containing $\frac{\partial^2 \omega_{\mathrm{eff}}^2 \left[\begin{smallmatrix} k \\ \nu \end{smallmatrix}\right]}{\partial \mathrm{v}_i \partial \mathrm{v}_j}$ for all $\left[\begin{smallmatrix} k \\ \nu \end{smallmatrix}\right]$, $\mathbf{B}_{ij}$ is a vector containing the right hand side of Eq. (6.11) for all $\left[\begin{smallmatrix} k \\ \nu \end{smallmatrix}\right]$, and the matrix $\mathbf{A}$ is given by Eq. (6.9). The first-order derivatives of $\omega_{\mathrm{eff}}^2 \left[\begin{smallmatrix} k \\ \nu \end{smallmatrix}\right]$ with respect to $\mathbf{v}$ are determined by evaluating Eq. (6.8).

The first-order derivative $\frac{\partial \omega^2 \left[\begin{smallmatrix} k \\ \nu \end{smallmatrix}\right]}{\partial T}$ is obtained by differentiating Eq. (5.19) with respect to T resulting in

$$\begin{aligned} \frac{\partial \omega_{\mathrm{eff}}^2 \left[\begin{smallmatrix} k \\ \nu \end{smallmatrix}\right]}{\partial T} = \frac{k_B}{2} \sum_{\left[\begin{smallmatrix} k' \\ \nu' \end{smallmatrix}\right]} V_4 \left[\begin{smallmatrix} k & -k & k' & -k' \\ \nu & \nu & \nu' & \nu' \end{smallmatrix}\right] \left(\omega_{\mathrm{eff}}^2 \left[\begin{smallmatrix} k' \\ \nu' \end{smallmatrix}\right]\right)^{-1} \\ - \frac{k_B T}{2} \sum_{\left[\begin{smallmatrix} k' \\ \nu' \end{smallmatrix}\right]} V_4 \left[\begin{smallmatrix} k & -k & k' & -k' \\ \nu & \nu & \nu' & \nu' \end{smallmatrix}\right] \frac{\partial \omega_{\mathrm{eff}}^2 \left[\begin{smallmatrix} k' \\ \nu' \end{smallmatrix}\right]}{\partial T} \left(\omega_{\mathrm{eff}}^2 \left[\begin{smallmatrix} k' \\ \nu' \end{smallmatrix}\right]\right)^{-2}. \end{aligned} \tag{6.13}$$

Rearranging the terms in Eq. (6.13) results in

$$\begin{aligned} \frac{\partial \omega_{\mathrm{eff}}^2 \left[\begin{smallmatrix} k \\ \nu \end{smallmatrix}\right]}{\partial T} + \frac{k_B T}{2} \sum_{\left[\begin{smallmatrix} k' \\ \nu' \end{smallmatrix}\right]} V_4 \left[\begin{smallmatrix} k & -k & k' & -k' \\ \nu & \nu & \nu' & \nu' \end{smallmatrix}\right] \left(\omega_{\mathrm{eff}}^2 \left[\begin{smallmatrix} k' \\ \nu' \end{smallmatrix}\right]\right)^{-2} \frac{\partial \omega_{\mathrm{eff}}^2 \left[\begin{smallmatrix} k' \\ \nu' \end{smallmatrix}\right]}{\partial T} \\ = \frac{k_B}{2} \sum_{\left[\begin{smallmatrix} k' \\ \nu' \end{smallmatrix}\right]} V_4 \left[\begin{smallmatrix} k & -k & k' & -k' \\ \nu & \nu & \nu' & \nu' \end{smallmatrix}\right] \left(\omega_{\mathrm{eff}}^2 \left[\begin{smallmatrix} k' \\ \nu' \end{smallmatrix}\right]\right)^{-1}. \end{aligned} \tag{6.14}$$

Similar to Eq. (6.11), the above equation when considered for all $\left[\begin{smallmatrix} k \\ \nu \end{smallmatrix}\right]$ is a system of linear equations that can be written in matrix form as

$$\mathbf{A} \frac{\partial \mathbf{X}}{\partial T} = \mathbf{B}_T, \tag{6.15}$$

where $\frac{\partial \mathbf{X}}{\partial T}$ is a vector containing $\frac{\partial \omega_{\mathrm{eff}}^2 \left[\begin{smallmatrix} k \\ \nu \end{smallmatrix}\right]}{\partial T}$ for all $\left[\begin{smallmatrix} k \\ \nu \end{smallmatrix}\right]$ and $\mathbf{B}_T$ is a vector containing the right hand side of Eq. (6.14) for all $\left[\begin{smallmatrix} k \\ \nu \end{smallmatrix}\right]$.

The second-order derivative $\frac{\partial^2 \omega_{\mathrm{eff}}^2 \left[\begin{smallmatrix} k \\ \nu \end{smallmatrix}\right]}{\partial T^2}$ is obtained by differentiating Eq. (6.14) with

respect to T resulting in

$$\begin{aligned}\frac{\partial^2\omega^2_{\text{eff}}\left[\substack{k\\\nu}\right]}{\partial T^2} &= k_BT\sum_{\left[\substack{k'\\\nu'}\right]} V_4\left[\substack{k-kk'-k'\\\nu\nu\ \ \nu'\nu'}\right]\left(\frac{\partial\omega^2_{\text{eff}}\left[\substack{k'\\\nu'}\right]}{\partial T}\right)^2\left(\omega^2_{\text{eff}}\left[\substack{k'\\\nu'}\right]\right)^{-3}\\ &- k_B\sum_{\left[\substack{k'\\\nu'}\right]} V_4\left[\substack{k-kk'-k'\\\nu\nu\ \ \nu'\nu'}\right]\frac{\partial\omega^2_{\text{eff}}\left[\substack{k'\\\nu'}\right]}{\partial T}\left(\omega^2_{\text{eff}}\left[\substack{k'\\\nu'}\right]\right)^{-2}\\ &- \frac{k_BT}{2}\sum_{\left[\substack{k'\\\nu'}\right]} V_4\left[\substack{k-kk'-k'\\\nu\nu\ \ \nu'\nu'}\right]\frac{\partial^2\omega^2_{\text{eff}}\left[\substack{k'\\\nu'}\right]}{\partial T^2}\left(\omega^2_{\text{eff}}\left[\substack{k'\\\nu'}\right]\right)^{-2}.\end{aligned} \tag{6.16}$$

Rearranging the terms in Eq. (6.16) results in

$$\begin{aligned}&\frac{\partial^2\omega^2_{\text{eff}}\left[\substack{k\\\nu}\right]}{\partial T^2} + \frac{k_BT}{2}\sum_{\left[\substack{k'\\\nu'}\right]} V_4\left[\substack{k-kk'-k'\\\nu\nu\ \ \nu'\nu'}\right]\left(\omega^2_{\text{eff}}\left[\substack{k'\\\nu'}\right]\right)^{-2}\frac{\partial^2\omega^2_{\text{eff}}\left[\substack{k'\\\nu'}\right]}{\partial T^2}\\ &= k_BT\sum_{\left[\substack{k'\\\nu'}\right]} V_4\left[\substack{k-kk'-k'\\\nu\nu\ \ \nu'\nu'}\right]\left(\frac{\partial\omega^2_{\text{eff}}\left[\substack{k'\\\nu'}\right]}{\partial T}\right)^2\left(\omega^2_{\text{eff}}\left[\substack{k'\\\nu'}\right]\right)^{-3}\\ &- k_B\sum_{\left[\substack{k'\\\nu'}\right]} V_4\left[\substack{k-kk'-k'\\\nu\nu\ \ \nu'\nu'}\right]\frac{\partial\omega^2_{\text{eff}}\left[\substack{k'\\\nu'}\right]}{\partial T}\left(\omega^2_{\text{eff}}\left[\substack{k'\\\nu'}\right]\right)^{-2}.\end{aligned} \tag{6.17}$$

Similar to Eq. (6.14), the above equation when considered for all $\left[\substack{k\\\nu}\right]$ is a system of linear equations that can be written in matrix form as

$$\mathbf{A}\frac{\partial^2\mathbf{X}}{\partial T^2} = \mathbf{B}_{TT}, \tag{6.18}$$

where $\frac{\partial^2\mathbf{X}}{\partial T^2}$ is a vector containing $\frac{\partial^2\omega^2_{\text{eff}}\left[\substack{k\\\nu}\right]}{\partial T^2}$ for all $\left[\substack{k\\\nu}\right]$ and $\mathbf{B}_{TT}$ is a vector containing the right hand side of Eq. (6.17) for all $\left[\substack{k\\\nu}\right]$. The right hand side of Eq. (6.17) requires the knowledge of first-order derivatives of $\omega^2_{\text{eff}}\left[\substack{k\\\nu}\right]$ with respect to T which are determined by evaluating Eq. (6.15).

Finally, the derivatives $\frac{\partial^2\omega^2\left[\substack{k\\\nu}\right]}{\partial \mathrm{v}_i\partial T}$ are obtained by differentiating Eq. (6.14) with respect

to v_i resulting in

$$\begin{aligned}\frac{\partial^2\omega^2_{\mathrm{eff}}\left[\substack{k\\\nu}\right]}{\partial \mathrm{v}_i\partial T} &= \frac{k_B}{2}\sum_{\left[\substack{k'\\\nu'}\right]}\left[\frac{\partial V_4\left[\substack{k-kk'-k'\\\nu\nu\ \ \nu'\nu'}\right]}{\partial \mathrm{v}_i}\left(\omega^2_{\mathrm{eff}}\left[\substack{k'\\\nu'}\right]\right)^{-1} - V_4\left[\substack{k-kk'-k'\\\nu\nu\ \ \nu'\nu'}\right]\frac{\partial\omega^2_{\mathrm{eff}}\left[\substack{k'\\\nu'}\right]}{\partial \mathrm{v}_i}\left(\omega^2_{\mathrm{eff}}\left[\substack{k'\\\nu'}\right]\right)^{-2}\right]\\ &- \frac{k_BT}{2}\sum_{\left[\substack{k'\\\nu'}\right]}\frac{\partial V_4\left[\substack{k-kk'-k'\\\nu\nu\ \ \nu'\nu'}\right]}{\partial \mathrm{v}_i}\frac{\partial\omega^2_{\mathrm{eff}}\left[\substack{k'\\\nu'}\right]}{\partial T}\left(\omega^2_{\mathrm{eff}}\left[\substack{k'\\\nu'}\right]\right)^{-2}\\ &+ k_BT\sum_{\left[\substack{k'\\\nu'}\right]}V_4\left[\substack{k-kk'-k'\\\nu\nu\ \ \nu'\nu'}\right]\frac{\partial\omega^2_{\mathrm{eff}}\left[\substack{k'\\\nu'}\right]}{\partial \mathrm{v}_i}\frac{\partial\omega^2_{\mathrm{eff}}\left[\substack{k'\\\nu'}\right]}{\partial T}\left(\omega^2_{\mathrm{eff}}\left[\substack{k'\\\nu'}\right]\right)^{-3}\\ &- \frac{k_BT}{2}\sum_{\left[\substack{k'\\\nu'}\right]}V_4\left[\substack{k-kk'-k'\\\nu\nu\ \ \nu'\nu'}\right]\frac{\partial^2\omega^2_{\mathrm{eff}}\left[\substack{k'\\\nu'}\right]}{\partial \mathrm{v}_i\partial T}\left(\omega^2_{\mathrm{eff}}\left[\substack{k'\\\nu'}\right]\right)^{-2}.\end{aligned} \tag{6.19}$$

Rearranging the terms in Eq. (6.19) results in

$$\begin{aligned}&\frac{\partial^2\omega^2_{\mathrm{eff}}\left[\substack{k\\\nu}\right]}{\partial \mathrm{v}_i\partial T} + \frac{k_BT}{2}\sum_{\left[\substack{k'\\\nu'}\right]}V_4\left[\substack{k-kk'-k'\\\nu\nu\ \ \nu'\nu'}\right]\left(\omega^2_{\mathrm{eff}}\left[\substack{k'\\\nu'}\right]\right)^{-2}\frac{\partial^2\omega^2_{\mathrm{eff}}\left[\substack{k'\\\nu'}\right]}{\partial \mathrm{v}_i\partial T}\\ &= \frac{k_B}{2}\sum_{\left[\substack{k'\\\nu'}\right]}\left[\frac{\partial V_4\left[\substack{k-kk'-k'\\\nu\nu\ \ \nu'\nu'}\right]}{\partial \mathrm{v}_i}\left(\omega^2_{\mathrm{eff}}\left[\substack{k'\\\nu'}\right]\right)^{-1} - V_4\left[\substack{k-kk'-k'\\\nu\nu\ \ \nu'\nu'}\right]\frac{\partial\omega^2_{\mathrm{eff}}\left[\substack{k'\\\nu'}\right]}{\partial \mathrm{v}_i}\left(\omega^2_{\mathrm{eff}}\left[\substack{k'\\\nu'}\right]\right)^{-2}\right]\\ &- \frac{k_BT}{2}\sum_{\left[\substack{k'\\\nu'}\right]}\frac{\partial V_4\left[\substack{k-kk'-k'\\\nu\nu\ \ \nu'\nu'}\right]}{\partial \mathrm{v}_i}\frac{\partial\omega^2_{\mathrm{eff}}\left[\substack{k'\\\nu'}\right]}{\partial T}\left(\omega^2_{\mathrm{eff}}\left[\substack{k'\\\nu'}\right]\right)^{-2}\\ &+ k_BT\sum_{\left[\substack{k'\\\nu'}\right]}V_4\left[\substack{k-kk'-k'\\\nu\nu\ \ \nu'\nu'}\right]\frac{\partial\omega^2_{\mathrm{eff}}\left[\substack{k'\\\nu'}\right]}{\partial \mathrm{v}_i}\frac{\partial\omega^2_{\mathrm{eff}}\left[\substack{k'\\\nu'}\right]}{\partial T}\left(\omega^2_{\mathrm{eff}}\left[\substack{k'\\\nu'}\right]\right)^{-3}.\end{aligned} \tag{6.20}$$

Similar to Eq. (6.17), the above equation when considered for all $\left[\substack{k\\\nu}\right]$ is a system of linear equations that can be written in matrix form as

$$\mathbf{A}\frac{\partial^2\mathbf{X}}{\partial \mathrm{v}_i\partial T} = \mathbf{B}_{iT}, \tag{6.21}$$

where $\frac{\partial \mathbf{X}}{\partial T}$ is a vector containing $\frac{\partial \omega^2_{\text{eff}}\left[\begin{smallmatrix}k\\ \nu\end{smallmatrix}\right]}{\partial T}$ for all $\left[\begin{smallmatrix}k\\ \nu\end{smallmatrix}\right]$ and $\mathbf{B}_{iT}$ is a vector containing the right hand side of Eq. (6.20) for all $\left[\begin{smallmatrix}k\\ \nu\end{smallmatrix}\right]$. The right hand side of Eq. (6.20) requires the knowledge of first-order derivatives of both $\omega^2\left[\begin{smallmatrix}k\\ \nu\end{smallmatrix}\right]$ and $V_4\left[\begin{smallmatrix}k & -k & k' & -k'\\ \nu & \nu & \nu' & \nu'\end{smallmatrix}\right]$ with respect to $\mathbf{v}$. These derivatives are evaluated based on the discussions from Sections 6.4 and 6.5. In addition, the first-order derivatives of $\omega^2_{\text{eff}}\left[\begin{smallmatrix}k\\ \nu\end{smallmatrix}\right]$ with respect to $\mathbf{v}$ and T are determined by evaluating Eqs. (6.8) and (6.15), respectively.

6.4 Derivatives of harmonic eigenvalues and eigenvectors

The derivatives of the effective harmonic frequencies $\omega^2_{\text{eff}}\left[\begin{smallmatrix}k\\ \nu\end{smallmatrix}\right]$ obtained in Section 6.3 require the corresponding derivatives of the harmonic eigenvalues $\omega^2\left[\begin{smallmatrix}k\\ \nu\end{smallmatrix}\right]$ and eigenvectors $\mathbf{e}\left[\begin{smallmatrix}k\\ \nu\end{smallmatrix}\right]$ of the harmonic dynamical matrix Eq. (4.20). Further, derivatives of the harmonic eigenvectors $\mathbf{e}\left[\begin{smallmatrix}k\\ \nu\end{smallmatrix}\right]$ are required to determine the derivatives of $V_4\left[\begin{smallmatrix}k & -k & k' & -k'\\ \nu & \nu & \nu' & \nu'\end{smallmatrix}\right]$ that are discussed in Section 6.5.

For a particular value of wave number k, the eigenvalue problem corresponding to the harmonic dynamical matrix Eq. (4.20) is given by

$$\left(\mathbb{K}[k] - \omega^2\left[\begin{smallmatrix}k\\ \nu\end{smallmatrix}\right]\mathbf{I}\right)\mathbf{e}\left[\begin{smallmatrix}k\\ \nu\end{smallmatrix}\right] = \mathbf{0}, \quad \nu = 1, 2, \ldots, M \tag{6.22}$$

where $\mathbf{I}$ is an identity matrix, $\mathbb{K}[k]$ is the harmonic dynamical matrix Eq. (4.20) of dimension $M \times M$ for a M-chain, $\omega^2\left[\begin{smallmatrix}k\\ \nu\end{smallmatrix}\right]$ is the real eigenvalue, and $\mathbf{e}\left[\begin{smallmatrix}k\\ \nu\end{smallmatrix}\right]$ is the corresponding normalized complex eigenvector of dimension $M \times 1$. Various algorithms (*Nelson*, 1976; *Andrew and Tan*, 1998; *der Aa et al.*, 2007) are present in the literature to determine the derivatives of eigenvalues and eigenvectors of an eigenvalue problem defined by Eq. (6.22). First, Nelson's algorithm (*Nelson*, 1976) was developed to determine the derivatives when the eigenvalues are distinct, i.e., $\omega^2\left[\begin{smallmatrix}k\\ \nu\end{smallmatrix}\right] \neq \omega^2\left[\begin{smallmatrix}k\\ \nu'\end{smallmatrix}\right]$ for all $\nu \neq \nu'$. Later on, more complicated algorithms (*Andrew and Tan*, 1998; *der Aa et al.*, 2007) were developed to determine the derivatives when some of the eigenvalues are repeated in value, i.e., $\omega^2\left[\begin{smallmatrix}k\\ \nu\end{smallmatrix}\right] = \omega^2\left[\begin{smallmatrix}k\\ \nu'\end{smallmatrix}\right]$ for some $\nu \neq \nu'$.

In this work, Nelsons's algorithm (*Nelson*, 1976) is used to evaluate the first- and second-order derivatives of harmonic eigenvalues $\omega^2\left[\begin{smallmatrix}k\\ \nu\end{smallmatrix}\right]$ and eigenvectors $\mathbf{e}\left[\begin{smallmatrix}k\\ \nu\end{smallmatrix}\right]$. However,

Nelson's algorithm can only be applied when the eigenvalues corresponding to an eigenvalue problem Eq. (6.22) are distinct. This imposes a constraint on the selection of k points corresponding to the summation in Eq. (5.28) such that for any particular wave number k all the eigenvalues are distinct.

The variation of harmonic frequencies with respect to wave number $k \in \left[-\frac{\pi}{a}, \frac{\pi}{a}\right)$ is schematically plotted in Fig. 6.1 for the case of a one-dimensional bi-atomic chain by considering a non-essential eight atom CB unit cell. Here, a is the reference unit cell length corresponding to the non-essential eight atom CB unit cell. From Fig. 6.1, it can be observed that the harmonic frequencies are not distinct for $k = -\frac{\pi}{a}$, $k = 0$, and $k = \frac{\pi}{a}$. This is due to the folding of dispersion curves which is the effect of considering the non-essential eight atom CB unit cell instead of the essential two atom CB unit cell. It is to be noted that, based upon previous experience (*Guthikonda and Elliott*, 2008b, 2009), considering a non-essential eight atom CB unit cell is important because it will allow for the identification of the onset of instability using the CB kinematics.

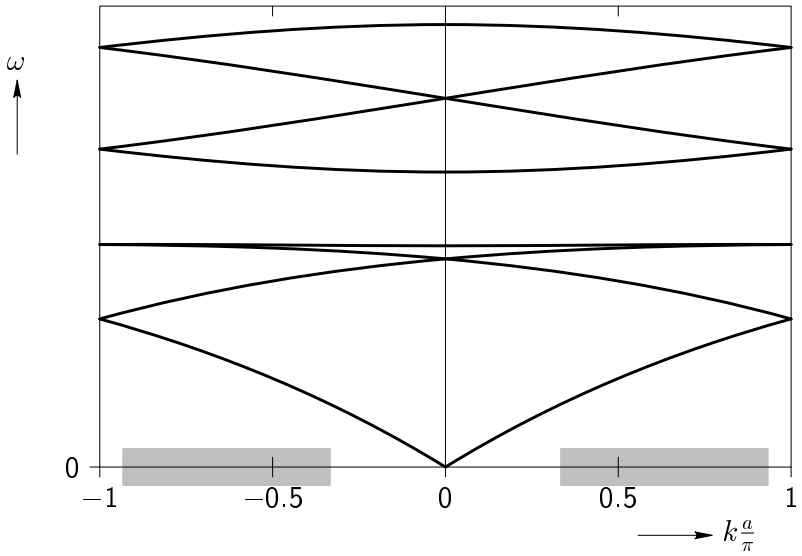

Figure 6.1: Variation of harmonic frequencies ω with respect to wave number k.

In this work, k points are selected from the shaded region as shown in Fig. 6.1 such that $k \in \left[-\frac{14}{15}\frac{\pi}{a}, -\frac{1}{3}\frac{\pi}{a}\right] \cup \left[\frac{1}{3}\frac{\pi}{a}, \frac{14}{15}\frac{\pi}{a}\right]$. This allows the use of Nelson's algorithm (*Nelson*,

1976) to determine the derivatives of eigenvalues and eigenvectors which is computationally efficient but recommended only when the eigenvalues are well separated. The results obtained by taking $k \in \left[-\frac{14}{15}\frac{\pi}{a}, -\frac{1}{3}\frac{\pi}{a}\right] \cup \left[\frac{1}{3}\frac{\pi}{a}, \frac{14}{15}\frac{\pi}{a}\right]$ are found to be essentially equal to the results for the full set of k points $\left[-\frac{\pi}{a}, \frac{\pi}{a}\right)$ when a sufficiently large number of k points are used for the summation in Eq. (5.28). The particular choice of restricting the values of k to be in $\left[-\frac{14}{15}\frac{\pi}{a}, -\frac{1}{3}\frac{\pi}{a}\right] \cup \left[\frac{1}{3}\frac{\pi}{a}, \frac{14}{15}\frac{\pi}{a}\right]$ is determined by trial and error such that Nelson's algorithm does not encounter any difficulties associated with the repeated frequencies at $k = 0$ and $k\frac{a}{\pi} = \pm 1$. It is noted that this interval of k points is likely to be problem dependent.

Nelson's algorithm determines the derivatives of harmonic eigenvalues and eigenvectors by differentiating Eq. (6.22) with respect to v_i resulting in

$$\left[\frac{\partial \mathbb{K}[k]}{\partial \mathrm{v}_i} - \frac{\partial \omega^2\left[\begin{smallmatrix}k\\ \nu\end{smallmatrix}\right]}{\partial \mathrm{v}_i}\mathbf{I}\right]\mathbf{e}\left[\begin{smallmatrix}k\\ \nu\end{smallmatrix}\right] + \left(\mathbb{K}[k] - \omega^2\left[\begin{smallmatrix}k\\ \nu\end{smallmatrix}\right]\mathbf{I}\right)\frac{\partial \mathbf{e}\left[\begin{smallmatrix}k\\ \nu\end{smallmatrix}\right]}{\partial \mathrm{v}_i} = \mathbf{0}. \tag{6.23}$$

Multiplying Eq. (6.23) with $\mathbf{e}^*\left[\begin{smallmatrix}k\\ \nu\end{smallmatrix}\right]$ and rearranging the terms gives an expression for the first-order derivative of the harmonic eigenvalue given by

$$\frac{\partial \omega^2\left[\begin{smallmatrix}k\\ \nu\end{smallmatrix}\right]}{\partial \mathrm{v}_i} = \mathbf{e}^*\left[\begin{smallmatrix}k\\ \nu\end{smallmatrix}\right]\frac{\partial \mathbb{K}[k]}{\partial \mathrm{v}_i}\mathbf{e}\left[\begin{smallmatrix}k\\ \nu\end{smallmatrix}\right]. \tag{6.24}$$

It is not possible to directly obtain the first-order derivatives of the harmonic eigenvectors from Eq. (6.23) since the matrix $\left(\mathbb{K}[k] - \omega^2\left[\begin{smallmatrix}k\\ \nu\end{smallmatrix}\right]\mathbf{I}\right)$ is singular. Nelson (*Nelson*, 1976) proposed that the harmonic eigenvector derivative can be written as

$$\frac{\partial \mathbf{e}\left[\begin{smallmatrix}k\\ \nu\end{smallmatrix}\right]}{\partial \mathrm{v}_i} = \mathbf{x}^i\left[\begin{smallmatrix}k\\ \nu\end{smallmatrix}\right] + c^i\left[\begin{smallmatrix}k\\ \nu\end{smallmatrix}\right]\mathbf{e}\left[\begin{smallmatrix}k\\ \nu\end{smallmatrix}\right], \tag{6.25}$$

where $\mathbf{x}^i\left[\begin{smallmatrix}k\\ \nu\end{smallmatrix}\right]$ is some vector and $c^i\left[\begin{smallmatrix}k\\ \nu\end{smallmatrix}\right]$ is a scalar constant which can be calculated. Substituting Eq. (6.25) into Eq. (6.23) and rearranging the terms result in

$$\left(\mathbb{K}[k] - \omega^2\left[\begin{smallmatrix}k\\ \nu\end{smallmatrix}\right]\mathbf{I}\right)\mathbf{x}^i\left[\begin{smallmatrix}k\\ \nu\end{smallmatrix}\right] = \mathbf{F}^i\left[\begin{smallmatrix}k\\ \nu\end{smallmatrix}\right], \tag{6.26}$$

where $\mathbf{F}^i\begin{bmatrix}k\\ \nu\end{bmatrix}$ is given by

$$\mathbf{F}^i\begin{bmatrix}k\\ \nu\end{bmatrix} = -\left[\frac{\partial \mathbb{K}[k]}{\partial \mathrm{v}_i} - \frac{\partial \omega^2\begin{bmatrix}k\\ \nu\end{bmatrix}}{\partial \mathrm{v}_i}\mathbf{I}\right]\mathbf{e}\begin{bmatrix}k\\ \nu\end{bmatrix}. \tag{6.27}$$

The matrix $\left(\mathbb{K}[k] - \omega^2\begin{bmatrix}k\\ \nu\end{bmatrix}\mathbf{I}\right)$ on the left hand side of Eq. (6.26) is still singular. Nelson proposed that the p^{th} component of $\mathbf{x}^i\begin{bmatrix}k\\ \nu\end{bmatrix}$ be set to zero, where p is the location at which the eigenvector $\mathbf{e}\begin{bmatrix}k\\ \nu\end{bmatrix}$ has the maximum absolute value. This is achieved by replacing the p^{th} row and column of matrix $\left(\mathbb{K}[k] - \omega^2\begin{bmatrix}k\\ \nu\end{bmatrix}\mathbf{I}\right)$ with zeros except for the diagonal term, which is set to one and setting the p^{th} component of the vector $\mathbf{F}^i\begin{bmatrix}k\\ \nu\end{bmatrix}$ to zero. This way, a unique value for $\mathbf{x}^i\begin{bmatrix}k\\ \nu\end{bmatrix}$ is determined. The scalar constant $c^i\begin{bmatrix}k\\ \nu\end{bmatrix}$ can be determined by differentiating the normalization condition of the harmonic eigenvector. Substituting the determined values of $\mathbf{x}^i\begin{bmatrix}k\\ \nu\end{bmatrix}$ and $c^i\begin{bmatrix}k\\ \nu\end{bmatrix}$ into Eq. (6.25) gives rise to the first-order derivative of harmonic eigenvector.

The second-order derivatives of harmonic eigenvalues and eigenvectors are obtained by differentiating Eq. (6.23) and following a similar procedure to that of first-order derivatives. The detailed explanation of Nelsons's algorithm for the case of first- and second-order derivatives of eigenvalues and eigenvectors of an eigenvalue problem Eq. (6.22) is given in Appendix F. Since the harmonic eigenvalues and eigenvectors are independent of temperature T it is only required to determine the first- and second-derivatives of $\omega^2\begin{bmatrix}k\\ \nu\end{bmatrix}$ and $\mathbf{e}\begin{bmatrix}k\\ \nu\end{bmatrix}$ with respect to macroscopic DOFs $\mathbf{v}$.

6.5 Derivatives of the interatomic potential

Finally, the derivatives of $\omega^2_{\text{eff}}\begin{bmatrix}k\\ \nu\end{bmatrix}$ given in Section 6.3 also require the corresponding derivatives of the fourth order terms $V_4\begin{bmatrix}k-k & k'-k'\\ \nu\nu & \nu'\nu'\end{bmatrix}$ defined by Eq. (4.27). The first- and second-order derivatives of $V_4\begin{bmatrix}k-k & k'-k'\\ \nu\nu & \nu'\nu'\end{bmatrix}$ with respect to macroscopic DOFs $\mathbf{v}$ are evaluated using the derivatives of eigenvectors $\mathbf{e}\begin{bmatrix}k\\ \nu\end{bmatrix}$ and the corresponding derivatives of $\overset{o}{\Phi}\begin{bmatrix}0 & \ell' & \ell'' & \ell'''\\ \alpha & \alpha' & \alpha'' & \alpha'''\end{bmatrix}$ which are obtained using CB kinematics Eq. (5.26). This requires up to sixth-order derivatives of the interatomic potential $\phi^{\eta(\alpha)\eta(\alpha')}(r)$ of Eq. (4.2) with respect to r.

6.6 Verification of the numerical implementation

The numerical implementation of the SCA model developed in Chapter 5 is done using C++ and the model is integrated with the BFBSymPac (*Elliott*, 2010) software package to utilize the advantages of the BFB method (*Elliott*, 2007; *Jusuf*, 2010). A number of consistency checks are done in order to verify the numerically implemented SCA model. For example, second-order derivatives of the CB free energy $\tilde{\mathcal{F}}$, effective harmonic frequencies $\omega^2_{\text{eff}}\left[\begin{smallmatrix}k\\ \nu\end{smallmatrix}\right]$, harmonic eigenvalues $\omega^2\left[\begin{smallmatrix}k\\ \nu\end{smallmatrix}\right]$ and eigenvectors $\mathbf{e}\left[\begin{smallmatrix}k\\ \nu\end{smallmatrix}\right]$, and fourth-order term $V_4\left[\begin{smallmatrix}k-kk'-k'\\ \nu\nu\ \ \nu'\nu'\end{smallmatrix}\right]$ discussed in this chapter should follow the symmetry of order of derivative given by

$$\frac{\partial^2(\cdot)}{\partial \mathrm{v}_i \partial \mathrm{v}_j} = \frac{\partial^2(\cdot)}{\partial \mathrm{v}_j \partial \mathrm{v}_i}, \tag{6.28}$$

where $(\cdot)$ is alternatively $\tilde{\mathcal{F}}$, $\omega^2_{\text{eff}}\left[\begin{smallmatrix}k\\ \nu\end{smallmatrix}\right]$, $\omega^2\left[\begin{smallmatrix}k\\ \nu\end{smallmatrix}\right]$, $\mathbf{e}\left[\begin{smallmatrix}k\\ \nu\end{smallmatrix}\right]$, and $V_4\left[\begin{smallmatrix}k-kk'-k'\\ \nu\nu\ \ \nu'\nu'\end{smallmatrix}\right]$. Further, the symmetry of the fourth-order term $V_4\left[\begin{smallmatrix}k-kk'-k'\\ \nu\nu\ \ \nu'\nu'\end{smallmatrix}\right]$ dictates that

$$V_4\left[\begin{smallmatrix}k-kk'-k'\\ \nu\nu\ \ \nu'\nu'\end{smallmatrix}\right] = V_4\left[\begin{smallmatrix}k'-k'k-k\\ \nu'\nu'\ \ \nu\nu\end{smallmatrix}\right]. \tag{6.29}$$

Combining Eqs. (6.28) and (6.29) results in

$$\frac{\partial^2 V_4\left[\begin{smallmatrix}k-kk'-k'\\ \nu\nu\ \ \nu'\nu'\end{smallmatrix}\right]}{\partial \mathrm{v}_i \partial \mathrm{v}_j} = \frac{\partial^2 V_4\left[\begin{smallmatrix}k-kk'-k'\\ \nu\nu\ \ \nu'\nu'\end{smallmatrix}\right]}{\partial \mathrm{v}_j \partial \mathrm{v}_i} = \frac{\partial^2 V_4\left[\begin{smallmatrix}k'-k'k-k\\ \nu'\nu'\ \ \nu\nu\end{smallmatrix}\right]}{\partial \mathrm{v}_i \partial \mathrm{v}_j} = \frac{\partial^2 V_4\left[\begin{smallmatrix}k'-k'k-k\\ \nu'\nu'\ \ \nu\nu\end{smallmatrix}\right]}{\partial \mathrm{v}_j \partial \mathrm{v}_i}. \tag{6.30}$$

All the symmetry relations of Eqs. (6.28), (6.29), and (6.30) are initially verified in the numerically implemented SCA model. Later, these symmetry relations are implemented into the final SCA model for one-dimensional bi-atomic chain in order to increase the computational efficiency of the model.

Chapter 7

Evaluation of SCA model

7.1 Introduction

The SCA model developed in Chapter 5 for the classical chain is implemented for a bi-atomic chain. The atomic interactions are modeled using the Morse pair potential given by

$$\phi(r) = A\left\{\exp\left[-2B\left(\frac{r}{\hat{r}}-1\right)\right]-2\exp\left[-B\left(\frac{r}{\hat{r}}-1\right)\right]\right\}, \tag{7.1}$$

where r is the distance between two interacting atoms, $\hat{r}$ is the zero force distance, A is related to the bond strength, and B is related to the bond stiffness. A bi-atomic chain consists of two types of atoms denoted by "a" and "b" and three types of atomic pair interactions which are modeled by three Morse potentials $\phi^{\mathrm{aa}}(r)$, $\phi^{\mathrm{bb}}(r)$, and $\phi^{\mathrm{ab}}(r)$. Hence, there are nine potential parameters that needs to be determined. In this work, the values for these nine parameters are chosen such that the model demonstrates a PT from a high symmetry, high temperature phase to a low symmetry, low temperature phase which is characteristic of the MTs found in SMAs. Normally these parameters should be determined by fitting the values obtained from experiments or first principles calculations of the material. The nine parameter values used for this work are given in Table 7.1.

Temperature is normalized such that $\theta = T/T_{\mathrm{ref}}$ where T is the temperature in Kelvin and T_{ref} is the reference temperature arbitrarily chosen as 300 K for this study. In theory, the number of k points corresponding to the summation in Eq. (5.28) is

	A (eV)	B	$\hat{r}$ (Å)
a – a	0.10	3.00	7.50
b – b	1.00	6.00	8.00
a – b	0.15	3.25	3.00

Table 7.1: Morse pair potential parameters for the bi-atomic chain used in the numerical calculations. The masses of the two types of atoms (a and b) present in the bi-atomic chain are considered to be $m_a = 196.97$ amu and $m_b = 112.41$ amu.

infinite but in practice it is taken to be a finite number such that the corresponding results are converged with reasonable accuracy. In this work, 50 k points are used which seems to be sufficient to obtain all the thermo-elastic properties discussed in Section 5.4 within a tolerance of 0.5% when compared to the corresponding results with 40 k points. A cutoff radius of $r_{\text{cut}} = 25$ Å is used which seems to be sufficient for the convergence of the summation in Eq. (4.2).

7.2 Temperature-induced MT associated with SCA model

The SCA model is evaluated by generating stress-free bifurcation diagrams of the material properties defined in Section 5.4 with respect to non-dimensional temperature θ for the case of an eight atom CB unit cell. These diagrams are generated using Branch-Following and Bifurcation techniques and the BFBSymPac software package (*Elliott*, 2010). The chain is considered to be free from external loads by taking $f^+ = f^- = 0$. At each temperature the equilibrium conditions Eqs. (5.29)–(5.30) and the stability conditions Eqs. (5.35)–(5.36) are evaluated. This involves solving the self-consistent Eq. (5.19) and evaluating the derivatives of the CB free energy $\tilde{\mathcal{F}}$, effective harmonic frequencies $\omega^2_{\text{eff}}\left[{k \atop \nu}\right]$, harmonic eigenvalues $\omega^2\left[{k \atop \nu}\right]$ and eigenvectors $\mathbf{e}\left[{k \atop \nu}\right]$, and interatomic potential $\phi^{\eta(\alpha)\eta(\alpha')}(r)$ as described in Chapter 6.

In this work, the self-consistent Eq. (5.19) is evaluated using the Newton-Raphson algorithm (*Press et al.*, 1992). The solution of the self-consistent Eq. (5.19) is then substituted into Eq. (5.28) in order to evaluate the free energy. The terms corresponding to $\omega^2_{\text{eff}}\left[{k' \atop \nu'}\right] < 0$ in the summation of Eq. (5.28) are not considered. In other words, the term involving V_4 in Eq. (5.28) is multiplied by the Heaviside step function $H\left(\omega^2_{\text{eff}}\left[{k' \atop \nu'}\right]\right)$

(*Abramowitz and Stegun*, 1972) and this augmented self-consistent equation is used to obtain the effective phonon frequencies. Physically this can be interpreted as restricting the vibrating atoms from moving along the deformation mode associated with $\omega_{\text{eff}}\begin{bmatrix} k \\ \nu \end{bmatrix}$ (which is negative and therefore unstable).

Due to the nonlinear nature of the self-consistent Eq. (5.19) there will generally be multiple solutions. The particular solution obtained will depend on the initial value given to the Newton-Raphson algorithm. Among these different solutions the one that minimizes the free energy of the material is chosen. This is determined by considering two approaches. The first approach considers the reference temperature to be $\theta_{\text{ref}} = 1$. For the present one-dimensional model, it is found from experience that the self-consistent Eq. (5.19) has a unique solution at the reference temperature $\theta = 1$. When the temperature is varied from θ to $\theta + d\theta$, the solution of the self-consistent Eq. (5.19) at θ is provided as the initial value to the Newton-Raphson algorithm which obtains the new solution to the self-consistent Eq. (5.19) at $\theta + d\theta$. The resulting free energy density corresponding to phase "*a*" (shown in Fig. 7.2) is schematically plotted in Fig. 7.1 and is denoted by red color. The second approach considers the reference

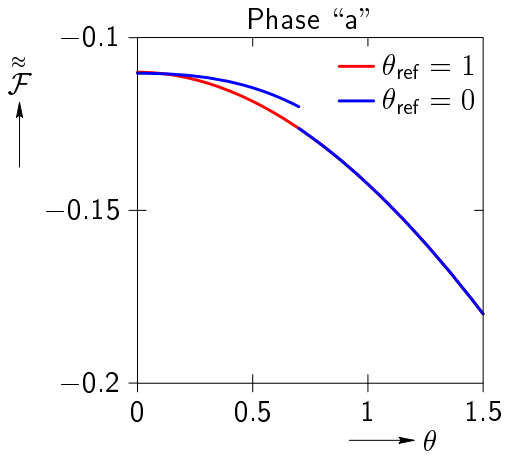

Figure 7.1: Schematic variation of the free energy density with respect to non-dimensional temperature θ when $\theta_{\text{ref}} = 1$ (red color) and $\theta_{\text{ref}} = 0$ (blue color).

temperature to be $\theta_{\text{ref}} = 0$. The self-consistent Eq. (5.19) has a unique solution at the reference temperature $\theta = 0$ where the effective harmonic frequencies become equal to

the corresponding harmonic frequencies. When the temperature is varied from θ to $\theta + d\theta$, the solution of the self-consistent Eq. (5.19) at θ is provided as the initial value to the Newton-Raphson algorithm which obtains the new solution to the self-consistent Eq. (5.19) at $\theta + d\theta$. The resulting free energy density is schematically plotted in Fig. 7.1 and is denoted by blue color. The jump in the blue color path is due to the singularity present in the self-consistent Eq. (5.19). This singularity is a consequence of truncating the infinite series in Eq. (5.18). Thus, in principle, it could be removed by including more terms in Eq. (5.19). From Fig. 7.1, it is observed that the red color path correspond to the minimum free energy density of the material. An exception to this occurs at very low temperatures ($\theta < 0.01$) where some of the effective harmonic frequencies $\omega^2_{\text{eff}}\left[{}^{k}_{\nu}\right]$ become negative. However, in this work the solution to Eq. (5.19) corresponding to the red curve in Fig. 7.1 is used for all temperatures because it gives the minimum free energy for all but very low temperatures ($T < 30$ K) and these temperatures are of little interest in the study of SMAs.

Figure 7.2 displays the stress-free bifurcation diagram of deformation gradient U versus non-dimensional temperature θ, along with the structure of the different phases found during the BFB investigation. Here, solid lines represent stable equilibrium configurations and dashed lines represent unstable configurations. Bifurcation points are represented by hollow circles whereas turning points are represented by solid circles. As the temperature is increased the uniform deformation U increases which implies that the chain expands as the temperature increases. This is in agreement with general thermodynamic observations. At high temperatures the only stable phase (red solid line) is the high symmetry structure. This structure, denoted with the label "a", is depicted in Fig. 7.2 and consists of equal spaced atoms. Phase "a" becomes unstable as the temperature is decreased with a bifurcation point occurring at $\theta = 0.97$. The low symmetry phase denoted by "b" (green line) originates from this bifurcation point. This phase is initially unstable as the temperature is increased but becomes stable when it reaches a turning point at around $\theta = 1.12$. It continues to be stable as temperature is decreased to 0 K. Two energetically distinct unstable phases represented by "c" (purple color) and "d" (gold color) emerge from the secondary bifurcation point of phase "a" at around $\theta = 0.44$. The phase "c" continues to be unstable as temperature is decreased to 0 K whereas the phase "d" is unstable until it reaches a bifurcation point at around

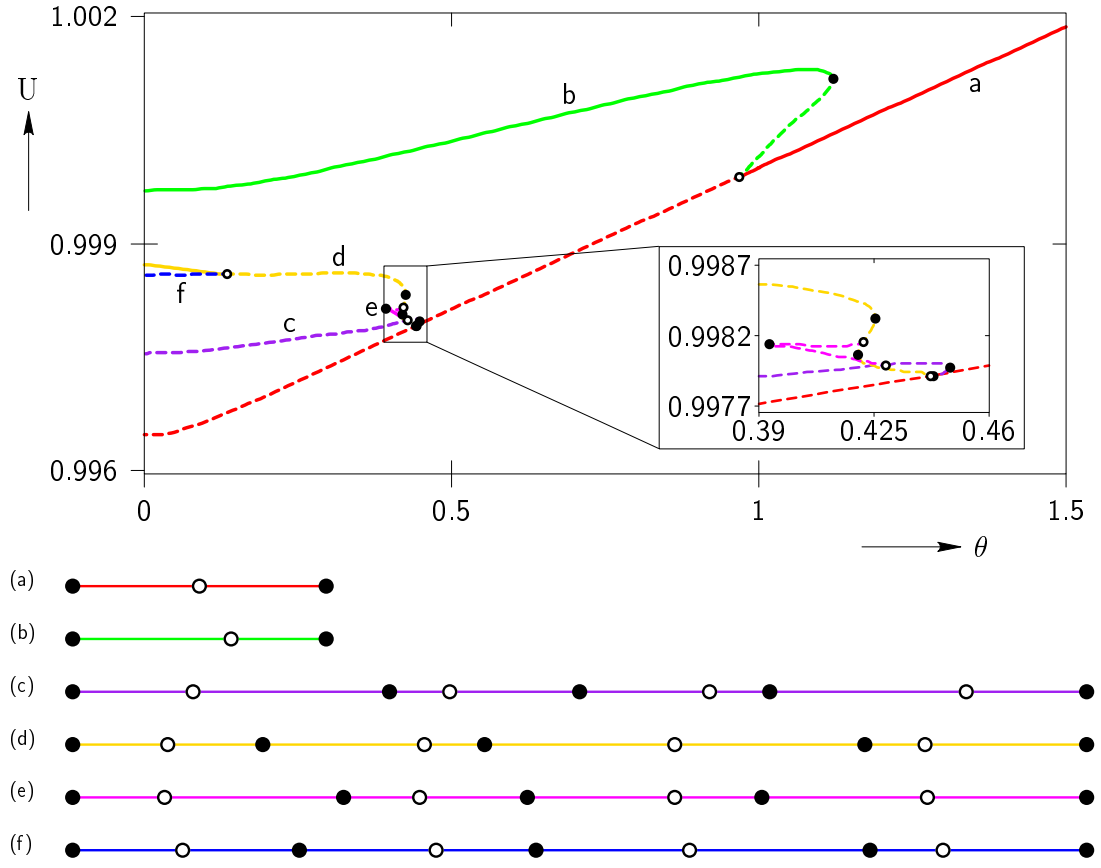

Figure 7.2: Variation of deformation gradient U with respect to non-dimensional temperature θ.

$\theta = 0.13$. From this bifurcation point onwards it is stable for all temperatures down to 0 K. Two additional unstable phases denoted by "e" (magenta color) and "f" (blue color) are also found originating from the bifurcation points on the phase "d".

Figure 7.3 shows the harmonic phonon frequencies for the stress-free phase "*a*" at 0 K. The imaginary phonon frequencies of the unstable modes plotted as negative values in Fig. 7.3 indicate that phase "a" is dynamically unstable at 0 K. However, phase "a" satisfies Eq. (5.36) (all $\omega^2_{\text{eff}}\left[{}^{k}_{\nu}\right] > 0$) at very low temperature ($\theta \leq 0.01$). The SCAILD method (*Souvatzis et al.*, 2008; *Souvatzis and Rudin*, 2008; *Souvatzis et al.*, 2009, 2010), which neglects the effects of thermal expansion, considers the temperature at which the material satisfies Eq. (5.36) as the transition point corresponding to the

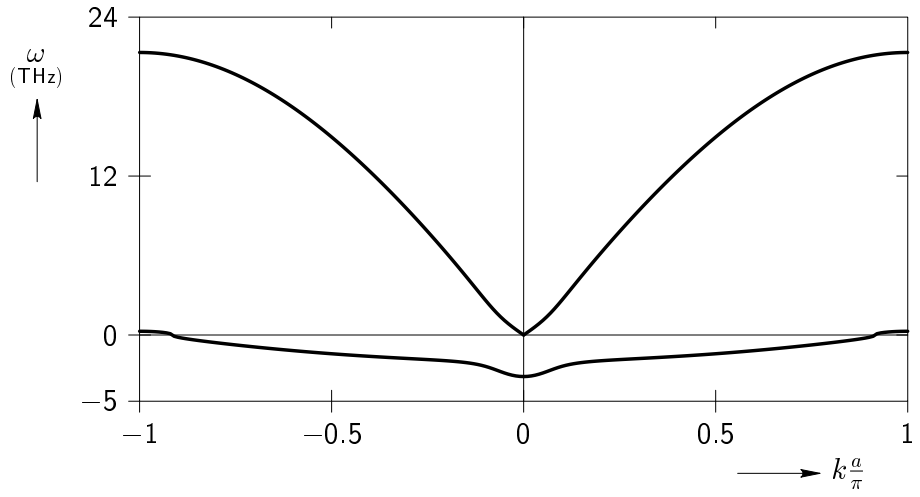

Figure 7.3: Harmonic phonon frequencies for the stress-free phase "a" at 0 K plotted for the essential 2-atom CB unit cell. The imaginary frequencies of the unstable modes are plotted as negative values.

phase transition. However, in the present case when the SCA method is applied without making any simplifying assumptions it is observed that at low temperatures phase "a" does not satisfy the CB stability criterion Eq. (5.35) indicating that the phase "a" is still unstable even though it satisfies Eq. (5.36). Phase "a" is stable (satisfies both Eqs. (5.35) and (5.36)) for $\theta > 0.97$. This implies that the transition temperature $\theta = 0.97$ depends significantly on the CB stability criterion Eq. (5.35).

The variation of the HC (Gibbs) free energy density $\overset{\approx}{\mathcal{F}}$ with respect to non-dimensional temperature θ is plotted in Fig. 7.4. The slope and curvature of all stress-free equilibrium paths are found to be negative for all temperatures. This indicates that the entropy and heat capacity at constant pressure are positive, as required by equilibrium thermodynamics.

At this point, we restrict our attention to the stable path segments of phases "a", "b", and "d" predicted by the SCA model. Figure 7.5 displays the variation of $\overset{\approx}{\mathcal{F}}$ for these phases with respect to θ. At high temperatures phase "a" is the only stable phase and at low temperatures two phases ("b" and "d") are stable. Figure 7.6 displays the variation of bulk (elastic) modulus K with respect to non-dimensional temperature θ. For phase "b", $K \to 0$ as a turning point is approached on the equilibrium path.

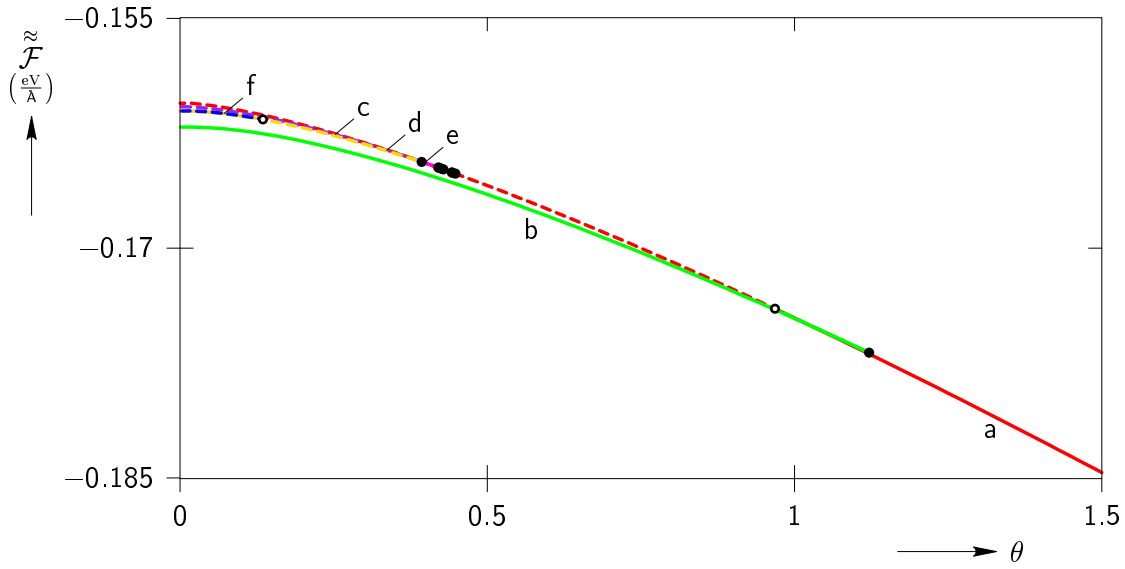

Figure 7.4: Variation of (Gibbs) free energy density with respect to non-dimensional temperature θ.

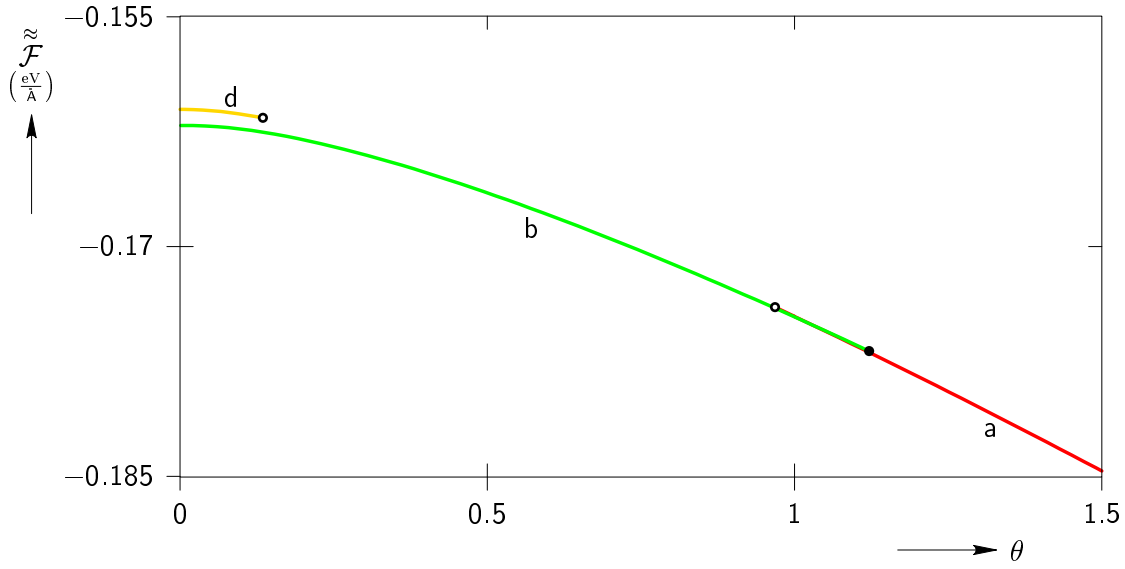

Figure 7.5: Variation of (Gibbs) free energy density corresponding to the stable segments of phases "a", "b", and "c" with respect to non-dimensional temperature θ.

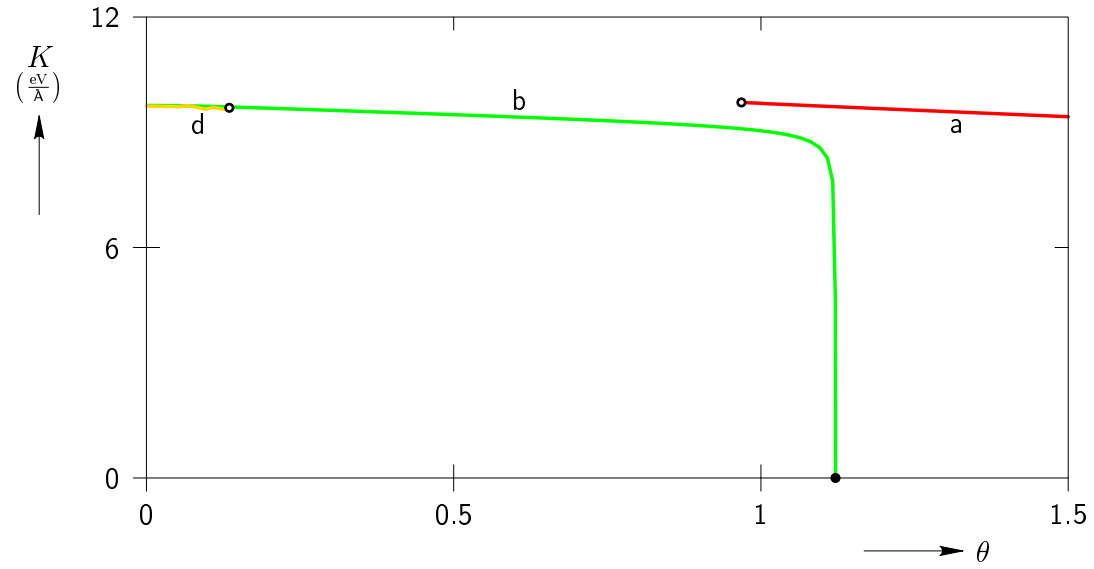

Figure 7.6: Variation of bulk (elastic) modulus K corresponding to the stable segments of phases "a", "b", and "d" with respect to non-dimensional temperature θ.

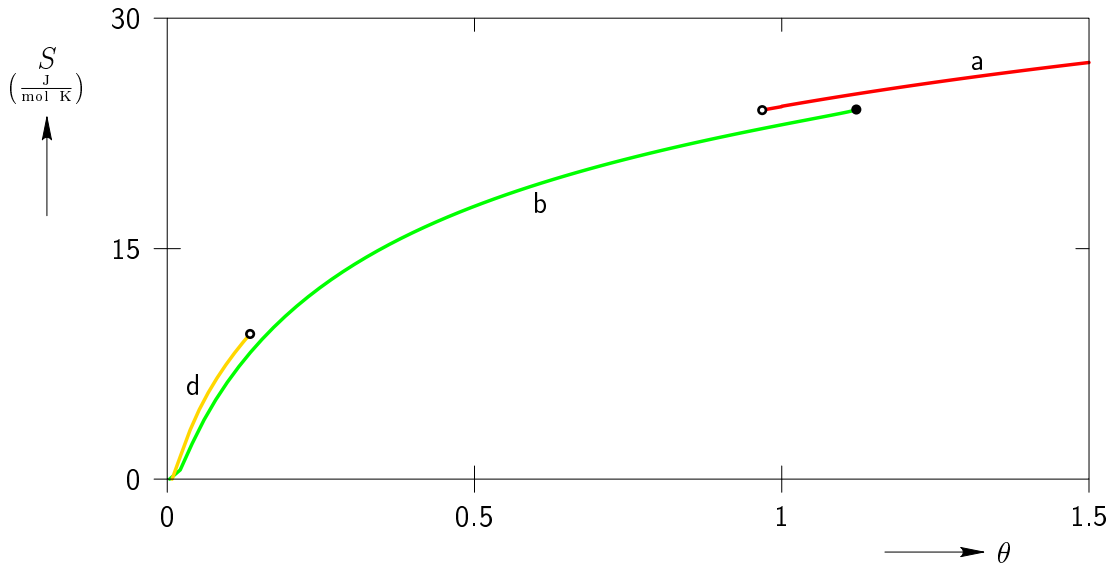

Figure 7.7: Variation of entropy S corresponding to the stable segments of phases "a", "b", and "d" with respect to non-dimensional temperature θ.

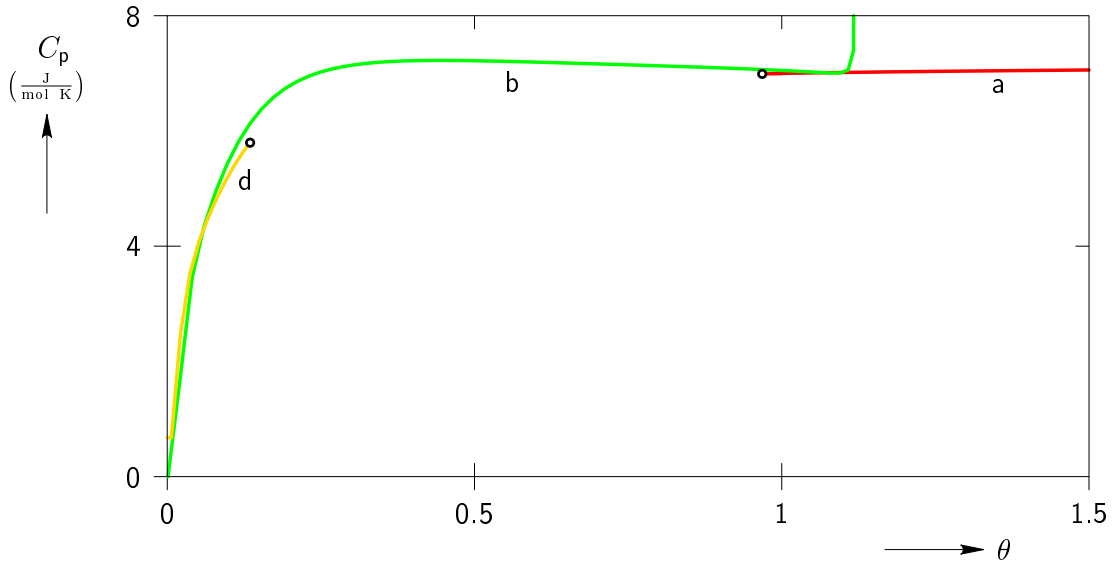

Figure 7.8: Variation of heat capacity at constant pressure C_p corresponding to the stable segments of phases "a", "b", and "d" with respect to non-dimensional temperature θ.

Figures 7.7 and 7.8 display the variation of entropy S and heat capacity at constant pressure C_p, respectively, with respect to non-dimensional temperature θ. In general, entropy and heat capacity are found to increase with temperature. This is in general agreement with thermodynamic theory. For the phase "b" C_p diverges to infinity as a turning point is approached on the equilibrium path. This is a result of the fact that the bulk modulus goes to zero at this point.

Although the results shown in Figs. 7.2–7.8 are for a one-dimensional bi-atomic chain, they are significantly better in terms of overall qualitative behavior when compared to the corresponding results of the EIP model for SMA AuCd shown in Figs. 2.9–2.15. For example, the maximum principle stretch λ_3 plotted in Fig. 2.9 increases nonlinearly whereas the uniform deformation gradient U plotted in Fig. 7.2 increases almost linearly with respect to non-dimensional temperature θ at higher temperatures. Qualitatively Fig. 7.2 is in better agreement with the general experimental observations when compared to Fig. 2.9. In addition, the linear variation of entropy S and heat capacity at constant pressure C_p plotted in Figs. 7.7 and 7.8 agrees with the general

experimental observations when compared to the nonlinear increase of S and C_{p} plotted in Figs. 2.14 and 2.15 at higher temperatures.

Returning to Fig. 7.5, it is observed that upon decreasing temperature phase "a" becomes metastable at the "equilibrium thermodynamics transition temperature" $\theta_{\mathrm{e}} = 1.05$ (with phase "b" having lower free energy for lower temperatures) and finally loses material stability at $\theta = 0.97$ which can be considered as the model's value for the austenite finish temperature A_f. At this temperature the only stable phase is "b". For lower temperatures phase "b" continues to be the stable phase with minimum free energy. Thus, a first-order transformation from the high symmetry phase "a" to the low symmetry phase "b" can be expected. In the case of increasing temperature, the low symmetry phase "b" has the global minimum free energy until $\theta_{\mathrm{e}} = 1.05$ where it becomes metastable with respect to phase "a". It loses material stability soon afterward at $\theta = 1.12$, which is the model's prediction for the martensite finish temperature M_f, where it ceases to exist for higher temperatures. Ideally, one should verify that no other equilibrium crystal structures exist with lower energy. This would ensure that the minimum energy phases shown in Fig. 7.5 capture the model's ground state phase at any given temperature. However, this theoretically infinite investigation is not pursued in this work.

The above discussion shows that the SCA model predicts a hysteretic MT between a high symmetry phase "a" and a low symmetry phase "b" for the case of a one-dimensional bi-atomic chain. Upon cooling the austenite to martensite transition begins at $\theta = 1.12$ and would complete at $\theta = 0.97$. The reverse transformation, upon heating, would begin at $\theta = 0.97$ and complete at $\theta = 1.12$. Therefore, the predicted maximum possible temperature hysteresis is $M_f - A_f = 1.12 - 0.97 = 0.15$ (45 K). Though this prediction is for a one dimensional bi-atomic chain, the temperature hysteresis (45 K) predicted is comparable to the general experiments and a significant improvement when compared to the large hysteresis (530 K) predicted by the EIP model.

7.3 Stress-induced MT associated with SCA model

In Section 7.2, it is observed that the SCA model is capable of simulating the temperature-induced MTs that are observed in SMAs. In addition to temperature-induced MTs,

SMAs exhibit stress-induced MTs when the material is subjected to mechanical load at high temperatures. In this section, similar to Section 7.2, the capability of the SCA model to simulate the stress-induced MTs that are observed in SMAs is evaluated by generating bifurcation diagrams with respect to mechanical load P. These diagrams are generated at a reference temperature $\theta = 1.2$ (360 K). The Gibbs free energy of the chain when subjected to external mechanical load P is given by

$$\tilde{\mathcal{G}} = \tilde{\mathcal{F}} - P(\mathrm{U} - 1), \tag{7.2}$$

where $\tilde{\mathcal{F}}$ is the CB free energy defined by Eq. (5.28) and U is the uniform deformation gradient. The equilibrium conditions corresponding to the Gibbs free energy Eq. (7.2) are given by

$$\left.\frac{\partial \tilde{\mathcal{G}}}{\partial \mathrm{U}}\right|_{(\overset{o}{\mathrm{U}},\overset{o}{\mathbf{S}})} = \left.\frac{\partial \tilde{\mathcal{F}}}{\partial \mathrm{U}}\right|_{(\overset{o}{\mathrm{U}},\overset{o}{\mathbf{S}})} - P = 0, \tag{7.3}$$

$$\left.\frac{\partial \tilde{\mathcal{G}}}{\partial S[\alpha]}\right|_{(\overset{o}{\mathrm{U}},\overset{o}{\mathbf{S}})} = \left.\frac{\partial \tilde{\mathcal{F}}}{\partial S[\alpha]}\right|_{(\overset{o}{\mathrm{U}},\overset{o}{\mathbf{S}})} = 0, \quad \alpha = 1, 2, \ldots, M-1. \tag{7.4}$$

Since the applied mechanical load P is a dead load, the stability conditions of the chain are identical to Eqs. (5.35)–(5.36). The temperature of the chain is fixed at $T = 360\ K$ and the mechanical load $f^+ = f^- = P$ is varied. At each value of P the equilibrium conditions Eqs. (7.3)–(7.4) and the stability conditions Eqs. (5.35)–(5.36) are evaluated. This involves solving the self-consistent Eq. (5.19) and evaluating the derivatives of the Gibbs free energy $\tilde{\mathcal{G}}$, effective harmonic frequencies $\omega^2_{\mathrm{eff}}\left[{}^{k}_{\nu}\right]$, harmonic eigenvalues $\omega^2\left[{}^{k}_{\nu}\right]$ and eigenvectors $\mathbf{e}\left[{}^{k}_{\nu}\right]$, and interatomic potential $\phi^{\eta(\alpha)\eta(\alpha')}(r)$ as described in Chapter 6.

Figure 7.9 shows the bifurcation diagram of mechanical load P versus deformation gradient U. Here, positive values of P indicate that the chain is under tension. At low values of P the only stable phase (red solid line) is the high symmetry structure. This structure, denoted with the label "a", is depicted in Fig. 7.2 and consists of equal spaced atoms. Phase "a" becomes unstable as the value of P is increased with a bifurcation point occurring at $P = 0.36\ \frac{\mathrm{eV}}{\mathrm{\AA}}$. A low symmetry phase denoted by "b" (green line) originates from this bifurcation point. This phase is initially unstable as the value of P is decreased but becomes stable when it reaches a turning point at around $P =$

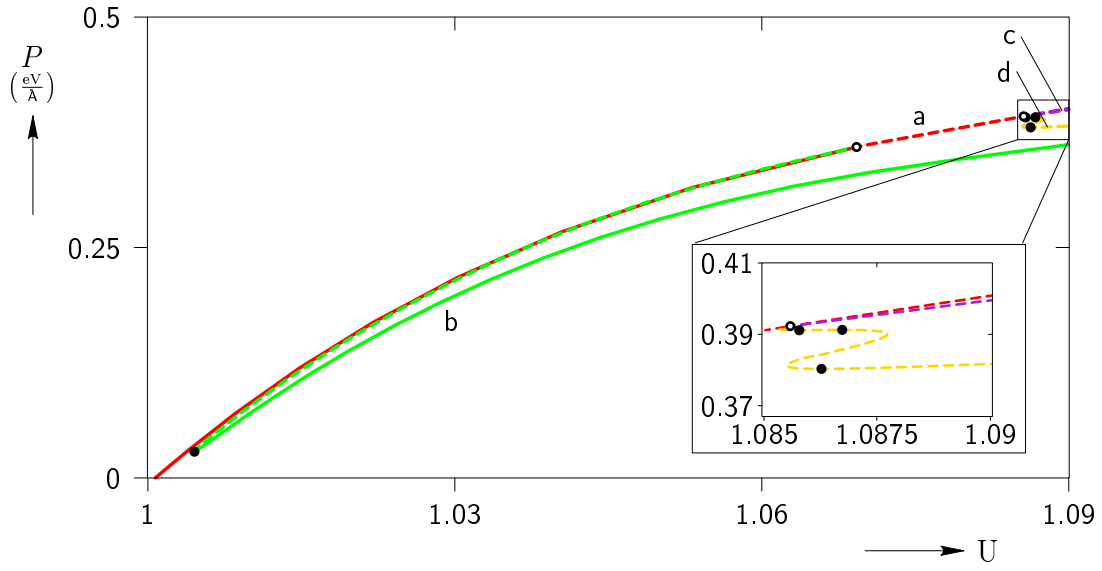

Figure 7.9: Variation of the mechanical load P with respect to deformation gradient U.

0.028 $\frac{\text{eV}}{\text{Å}}$. It continues to be stable as P is increased. Two energetically distinct unstable phases represented by "c" (purple color) and "d" (gold color) emerge from the secondary bifurcation point of phase "a" at around $P = 0.39$ $\frac{\text{eV}}{\text{Å}}$.

Similar to Eq. (5.37), the Gibb free energy $\tilde{\mathcal{G}}$ is homogenized such that $\tilde{\tilde{\mathcal{G}}}(\text{U};T) \equiv \frac{1}{na}\tilde{\mathcal{G}}(\text{U}, \mathbf{S}(\text{U};T);T)$. The variation of the Gibbs free energy density $\tilde{\tilde{\mathcal{G}}}$ corresponding to the stable phases "a" and "b" with respect to the mechanical load P is plotted in Fig. 7.10. The stable phase "a" becomes metastable at the transition load $P_{\text{e}} = 0.12$ $\frac{\text{eV}}{\text{Å}}$ (with phase "b" having lower free energy for higher values of P) and finally loses its stability at $P = 0.36$ $\frac{\text{eV}}{\text{Å}}$. At this load the only stable phase is the low symmetry phase "b". For higher mechanical loads phase "b" continues to be stable. Thus, a first-order transformation from a high symmetry phase "a" to low symmetry phase "b" can be expected. In the case of decreasing P, the low symmetry phase "b" has the minimum free energy density until $P_{\text{e}} = 0.12$ $\frac{\text{eV}}{\text{Å}}$ where it becomes metastable with respect to the phase "a". It loses material stability soon afterward at $P = 0.028$ $\frac{\text{eV}}{\text{Å}}$ where it ceases to exist for lower values of P. These observations indicate that the SCA model predicts a stress-induced hysteretic MT between a high symmetric phase "a" and a low symmetric

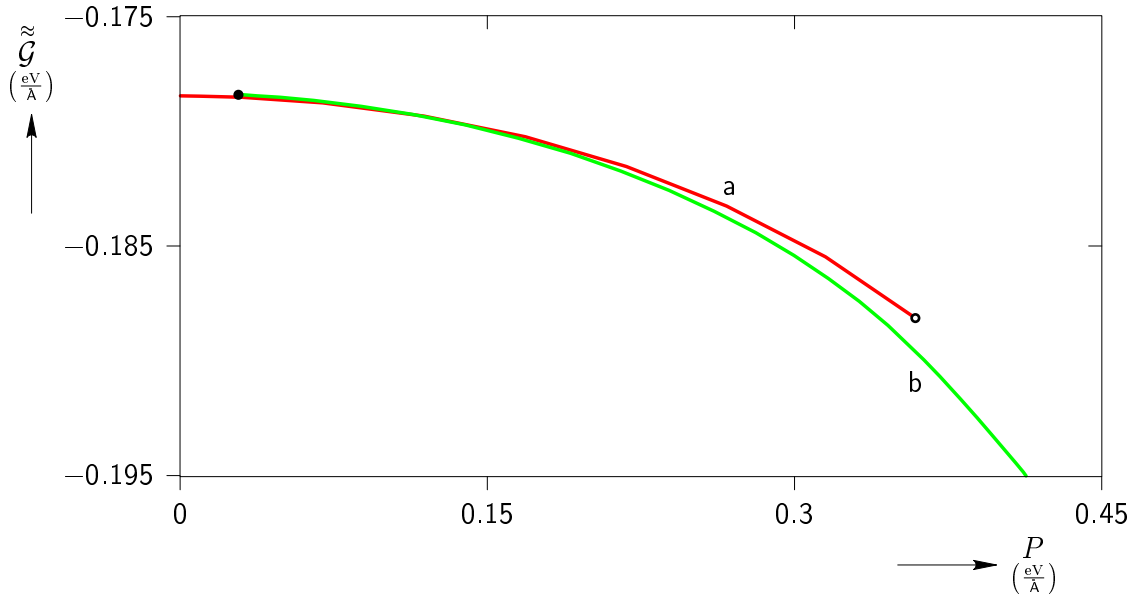

Figure 7.10: Variation of the Gibbs free energy density corresponding to the stable segments of phases “a” and “b” with respect to mechanical load P.

phase “b” for the case of a one-dimensional bi-atomic chain.

Chapter 8

Summary and discussion

This thesis is concerned with developing lattice level atomistic models to simulate the properties of shape memory alloys (SMAs).

In the first part of this work, an Effective Interaction Potential (EIP) model is developed to study the properties of crystalline materials. In this model, effective pair potentials are used for the material's atomic interactions and the deformations of the crystal are described by Cauchy-Born (CB) kinematics. The crystal's free energy density and equilibrium equations are formulated and stability criteria (both CB and phonon) are used to evaluate the material's stability at any equilibrium configuration. This general model is then applied to study the properties of the shape memory alloy (SMA) Au-47.5at%Cd.

A model is developed using a general form of the Morse EIP that is capable of capturing the qualitative behavior of multiple properties of pure Au, pure Cd, and B2 AuCd as temperature is varied. After extensive analysis and experimentation a model is chosen such that the pair equilibrium spacing parameter increases exponentially as temperature is increased, the bond stiffness parameter decreases polynomially as temperature is increased, and the bond strength parameter varies polynomially with temperature. The adjustable parameters in each potential are fit by matching the experimental values of lattice parameter, instantaneous bulk modulus, cohesive energy, linear thermal expansion coefficient, and heat capacity at constant pressure at the transformation temperature. Further, the lattice parameter and cohesive energy are fit for a number of different temperatures. The fitting of all data is performed simultaneously

as an unconstrained optimization problem.

A stress-free bifurcation diagram is generated to evaluate the model's ability to correctly predict the MT between the B2 and B19 structures. From the plots of the maximum principal stretch and Gibbs free energy density versus non-dimensional temperature it is observed that a $B2 \leftrightarrow B19$ MT occurs with a reasonable temperature hysteresis. The transformation stretch is found to be in good agreement with the experimental value. Further, it is found that this model is able to capture the (approximately) volume preserving nature of the martensitic transformation in AuCd. Finally, it is found that the model predicts the latent heat of transformation to within an order of magnitude. It should be noted that the fitting procedure used in the model's development did not include any data associated with the B19 martensite phase of the material. A more general EIP model is likely to be capable of improving the prediction of latent heat and thermal hysteresis. However, the development of this model is left to future work.

The above positive results indicate that the EIP models have the potential to accurately capture the entire range of SMA behavior. These EIP models are computationally inexpensive when compared to Molecular Dynamics, Monté Carlo, and Density Functional Theory models. Thus, EIP models are an appealing accurate and computationally efficient alternative to more traditional simulation methodologies when one is interested in performing large scale simulations (such as the formation of complicated microstructures, or the interaction of a crack tip with the phase transformation) for materials that exhibit MTs including SMAs.

The second part of this work develops a lattice dynamics model using the first-order self-consistent approach (SCA). To this author's knowledge, the SCA method is implemented completely for the first time in this work. The complete implementation is necessary for the model to be fully integrated into the Branch-Following Bifurcation (BFB) methods. This integration of the SCA method into a BFB framework allows the model to be useful in parametrically exploring the configuration space of the material in a computationally efficient way. The SCA method requires minimal fitting due to the use of temperature independent interatomic potentials. The temperature dependence of material properties is modeled by considering the effects of atomic vibrations. These effects are captured by renormalizing the frequencies of atomic vibration using a set of self-consistent equations. These renormalized frequencies are not only dependent on

the configuration but also temperature. This explicit dependence of the renormalized frequencies on both the configuration and temperature enables the SCA method to capture entropic stabilization and simulate the MTs that occur in SMAs. The theoretical picture is that at temperatures above the transition temperature, certain harmonic frequencies are imaginary but all the renormalized phonon frequencies are real. This implies that although the material is unstable according to the harmonic approximation it may be stable due to the anharmonic effects which are considered in calculating the renormalized phonon frequencies. As the temperature is decreased the magnitude of renormalized phonon frequencies decreases which leads to the material becoming unstable at the transition temperature.

In this work, the SCA method is developed using a classical mechanics approach and applied for the case of a one-dimensional bi-atomic chain. First, a generalized lattice dynamics problem is formulated in one dimension and the first-order SCA model is developed using concepts from the statistical perturbation method. Then, the critical aspects involved in the numerical implementation of the SCA model such that BFB methods can be exploited to systematically investigate the SMA behavior are discussed. Finally, the SCA model is applied to a one dimensional bi-atomic chain. The atomic interactions are modeled using Morse pair potentials and the constant potential parameters are chosen to demonstrate the usefulness of the current model. The resulting model is evaluated by generating equilibrium paths with temperature and mechanical load as loading parameters. These plots are generated using BFB techniques.

The current model successfully predicts a first-order MT which involves a transformation from a high symmetry phase to a low symmetry phase as the temperature is decreased for a fixed (zero value of) mechanical load and a transformation from a high symmetry phase to a low symmetry phase when the mechanical load is increased for a fixed temperature. Thus, the current model is able to qualitatively capture both temperature- and stress-induced MTs that are responsible for the peculiar properties of SMAs. This indicates that the current model applied to three-dimensional structures will be likely to capture the first-order MTs that occur in real SMAs. This qualitative prediction of both temperature- and stress-induced MTs indicates that such a model could be used for the computational design and discovery of new SMAs with better

properties. Such an undertaking would involve, first, determining the potential parameters of new alloys from first-principles calculations and, second, using these parameter values with a three-dimensional version of the SCA model to evaluate the shape memory behavior of the new previously unstudied materials.

References

M. Abramowitz and I. A. Stegun. *Handbook of Mathematical Functions with Formulas, Graphs, and Mathematical Tables*. New York: Dover, 1972.

A. L. Andrew and R. C. E. Tan. Computation of derivatives of repeated eigenvalues and the corresponding eigenvectors of symmetric matrix pencils. *SIAM Journal on Matrix Analysis and Applications*, 20:78–100, 1998.

A. B. Belonoshko, N. V. Skorodumova, A. Rosengren, and B. Johansson. Elastic anisotropy of earth's inner core. *Science*, 319:797–800, 2008.

K. Bhattacharya. *Microstructure of Martensite: Why It Forms and How It Gives Rise to the Shape-Memory Effect*. Oxford University Press, 2003.

N. Boccara and G. Sarma. Inelastic scattering of neutrons. *Physics*, 1, 1965.

L. C. Brinson. One dimensional constitutive behavior of shape memory alloys: thermomechanical derivation with non-constant material functions. *Journal of Intelligent Material Systems and Structures*, 4(2):229–242, 1993.

L. C. Brinson and M. S. Huang. Simplifications and comparisons of shape memory alloy constitutive models. *Journal of Intelligent Material Systems and Structures*, 7(1):108–114, 1996.

K. S. Brown and J. P. Sethna. Statistical mechanical approaches to models with many poorly known parameters. *Physical Review E*, 68(2):021904, 2003.

A. Bystrom and K. E. Almin. X-ray investigation of AuCd alloys rich in Au. *Acta Chemica Scandinavica*, 1(1):76–89, 1947.

R. Car and M. Parrinello. Unified approach for molecular-dynamics and density-functional theory. *Physical Review Letters*, 55:2471–2474, 1985.

L. C. Chang and T. A. Read. Plastic deformation and diffusionless phase changes in metals - the AuCd β-phase. *Transactions of the American Institute of Mining and Metallurgical Engineers*, 191(1):47–52, 1951.

Y. A. Chang and L. Himmel. Elastic constants of cadmium from 300^o to 575^o K. *Journal of Applied Physics*, 37(10):3786–3790, 1966a.

Y. A. Chang and L. Himmel. Temperature dependence of the elastic constants of Cu, Ag, and Au above room temperature. *Journal of Applied Physics*, 37(9):3565–3572, 1966b.

P. Choquard. *The Anharmonic Crystal*. W. A. Benjamin, Inc., 1967.

J. Cui, Y. S. Chu, O. O. Famodu, Y. Furuya, J. Hattrick-Simpers, R. D. James, A. Ludwig, S. Thienhaus, M. Wuttig, Z. Zhang, and I. Takeuchi. Combinatorial search of thermoelastic shape-memory alloys with extremely small hysteresis width. *Nature Materials*, 5:286–290, 2006.

B. C. Daniels, Y. J. Chen, J. P. Sethna, R. N. Gutenkunst, and C. R. Myers. Sloppiness, robustness, and evolvability in systems biology. *Current Opinion in Biotechnology*, 19(4):389–395, 2008.

R. Delville, D. Schryvers, Z. Zhang, and R. D. James. Transmission electron microscopy investigation of microstructures in low-hysteresis alloys with special lattice parameters. *Scripta Materiallia*, 60(5):293–296, 2008.

N. P. V. der Aa, H. G. T. Morsche, and R. R. M. Mattheij. Computation of eigenvalue and eigenvector derivatives for a general complexvalued eigensystem. *Electronic Journal of Linear Algebra*, 16:300–314, 2007.

P. A. M. Dirac. *Quantum Mechanics*. Clarendon Press, Oxford, 1948.

N. D. Drummond and G. J. Ackland. Ab initio quasiharmonic equations of state for dynamically stabilized soft-mode materials. *Physical Review B*, 65(184104), 2002.

T. W. Duerig, K. N. Melton, D. Stockel, and C. M. Wayman. *Engineering Aspects of Shape Memory Alloys*. Butterworth-Heinemann, 1990.

D. A. Edwards, W. E. Wallace, and R. S. Craig. Magnesium-Cadmium alloys. IV. The Cadmium-Rich Alloys; Some Lattice Parameters and Phase Relationships between 25^o and 300^o. Structure of the $MgCd_3$ Superlattice. Schottky Defects and the Anomalous Entropy. *Journal of American Chemical Society*, 74(21):5256–5261, 1952.

R. S. Elliott. *Lattice-level instabilities in bi-atomic alloys*. Ph.D. thesis, Department of Aerospace Engineering, The University of Michigan, Ann Arbor, MI, U.S.A., 2004.

R. S. Elliott. Multiscale bifurcation and stability of multilattices. *Journal of Computer-Aided Materials Design*, 14(Suppl. 1):143–157, 2007.

R. S. Elliott. Branch-following and bifurcation with symmetry package (BFBSympac), 2010. Available by request from the author, elliott@aem.umn.edu.

R. S. Elliott and D. S. Karls. Entropic stabilization of austenite in shape memory alloys. *Journal of the Mechanics and Physics of Solids*, 2010. Submitted, under revision.

R. S. Elliott, J. A. Shaw, and N. Triantafyllidis. Stability of thermally-induced martensitic transformations in bi-atomic crystals. *Journal of the Mechanics and Physics of Solids*, 50(11):2463–2493, 2002b.

R. S. Elliott, N. Triantafyllidis, and J. A. Shaw. Stability of crystalline solids–I: Continuum and atomic-lattice considerations. *Journal of the Mechanics and Physics of Solids*, 54(1):161–192, 2006a.

R. S. Elliott, N. Triantafyllidis, and J. A. Shaw. Stability of crystalline solids–II: Application to temperature-induced martensitic phase transformations in a bi-atomic crystal. *Journal of the Mechanics and Physics of Solids*, 54(1):193–232, 2006b.

P. Entel, K. Kadau, R. Meyer, H. C. Herper, M. Schroter, and E. Hoffmann. Large-scale molecular-dynamics simulations of martensitic nucleation and shape-memory effects in transition metal alloys. *Phase Transitions*, 65:79–108, 1999.

P. Entel, R. Meyer, and K. Kadau. Molecular dynamics simulations of martensitic transitions. *Philosophical Magazine B-Physics of Condensed Matter Statistical Mechanics Electronic Optical and Magnetic Properties*, 80(2):183–194, 2000.

O. Eriksson, J. M. Wills, and D. Wallace. Electronic, quasi-harmonic, and anharmonic entropies of transition-metals. *Physical Review B*, 46:5221–5228, 1992.

N. S. Gillis, N. R. Werthamer, and T. R. Koehler. Properties of crystalline Argon and Neon in the self-consistent phonon approximation. *Physics Review B*, 165(3):951–959, 1968.

B. C. Goo and C. Lexcellent. Micromechanics based modeling of two-way memory effect of a single crystalline shape memory alloy. *Acta Metallurgica*, 45:727–737, 1997.

M. Grujicic and P. Dang. Computer simulation of martensitic transformation in Fe-Ni face-centered cubic alloys. *Materials Science & Engineering A*, 201:194–204, 1995.

V. S. Guthikonda and R. S. Elliott. Stability and elastic properties of the stress-free B2 (CsCl-type) crystal for the Morse pair potential model. *Journal of Elasticity*, 92:151–186, 2008a.

V. S. Guthikonda and R. S. Elliott. Stability and elastic properties of the stress-free B2 (CsCl-type) crystal for the Morse pair potential model. *Journal of Elasticity*, 92(2):151–186, 2008b.

V. S. Guthikonda and R. S. Elliott. Towards an effective interaction potential model for the shape memory alloy AuCd, 2008c. AEM Report 2008-1.

V. S. Guthikonda and R. S. Elliott. An effective interaction potential model for the shape memory alloy AuCd. *Continuum Mechanics and Thermodynamics*, 21(4):269–295, 2009.

V. S. R. Guthikonda, M. K. Kiran, S. M. Sivakumar, and A. R. Srinivasa. On smeared and micromechanical approaches to modeling martensitic transformations in SMA. *Nonlinear Analysis: Real World Applications*, 9:990–1011, 2008.

W. Heisenberg. *The Physical Principles of Quantum Theory*. Uiversity of Chicago Press, Chicago, 1930.

D. J. Hoh, B. L. Hoh, A. P. Amar, and M. Y. Wang. Shape memory alloys: Metallurgy, biocompatibility, and biomechanics for neurosurgical applications. *Neurosurgery*, 64:199–214, 2009.

P. Hohenberg. Inhomogeneous electron gas. *Physical Review B*, 136:B864–B871, 1964.

D. J. Hooton. A new treatment of anharmonicity in lattice thermodynamics 1. *Philosophical Magazine*, 46:422–432, 1955a.

D. J. Hooton. A new treatment of anharmonicity in lattice thermodynamics 2. *Philosophical Magazine*, 46:433–442, 1955b.

D. J. Hooton. The use of a model in anharmonic lattice dynamics. *Philosophical Magazine*, 3:49–54, 1958.

L. V. Hove, N. M. Hugenholtz, and L. P. Howland. *Quantum Theory of Many Particle Systems*. Benjamin, New York, 1961.

K. Huang and M. Born. *Dynamical Theory of Crystal Lattices*. Oxford University Press, 1962.

M. S. Huang and L. C. Brinson. A multivariant model for single crystal shape memory alloys. *Journal of the Mechanics and Physics of Solids*, 46:1379–1409, 1998.

X. Huang, C. Bungarao, V. Godlevsky, and K. M. Rabe. Lattice instabilities of cubic NiTi from first principles. *Physical Review B-Condensed Matter*, 65(1):1–5, 2001.

X. Huang, K. M. Rabe, and G. J. Ackland. Crystal structures and shape-memory behavior of NiTi. *Nature Materials*, 2(5):307–311, 2003.

R. Hultgren, P. D. Desai, D. T. Hawkins, M. Gleiser, and K. K. Kelley. *Selected Values of the Thermodynamic Properties of Metals and Alloys*. John Wiley & Sons Inc, 1963.

R. Hultgren, P. D. Desai, D. T. Hawkins, M. Gleiser, and K. K. Kelley. *Selected Values of the Thermodynamic Properties of Binary Alloys*. John Wiley & Sons Inc, 1973.

H. Ishida and Y. Hiwatari. MD simulation of martensitc transformations in TiNi alloys with MEAM. *Molecular Simulation*, 33:459–461, 2007.

Y. Ivshin and T. J. Pence. A constitutive model for hysteretic phase transition behavior. *International Journal of Engineering Science*, 32:681–704, 1994.

R. D. James and K. F. Hane. Martensitic transformations and shape-memory materials. *Acta Materialia*, 48(1):197–222, 2000.

R. D. James, R. V. Kohn, and T. W. Shield. Modeling of branched needle microstructures at the edge of a martensite laminate. *Journal De Physique IV*, 5(C8):253–259, 1995.

R. D. James and Z. Zhang. A way to search for multiferroic materials with "unlikely" combinations of physical properties. In A. Planes, L. Manosa, and A. Saxena, editors, *Magnetism and Structure in Functional Materials*, volume 79 of *Springer Series in Materials Science*, chapter 9, pages 159–176. Springer, 2006.

S. C. Johnson and T. D. Gutierrez. Visualizing the phonon wave function. *American Journal of Physics*, 70:227–237, 2002.

V. Jusuf. *Algorithms for Branch-Following and Critical Point Identification in the Presence of Symmetry.* Master's thesis, Department of Aerospace Engineering and Mechanics, The University of Minnesota, Minneapolis, MN, U.S.A., 2010.

P. G. Laing, A. B. Ferguson, and E. S. Hodges. Tissue reaction in rabbit muscle exposed to metallic implants. *Journal of Biomedical Materials Research*, 1(1):135–149, 1967.

P. H. Leo, T. H. Shield, and O. P. Bruno. Transient heat-transfer effects on the pseudoelastic behavior of shape-memory wires. *Acta Metallurgica ET Materialia*, 41(8):2477–2485, 1993.

C. Liang and A. Rogers. One-dimensional thermomechanical constitutive relations for shape memory materials. *Journal of Intelligent Material Systems and Structures*, 1(2):207–234, 1990.

Z. K. Lu and G. J. Weng. Martensitic transformations and stress-strain relations of shape-memory alloys. *Journal of the Mechanics of Physics of Solids*, 45:1905–1928, 1997.

K. Masuda-Jindo, S. R. Nishitani, and V. V. Huang. hcp-bcc structural phase transformation of Titanium: Analytic model calculations. *Physical Review B*, 70(184122), 2004.

Mathworks. 2009. http://www.mathworks.com.

T. May, W. Muller, and D. Strauch. Anharmonic lattice dynamics and neutron-scattering spectra in bcc transition metals. *Physical Review B*, 57:5758–5763, 1998.

T. Mehaddene, J. Neuhaus, W. Petry, K. Hradil, P. Bourges, and A. Hiess. Phonon dispersions of Ni-Mn-Al shape memory alloy. *Materials Science and Engineering A - Structural Material Properties Microstructure and Processing*, 481(SI):197–200, 2008.

R. Meyer and P. Entel. Martensite-austenite transition and phonon dispersion curves of $Fe_{1-x}Ni_x$ studied by molecular-dynamics simulations. *Physical Review B*, 57(9):5140–5147, 1998.

E. G. Moroni, G. Grimvall, and T. Jarlborg. Free energy contributions to the hcp-bcc transformation in transition metals. *Physical Review Letters*, 76:2758–2761, 1996.

N. Nakanishi, T. Mori, S. Miura, Y. Murakami, and S. Kachi. Pseudoelasticity in Au-Cd thermoelastic martensite. *Philosophical Magazine*, 28:277–292, 1973.

R. B. Nelson. Simplified calculation of eigenvector derivatives. *AIAA Journal*, 14:1201–1205, 1976.

S. R. Nishitani, H. Kawabe, and M. Aoki. First-principles calculations on bcc-hcp transition of titanium. *Material Science and Engineering A-Structural Materials Properties Microstructure and Processing*, 312:77–83, 2001.

T. Ohba, Y. Emura, S. Miyazaki, and K. Otsuka. Crystal structure of γ_2' martensite in Au-47.5%Cd alloy. *Materials Transactions JIM*, 31(1):12–17, 1990.

A. Olander. The crystal structure of AuCd. *Zeitschrift Fur Kristallographie*, 83(1/2):145–148, 1932.

K. Otsuka and C. M. Wayman. *Shape Memory Materials*. Cambridge University Press, 1998.

S. Ozgen and O. Adiguzel. Molecular dynamics simulations of diffusionless phase transformation in quenched NiAl alloy model. *Journal of Physics and Chemistry of Solids*, 64(3):459–464, 2003.

K. Parlinski, M. Parlinska, and R. Gotthardt. Phonons in austenite and martensite NiTi crystals. *Journal De Physique IV*, 112:635–638, 2003.

K. Parlinski and M. Parlinska-Wojtan. Lattice dynamics of NiTi austenite, martensite, and R phase. *Physical Review B*, 67(064307):1–8, 2002.

E. Patoor, A. Eberhardt, and M. Berveiller. Thermomechanical behavior of shape memory alloys. *Archives of Mechanics*, 40(5-6):775–794, 1988.

E. Patoor, A. Eberhardt, and M. Berveiller. Micromechanical modelling of the shape memory alloys. *Pitman Research Notes in Mathematics Series*, 296:38–54, 1993.

K. Persson, M. Ekman, and V. Ozolins. Phonon instabilities in bcc Sc, Ti, La, and Hf. *Physical Review B*, 61:11221–11224, 2000.

A. Petit and P. L. Dulong. Recherches sur quelques points importants de la théorie de la chaleur. *Annales de Chimie et de Physique*, 10:395–413, 1819.

M. Pitteri and G. Zanzotto. *Continuum Models for Phase Transitions and Twinning in Crystals*, volume 19 of *Applied Mathematics*. CRC Press, 2002.

W. H. Press, S. A. Teukolsky, W. T. Vetterling, and B. P. Flannery. *Numerical Recipes in C: The Art of Scientific Computing*. Cambridge University Press, 1992.

J. L. M. Putters, D. M. K. S. K. Sukul, G. R. D. Zeeuw, A. Bijma, and P. A. Besselink. Comparative cell culture effects of shape memory metal <nitinol ®>, Nickel and Titanium: A biocompatibility estimation. *European Surgical Research*, 24(6):378–382, 1992.

X. Ren, N. Miura, J. Zhang, K. Otsuka, K. Tanaka, M. Koiwa, T. Suzuki, and Y. I. Chumlyakov. A comparative study of elastic constants of Ti-Ni-based alloys prior to martensitic transformation. *Material Science and Engineering A - Structural Mateirals Properties Microstructure and Processing*, 312(1–2):196–206, 2001.

S. Rubini and P. Ballone. Martensitic transformations and phonon localization in Ni-Al alloys by atomistic simulations. *Meccanica*, 30:439–448, 1995.

F. Seitz and D. Turnbull. *Solid State Physics: Advances in Research and Applications*, volume 12. Academic Press, 1961.

Y. Shao, P. C. Clapp, and J. A. Rifkin. Molecular dynamics simulation of martensitic transformations in NiAl. *Metallurgical and Materials Transactions A*, 27A:1477–1489, 1996.

J. A. Shaw. *Material Instabilities in a Nickel-Titanium Shape Memory Alloy.* Phd thesis, The Univeristy of Texas at Austin, Austin, TX 78712, 1997.

J. A. Shaw. A thermomechanical model for a 1-D shape memory alloy wire with propagating instabilities. *International Journal of Solids and Structures*, 39(5):1275–1305, 2002.

J. A. Shaw and S. Kyriakides. Thermomechanical aspects of NiTi. *Journal of the Mechanics and Physics of Solids*, 43(8):1243–1281, 1995.

T. W. Shield. Orientation dependence of the pseudoelastic behavior of single-crystals of Cu-Al-Ni in tension. *Journal of the Mechanics and Physics of Solids*, 43(6):869–895, 1995.

R. C. Shukla. Derivation of the Self-Consistent Phonon Theory from Zubarev Type Green's Function. *Physica Status Solidi B*, 205:481–492, 1998.

R. C. Shukla and E. R. Cowley. Inclusion of higher order anharmonic contributions in self-consistent phonon theory. *Physica Review B*, 62(5):3232–3236, 2000.

M. B. Smirnov. Lattice dynamics and thermal expansion of quartz. *Physical Review B*, 59:4036–4043, 1999.

P. Souvatzis, O. Eriksson, M. I. Katsnelson, and S. P. Rudin. Entropy driven stabilization of energetically unstable crystal structures explained from first principles theory. *Physical Review Letters*, 100(095901), 2008.

P. Souvatzis, O. Eriksson, M. I. Katsnelson, and S. P. Rudin. The self-consistent ab initio lattice dynamical method. *Computational Material Science*, 44:888–894, 2009.

P. Souvatzis, D. Legut, O. Eriksson, and M. I. Katsnelson. Ab initio study of interacting lattice vibrations and stabilization of the beta phase in Ni-Ti shape-memory alloy. *Physical Review B*, 81(092201), 2010.

P. Souvatzis and S. P. Rudin. Dynamical stabilization of cubic ZrO_2 by phonon-phonon interactions: Ab initio calculations. *Physical Review B*, 78(184304), 2008.

M. Sternik and K. Parlinski. Free-energy calculations for the cubic ZrO_2 crystal as an example of a system with a soft mode. *Journal of Chemical Physics*, 123(204708), 2005.

Q. P. Sun and K. C. Hwang. Micromechanics modelling for the constitutive behavior of polycrystalline shape memory alloys–I. Derivation of general relations. *Journal of the Mechanics and Physics of Solids*, 41(1):1–17, 1993a.

Q. P. Sun and K. C. Hwang. Micromechanics modelling for the constitutive behavior of polycrystalline shape memory alloys–II. Study of the individual phenomena. *Journal of the Mechanics and Physics of Solids*, 41(1):19–33, 1993b.

E. B. Tadmor, G. S. Smith, N. Bernstein, and E. Kaxiras. Mixed finite element and atomistic formulations for complex crystals. *Physical Review B*, 59(1):235–245, 1999.

K. Tanaka and S. Nagaki. A thermomechanical description of materials with internal variables in the process of phase-transitions. *Ingenieur Archiv*, 51(5):287–299, 1982.

P. Villars, L. D. Calvert, and W. B. Pearson. *Pearson's handbook of crystallographic data for intermetallic phases*. Metals Park, 1985.

A. Vivet and C. Lexcellent. Micromechanical modelling for tension-compression pseudoelastic behavior of AuCd single crystals. *The European Journal Applied Physics*, 4(2):125–132, 1998.

L. Vocadlo, D. Alfe, M. J. Gillan, I. G. Wood, J. P. Brodholt, and G. D. Price. Possible thermal and chemical stabilization of body-centred-cubic iron in the earth's core. *Nature*, 424:536–539, 2003.

D. C. Wallace. Renormalization and statistical mechanics in many-particle systems. II. statistical perturbation method. *Physical Review*, 152(1):261–269, 1966.

D. C. Wallace. *Thermodynamics of Crystals*. Courier Dover Publications, 1998.

D. C. Wallace. *Statistical Physics of Crystals and Liquids*. World Scientific, 2002.

J. Wang, Y. Wang, R. Schaublin, C. Abromeit, and R. Gotthardt. The effect of point defects on the martensitic phase transformation. *Material Science and Engineering A - Structural Material Properties Microstructure and Processing*, 438:102–108, 2006.

J. C. Watah, N. L. O'Dell, B. B. Singh, M. Ghazi, G. M. Whitford, and P. E. Lockwood. Relating Nickel induced tissue inflammation to Nickel release in vivo. *Journal of Biomedical Materials Research*, 58(5):537–544, 2001.

J. H. Weiner. *Statistical Mechanics of Elasticity*. Dover Publications, 2002.

Y. Y. Ye, C. T. Chan, and K. M. Ho. Structural and electronic properties of the martensitic alloys TiNi, TiPd, and TiPt. *Physical Review B*, 56(7):3678–3689, 1997.

C. Zener. Contributions to the theory of beta-phase alloys. *Physical Review*, 71(12):846–851, 1947.

A. Zheludev, S. M. Shapiro, P. Wochner, A. Schwartz, M. Wall, and L. E. Tanner. Phonon anomaly, central peak, and microstructures in Ni_2MnGa. *Physical Review B*, 51(17):11310–11314, 1995.

S. Zirinsky. The temperature dependence of the elastic constants of Gold-Cadmium alloys. *Acta Metallurgica*, 4(2):164–171, 1956.

Appendix A

Bulk modulus

The instantaneous second-order elastic moduli may be obtained by defining a new energy density with reference configuration taken as the current configuration $(\mathbf{U}_0;\theta_0)$, $\overset{\approx}{W}{}^{*}(\mathbf{U}^*;\theta_0) \equiv \overset{\approx}{W}(\mathbf{U}^*\cdot\mathbf{U}_0;\theta_0)/\det(\mathbf{U}_0)$. The instantaneous moduli are,

$$\mathcal{L}_{ijkl} \equiv \left.\frac{\partial^2 \overset{\approx}{W}{}^{*}}{\partial U^*_{ij}\partial U^*_{kl}}\right|_{(\mathbf{U}^*=\mathbf{I};\theta_0)} \tag{A.1}$$

The derivation of $\mathcal{L}_{ijkl}$ is as follows:

$$\begin{aligned}
\frac{\partial \overset{\approx}{W}{}^{*}}{\partial U^*_{ij}} &= \frac{1}{\det(\mathbf{U}_0)}\left[\frac{\partial \overset{\approx}{W}}{\partial U_{pq}}\frac{\partial\left(U^*_{pr}U_{0rq}\right)}{\partial U^*_{ij}}\right] \\
&= \frac{1}{\det(\mathbf{U}_0)}\left[\frac{\partial \overset{\approx}{W}}{\partial U_{pq}}\frac{1}{2}\left(\delta_{pi}\delta_{rj}+\delta_{pj}\delta_{ri}\right)U_{0rq}\right] \\
&= \frac{1}{2\det(\mathbf{U}_0)}\left[\frac{\partial \overset{\approx}{W}}{\partial U_{iq}}U_{0jq}+\frac{\partial \overset{\approx}{W}}{\partial U_{jq}}U_{0iq}\right].
\end{aligned} \tag{A.2}$$

$$
\begin{aligned}
\mathcal{L}_{ijkl} &= \left.\frac{\partial^2 \overset{\approx}{W}{}^*}{\partial U^*_{ij}\partial U^*_{kl}}\right|_{(\mathbf{U}^*=\mathbf{I};\theta_0)} \\
&= \left.\frac{\partial}{\partial U^*_{kl}}\left(\frac{1}{2\det(\mathbf{U}_0)}\left[\frac{\partial \overset{\approx}{W}}{\partial U_{iq}}U_{0jq}+\frac{\partial \overset{\approx}{W}}{\partial U_{jq}}U_{0iq}\right]\right)\right|_{(\mathbf{U}^*=\mathbf{I};\theta_0)} \\
&= \left.\frac{1}{2\det(\mathbf{U}_0)}\left(\frac{\partial^2 \overset{\approx}{W}}{\partial U_{iq}\partial U_{rs}}U_{0jq}\frac{\partial\left(U^*_{rt}U_{0ts}\right)}{U^*_{kl}}+\frac{\partial^2 \overset{\approx}{W}}{\partial U_{jq}\partial U_{rs}}U_{0iq}\frac{\partial\left(U^*_{rt}U_{0ts}\right)}{U^*_{kl}}\right)\right|_{(\mathbf{U}^*=\mathbf{I};\theta_0)} \\
&= \frac{1}{2\det(\mathbf{U}_0)}\left(\frac{\partial^2 \overset{\approx}{W}}{\partial U_{iq}\partial U_{rs}}U_{0jq}\frac{1}{2}\left(\delta_{rk}\delta_{tl}+\delta_{rl}\delta_{tk}\right)U_{0ts}+\right. \\
&\qquad \left.\left.\frac{\partial^2 \overset{\approx}{W}}{\partial U_{jq}\partial U_{rs}}U_{0iq}\frac{1}{2}\left(\delta_{rk}\delta_{tl}+\delta_{rl}\delta_{tk}\right)U_{0ts}\right)\right|_{(\mathbf{U}^*=\mathbf{I};\theta_0)} \\
&= \frac{1}{4\det(\mathbf{U}_0)}\left(\frac{\partial^2 \overset{\approx}{W}}{\partial U_{iq}\partial U_{ks}}U_{0jq}U_{0ls}+\frac{\partial^2 \overset{\approx}{W}}{\partial U_{iq}\partial U_{ls}}U_{0jq}U_{0ks}+\right. \\
&\qquad \left.\left.\frac{\partial^2 \overset{\approx}{W}}{\partial U_{jq}\partial U_{ks}}U_{0iq}U_{0ls}+\frac{\partial^2 \overset{\approx}{W}}{\partial U_{jq}\partial U_{ls}}U_{0iq}U_{0ks}\right)\right|_{(\mathbf{U}^*=\mathbf{I};\theta_0)}.
\end{aligned}
\tag{A.3}
$$

Note that the symmetrization is required to ensure that $\mathcal{L}_{ijkl}$ has the appropriate minor symmetries. For small deformations from the current configuration the incremental stress/strain relationship for the stress-free configuration $(\mathbf{U}^* = \mathbf{I}; \theta_0)$ is given by

$$
\delta\boldsymbol{\sigma} = \boldsymbol{\mathcal{L}} : \delta\boldsymbol{\epsilon}, \tag{A.4}
$$

where $\delta\boldsymbol{\sigma}$ is the increment of Cauchy stress and $\delta\boldsymbol{\epsilon}$ is the increment of small strain.

The instantaneous bulk modulus K relates the change in volume to an increment in an applied hydrostatic pressure. That is,

$$
K = \frac{\delta P}{\delta V}. \tag{A.5}
$$

Taking

$$\delta\boldsymbol{\sigma} = \delta P\ \mathbf{I}, \tag{A.6}$$

where $\mathbf{I}$ is the identity tensor, and substituting Eq. (A.6) into Eq. (A.4) leads to (after rearrangement)

$$\delta\boldsymbol{\epsilon} = \boldsymbol{\mathcal{L}}^{-1} : \delta\boldsymbol{\sigma} = \delta P \left(\boldsymbol{\mathcal{L}}^{-1} : \mathbf{I}\right). \tag{A.7}$$

Now, a change in volume is calculated to leading order by taking the trace of $\delta\boldsymbol{\epsilon}$ which gives

$$\delta V = \mathbf{I} : \delta\boldsymbol{\epsilon} = \delta P \left(\mathbf{I} : \boldsymbol{\mathcal{L}}^{-1} : \mathbf{I}\right). \tag{A.8}$$

Finally, substituting Eq. (A.8) into Eq. (A.5) gives the instantaneous bulk modulus K for a material as

$$K = \frac{1}{\left[\mathbf{I} : \boldsymbol{\mathcal{L}}^{-1} : \mathbf{I}\right]}. \tag{A.9}$$

Some authors define the instantaneous bulk modulus as the proportionality constant relating a change in the spherical part of the stress to an increment of an applied pure dilatation. That is

$$K = \frac{\delta P}{\delta V}, \tag{A.10}$$

where

$$\delta\boldsymbol{\epsilon} = \frac{1}{3}\delta V\ \mathbf{I}. \tag{A.11}$$

Substituting Eq. (A.11) into Eq. (A.4) and recalling that $\mathbf{I} : \delta\boldsymbol{\sigma} = 3\ \delta P$ results in

$$3\ \delta P = \mathbf{I} : \delta\boldsymbol{\sigma} = \frac{1}{3}\delta V \left(\mathbf{I} : \boldsymbol{\mathcal{L}} : \mathbf{I}\right). \tag{A.12}$$

From Eq. (A.12), the instantaneous bulk modulus K is found to be

$$K = \frac{1}{9} \left[\mathbf{I} : \boldsymbol{\mathcal{L}} : \mathbf{I} \right]. \tag{A.13}$$

As mentioned in Section 2.2, these two definitions (Eq. (A.9) and Eq. (A.13)) are equal only for cubic or isotropic materials. Comparing the derivation of Eqs. (A.9) and (A.13), Eq. (A.9) more accurately represents the common interpretation of the instantaneous bulk modulus.

Appendix B

Harmonic approximation

The harmonic approximation assumes the atomic vibrations to be very small when compared to the inter-atomic distance. This assumption simplifies the total hamiltonian Eq. (4.5) where the contribution of the third- and higher-order potential energy terms are considered to be negligible. The resulting harmonic hamiltonian of a chain of atoms vibrating about an equilibrium configuration $\overset{o}{\mathbf{u}}$ is given by

$$\begin{aligned}\mathcal{H}_{\mathrm{H}} &= KE + \Phi_0 + \Phi_2, \\ &= \frac{1}{2}\sum_{\left[\substack{\ell \\ \alpha}\right]} m_\alpha \left(\delta\dot{u}\left[\substack{\ell \\ \alpha}\right]\right)^2 + naW(\overset{o}{\mathbf{u}}) + \frac{1}{2}\sum_{\left[\substack{\ell \\ \alpha}\right]}\sum_{\left[\substack{\ell' \\ \alpha'}\right]} \overset{o}{\Phi}\left[\substack{\ell\,\ell' \\ \alpha\alpha'}\right] \delta u\left[\substack{\ell \\ \alpha}\right] \delta u\left[\substack{\ell' \\ \alpha'}\right].\end{aligned} \tag{B.1}$$

Here, the first-order term Φ_1 Eq. (4.17) is dropped due to mechanical equilibrium condition Eq. (4.13) corresponding to an equilibrium configuration $\overset{o}{\mathbf{u}}$.

Rewriting the harmonic hamiltonian Eq. (B.1) in terms of normal mode coordinates Eq. (4.18) results in

$$\mathcal{H}_{\mathrm{H}} = \Phi_0 + \frac{1}{2}\sum_{\left[\substack{k \\ \nu}\right]} \dot{q}^*\left[\substack{k \\ \nu}\right] \dot{q}\left[\substack{k \\ \nu}\right] + \frac{1}{2}\sum_{\left[\substack{k \\ \nu}\right]} \omega^2\left[\substack{k \\ \nu}\right] q^*\left[\substack{k \\ \nu}\right] q\left[\substack{k \\ \nu}\right], \tag{B.2}$$

where $\omega^2\left[\substack{k \\ \nu}\right]$ are the eigenvalues of the harmonic *dynamical matrix* Eq. (4.20) and $q^*\left[\substack{k \\ \nu}\right]$ is the complex conjugate of $q\left[\substack{k \\ \nu}\right]$.

The harmonic partition function Z_{H} corresponding to an equilibrium configuration

$\overset{o}{\mathbf{u}}$ is given by

$$Z_{\mathrm{H}}(\overset{o}{\mathbf{u}};T) = \int \exp\left\{-\frac{\mathcal{H}_{\mathrm{H}}}{k_B T}\right\} d\mathbf{p}\; d\mathbf{q}, \tag{B.3}$$

where $\mathbf{p} = \left\{p\begin{bmatrix}k\\ \nu\end{bmatrix}\right\}$, $\mathbf{q} = \left\{q\begin{bmatrix}k\\ \nu\end{bmatrix}\right\}$, $\mathcal{H}_{\mathrm{H}}$ is the harmonic hamiltonian Eq. (B.2), k_B is the Boltzmann constant, and T is the thermodynamic temperature.

Using the relation

$$\int_{-\infty}^{+\infty} \exp\left\{-ax^2\right\} dx = \left(\frac{\pi}{a}\right)^{1/2}, \tag{B.4}$$

the harmonic partition function Eq. (B.3) can be analytically evaluated and the final resulting expression is given by

$$Z_{\mathrm{H}}(\overset{o}{\mathbf{u}};T) = \exp\left\{-\frac{\Phi_0(\overset{o}{\mathbf{u}})}{k_B T}\right\} \prod_{\begin{bmatrix}k\\ \nu\end{bmatrix}} \left[\frac{k_B T}{\hbar\omega\begin{bmatrix}k\\ \nu\end{bmatrix}}\right]. \tag{B.5}$$

The harmonic Helmholtz free energy is given by

$$\begin{aligned}\mathcal{F}_{\mathrm{H}}(\overset{o}{\mathbf{u}};T) &= -k_B T\ \mathrm{ln}\mathrm{Z}_{\mathrm{H}}, \\ &= \Phi_0(\overset{o}{\mathbf{u}}) - k_B T \sum_{\begin{bmatrix}k\\ \nu\end{bmatrix}} \ln\left[\frac{k_B T}{\hbar\omega\begin{bmatrix}k\\ \nu\end{bmatrix}}\right].\end{aligned} \tag{B.6}$$

The harmonic Helmholtz free energy Eq. (B.6) is homogenized using the CB kinematics Eq. (5.26) such that the harmonic CB Helmholtz free energy is given by

$$\tilde{\mathcal{F}}_{\mathrm{H}}(\overset{o}{\mathrm{U}}, \overset{o}{\mathbf{S}};T) \equiv \mathcal{F}_{\mathrm{H}}(\overset{o}{\mathbf{u}}(\overset{o}{\mathrm{U}}, \overset{o}{\mathbf{S}});T), \tag{B.7}$$

where $\mathcal{F}_{\mathrm{H}}(\overset{o}{\mathbf{u}}(\overset{o}{\mathrm{U}}, \overset{o}{\mathbf{S}});T)$ is the harmonic free energy Eq. (B.6) such that the atomic DOF's are restricted by CB kinematics. Corresponding to Eq. (B.6), the harmonic CB Helmholtz free energy $\tilde{\mathcal{F}}$ is given by

$$\tilde{\mathcal{F}}_{\mathrm{H}}(\overset{o}{\mathrm{U}}, \overset{o}{\mathbf{S}};T) = \Phi_0(\overset{o}{\mathrm{U}}, \overset{o}{\mathbf{S}}) - k_B T \sum_{\begin{bmatrix}k\\ \nu\end{bmatrix}} \ln\left[\frac{k_B T}{\hbar\omega\begin{bmatrix}k\\ \nu\end{bmatrix}}\right]. \tag{B.8}$$

Here, the harmonic approximation assumes the frequencies of atomic vibrations $\omega^2\begin{bmatrix}k\\ \nu\end{bmatrix}$ to be constant corresponding to the static equilibrium configuration.

The harmonic HC free energy density corresponding to Eq. (5.37) is given by

$$\overset{\approx}{\mathcal{F}}_{\mathrm{H}}(\overset{o}{\mathrm{U}};T) \equiv \frac{1}{na}\tilde{\mathcal{F}}_{\mathrm{H}}(\overset{o}{\mathrm{U}},\overset{o}{\mathbf{S}}(\overset{o}{\mathrm{U}},T);T), \tag{B.9}$$

where a is the unit cell length and n is the total number of unit cells in the chain.

Corresponding to Eq. (5.38), the entropy per mole S of a general M-chain is given by

$$\begin{aligned} S &= -\frac{\partial \overset{\approx}{\mathcal{F}}_{\mathrm{H}}}{\partial T}\bigg|_{(\overset{o}{\mathrm{U}};T)} \frac{aN_A}{M}, \\ &= \left(k_B \sum_{\left[\substack{k \\ \nu}\right]} \ln\left[\frac{k_B T}{\hbar\omega_{\left[\substack{k \\ \nu}\right]}}\right] + k_B T \sum_{\left[\substack{k \\ \nu}\right]} \frac{1}{T} \right) \frac{N_A}{nM}, \\ &= \frac{k_B N_A}{nM} \sum_{\left[\substack{k \\ \nu}\right]} \ln\left[\frac{k_B T}{\hbar\omega_{\left[\substack{k \\ \nu}\right]}}\right] + \frac{k_B N_A}{n}, \end{aligned} \tag{B.10}$$

where n is the total number of unit cells in the chain, a is the reference unit cell length, M is the number of atoms in the unit cell, and N_A is the Avogadro's constant (6.023×10^{23}).

The heat capacity per mole at constant volume C_{v} of a general M-chain corresponding to Eq. (5.41) is given by

$$\begin{aligned} C_{\mathrm{v}} &= -\left(T \frac{\partial^2 \overset{\approx}{\mathcal{F}}_{\mathrm{H}}}{\partial T^2} \right)_{(\overset{o}{\mathrm{U}};T)} \frac{aN_A}{M}, \\ &= -\left(T \left[-k_B \sum_{\left[\substack{k \\ \nu}\right]} \frac{1}{T} - k_B \sum_{\left[\substack{k \\ \nu}\right]} \frac{1}{T} + k_B T \sum_{\left[\substack{k \\ \nu}\right]} \frac{1}{T^2} \right] \right)_{(\overset{o}{\mathrm{U}};T)} \frac{N_A}{nM}, \\ &= \frac{k_B N_A}{n}. \end{aligned} \tag{B.11}$$

Corresponding to Eq. (5.40), the linear thermal expansion α is given by

$$\alpha = -\overset{o}{\mathrm{U}}^{-1} \left[\left(\frac{\partial^2 \overset{\approx}{\mathcal{F}}_{\mathrm{H}}}{\partial \mathrm{U}^2} \right)^{-1} \left(\frac{\partial^2 \overset{\approx}{\mathcal{F}}_{\mathrm{H}}}{\partial \mathrm{U} \partial T} \right) \right]_{(\overset{o}{\mathrm{U}},T)} = 0, \tag{B.12}$$

where $\frac{\partial^2 \widetilde{\widetilde{\mathcal{F}}}_{\mathrm{H}}}{\partial \mathrm{U} \partial T} = 0$ since $\omega\left[\begin{smallmatrix} k \\ \nu \end{smallmatrix}\right]$ are constants corresponding to static equilibrium configuration.

From Eqs. (B.12)–(B.11), it is clear that the classical harmonic approximation predicts the heat capacity to be constant and linear thermal expansion to be zero. This is in contradiction with general experimental observations.

Appendix C

Quasi-harmonic approximation

Quasi-harmonic approximation (QHA) method is an improvement over harmonic approximation method described in Chapter B. In this method, the phonon frequencies $\omega\begin{bmatrix}k\\ \nu\end{bmatrix}$ are calculated using the harmonic approximation. The square of these phonon frequencies are obtained as eigenvalues of the harmonic dynamical matrix Eq. (4.20). However, these frequencies are considered to be dependent on the equilibrium configuration $\overset{o}{\mathbf{u}} \equiv (\overset{o}{\mathrm{U}}, \overset{o}{\mathbf{S}})$. The resultant CB Helmholtz free energy corresponding to Eq. (B.8) is given by

$$\tilde{\mathcal{F}}_{\mathrm{QH}}\left(\overset{o}{\mathrm{U}}, \overset{o}{\mathbf{S}}; T\right) = \Phi_0(\overset{o}{\mathrm{U}}, \overset{o}{\mathbf{S}}) - k_B T \sum_{\begin{bmatrix}k\\ \nu\end{bmatrix}} \ln\left[\frac{k_B T}{\hbar\omega\begin{bmatrix}k\\ \nu\end{bmatrix}}\right], \tag{C.1}$$

where $\omega\begin{bmatrix}k\\ \nu\end{bmatrix} \equiv \omega\begin{bmatrix}k\\ \nu\end{bmatrix}(\overset{o}{\mathrm{U}}, \overset{o}{\mathbf{S}})$.

The HC free energy density corresponding to Eq. (5.37) is given by

$$\overset{\approx}{\mathcal{F}}_{\mathrm{QH}}(\overset{o}{\mathrm{U}}; T) \equiv \frac{1}{na}\tilde{\mathcal{F}}_{\mathrm{QH}}(\overset{o}{\mathrm{U}}, \overset{o}{\mathbf{S}}(\overset{o}{\mathrm{U}}; T); T). \tag{C.2}$$

Corresponding to Eq. (5.38), the entropy per mole S of a general M-chain is given by

$$\begin{aligned} S &= -\frac{\partial \overset{\approx}{\mathcal{F}}_{\mathrm{QH}}}{\partial T}\bigg|_{(\overset{o}{\mathrm{U}};T)} \frac{aN_A}{M} = \left(k_B \sum_{\begin{bmatrix}k\\ \nu\end{bmatrix}} \ln\left[\frac{k_B T}{\hbar\omega\begin{bmatrix}k\\ \nu\end{bmatrix}}\right] + k_B T \sum_{\begin{bmatrix}k\\ \nu\end{bmatrix}} \frac{1}{T}\right)\frac{N_A}{nM}, \\ &= \frac{k_B N_A}{nM} \sum_{\begin{bmatrix}k\\ \nu\end{bmatrix}} \ln\left[\frac{k_B T}{\hbar\omega\begin{bmatrix}k\\ \nu\end{bmatrix}}\right] + \frac{k_B N_A}{n}. \end{aligned} \tag{C.3}$$

Corresponding to Eq. (5.41), the heat capacity per mole at constant volume $C_{\rm v}$ of a general M-chain is given by

$$\begin{aligned} C_{\rm v} &= -\left(T\frac{\partial^2 \overset{\approx}{\mathcal{F}}_{\rm QH}}{\partial T^2} \right)_{\overset{o}{(\mathrm{U};T)}} \frac{aN_A}{M}, \\ &= -\left(T\left[-k_B \sum_{\left[\nu\right]}^{k} \frac{1}{T} - k_B \sum_{\left[\nu\right]}^{k} \frac{1}{T} + k_B T \sum_{\left[\nu\right]}^{k} \frac{1}{T^2} \right] \right)_{\overset{o}{(\mathrm{U};T)}} \frac{N_A}{nM}, \\ &= \frac{k_B N_A}{n}. \end{aligned} \tag{C.4}$$

The linear thermal expansion corresponding to Eq. (5.40) is given by

$$\alpha = -(\overset{o}{\mathrm{U}})^{-1} \left[\left(\frac{\partial^2 \overset{\approx}{\mathcal{F}}_{\rm QH}}{\partial \mathrm{U}^2} \right)^{-1} \left(\frac{\partial^2 \overset{\approx}{\mathcal{F}}_{\rm QH}}{\partial \mathrm{U} \partial T} \right) \right]_{\overset{o}{(\mathrm{U};T)}}, \tag{C.5}$$

where

$$\frac{\partial^2 \overset{\approx}{\mathcal{F}}_{\rm QH}}{\partial \mathrm{U} \partial T} = k_B \sum_{\left[\nu\right]}^{k} \frac{1}{\omega_{\left[\nu\right]}^{k}} \frac{\partial \omega_{\left[\nu\right]}^{k}}{\partial \mathrm{U}}. \tag{C.6}$$

From Eqs. (C.5)–(C.6), it can be observed that the linear thermal expansion using QHA method is not zero where as it is zero from harmonic approximation Eq. (B.12).

Appendix D

Self-consistent equation

The self-consistent equation of Eq. (5.18) is derived in detail starting from Eq. (5.13). The contribution of $\widetilde{\mathcal{PT}}$ in calculating the total partition function Z is minimized by making the first-order contribution of $\widetilde{\mathcal{PT}}$ zero:

$$Z_1 = -\frac{1}{h^{\mathcal{N}}} \int \exp\left\{-\frac{\mathcal{H}_{\text{eff}}}{k_B T}\right\} \left(\frac{\widetilde{\mathcal{PT}}}{k_B T}\right) \, d\mathbf{p} \, d\mathbf{q} = 0, \tag{D.1}$$

where $\mathbf{p} = \left\{p\begin{bmatrix}k\\ \nu\end{bmatrix}\right\}$ and $\mathbf{q} = \left\{q\begin{bmatrix}k\\ \nu\end{bmatrix}\right\}$ indicate the momenta and coordinates corresponding to all modes of vibrations and $\mathcal{H}_{\text{eff}}$ is given by

$$\begin{aligned} \mathcal{H}_{\text{eff}} &= \Phi_0 + \widetilde{KE} + \widetilde{\Phi}_{\text{eff}}, \\ &= \Phi_0 + \frac{1}{2} \sum_{\begin{bmatrix}k\\ \nu\end{bmatrix}} p^* \begin{bmatrix}k\\ \nu\end{bmatrix} p \begin{bmatrix}k\\ \nu\end{bmatrix} + \frac{1}{2} \sum_{\begin{bmatrix}k\\ \nu\end{bmatrix}} \omega_{\text{eff}}^2 \begin{bmatrix}k\\ \nu\end{bmatrix} q^* \begin{bmatrix}k\\ \nu\end{bmatrix} q \begin{bmatrix}k\\ \nu\end{bmatrix}. \end{aligned} \tag{D.2}$$

Factoring out the Φ_0 term in Eq. (D.1) and substituting the terms contained in $\widetilde{\mathcal{PT}}$ results in

$$\int_{\mathbb{R}^{\mathcal{N}}} \int_{\mathbb{R}^{\mathcal{N}}} \exp\left\{-\frac{\widetilde{KE} + \widetilde{\Phi}_{\text{eff}}}{k_B T}\right\} \left(-\widetilde{\Phi}_{\text{eff}} + \widetilde{\Phi}_1 + \widetilde{\Phi}_2 + \widetilde{\Phi}_3 + \widetilde{\Phi}_4 + \dots\right) \, d\mathbf{p} \, d\mathbf{q} = 0, \tag{D.3}$$

where

$$\widetilde{\Phi}_{\text{eff}} = \frac{1}{2}\sum_{\left[\substack{k\\ \nu}\right]} \omega_{\text{eff}}^2\left[\substack{k\\ \nu}\right] q^*\left[\substack{k\\ \nu}\right] q\left[\substack{k\\ \nu}\right], \tag{D.4}$$

$$\widetilde{\Phi}_1 = \sum_{\left[\substack{k\\ \nu}\right]} V_1\left[\substack{k\\ \nu}\right] q\left[\substack{k\\ \nu}\right], \tag{D.5}$$

$$\widetilde{\Phi}_2 = \frac{1}{2}\sum_{\left[\substack{k\\ \nu}\right]} \omega^2\left[\substack{k\\ \nu}\right] q^*\left[\substack{k\\ \nu}\right] q\left[\substack{k\\ \nu}\right], \tag{D.6}$$

$$\widetilde{\Phi}_3 = \frac{1}{3!}\sum_{\left[\substack{k\\ \nu}\right]}\sum_{\left[\substack{k'\\ \nu'}\right]}\sum_{\left[\substack{k''\\ \nu''}\right]} V_3\left[\substack{kk'k''\\ \nu\nu'\nu''}\right] q\left[\substack{k\\ \nu}\right] q\left[\substack{k'\\ \nu'}\right] q\left[\substack{k''\\ \nu''}\right] \Delta(k+k'+k''), \tag{D.7}$$

$$\widetilde{\Phi}_4 = \frac{1}{4!}\sum_{\left[\substack{k\\ \nu}\right]}\sum_{\left[\substack{k'\\ \nu'}\right]}\sum_{\left[\substack{k''\\ \nu''}\right]}\sum_{\left[\substack{k'''\\ \nu'''}\right]} V_4\left[\substack{kk'k''k'''\\ \nu\nu'\nu''\nu'''}\right] q\left[\substack{k\\ \nu}\right] q\left[\substack{k'\\ \nu'}\right] q\left[\substack{k''\\ \nu''}\right] q\left[\substack{k'''\\ \nu'''}\right] \Delta(k+k'+k''+k'''). \tag{D.8}$$

Here, the function $\Delta(K)$ is defined such that $\Delta(K) = 1$ if K is a reciprocal lattice point and zero otherwise.

Separating the momenta in Eq. (D.3) results in

$$\int_{\mathbb{R}^{\mathcal{N}}} \exp\left\{-\frac{\widetilde{\Phi}_{\text{eff}}}{k_B T}\right\}\left(-\widetilde{\Phi}_{\text{eff}} + \widetilde{\Phi}_1 + \widetilde{\Phi}_2 + \widetilde{\Phi}_3 + \widetilde{\Phi}_4 + \dots\right)\, d\mathbf{q} = 0. \tag{D.9}$$

Substituting $\widetilde{\Phi}_{\text{eff}}$ from Eq. (5.10) into Eq. (D.9) results in

$$\int_{\mathbb{R}^{\mathcal{N}}} \exp\left\{-\frac{\sum_{\left[\substack{k_1\\ \nu_1}\right]} \omega_{\text{eff}}^2\left[\substack{k_1\\ \nu_1}\right] q^2\left[\substack{k_1\\ \nu_1}\right]}{2k_B T}\right\}\left(-\widetilde{\Phi}_{\text{eff}} + \widetilde{\Phi}_1 + \widetilde{\Phi}_2 + \widetilde{\Phi}_3 + \widetilde{\Phi}_4 + \dots\right)\, d\mathbf{q} = 0. \tag{D.10}$$

The analytical evaluation of Eq. (D.10) involves extensive use of the following integral

relations

$$\int_{-\infty}^{\infty} \exp\left\{-ax^2\right\}\, dx = \left(\frac{\pi}{a}\right)^{1/2}, \tag{D.11}$$

$$\int_{-\infty}^{\infty} \exp\left\{-ax^2\right\}x^2\, dx = \frac{1}{2}\left(\frac{\pi}{a^3}\right)^{1/2}, \tag{D.12}$$

$$\int_{-\infty}^{\infty} \exp\left\{-ax^2\right\}x^4\, dx = \frac{3}{4}\left(\frac{\pi}{a^5}\right)^{1/2}, \tag{D.13}$$

$$\int_{-\infty}^{\infty} \exp\left\{-ax^2\right\}x^{2s-1}\, dx = 0 \quad \text{for s} \in \mathbb{Z}. \tag{D.14}$$

The integral in Eq. (D.10) is symmetric with respect to the sign of the coordinate $\mathbf{q}$. This implies that based on Eq. (D.14) the odd power terms $\widetilde{\Phi}_1, \widetilde{\Phi}_3, \ldots$ in Eq. (D.10) average out to zero resulting in

$$\int_{\mathbb{R}^{\mathcal{N}}} \exp\left\{-\frac{\sum_{\left[\substack{k_1\\ \nu_1}\right]} \omega^2_{\text{eff}}\left[\substack{k_1\\ \nu_1}\right] q^2\left[\substack{k_1\\ \nu_1}\right]}{2k_BT}\right\}\left(-\widetilde{\Phi}_{\text{eff}} + \widetilde{\Phi}_2 + \widetilde{\Phi}_4 + \ldots\right)\, d\mathbf{q} = 0. \tag{D.15}$$

Eq. (D.15) can be analytically solved. Here we will consider each of the first three terms in the integral of Eq. (D.15) separately for clarity. The first part of the integral is given by

$$I_1 = -\int_{\mathbb{R}^{\mathcal{N}}} \exp\left\{-\frac{\sum_{\left[\substack{k_1\\ \nu_1}\right]} \omega^2_{\text{eff}}\left[\substack{k_1\\ \nu_1}\right] q^2\left[\substack{k_1\\ \nu_1}\right]}{2k_BT}\right\}\widetilde{\Phi}_{\text{eff}}\, d\mathbf{q}. \tag{D.16}$$

Substituting Eq. (D.4) into Eq. (D.16) results in

$$I_1 = -\frac{1}{2}\sum_{\left[\substack{k\\ \nu}\right]} \omega^2_{\text{eff}}\left[\substack{k\\ \nu}\right] \int_{\mathbb{R}^{\mathcal{N}}} \exp\left\{-\frac{\sum_{\left[\substack{k_1\\ \nu_1}\right]} \omega^2_{\text{eff}}\left[\substack{k_1\\ \nu_1}\right] q^2\left[\substack{k_1\\ \nu_1}\right]}{2k_BT}\right\} q^2\left[\substack{k\\ \nu}\right]\, d\mathbf{q}. \tag{D.17}$$

Using Eqs. (D.11) and (D.12), the integral I_1 in Eq. (D.17) can be solved and the

resulting final form of I_1 is given by

$$\begin{aligned} I_1 &= -\frac{1}{2}\sum_{\begin{bmatrix}k\\ \nu\end{bmatrix}} \omega_{\text{eff}}^2\begin{bmatrix}k\\ \nu\end{bmatrix}\left[\frac{\sqrt{\pi}}{2}\left(\frac{2k_BT}{\omega_{\text{eff}}^2\begin{bmatrix}k\\ \nu\end{bmatrix}}\right)^{3/2}\right]\left\{\prod_{\substack{\begin{bmatrix}k_1\\ \nu_1\end{bmatrix}\neq\begin{bmatrix}k\\ \nu\end{bmatrix}}}\left[\sqrt{\pi}\left(\frac{2k_BT}{\omega_{\text{eff}}^2\begin{bmatrix}k_1\\ \nu_1\end{bmatrix}}\right)^{1/2}\right]\right\}, \\ &= -\sum_{\begin{bmatrix}k\\ \nu\end{bmatrix}}\left(\frac{k_BT}{2}\right)\left\{\prod_{\begin{bmatrix}k_1\\ \nu_1\end{bmatrix}}\left[\sqrt{\pi}\left(\frac{2k_BT}{\omega_{\text{eff}}^2\begin{bmatrix}k_1\\ \nu_1\end{bmatrix}}\right)^{1/2}\right]\right\}, \end{aligned} \tag{D.18}$$

Here, the terms $\left(\frac{k_BT}{2}\right)$ and $\left\{\prod_{\begin{bmatrix}k_1\\ \nu_1\end{bmatrix}}\left[\sqrt{\pi}\left(\frac{2k_BT}{\omega_{\text{eff}}^2\begin{bmatrix}k_1\\ \nu_1\end{bmatrix}}\right)^{1/2}\right]\right\}$ are independent of the summation $\begin{bmatrix}k\\ \nu\end{bmatrix}$. These terms are retained inside the summation of Eq. (D.18) due to the advantage in rearranging the terms when all three integrals corresponding to Eq. (D.15) are combined later.

The second part of the integral in Eq. (D.15) is given by

$$I_2 = \int_{\mathbb{R}^{\mathcal{N}}} \exp\left\{-\frac{\sum_{\begin{bmatrix}k_1\\ \nu_1\end{bmatrix}} \omega_{\text{eff}}^2\begin{bmatrix}k_1\\ \nu_1\end{bmatrix} q^2\begin{bmatrix}k_1\\ \nu_1\end{bmatrix}}{2k_BT}\right\}\widetilde{\Phi}_2\ d\mathbf{q}. \tag{D.19}$$

The integral I_2 is similar to the integral I_1 and the corresponding analytical solution for I_2 based on Eq. (D.18) is given by

$$\begin{aligned} I_2 &= \frac{1}{2}\sum_{\begin{bmatrix}k\\ \nu\end{bmatrix}} \omega^2\begin{bmatrix}k\\ \nu\end{bmatrix}\left[\frac{\sqrt{\pi}}{2}\left(\frac{2k_BT}{\omega_{\text{eff}}^2\begin{bmatrix}k\\ \nu\end{bmatrix}}\right)^{3/2}\right]\left\{\prod_{\substack{\begin{bmatrix}k_1\\ \nu_1\end{bmatrix}\neq\begin{bmatrix}k\\ \nu\end{bmatrix}}}\left[\sqrt{\pi}\left(\frac{2k_BT}{\omega_{\text{eff}}^2\begin{bmatrix}k_1\\ \nu_1\end{bmatrix}}\right)^{1/2}\right]\right\}, \\ &= \sum_{\begin{bmatrix}k\\ \nu\end{bmatrix}}\left(\frac{k_BT}{2}\right)\left(\frac{\omega^2\begin{bmatrix}k\\ \nu\end{bmatrix}}{\omega_{\text{eff}}^2\begin{bmatrix}k\\ \nu\end{bmatrix}}\right)\left\{\prod_{\begin{bmatrix}k_1\\ \nu_1\end{bmatrix}}\left[\sqrt{\pi}\left(\frac{2k_BT}{\omega_{\text{eff}}^2\begin{bmatrix}k_1\\ \nu_1\end{bmatrix}}\right)^{1/2}\right]\right\}. \end{aligned} \tag{D.20}$$

The final part of the integral in Eq. (D.15) is given by

$$I_3 = \int_{\mathbb{R}^{\mathcal{N}}} \exp\left\{-\frac{\sum_{\begin{bmatrix}k_1\\ \nu_1\end{bmatrix}} \omega_{\text{eff}}^2\begin{bmatrix}k_1\\ \nu_1\end{bmatrix} q^2\begin{bmatrix}k_1\\ \nu_1\end{bmatrix}}{2k_BT}\right\}\widetilde{\Phi}_4\ d\mathbf{q} \tag{D.21}$$

The fourth order term $\widetilde{\Phi}_4$ of Eq. (D.8) consists of the function $\Delta(k+k'+k''+k''')$ where $\Delta(k+k'+k''+k''') = 1$ if $k+k'+k''+k'''$ is a reciprocal lattice point and zero otherwise. The integral in Eq. (D.21) is symmetric with respect to sign of the coordinate $\mathbf{q}$. This imposes the condition on $k+k'+k''+k'''$ such that only two kinds of combinations given by $k-k+k'-k'$ and $k-k+k-k$ will survive the symmetric integral without averaging out to zero. The combination $k-k+k'-k'$ gives rise to six identical terms and the combination $k-k+k-k$ gives rise to two identical terms. This simplifies Eq. (D.21) such that

$$I_3 = \int_{\mathbb{R}^{\mathcal{N}}} \exp\left\{-\frac{\sum_{\left[\begin{smallmatrix}k_1\\ \nu_1\end{smallmatrix}\right]} \omega^2\left[\begin{smallmatrix}k_1\\ \nu_1\end{smallmatrix}\right] q^2\left[\begin{smallmatrix}k_1\\ \nu_1\end{smallmatrix}\right]}{2k_BT}\right\}\approx{\Phi}_4\, d\mathbf{q} \tag{D.22}$$

where

$$\approx{\Phi}_4 = \frac{6}{4!}\sum_{\left[\begin{smallmatrix}k\\ \nu\end{smallmatrix}\right]}\sum_{\left[\begin{smallmatrix}k'\\ \nu'\end{smallmatrix}\right]\neq\left[\begin{smallmatrix}k\\ \nu\end{smallmatrix}\right]} V_4\left[\begin{smallmatrix}k\,-k\,k'\,-k'\\ \nu\,\nu\,\nu'\,\nu'\end{smallmatrix}\right] q^2\left[\begin{smallmatrix}k\\ \nu\end{smallmatrix}\right] q^2\left[\begin{smallmatrix}k'\\ \nu'\end{smallmatrix}\right] + \frac{2}{4!}\sum_{\left[\begin{smallmatrix}k\\ \nu\end{smallmatrix}\right]} V_4\left[\begin{smallmatrix}k\,-k\,k\,-k\\ \nu\,\nu\,\nu\,\nu\end{smallmatrix}\right] q^4\left[\begin{smallmatrix}k\\ \nu\end{smallmatrix}\right]. \tag{D.23}$$

Substituting Eq. (D.23) into Eq. (D.22) and using Eqs. (D.11)–(D.13) results in

$$\begin{aligned} I_3 = {} & \frac{6}{4!}\sum_{\left[\begin{smallmatrix}k\\ \nu\end{smallmatrix}\right]}\sum_{\left[\begin{smallmatrix}k'\\ \nu'\end{smallmatrix}\right]\neq\left[\begin{smallmatrix}k\\ \nu\end{smallmatrix}\right]} V_4\left[\begin{smallmatrix}k\,-k\,k'\,-k'\\ \nu\,\nu\,\nu'\,\nu'\end{smallmatrix}\right]\left(\frac{k_BT}{\omega_{\mathrm{eff}}^2\left[\begin{smallmatrix}k\\ \nu\end{smallmatrix}\right]}\right)\left(\frac{k_BT}{\omega_{\mathrm{eff}}^2\left[\begin{smallmatrix}k'\\ \nu'\end{smallmatrix}\right]}\right)\left\{\prod_{\left[\begin{smallmatrix}k_1\\ \nu_1\end{smallmatrix}\right]}\left[\sqrt{\pi}\left(\frac{2k_BT}{\omega_{\mathrm{eff}}^2\left[\begin{smallmatrix}k_1\\ \nu_1\end{smallmatrix}\right]}\right)^{1/2}\right]\right\} \\ & + \frac{2}{4!}\sum_{\left[\begin{smallmatrix}k\\ \nu\end{smallmatrix}\right]} V_4\left[\begin{smallmatrix}k\,-k\,k\,-k\\ \nu\,\nu\,\nu\,\nu\end{smallmatrix}\right]\left[\frac{3\sqrt{\pi}}{4}\left(\frac{2k_BT}{\omega_{\mathrm{eff}}^2\left[\begin{smallmatrix}k\\ \nu\end{smallmatrix}\right]}\right)^{5/2}\right]\left\{\prod_{\left[\begin{smallmatrix}k_1\\ \nu_1\end{smallmatrix}\right]\neq\left[\begin{smallmatrix}k\\ \nu\end{smallmatrix}\right]}\left[\sqrt{\pi}\left(\frac{2k_BT}{\omega_{\mathrm{eff}}^2\left[\begin{smallmatrix}k_1\\ \nu_1\end{smallmatrix}\right]}\right)^{1/2}\right]\right\}. \end{aligned} \tag{D.24}$$

Rearranging the terms in Eq. (D.24) gives the final analytical expression for I_3 given by

$$I_3 = \left\{\left(\frac{k_BT}{2}\right)^2\sum_{\left[\begin{smallmatrix}k\\ \nu\end{smallmatrix}\right]}\sum_{\left[\begin{smallmatrix}k'\\ \nu'\end{smallmatrix}\right]}\frac{V_4\left[\begin{smallmatrix}k\,-k\,k'\,-k'\\ \nu\,\nu\,\nu'\,\nu'\end{smallmatrix}\right]}{\omega_{\mathrm{eff}}^2\left[\begin{smallmatrix}k\\ \nu\end{smallmatrix}\right]\omega_{\mathrm{eff}}^2\left[\begin{smallmatrix}k'\\ \nu'\end{smallmatrix}\right]}\right\}\left\{\prod_{\left[\begin{smallmatrix}k_1\\ \nu_1\end{smallmatrix}\right]}\left[\sqrt{\pi}\left(\frac{2k_BT}{\omega_{\mathrm{eff}}^2\left[\begin{smallmatrix}k_1\\ \nu_1\end{smallmatrix}\right]}\right)^{1/2}\right]\right\}. \tag{D.25}$$

Substituting the analytical expressions of integrals I_1, I_2, and I_3 from Eqs. (D.18), (D.20), and (D.25) into Eq. (D.15) and separating the constant terms $\left(\frac{k_BT}{2}\right)$ and

$\left\{\prod_{\left[\begin{smallmatrix}k_1\\ \nu_1\end{smallmatrix}\right]}\left[\sqrt{\pi}\left(\frac{2k_BT}{\omega^2_{\text{eff}}\left[\begin{smallmatrix}k_1\\ \nu_1\end{smallmatrix}\right]}\right)^{1/2}\right]\right\}$ results in

$$\sum_{\left[\begin{smallmatrix}k\\ \nu\end{smallmatrix}\right]}\left\{-1+\frac{\omega^2\left[\begin{smallmatrix}k\\ \nu\end{smallmatrix}\right]}{\omega^2_{\text{eff}}\left[\begin{smallmatrix}k\\ \nu\end{smallmatrix}\right]}+\frac{k_BT}{2}\sum_{\left[\begin{smallmatrix}k'\\ \nu'\end{smallmatrix}\right]}\frac{V_4\left[\begin{smallmatrix}k-kk'-k'\\ \nu\nu\ \ \nu'\nu'\end{smallmatrix}\right]}{\omega^2_{\text{eff}}\left[\begin{smallmatrix}k\\ \nu\end{smallmatrix}\right]\omega^2_{\text{eff}}\left[\begin{smallmatrix}k'\\ \nu'\end{smallmatrix}\right]}+\dots\right\}=0. \tag{D.26}$$

It is possible that many sets of $\omega^2_{\text{eff}}\left[\begin{smallmatrix}k\\ \nu\end{smallmatrix}\right]$ satisfy Eq. (D.26). Even at $T=0$ K, many sets of $\omega^2_{\text{eff}}\left[\begin{smallmatrix}k\\ \nu\end{smallmatrix}\right]$ satisfy Eq. (D.26). However, at $T=0$ K the effective harmonic potential should coincide with the harmonic potential such that $\omega^2_{\text{eff}}\left[\begin{smallmatrix}k\\ \nu\end{smallmatrix}\right]=\omega^2\left[\begin{smallmatrix}k\\ \nu\end{smallmatrix}\right]$ for all $\left[\begin{smallmatrix}k\\ \nu\end{smallmatrix}\right]$. Based on this observation, a particular solution is considered by making each term in Eq. (D.26) to be zero. This results in a set of equations given by

$$-1+\frac{\omega^2\left[\begin{smallmatrix}k\\ \nu\end{smallmatrix}\right]}{\omega^2_{\text{eff}}\left[\begin{smallmatrix}k\\ \nu\end{smallmatrix}\right]}+\frac{k_BT}{2}\sum_{\left[\begin{smallmatrix}k'\\ \nu'\end{smallmatrix}\right]}\frac{V_4\left[\begin{smallmatrix}k-kk'-k'\\ \nu\nu\ \ \nu'\nu'\end{smallmatrix}\right]}{\omega^2_{\text{eff}}\left[\begin{smallmatrix}k\\ \nu\end{smallmatrix}\right]\omega^2_{\text{eff}}\left[\begin{smallmatrix}k'\\ \nu'\end{smallmatrix}\right]}+\dots=0. \tag{D.27}$$

Multiplying Eq. (D.27) with $\omega^2_{\text{eff}}\left[\begin{smallmatrix}k\\ \nu\end{smallmatrix}\right]$ and rearranging the terms result in the self-consistent equation to determine the effective harmonic frequencies $\omega^2_{\text{eff}}\left[\begin{smallmatrix}k\\ \nu\end{smallmatrix}\right]$ given by

$$\omega^2_{\text{eff}}\left[\begin{smallmatrix}k\\ \nu\end{smallmatrix}\right]=\omega^2\left[\begin{smallmatrix}k\\ \nu\end{smallmatrix}\right]+\frac{k_BT}{2}\sum_{\left[\begin{smallmatrix}k'\\ \nu'\end{smallmatrix}\right]}V_4\left[\begin{smallmatrix}k-kk'-k'\\ \nu\nu\ \ \nu'\nu'\end{smallmatrix}\right]\frac{1}{\omega^2_{\text{eff}}\left[\begin{smallmatrix}k'\\ \nu'\end{smallmatrix}\right]}+\dots. \tag{D.28}$$

Appendix E

Quantum mechanics formulation of the self-consistent approach

E.1 Introduction

The formulation of the SCA method (*Hooton*, 1955a,b; *Huang and Born*, 1962; *Choquard*, 1967; *Wallace*, 1998) is generally done using quantum mechanics. In this chapter, first-order SCA method is formulated within quantum mechanics for the case of a one dimensional chain. This is based on the statistical perturbation method (*Wallace*, 1966) and first-order SCA method developed in *Wallace* (1998) which uses the operator-renormalization technique. The resultant self-consistent equation and free energy from this formulation are compared with the corresponding results from the SCA method formulation within classical mechanics done in Chapter 5.

In Chapter 4, the normal modes of vibration are described as a wave-like phenomena within classical mechanics. In formulations using quantum mechanics, these normal modes of vibration are treated as particles and hence the energy corresponding to each mode of vibration is quantized. Each quanta of a mode of vibration is called a *phonon*. The classical hamiltonian $\mathcal{H}$ Eq. (4.17), real space coordinates $\delta u\left[\begin{smallmatrix}\ell\\ \alpha\end{smallmatrix}\right]$, normal mode coordinates $q\left[\begin{smallmatrix}k\\ \nu\end{smallmatrix}\right]$, and momenta $p\left[\begin{smallmatrix}k\\ \nu\end{smallmatrix}\right]$ are introduced into quantum mechanical formulation as hamiltonian operator $\widehat{\mathcal{H}}$, real space coordinate operator $\delta\hat{u}\left[\begin{smallmatrix}\ell\\ \alpha\end{smallmatrix}\right]$, normal mode coordinate operator $\hat{q}\left[\begin{smallmatrix}k\\ \nu\end{smallmatrix}\right]$, and momentum operator $\hat{p}\left[\begin{smallmatrix}k\\ \nu\end{smallmatrix}\right]$ respectively.

The hamiltonian operator of a chain of atoms vibrating about the configuration $\overset{o}{\mathbf{u}}$

corresponding to Eq. (4.17) is given by

$$\begin{aligned}
\widehat{\mathcal{H}} &= \widehat{KE} + \Phi_0 + \widehat{\Phi}_1 + \widehat{\Phi}_2 + \widehat{\Phi}_3 + \widehat{\Phi}_4 + \ldots, \\
\widehat{KE} &\equiv \frac{1}{2}\sum_{\left[\substack{\ell \\ \alpha}\right]} m_\alpha \left(\delta\hat{\dot{u}}\left[\substack{\ell \\ \alpha}\right]\right)^2, \\
\Phi_0 &\equiv naW(\overset{o}{\mathbf{u}}), \\
\widehat{\Phi}_1 &\equiv \sum_{\left[\substack{\ell \\ \alpha}\right]} \overset{o}{\Phi}\left[\substack{\ell \\ \alpha}\right] \delta\hat{u}\left[\substack{\ell \\ \alpha}\right], \\
\widehat{\Phi}_2 &\equiv \frac{1}{2!}\sum_{\left[\substack{\ell \\ \alpha}\right]}\sum_{\left[\substack{\ell' \\ \alpha'}\right]} \overset{o}{\Phi}\left[\substack{\ell\,\ell' \\ \alpha\alpha'}\right] \delta\hat{u}\left[\substack{\ell \\ \alpha}\right] \delta\hat{u}\left[\substack{\ell' \\ \alpha'}\right], \\
&\vdots
\end{aligned} \tag{E.1}$$

Corresponding to Eq. (4.18), the normal mode operators are given by

$$\begin{aligned}
\delta\hat{u}\left[\substack{\ell \\ \alpha}\right] &= (nm_\alpha)^{-1/2}\sum_{\left[\substack{k \\ \nu}\right]} \hat{q}\left[\substack{k \\ \nu}\right] \mathrm{e}\left[\substack{k \\ \nu\alpha}\right] \exp\{ikX[\ell]\}, \\
\delta\hat{\dot{u}}\left[\substack{\ell \\ \alpha}\right] &= (nm_\alpha)^{-1/2}\sum_{\left[\substack{k \\ \nu}\right]} \hat{p}^*\left[\substack{k \\ \nu}\right] \mathrm{e}\left[\substack{k \\ \nu\alpha}\right] \exp\{ikX[\ell]\},
\end{aligned} \tag{E.2}$$

The total hamiltonian operator Eq. (E.1) rewritten in terms normal mode operators Eq. (E.2) is given by

$$\begin{aligned}
\widehat{\mathcal{H}} = {} & \frac{1}{2}\sum_{\left[\substack{k \\ \nu}\right]} \hat{p}\left[\substack{k \\ \nu}\right] \hat{p}^\dagger\left[\substack{k \\ \nu}\right] + \Phi_0 + \sum_{\left[\substack{k \\ \nu}\right]} V_1\left[\substack{k \\ \nu}\right] \hat{q}\left[\substack{k \\ \nu}\right] + \frac{1}{2}\sum_{\left[\substack{k \\ \nu}\right]} \omega^2\left[\substack{k \\ \nu}\right] \hat{q}\left[\substack{k \\ \nu}\right] \hat{q}^\dagger\left[\substack{k \\ \nu}\right] \\
& + \frac{1}{3!}\sum_{\left[\substack{k \\ \nu}\right]}\sum_{\left[\substack{k' \\ \nu'}\right]}\sum_{\left[\substack{k'' \\ \nu''}\right]} V_3\left[\substack{kk'k'' \\ \nu\nu'\nu''}\right] \hat{q}\left[\substack{k \\ \nu}\right] \hat{q}\left[\substack{k' \\ \nu'}\right] \hat{q}\left[\substack{k'' \\ \nu''}\right] \Delta(k+k'+k'') \\
& + \frac{1}{4!}\sum_{\left[\substack{k \\ \nu}\right]}\sum_{\left[\substack{k' \\ \nu'}\right]}\sum_{\left[\substack{k'' \\ \nu''}\right]}\sum_{\left[\substack{k''' \\ \nu'''}\right]} V_4\left[\substack{kk'k''k''' \\ \nu\nu'\nu''\nu'''}\right] \hat{q}\left[\substack{k \\ \nu}\right] \hat{q}\left[\substack{k' \\ \nu'}\right] \hat{q}\left[\substack{k'' \\ \nu''}\right] \hat{q}\left[\substack{k''' \\ \nu'''}\right] \Delta(k+k'+k''+k''') \\
& + \ldots,
\end{aligned} \tag{E.3}$$

where V_1, V_3, and V_4 are defined by Eqs. (4.25)-(4.27) respectively. The function $\Delta(K)$ is defined such that $\Delta(K) = 1$ if K is a reciprocal lattice point and zero otherwise.

The superscript † denotes the adjoint of the operator and $\omega^2\left[\begin{smallmatrix}k\\ \nu\end{smallmatrix}\right]$ are the eigenvalues of harmonic dynamical matrix Eq. (4.20).

In order to find the energy levels and the corresponding energy eigenstates of an oscillator, one must solve the time-independent Schrödinger equation

$$\widehat{\mathcal{H}}\psi = E\psi, \tag{E.4}$$

where $\psi = \psi(\mathbf{q})$ is the many-dimensional wave function which describes a state of the system defined by normal mode coordinates $\mathbf{q} = \left\{q\left[\begin{smallmatrix}k\\ \nu\end{smallmatrix}\right]\right\}$ (*Johnson and Gutierrez*, 2002). The squares of the absolute values of wave function gives the probability distribution that the system will be in any of the possible states. The wave function is normalized such that

$$\int \psi^*\psi \; d\mathbf{q} = \mathbf{1}, \tag{E.5}$$

where ψ^* is the complex conjugate of ψ and the integration is done over all the configuration space of normal mode coordinates $\mathbf{q}$. The E in Eq. (E.4) is the energy corresponding to the state described by the wave function ψ. The Schrödinger equation Eq. (E.4) can be considered as an eigen equation, with ψ as the eigenvector and E as the corresponding eigenvalue.

The coordinate operator $\hat{q}\left[\begin{smallmatrix}k\\ \nu\end{smallmatrix}\right]$ and momentum operator $\hat{p}\left[\begin{smallmatrix}k\\ \nu\end{smallmatrix}\right]$ satisfy the relations

$$\begin{aligned} \hat{q}\begin{bmatrix}k\\ \nu\end{bmatrix}\psi &= q\begin{bmatrix}k\\ \nu\end{bmatrix}\psi, \\ \hat{p}\begin{bmatrix}k\\ \nu\end{bmatrix}\psi &= -i\hbar\frac{\partial\psi}{\partial q\left[\begin{smallmatrix}k\\ \nu\end{smallmatrix}\right]}. \end{aligned} \tag{E.6}$$

The *average value* of any quantity χ, also called as *mean value* or *expectation value*, is given by the integral

$$\overline{\chi} = \int \psi^*\chi\psi \; d\mathbf{q}. \tag{E.7}$$

In quantum mechanical formulations, Bra-ket notation invented by Paul Dirac (*Dirac*, 1948) is often used. According to this notation, the wave function corresponding to a state of a system of vibrating atoms is given by $|\mathbf{n}\rangle$ called as *ket*. Here, $\mathbf{n}$ denotes the set of *occupation numbers* $n\left[\begin{smallmatrix}k\\ \nu\end{smallmatrix}\right]$ representing the number of each kind of allowed phonon.

Every *ket* has a dual *bra* represented by $\langle \mathbf{n}|$. The normalization of the wave function Eq. (E.5) written in Bra-ket notation is given by

$$\langle \mathbf{n} \,|\, \mathbf{n} \rangle = \mathbf{1}, \tag{E.8}$$

and the expectation value of any quantity χ Eq. (E.7) is given by

$$\overline{\chi} = \langle \mathbf{n} \,|\chi|\, \mathbf{n} \rangle \,, \tag{E.9}$$

where *bra*, $\langle \mathbf{n}|$, corresponds to ψ^* and *ket*, $|\mathbf{n}\rangle$, corresponds to ψ in Eq. (E.7).

Particles subjected to the Pauli exclusion principle, such as electrons, are called as *fermions*. The values of each $n\begin{bmatrix} k \\ \nu \end{bmatrix}$ for fermions are restricted to zero or one. However, the quanta of lattice vibrations (*phonons*) are not subjected to this restriction so that each $n\begin{bmatrix} k \\ \nu \end{bmatrix}$ can take on any positive integer value including zero. The family of particles with this property are called *bosons*. Any particle is either a fermion or a boson. The case of $n\begin{bmatrix} k \\ \nu \end{bmatrix} = 0$ for all $\begin{bmatrix} k \\ \nu \end{bmatrix}$ is the lowest energy state called as the *ground state* and the wave function in this case is simply written as $|\mathbf{0}\rangle$. The ground state corresponds to the state at temperature 0 K.

The concept of commutation is used in many applications of quantum mechanics. For any two operators, say $\hat{A}$ and $\hat{B}$, the *commutation relation* is defined as

$$\left[\hat{A}, \hat{B}\right] \equiv \hat{A}\hat{B} - \hat{B}\hat{A}. \tag{E.10}$$

Any two operators are said to *commute* if their commutation relation equals to zero. If any two operators have a Heisenberg uncertainty relation (*Heisenberg*, 1930) then they will not commute. For the case of position operator $\hat{q}\begin{bmatrix} k \\ \nu \end{bmatrix}$ and momentum operator $\hat{p}\begin{bmatrix} k \\ \nu \end{bmatrix}$, the commutation relation is given by

$$\left[\hat{q}\begin{bmatrix} k \\ \nu \end{bmatrix}, \hat{p}\begin{bmatrix} k' \\ \nu' \end{bmatrix}\right] = i\hbar\delta_{kk'}\delta_{\nu\nu'}. \tag{E.11}$$

Clearly the position operator $\hat{q}\begin{bmatrix} k \\ \nu \end{bmatrix}$ and momentum operator $\hat{p}\begin{bmatrix} k \\ \nu \end{bmatrix}$ do not commute. This is the fundamental difference between classical and quantum approaches. Thus, there is a Heisenberg uncertainty relation and one cannot expect to simultaneously know the

position and momentum of a quantum particle.

At this point, it is convenient to formulate the description of $\widehat{\mathcal{H}}$ Eq. (E.3) in terms of phonon creation and annihilation operators. The phonon creation and annihilation operators, denoted by $\hat{A}^\dagger\left[{k \atop \nu}\right]$ and $\hat{A}\left[{k \atop \nu}\right]$ respectively, are defined as

$$\begin{aligned}\hat{A}^\dagger\left[{k \atop \nu}\right] &= \left(2\hbar\omega\left[{k \atop \nu}\right]\right)^{-1/2}\left(\omega\left[{k \atop \nu}\right]\hat{q}\left[{-k \atop \nu}\right] - i\hat{p}\left[{k \atop \nu}\right]\right),\\ \hat{A}\left[{k \atop \nu}\right] &= \left(2\hbar\omega\left[{k \atop \nu}\right]\right)^{-1/2}\left(\omega\left[{k \atop \nu}\right]\hat{q}\left[{k \atop \nu}\right] + i\hat{p}\left[{-k \atop \nu}\right]\right).\end{aligned} \tag{E.12}$$

These operators are dimensionless, and also $\hat{A}^\dagger\left[{k \atop \nu}\right] = \hat{A}^*\left[{k \atop \nu}\right]$. From Eq. (E.12), the coordinate operator $\hat{q}\left[{k \atop \nu}\right]$ and momentum operator $\hat{p}\left[{k \atop \nu}\right]$ are given by

$$\begin{aligned}\hat{q}\left[{k \atop \nu}\right] &= \left(\frac{\hbar}{2\omega\left[{k \atop \nu}\right]}\right)^{1/2}\left(\hat{A}\left[{k \atop \nu}\right] + \hat{A}^\dagger\left[{-k \atop \nu}\right]\right),\\ \hat{p}\left[{k \atop \nu}\right] &= i\left(\frac{\hbar\omega\left[{k \atop \nu}\right]}{2}\right)^{1/2}\left(\hat{A}^\dagger\left[{k \atop \nu}\right] - \hat{A}\left[{-k \atop \nu}\right]\right).\end{aligned} \tag{E.13}$$

Using Eqs. (E.11) and (E.12), the commutation relations for creation and annihilation operators are given by

$$\begin{aligned}\left[\hat{A}\left[{k \atop \nu}\right], \hat{A}^\dagger\left[{k' \atop \nu'}\right]\right] &= \delta_{kk'}\delta_{\nu\nu'},\\ \left[\hat{A}\left[{k \atop \nu}\right], \hat{A}\left[{k' \atop \nu'}\right]\right] &= \left[\hat{A}^\dagger\left[{k \atop \nu}\right], \hat{A}^\dagger\left[{k' \atop \nu'}\right]\right] = 0.\end{aligned} \tag{E.14}$$

The hamiltonian operator Eq. (E.3) rewritten in terms of creation and annihilation operators Eq. (E.13) is given by

$$\widehat{\mathcal{H}} = \Phi_0 + \sum_{\left[{k \atop \nu}\right]}\hbar\omega\left[{k \atop \nu}\right]\left(\frac{1}{2} + \hat{A}^\dagger\left[{k \atop \nu}\right]\hat{A}\left[{k \atop \nu}\right]\right) + \widehat{\widetilde{\Phi}}_1 + \widehat{\widetilde{\Phi}}_3 + \widehat{\widetilde{\Phi}}_4 + \ldots, \tag{E.15}$$

where

$$\widehat{\widetilde{\Phi}}_1 \equiv \sum_{\left[{k \atop \nu}\right]} V_1\left[{k \atop \nu}\right]\left(\frac{\hbar}{2\omega\left[{k \atop \nu}\right]}\right)^{1/2}\left(\hat{A}\left[{k \atop \nu}\right] + \hat{A}^\dagger\left[{-k \atop \nu}\right]\right), \tag{E.16}$$

$$\widehat{\widetilde{\Phi}}_3 \equiv \frac{1}{3!}\sum_{\left[\substack{k\\\nu}\right]}\sum_{\left[\substack{k'\\\nu'}\right]}\sum_{\left[\substack{k''\\\nu''}\right]} V_3\left[\substack{kk'k''\\\nu\nu'\nu''}\right]\left(\frac{\hbar}{2}\right)^{3/2}\left(\omega\left[\substack{k\\\nu}\right]\omega\left[\substack{k'\\\nu'}\right]\omega\left[\substack{k''\\\nu''}\right]\right)^{-1/2}\left(\hat{A}\left[\substack{k\\\nu}\right]+\hat{A}^\dagger\left[\substack{-k\\\nu}\right]\right)$$
$$\left(\hat{A}\left[\substack{k'\\\nu'}\right]+\hat{A}^\dagger\left[\substack{-k'\\\nu'}\right]\right)\left(\hat{A}\left[\substack{k''\\\nu''}\right]+\hat{A}^\dagger\left[\substack{-k''\\\nu''}\right]\right)\Delta(k+k'+k''), \tag{E.17}$$

$$\begin{aligned}\widehat{\widetilde{\Phi}}_4 \equiv \frac{1}{4!}\sum_{\left[\substack{k\\\nu}\right]}\sum_{\left[\substack{k'\\\nu'}\right]}\sum_{\left[\substack{k''\\\nu''}\right]}\sum_{\left[\substack{k'''\\\nu'''}\right]} V_4\left[\substack{kk'k''k'''\\\nu\nu'\nu''\nu'''}\right]\left(\frac{\hbar}{2}\right)^{2}\left(\omega\left[\substack{k\\\nu}\right]\omega\left[\substack{k'\\\nu'}\right]\omega\left[\substack{k''\\\nu''}\right]\omega\left[\substack{k'''\\\nu'''}\right]\right)^{-1/2}\\ \left(\hat{A}\left[\substack{k\\\nu}\right]+\hat{A}^\dagger\left[\substack{-k\\\nu}\right]\right)\left(\hat{A}\left[\substack{k'\\\nu'}\right]+\hat{A}^\dagger\left[\substack{-k'\\\nu'}\right]\right)\left(\hat{A}\left[\substack{k''\\\nu''}\right]+\hat{A}^\dagger\left[\substack{-k''\\\nu''}\right]\right)\\ \left(\hat{A}\left[\substack{k'''\\\nu'''}\right]+\hat{A}^\dagger\left[\substack{-k'''\\\nu'''}\right]\right)\Delta(k+k'+k''+k''').\end{aligned} \tag{E.18}$$

E.2 Statistical perturbation method

This section explains the statistical perturbation method whose results will be used in the self-consistent approach discussed later in Section E.3. The statistical perturbation method is a general method for approximating statistical averages in a many-body problem (*Wallace*, 1966). Here, an overview of this method is described. See *Wallace* (1966) for more details about statistical perturbation method.

The basic idea in this method is that if $\hat{A}^\dagger\left[\substack{k\\\nu}\right]$ and $\hat{A}\left[\substack{k\\\nu}\right]$ are *approximate* creation and annihilation operators, respectively, such that they satisfy the hamiltonian commutator relations

$$\left[\widehat{\mathcal{H}}, \hat{A}^\dagger\left[\substack{k\\\nu}\right]\right] = \hbar\omega\left[\substack{k\\\nu}\right]\hat{A}^\dagger\left[\substack{k\\\nu}\right] + \hat{R}^\dagger\left[\substack{k\\\nu}\right], \tag{E.19}$$

$$\left[\widehat{\mathcal{H}}, \hat{A}\left[\substack{k\\\nu}\right]\right] = -\hbar\omega\left[\substack{k\\\nu}\right]\hat{A}\left[\substack{k\\\nu}\right] - \hat{R}\left[\substack{k\\\nu}\right], \tag{E.20}$$

where $\hbar\omega\left[\substack{k\\\nu}\right]$ are real positive energies and remainders $\hat{R}^\dagger\left[\substack{k\\\nu}\right]$ and $\hat{R}\left[\substack{k\\\nu}\right]$ are *small* operators such that the statistical averages $\left\langle \hat{A}^\dagger\left[\substack{k\\\nu}\right]\widehat{\chi}\right\rangle$ and $\left\langle \widehat{\chi}^\dagger\hat{A}\left[\substack{k\\\nu}\right]\right\rangle$ can be obtained in terms of the remainders. Here, $\widehat{\chi}$ is any operator and $\widehat{\chi}^\dagger$ is the complex conjugate of $\widehat{\chi}$. The remainders have to be small in the sense that they give small contributions to statistical averages. It is important to note that the operators $\hat{A}^\dagger\left[\substack{k\\\nu}\right]$ and $\hat{A}\left[\substack{k\\\nu}\right]$ are

approximate operators which implies that these operators satisfy the commutation relations Eq. (E.14) approximately. Further, the energies $\hbar\omega\begin{bmatrix}k\\ \nu\end{bmatrix}$ and the operators $\hat{A}^\dagger\begin{bmatrix}k\\ \nu\end{bmatrix}$ and $\hat{A}\begin{bmatrix}k\\ \nu\end{bmatrix}$ may be temperature-dependent.

The statical average $\left\langle \hat{A}^\dagger\begin{bmatrix}k\\ \nu\end{bmatrix}\widehat{\chi}\right\rangle$ can be obtained by starting with the hamiltonian commutator relation Eq. (E.19). Using the definition of commutation Eq. (E.10), Eq. (E.19) can be rewritten as

$$\widehat{\mathcal{H}}\hat{A}^\dagger\begin{bmatrix}k\\ \nu\end{bmatrix} = \hat{A}^\dagger\begin{bmatrix}k\\ \nu\end{bmatrix}\left(\widehat{\mathcal{H}} + \hbar\omega\begin{bmatrix}k\\ \nu\end{bmatrix}\right) + \hat{R}^\dagger\begin{bmatrix}k\\ \nu\end{bmatrix}. \tag{E.21}$$

Operating $\widehat{\mathcal{H}}$ on Eq.(E.21) and using Eq. (E.21) again results in

$$\begin{aligned}\widehat{\mathcal{H}}^2\hat{A}^\dagger\begin{bmatrix}k\\ \nu\end{bmatrix} &= \widehat{\mathcal{H}}\hat{A}^\dagger\begin{bmatrix}k\\ \nu\end{bmatrix}\left(\widehat{\mathcal{H}} + \hbar\omega\begin{bmatrix}k\\ \nu\end{bmatrix}\right) + \widehat{\mathcal{H}}\hat{R}^\dagger\begin{bmatrix}k\\ \nu\end{bmatrix}, \\ &= \hat{A}^\dagger\begin{bmatrix}k\\ \nu\end{bmatrix}\left(\widehat{\mathcal{H}} + \hbar\omega\begin{bmatrix}k\\ \nu\end{bmatrix}\right)^2 + \hat{R}^\dagger\begin{bmatrix}k\\ \nu\end{bmatrix}\left(\widehat{\mathcal{H}} + \hbar\omega\begin{bmatrix}k\\ \nu\end{bmatrix}\right) + \widehat{\mathcal{H}}\hat{R}^\dagger\begin{bmatrix}k\\ \nu\end{bmatrix}.\end{aligned} \tag{E.22}$$

Repeating the same procedure s times results in

$$\widehat{\mathcal{H}}^s\hat{A}^\dagger\begin{bmatrix}k\\ \nu\end{bmatrix} = \hat{A}^\dagger\begin{bmatrix}k\\ \nu\end{bmatrix}\left(\widehat{\mathcal{H}} + \hbar\omega\begin{bmatrix}k\\ \nu\end{bmatrix}\right)^s + \sum_{t=0}^{s-1}\widehat{\mathcal{H}}^t\hat{R}^\dagger\begin{bmatrix}k\\ \nu\end{bmatrix}\left(\widehat{\mathcal{H}} + \hbar\omega\begin{bmatrix}k\\ \nu\end{bmatrix}\right)^{s-t-1}, \quad s = 1, 2, \ldots. \tag{E.23}$$

Using Eq. (E.23) and the relation

$$\exp\left\{-\frac{\widehat{\mathcal{H}}}{k_BT}\right\} = \sum_{s=0}^{\infty}(s!)^{-1}\left(-k_BT\right)^{-s}\widehat{\mathcal{H}}^s, \tag{E.24}$$

it is possible to obtain the relation

$$\begin{aligned}\exp\left\{-\frac{\widehat{\mathcal{H}}}{k_BT}\right\}\hat{A}^\dagger\begin{bmatrix}k\\ \nu\end{bmatrix} = \hat{A}^\dagger\begin{bmatrix}k\\ \nu\end{bmatrix}\exp\left\{-\frac{\left(\widehat{\mathcal{H}} + \hbar\omega\begin{bmatrix}k\\ \nu\end{bmatrix}\right)}{k_BT}\right\} \\ + \sum_{s=1}^{\infty}(s!)^{-1}\left(-k_BT\right)^{-s}\sum_{t=0}^{s-1}\widehat{\mathcal{H}}^t\hat{R}^\dagger\begin{bmatrix}k\\ \nu\end{bmatrix}\left(\widehat{\mathcal{H}} + \hbar\omega\begin{bmatrix}k\\ \nu\end{bmatrix}\right)^{s-t-1}.\end{aligned} \tag{E.25}$$

The partition function Z is given by

$$Z = \mathrm{Tr}\left(\exp\left\{-\frac{\widehat{\mathcal{H}}}{k_B T}\right\}\right), \tag{E.26}$$

and the statistical average $\left\langle \hat{A}^\dagger \begin{bmatrix} k \\ \nu \end{bmatrix} \widehat{\chi} \right\rangle$ is defined by

$$\left\langle \hat{A}^\dagger \begin{bmatrix} k \\ \nu \end{bmatrix} \widehat{\chi} \right\rangle = Z^{-1}\mathrm{Tr}\left(\hat{A}^\dagger \begin{bmatrix} k \\ \nu \end{bmatrix} \widehat{\chi} \exp\left\{-\frac{\widehat{\mathcal{H}}}{k_B T}\right\}\right). \tag{E.27}$$

By the cyclic permutation theorem for traces, Eq. (E.27) can be rewritten as

$$\left\langle \hat{A}^\dagger \begin{bmatrix} k \\ \nu \end{bmatrix} \widehat{\chi} \right\rangle = Z^{-1}\mathrm{Tr}\left(\widehat{\chi} \exp\left\{-\frac{\widehat{\mathcal{H}}}{k_B T}\right\} \hat{A}^\dagger \begin{bmatrix} k \\ \nu \end{bmatrix}\right). \tag{E.28}$$

Using Eq. (E.25), the statistical average $\left\langle \hat{A}^\dagger \begin{bmatrix} k \\ \nu \end{bmatrix} \widehat{\chi} \right\rangle$ Eq. (E.28) becomes

$$\begin{aligned}\left\langle \hat{A}^\dagger \begin{bmatrix} k \\ \nu \end{bmatrix} \widehat{\chi} \right\rangle = \exp\left\{-\frac{\hbar\omega \begin{bmatrix} k \\ \nu \end{bmatrix}}{k_B T}\right\} \left\langle \widehat{\chi} \hat{A}^\dagger \begin{bmatrix} k \\ \nu \end{bmatrix} \right\rangle \\ + Z^{-1}\mathrm{Tr}\left(\widehat{\chi} \sum_{s=1}^{\infty} (s!)^{-1} (-k_B T)^{-s} \sum_{t=0}^{s-1} \widehat{\mathcal{H}}^t \hat{R}^\dagger \begin{bmatrix} k \\ \nu \end{bmatrix} \left(\widehat{\mathcal{H}} + \hbar\omega \begin{bmatrix} k \\ \nu \end{bmatrix}\right)^{s-t-1}\right).\end{aligned} \tag{E.29}$$

Similarly, the statical average $\left\langle \widehat{\chi}^\dagger \hat{A} \begin{bmatrix} k \\ \nu \end{bmatrix} \right\rangle$ can be obtained by starting with the hamiltonian commutator relation Eq. (E.20). Using the definition of commutation Eq. (E.10), Eq. (E.20) can be rewritten as

$$\hat{A} \begin{bmatrix} k \\ \nu \end{bmatrix} \widehat{\mathcal{H}} = \left(\widehat{\mathcal{H}} + \hbar\omega \begin{bmatrix} k \\ \nu \end{bmatrix}\right) \hat{A} \begin{bmatrix} k \\ \nu \end{bmatrix} + \hat{R} \begin{bmatrix} k \\ \nu \end{bmatrix}. \tag{E.30}$$

Operating Eq. (E.30) on $\widehat{\mathcal{H}}$ and using Eq. (E.30) again gives

$$\begin{aligned}\hat{A} \begin{bmatrix} k \\ \nu \end{bmatrix} \widehat{\mathcal{H}}^2 &= \left(\widehat{\mathcal{H}} + \hbar\omega \begin{bmatrix} k \\ \nu \end{bmatrix}\right) \hat{A} \begin{bmatrix} k \\ \nu \end{bmatrix} \widehat{\mathcal{H}} + \hat{R} \begin{bmatrix} k \\ \nu \end{bmatrix} \widehat{\mathcal{H}}, \\ &= \left(\widehat{\mathcal{H}} + \hbar\omega \begin{bmatrix} k \\ \nu \end{bmatrix}\right)^2 \hat{A} \begin{bmatrix} k \\ \nu \end{bmatrix} + \left(\widehat{\mathcal{H}} + \hbar\omega \begin{bmatrix} k \\ \nu \end{bmatrix}\right) \hat{R} \begin{bmatrix} k \\ \nu \end{bmatrix} + \hat{R} \begin{bmatrix} k \\ \nu \end{bmatrix} \widehat{\mathcal{H}}.\end{aligned} \tag{E.31}$$

Repeating the same procedure for s times results in

$$\hat{A}\begin{bmatrix}k\\ \nu\end{bmatrix}\widehat{\mathcal{H}}^{s}=\left(\widehat{\mathcal{H}}+\hbar\omega\begin{bmatrix}k\\ \nu\end{bmatrix}\right)^{s}\hat{A}\begin{bmatrix}k\\ \nu\end{bmatrix}+\sum_{t=0}^{s-1}\left(\widehat{\mathcal{H}}+\hbar\omega\begin{bmatrix}k\\ \nu\end{bmatrix}\right)^{s-t-1}\hat{R}\begin{bmatrix}k\\ \nu\end{bmatrix}\widehat{\mathcal{H}}^{t},\quad s=1,2,\ldots. \tag{E.32}$$

Using Eqs. (E.32) and (E.24), it is possible to obtain the relation

$$\begin{aligned}\hat{A}\begin{bmatrix}k\\ \nu\end{bmatrix}\exp\left\{-\frac{\widehat{\mathcal{H}}}{k_BT}\right\}&=\exp\left\{-\frac{\left(\widehat{\mathcal{H}}+\hbar\omega\begin{bmatrix}k\\ \nu\end{bmatrix}\right)}{k_BT}\right\}\hat{A}\begin{bmatrix}k\\ \nu\end{bmatrix}\\&\quad+\sum_{s=1}^{\infty}(s!)^{-1}\left(-k_BT\right)^{-s}\sum_{t=0}^{s-1}\left(\widehat{\mathcal{H}}+\hbar\omega\begin{bmatrix}k\\ \nu\end{bmatrix}\right)^{s-t-1}\hat{R}\begin{bmatrix}k\\ \nu\end{bmatrix}\widehat{\mathcal{H}}^{t}.\end{aligned} \tag{E.33}$$

The statistical average $\left\langle\widehat{\chi}^{\dagger}\hat{A}\begin{bmatrix}k\\ \nu\end{bmatrix}\right\rangle$ is given by

$$\left\langle\widehat{\chi}^{\dagger}\hat{A}\begin{bmatrix}k\\ \nu\end{bmatrix}\right\rangle=Z^{-1}\mathrm{Tr}\left(\widehat{\chi}^{\dagger}\hat{A}\begin{bmatrix}k\\ \nu\end{bmatrix}\exp\left\{-\frac{\widehat{\mathcal{H}}}{k_BT}\right\}\right), \tag{E.34}$$

and using Eq. (E.33) gives

$$\begin{aligned}\left\langle\widehat{\chi}^{\dagger}\hat{A}\begin{bmatrix}k\\ \nu\end{bmatrix}\right\rangle&=\exp\left\{-\frac{\hbar\omega\begin{bmatrix}k\\ \nu\end{bmatrix}}{k_BT}\right\}Z^{-1}\mathrm{Tr}\left(\widehat{\chi}^{\dagger}\exp\left\{-\frac{\widehat{\mathcal{H}}}{k_BT}\right\}\hat{A}\begin{bmatrix}k\\ \nu\end{bmatrix}\right)\\&\quad+Z^{-1}\mathrm{Tr}\left(\widehat{\chi}^{\dagger}\sum_{s=1}^{\infty}(s!)^{-1}\left(-k_BT\right)^{-s}\sum_{t=0}^{s-1}\left(\widehat{\mathcal{H}}+\hbar\omega\begin{bmatrix}k\\ \nu\end{bmatrix}\right)^{s-t-1}\hat{R}\begin{bmatrix}k\\ \nu\end{bmatrix}\widehat{\mathcal{H}}^{t}\right).\end{aligned} \tag{E.35}$$

Using the cyclic permutation theorem for traces, Eq. (E.35) is rewritten as

$$\begin{aligned}\left\langle\widehat{\chi}^{\dagger}\hat{A}\begin{bmatrix}k\\ \nu\end{bmatrix}\right\rangle&=\exp\left\{-\frac{\hbar\omega\begin{bmatrix}k\\ \nu\end{bmatrix}}{k_BT}\right\}Z^{-1}\mathrm{Tr}\left(\hat{A}\begin{bmatrix}k\\ \nu\end{bmatrix}\widehat{\chi}^{\dagger}\exp\left\{-\frac{\widehat{\mathcal{H}}}{k_BT}\right\}\right)\\&\quad+Z^{-1}\mathrm{Tr}\left(\widehat{\chi}^{\dagger}\sum_{s=1}^{\infty}(s!)^{-1}\left(-k_BT\right)^{-s}\sum_{t=0}^{s-1}\left(\widehat{\mathcal{H}}+\hbar\omega\begin{bmatrix}k\\ \nu\end{bmatrix}\right)^{s-t-1}\hat{R}\begin{bmatrix}k\\ \nu\end{bmatrix}\widehat{\mathcal{H}}^{t}\right).\end{aligned} \tag{E.36}$$

Using Eq. (E.27), Eq. (E.36) is further reduced to

$$\left\langle \widehat{\chi}^{\dagger}\hat{A}\begin{bmatrix}k\\ \nu\end{bmatrix}\right\rangle = \exp\left\{-\frac{\hbar\omega\begin{bmatrix}k\\ \nu\end{bmatrix}}{k_BT}\right\}\left\langle \hat{A}\begin{bmatrix}k\\ \nu\end{bmatrix}\widehat{\chi}^{\dagger}\right\rangle + Z^{-1}\mathrm{Tr}\left(\widehat{\chi}^{\dagger}\sum_{s=1}^{\infty}(s!)^{-1}\left(-k_BT\right)^{-s}\sum_{t=0}^{s-1}\left(\widehat{\mathcal{H}}+\hbar\omega\begin{bmatrix}k\\ \nu\end{bmatrix}\right)^{s-t-1}\hat{R}\begin{bmatrix}k\\ \nu\end{bmatrix}\widehat{\mathcal{H}}^{t}\right). \tag{E.37}$$

The basic equations of the statistical perturbation method for $\left\langle \hat{A}^{\dagger}\begin{bmatrix}k\\ \nu\end{bmatrix}\widehat{\chi}\right\rangle$ and $\left\langle \widehat{\chi}^{\dagger}\hat{A}\begin{bmatrix}k\\ \nu\end{bmatrix}\right\rangle$ are given by Eqs. (E.29) and (E.37). Since remainders $\hat{R}^{\dagger}\begin{bmatrix}k\\ \nu\end{bmatrix}$ and $\hat{R}\begin{bmatrix}k\\ \nu\end{bmatrix}$ are considered to be small, the statistical perturbation method considers the last terms in Eqs. (E.29) and (E.37) as the perturbation terms and may be approximated.

E.2.1 Zeroth-order perturbation

The zeroth-order statistical perturbation method considers the first-order terms in remainders $O\left(\hat{R}^{\dagger}\begin{bmatrix}k\\ \nu\end{bmatrix}\right)$ and $O\left(\hat{R}\begin{bmatrix}k\\ \nu\end{bmatrix}\right)$ as negligible. The hamiltonian commutator relations Eqs. (E.19) and (E.20) with first-order terms in remainders neglected are given by

$$\left[\widehat{\mathcal{H}},\hat{A}^{\dagger}\begin{bmatrix}k\\ \nu\end{bmatrix}\right] = \hbar\omega\begin{bmatrix}k\\ \nu\end{bmatrix}\hat{A}^{\dagger}\begin{bmatrix}k\\ \nu\end{bmatrix}, \tag{E.38}$$

$$\left[\widehat{\mathcal{H}},\hat{A}\begin{bmatrix}k\\ \nu\end{bmatrix}\right] = -\hbar\omega\begin{bmatrix}k\\ \nu\end{bmatrix}\hat{A}\begin{bmatrix}k\\ \nu\end{bmatrix}. \tag{E.39}$$

A simple expression for the statistical average $\left\langle \hat{A}^{\dagger}\begin{bmatrix}k\\ \nu\end{bmatrix}\widehat{\chi}\right\rangle$ correct to zeroth-order in remainders can be obtained by neglecting the remainder terms in Eq. (E.29) given by

$$\left\langle \hat{A}^{\dagger}\begin{bmatrix}k\\ \nu\end{bmatrix}\widehat{\chi}\right\rangle = \exp\left\{-\frac{\hbar\omega\begin{bmatrix}k\\ \nu\end{bmatrix}}{k_BT}\right\}\left\langle \widehat{\chi}\hat{A}^{\dagger}\begin{bmatrix}k\\ \nu\end{bmatrix}\right\rangle. \tag{E.40}$$

Eq. (E.40) can be rewritten in a form containing operator commutators as follows

$$\left(\exp\left\{\frac{\hbar\omega\begin{bmatrix}k\\ \nu\end{bmatrix}}{k_BT}\right\}-1\right)\left\langle \hat{A}^{\dagger}\begin{bmatrix}k\\ \nu\end{bmatrix}\widehat{\chi}\right\rangle = \left\langle \widehat{\chi}\hat{A}^{\dagger}\begin{bmatrix}k\\ \nu\end{bmatrix}-\hat{A}^{\dagger}\begin{bmatrix}k\\ \nu\end{bmatrix}\widehat{\chi}\right\rangle. \tag{E.41}$$

From Eq. (E.41) it follows that

$$\left\langle \hat{A}^{\dagger}\begin{bmatrix} k \\ \nu \end{bmatrix} \widehat{\chi} \right\rangle = \left(\exp\left\{ \frac{\hbar\omega\begin{bmatrix} k \\ \nu \end{bmatrix}}{k_B T} \right\} - 1 \right)^{-1} \left\langle \left[\widehat{\chi}, \hat{A}^{\dagger}\begin{bmatrix} k \\ \nu \end{bmatrix} \right] \right\rangle . \tag{E.42}$$

Similarly, a simple expression for the statistical average $\left\langle \widehat{\chi}^{\dagger} \hat{A}\begin{bmatrix} k \\ \nu \end{bmatrix} \right\rangle$ correct to zeroth-order in remainders can be obtained by neglecting the remainder terms in Eq. (E.37) given by

$$\left\langle \widehat{\chi}^{\dagger} \hat{A}\begin{bmatrix} k \\ \nu \end{bmatrix} \right\rangle = \exp\left\{ -\frac{\hbar\omega\begin{bmatrix} k \\ \nu \end{bmatrix}}{k_B T} \right\} \left\langle \hat{A}^{\dagger}\begin{bmatrix} k \\ \nu \end{bmatrix} \widehat{\chi}^{\dagger} \right\rangle . \tag{E.43}$$

Eq. (E.43) can be rewritten in a form containing operator commutators as

$$\left(\exp\left\{ \frac{\hbar\omega\begin{bmatrix} k \\ \nu \end{bmatrix}}{k_B T} \right\} - 1 \right) \left\langle \widehat{\chi}^{\dagger} \hat{A}\begin{bmatrix} k \\ \nu \end{bmatrix} \right\rangle = \left\langle \hat{A}^{\dagger}\begin{bmatrix} k \\ \nu \end{bmatrix} \widehat{\chi}^{\dagger} - \widehat{\chi}^{\dagger} \hat{A}\begin{bmatrix} k \\ \nu \end{bmatrix} \right\rangle . \tag{E.44}$$

From Eq. (E.44) it follows that

$$\left\langle \widehat{\chi}^{\dagger} \hat{A}\begin{bmatrix} k \\ \nu \end{bmatrix} \right\rangle = \left(\exp\left\{ \frac{\hbar\omega\begin{bmatrix} k \\ \nu \end{bmatrix}}{k_B T} \right\} - 1 \right)^{-1} \left\langle \left[\hat{A}^{\dagger}\begin{bmatrix} k \\ \nu \end{bmatrix} \widehat{\chi}^{\dagger} \right] \right\rangle . \tag{E.45}$$

Eqs. (E.42) and (E.45) are the zeroth-order basic equations of the statistical perturbation method.

Since the remainders $\hat{R}^{\dagger}\begin{bmatrix} k \\ \nu \end{bmatrix}$ and $\hat{R}\begin{bmatrix} k \\ \nu \end{bmatrix}$ are assumed to be very small and neglected, the operator $\hat{A}^{\dagger}\begin{bmatrix} k \\ \nu \end{bmatrix}$ creates an excitation of energy $\hbar\omega\begin{bmatrix} k \\ \nu \end{bmatrix}$ and the operator $\hat{A}\begin{bmatrix} k \\ \nu \end{bmatrix}$ annihilates the excitation of energy $\hbar\omega\begin{bmatrix} k \\ \nu \end{bmatrix}$. This implies that the operators $\hat{A}^{\dagger}\begin{bmatrix} k \\ \nu \end{bmatrix}$ and $\hat{A}\begin{bmatrix} k \\ \nu \end{bmatrix}$ satisfy the commutation relations Eq. (E.14) exactly. Eq. (E.42) with $\widehat{\chi} = \hat{A}\begin{bmatrix} k' \\ \nu' \end{bmatrix}$ results in

$$\left\langle \hat{A}^{\dagger}\begin{bmatrix} k \\ \nu \end{bmatrix} \hat{A}\begin{bmatrix} k' \\ \nu' \end{bmatrix} \right\rangle = \delta_{kk'}\delta_{\nu\nu'} \left(\exp\left\{ \frac{\hbar\omega\begin{bmatrix} k \\ \nu \end{bmatrix}}{k_B T} \right\} - 1 \right)^{-1} . \tag{E.46}$$

Eq. (E.46) results in the well known Bose-Einstein distribution which gives the mean number of phonons $\left\langle n\begin{bmatrix} k \\ \nu \end{bmatrix} \right\rangle$ of a single-particle state $\begin{bmatrix} k \\ \nu \end{bmatrix}$ given by

$$\left\langle n\begin{bmatrix} k \\ \nu \end{bmatrix} \right\rangle = \left\langle \hat{A}^{\dagger}\begin{bmatrix} k \\ \nu \end{bmatrix} \hat{A}\begin{bmatrix} k \\ \nu \end{bmatrix} \right\rangle = \left(\exp\left\{ \frac{\hbar\omega\begin{bmatrix} k \\ \nu \end{bmatrix}}{k_B T} \right\} - 1 \right)^{-1} . \tag{E.47}$$

E.2.2 First-order perturbation

The first-order statistical perturbation method involves the calculation of the statistical averages $\left\langle \hat{A}^\dagger\left[{}^{k}_{\nu}\right] \widehat{\chi} \right\rangle$ by considering the second-order contributions of the remainders $O\left(\hat{R}^\dagger\left[{}^{k}_{\nu}\right] \hat{R}\left[{}^{k}_{\nu}\right]\right)$ as negligible.

The hamiltonian commutator equations are given by Eqs. (E.19) and (E.20) and the corresponding statistical averages $\left\langle \hat{A}^\dagger\left[{}^{k}_{\nu}\right] \widehat{\chi} \right\rangle$ and $\left\langle \widehat{\chi}^\dagger \hat{A}\left[{}^{k}_{\nu}\right] \right\rangle$ are given by Eqs. (E.29) and (E.37) respectively.

A particular useful average $\left\langle \hat{A}^\dagger\left[{}^{k}_{\nu}\right] \hat{A}\left[{}^{k}_{\nu}\right] \right\rangle$ is obtained by setting $\widehat{\chi} = \hat{A}\left[{}^{k}_{\nu}\right]$ in Eq. (E.29). For this case, the perturbation term in Eq. (E.29) is easily evaluated as a power series in $\hat{R}^\dagger\left[{}^{k}_{\nu}\right]$. The perturbation term (last term in Eq. (E.29)) with $\widehat{\chi} = \hat{A}\left[{}^{k}_{\nu}\right]$ is

$$Z^{-1}\mathrm{Tr}\left(\hat{A}\left[{}^{k}_{\nu}\right]\sum_{s=1}^{\infty}(s!)^{-1}\left(-k_BT\right)^{-s}\sum_{t=0}^{s-1}\widehat{\mathcal{H}}^t\hat{R}^\dagger\left[{}^{k}_{\nu}\right]\left(\widehat{\mathcal{H}}+\hbar\omega\left[{}^{k}_{\nu}\right]\right)^{s-t-1}\right), \tag{E.48}$$

and permutating $\hat{A}\left[{}^{k}_{\nu}\right]$ inside the trace results in

$$Z^{-1}\mathrm{Tr}\left(\sum_{s=1}^{\infty}(s!)^{-1}\left(-k_BT\right)^{-s}\sum_{t=0}^{s-1}\widehat{\mathcal{H}}^t\hat{R}^\dagger\left[{}^{k}_{\nu}\right]\left(\widehat{\mathcal{H}}+\hbar\omega\left[{}^{k}_{\nu}\right]\right)^{s-t-1}\hat{A}\left[{}^{k}_{\nu}\right]\right). \tag{E.49}$$

Further evaluation of the perturbation term Eq. (E.49) can be done by considering Eq. (E.32). Replacing s by $s-t-1$ in Eq. (E.32) results in

$$\hat{A}\left[{}^{k}_{\nu}\right]\widehat{\mathcal{H}}^{s-t-1} = \left(\widehat{\mathcal{H}}+\hbar\omega\left[{}^{k}_{\nu}\right]\right)^{s-t-1}\hat{A}\left[{}^{k}_{\nu}\right] + O\left(\hat{R}\left[{}^{k}_{\nu}\right]\right), \tag{E.50}$$

where details of the terms $O\left(\hat{R}\left[{}^{k}_{\nu}\right]\right)$ are not necessary. Using Eq. (E.50), the perturbation term Eq. (E.49) can be written as

$$Z^{-1}\mathrm{Tr}\left(\sum_{s=1}^{\infty}(s!)^{-1}\left(-k_BT\right)^{-s}\sum_{t=0}^{s-1}\widehat{\mathcal{H}}^t\hat{R}^\dagger\left[{}^{k}_{\nu}\right]\hat{A}\left[{}^{k}_{\nu}\right]\widehat{\mathcal{H}}^{s-t-1}\right) + O(\hat{R}^\dagger\left[{}^{k}_{\nu}\right]\hat{R}\left[{}^{k}_{\nu}\right]), \tag{E.51}$$

and permuting $\widehat{\mathcal{H}}^t$ inside the trace of Eq. (E.51) results in

$$Z^{-1}\mathrm{Tr}\left(\sum_{s=1}^{\infty}(s!)^{-1}\left(-k_BT\right)^{-s}\sum_{t=0}^{s-1}\hat{R}^\dagger\left[{}^{k}_{\nu}\right]\hat{A}\left[{}^{k}_{\nu}\right]\widehat{\mathcal{H}}^{s-1}\right) + O(\hat{R}^\dagger\left[{}^{k}_{\nu}\right]\hat{R}\left[{}^{k}_{\nu}\right]). \tag{E.52}$$

Eq. (E.52) has the sum on t which contains s same terms. So $\sum_t$ in Eq. (E.52) can be replaced by s such that the resulting perturbation term becomes

$$\begin{aligned}
&-(k_BT)^{-1}\,Z^{-1}\mathrm{Tr}\left(\hat{R}^{\dagger}\begin{bmatrix}k\\ \nu\end{bmatrix}\hat{A}\begin{bmatrix}k\\ \nu\end{bmatrix}\sum_{s=1}^{\infty}[(s-1)!]^{-1}\,(-k_BT)^{-(s-1)}\,\widehat{\mathcal{H}}^{s-1}\right)+O(\hat{R}^{\dagger}\begin{bmatrix}k\\ \nu\end{bmatrix}\hat{R}\begin{bmatrix}k\\ \nu\end{bmatrix})\\
&=-(k_BT)^{-1}\,Z^{-1}\mathrm{Tr}\left(\hat{R}^{\dagger}\begin{bmatrix}k\\ \nu\end{bmatrix}\hat{A}\begin{bmatrix}k\\ \nu\end{bmatrix}\exp\left\{-\frac{\widehat{\mathcal{H}}}{k_BT}\right\}\right)+O(\hat{R}^{\dagger}\begin{bmatrix}k\\ \nu\end{bmatrix}\hat{R}\begin{bmatrix}k\\ \nu\end{bmatrix}),\\
&=-(k_BT)^{-1}\left\langle\hat{R}^{\dagger}\begin{bmatrix}k\\ \nu\end{bmatrix}\hat{A}\begin{bmatrix}k\\ \nu\end{bmatrix}\right\rangle+O(\hat{R}^{\dagger}\begin{bmatrix}k\\ \nu\end{bmatrix}\hat{R}\begin{bmatrix}k\\ \nu\end{bmatrix}).
\end{aligned}\tag{E.53}$$

Here, the perturbation term Eq. (E.53) is evaluated to the first-order of $\hat{R}^{\dagger}\begin{bmatrix}k\\ \nu\end{bmatrix}$ with second-order term $O(\hat{R}^{\dagger}\begin{bmatrix}k\\ \nu\end{bmatrix}\hat{R}\begin{bmatrix}k\\ \nu\end{bmatrix})$ considered to be negligible. Finally, using Eq. (E.53), the statistical average $\left\langle\hat{A}^{\dagger}\begin{bmatrix}k\\ \nu\end{bmatrix}\hat{A}\begin{bmatrix}k\\ \nu\end{bmatrix}\right\rangle$ Eq. (E.29) is given by

$$\begin{aligned}
\left\langle\hat{A}^{\dagger}\begin{bmatrix}k\\ \nu\end{bmatrix}\hat{A}\begin{bmatrix}k\\ \nu\end{bmatrix}\right\rangle=\exp\left\{-\frac{\hbar\omega\begin{bmatrix}k\\ \nu\end{bmatrix}}{k_BT}\right\}\left\langle\hat{A}\begin{bmatrix}k\\ \nu\end{bmatrix}\hat{A}^{\dagger}\begin{bmatrix}k\\ \nu\end{bmatrix}\right\rangle\\
-(k_BT)^{-1}\left\langle\hat{R}^{\dagger}\begin{bmatrix}k\\ \nu\end{bmatrix}\hat{A}\begin{bmatrix}k\\ \nu\end{bmatrix}\right\rangle.
\end{aligned}\tag{E.54}$$

Multiplying Eq. (E.54) with $\exp\left\{\frac{\hbar\omega\begin{bmatrix}k\\ \nu\end{bmatrix}}{k_BT}\right\}$ and subtracting $\left\langle\hat{A}^{\dagger}\begin{bmatrix}k\\ \nu\end{bmatrix}\hat{A}\begin{bmatrix}k\\ \nu\end{bmatrix}\right\rangle$ on both left hand side and right hand side of Eq. (E.54) results in

$$\begin{aligned}
\left(\exp\left\{\frac{\hbar\omega\begin{bmatrix}k\\ \nu\end{bmatrix}}{k_BT}\right\}-1\right)\left\langle\hat{A}^{\dagger}\begin{bmatrix}k\\ \nu\end{bmatrix}\hat{A}\begin{bmatrix}k\\ \nu\end{bmatrix}\right\rangle=\left\langle\hat{A}\begin{bmatrix}k\\ \nu\end{bmatrix}\hat{A}^{\dagger}\begin{bmatrix}k\\ \nu\end{bmatrix}-\hat{A}^{\dagger}\begin{bmatrix}k\\ \nu\end{bmatrix}\hat{A}\begin{bmatrix}k\\ \nu\end{bmatrix}\right\rangle\\
-(k_BT)^{-1}\exp\left\{\frac{\hbar\omega\begin{bmatrix}k\\ \nu\end{bmatrix}}{k_BT}\right\}\left\langle\hat{R}^{\dagger}\begin{bmatrix}k\\ \nu\end{bmatrix}\hat{A}\begin{bmatrix}k\\ \nu\end{bmatrix}\right\rangle.
\end{aligned}\tag{E.55}$$

Rearranging the terms in Eq. (E.55) results in the first-order basic equation of the statistical perturbation method given by

$$\begin{aligned}
\left\langle\hat{A}^{\dagger}\begin{bmatrix}k\\ \nu\end{bmatrix}\hat{A}\begin{bmatrix}k\\ \nu\end{bmatrix}\right\rangle=\left(\exp\left\{\frac{\hbar\omega\begin{bmatrix}k\\ \nu\end{bmatrix}}{k_BT}\right\}-1\right)^{-1}\left\langle\left[\hat{A}\begin{bmatrix}k\\ \nu\end{bmatrix},\hat{A}^{\dagger}\begin{bmatrix}k\\ \nu\end{bmatrix}\right]\right\rangle\\
-(k_BT)^{-1}\left[\frac{\exp\left\{\frac{\hbar\omega\begin{bmatrix}k\\ \nu\end{bmatrix}}{k_BT}\right\}}{\exp\left\{\frac{\hbar\omega\begin{bmatrix}k\\ \nu\end{bmatrix}}{k_BT}\right\}-1}\right]\left\langle\hat{R}^{\dagger}\begin{bmatrix}k\\ \nu\end{bmatrix}\hat{A}\begin{bmatrix}k\\ \nu\end{bmatrix}\right\rangle.
\end{aligned}\tag{E.56}$$

This equation is useful for calculating the averages $\left\langle \hat{A}^\dagger\left[{k \atop \nu}\right] \hat{A}\left[{k \atop \nu}\right] \right\rangle$ correct to first-order in $\hat{R}^\dagger\left[{k \atop \nu}\right]$.

E.2.3 Renormalized energies

A further procedure of the statistical perturbation method consists of introducing the renormalized energies $\hbar\widetilde{\omega}\left[{k \atop \nu}\right]$ defined as

$$\hbar\widetilde{\omega}\left[{k \atop \nu}\right] = \hbar\omega\left[{k \atop \nu}\right] + \hbar\delta\omega\left[{k \atop \nu}\right], \tag{E.57}$$

where energy shifts $\hbar\delta\omega\left[{k \atop \nu}\right]$ are assumed to be of same order as the statistical average of operators linear in $\hat{R}^\dagger\left[{k \atop \nu}\right]$ or $\hat{R}\left[{k \atop \nu}\right]$.

By making the first-order perturbation terms in Eq. (E.56) vanish identically, it is possible to calculate the renormalized energies $\hbar\widetilde{\omega}\left[{k \atop \nu}\right]$. This can be done by using Eq. (E.57) to rewrite the Hamiltonian commutator equation Eq. (E.19) as

$$\left[\widehat{\mathcal{H}}, \hat{A}^\dagger\left[{k \atop \nu}\right]\right] = \hbar\widetilde{\omega}\left[{k \atop \nu}\right] \hat{A}^\dagger\left[{k \atop \nu}\right] + \left(\hat{R}^\dagger\left[{k \atop \nu}\right] - \hbar\delta\omega\left[{k \atop \nu}\right] \hat{A}^\dagger\left[{k \atop \nu}\right]\right). \tag{E.58}$$

In view of Eq. (E.58) all the derivations in Sections E.2.1 and E.2.2 are valid with $\hbar\omega\left[{k \atop \nu}\right]$ replaced by $\hbar\widetilde{\omega}\left[{k \atop \nu}\right]$ and $\hat{R}^\dagger\left[{k \atop \nu}\right]$ replaced by $\left(\hat{R}^\dagger\left[{k \atop \nu}\right] - \hbar\delta\omega\left[{k \atop \nu}\right] \hat{A}^\dagger\left[{k \atop \nu}\right]\right)$. In particular, Eq. (E.56) becomes

$$\begin{aligned}\left\langle \hat{A}^\dagger\left[{k \atop \nu}\right] \hat{A}\left[{k \atop \nu}\right] \right\rangle = &\left(\exp\left\{\frac{\hbar\widetilde{\omega}\left[{k \atop \nu}\right]}{k_B T}\right\} - 1\right)^{-1} \left\langle \left[\hat{A}\left[{k \atop \nu}\right], \hat{A}^\dagger\left[{k \atop \nu}\right]\right] \right\rangle \\ &- (k_B T)^{-1} \left[\frac{\exp\left\{\frac{\hbar\widetilde{\omega}\left[{k \atop \nu}\right]}{k_B T}\right\}}{\exp\left\{\frac{\hbar\widetilde{\omega}\left[{k \atop \nu}\right]}{k_B T}\right\} - 1}\right] \left\langle \left(\hat{R}^\dagger\left[{k \atop \nu}\right] - \hbar\delta\omega\left[{k \atop \nu}\right] \hat{A}^\dagger\left[{k \atop \nu}\right]\right) \hat{A}\left[{k \atop \nu}\right] \right\rangle.\end{aligned} \tag{E.59}$$

The first-order perturbation term in Eq. (E.59) vanishes if

$$\left\langle \left(\hat{R}^\dagger\left[{k \atop \nu}\right] - \hbar\delta\omega\left[{k \atop \nu}\right] \hat{A}^\dagger\left[{k \atop \nu}\right]\right) \hat{A}\left[{k \atop \nu}\right] \right\rangle = \left\langle \hat{R}^\dagger\left[{k \atop \nu}\right] \hat{A}\left[{k \atop \nu}\right] \right\rangle - \hbar\delta\omega\left[{k \atop \nu}\right] \left\langle \hat{A}^\dagger\left[{k \atop \nu}\right] \hat{A}\left[{k \atop \nu}\right] \right\rangle = 0, \tag{E.60}$$

which gives

$$\hbar\delta\omega\left[\begin{smallmatrix}k\\ \nu\end{smallmatrix}\right] = \frac{\left\langle \hat{R}^{\dagger}\left[\begin{smallmatrix}k\\ \nu\end{smallmatrix}\right] \hat{A}\left[\begin{smallmatrix}k\\ \nu\end{smallmatrix}\right]\right\rangle}{\left\langle \hat{A}^{\dagger}\left[\begin{smallmatrix}k\\ \nu\end{smallmatrix}\right] \hat{A}\left[\begin{smallmatrix}k\\ \nu\end{smallmatrix}\right]\right\rangle}. \tag{E.61}$$

Thus, with the energy shifts $\hbar\delta\omega\left[\begin{smallmatrix}k\\ \nu\end{smallmatrix}\right]$ given by Eq. (E.61), the first-order basic equation Eq. (E.59) reduces to a zeroth-order basic equation with renormalized energies $\hbar\widetilde{\omega}\left[\begin{smallmatrix}k\\ \nu\end{smallmatrix}\right]$ given by

$$\left\langle \hat{A}^{\dagger}\left[\begin{smallmatrix}k\\ \nu\end{smallmatrix}\right] \hat{A}\left[\begin{smallmatrix}k\\ \nu\end{smallmatrix}\right]\right\rangle = \left(\exp\left\{\frac{\hbar\widetilde{\omega}\left[\begin{smallmatrix}k\\ \nu\end{smallmatrix}\right]}{k_B T}\right\} - 1\right)^{-1} \left\langle \left[\hat{A}\left[\begin{smallmatrix}k\\ \nu\end{smallmatrix}\right], \hat{A}^{\dagger}\left[\begin{smallmatrix}k\\ \nu\end{smallmatrix}\right]\right]\right\rangle. \tag{E.62}$$

The coupled equations Eqs. (E.61) and (E.62) must be solved self-consistently. However, all the above calculations were carried only to first-order in $\hat{R}^{\dagger}\left[\begin{smallmatrix}k\\ \nu\end{smallmatrix}\right]$ and $\hat{R}\left[\begin{smallmatrix}k\\ \nu\end{smallmatrix}\right]$ operators. Hence, it is consistent to evaluate Eq. (E.60) correct to first-order in remainder operators. This can be achieved by evaluating all the terms of Eq. (E.60) in zeroth-order. The zeroth-order expression for $\left\langle \hat{R}^{\dagger}\left[\begin{smallmatrix}k\\ \nu\end{smallmatrix}\right] \hat{A}\left[\begin{smallmatrix}k\\ \nu\end{smallmatrix}\right]\right\rangle$ is obtained by setting $\widehat{\chi}^{\dagger} = \hat{R}^{\dagger}\left[\begin{smallmatrix}k\\ \nu\end{smallmatrix}\right]$ in Eq. (E.37) which results in

$$\left\langle \hat{R}^{\dagger}\left[\begin{smallmatrix}k\\ \nu\end{smallmatrix}\right] \hat{A}\left[\begin{smallmatrix}k\\ \nu\end{smallmatrix}\right]\right\rangle = \exp\left\{-\frac{\hbar\omega\left[\begin{smallmatrix}k\\ \nu\end{smallmatrix}\right]}{k_B T}\right\} \left\langle \hat{A}\left[\begin{smallmatrix}k\\ \nu\end{smallmatrix}\right] \hat{R}^{\dagger}\left[\begin{smallmatrix}k\\ \nu\end{smallmatrix}\right]\right\rangle + O\left(\hat{R}^{\dagger}\left[\begin{smallmatrix}k\\ \nu\end{smallmatrix}\right] \hat{R}\left[\begin{smallmatrix}k\\ \nu\end{smallmatrix}\right]\right). \tag{E.63}$$

Multiplying Eq. (E.63) with $\exp\left\{\frac{\hbar\omega\left[\begin{smallmatrix}k\\ \nu\end{smallmatrix}\right]}{k_B T}\right\}$ and subtracting $\left\langle \hat{R}^{\dagger}\left[\begin{smallmatrix}k\\ \nu\end{smallmatrix}\right] \hat{A}\left[\begin{smallmatrix}k\\ \nu\end{smallmatrix}\right]\right\rangle$ on both left hand side and right hand side of Eq. (E.63) results in

$$\begin{aligned}\left(\exp\left\{\frac{\hbar\omega\left[\begin{smallmatrix}k\\ \nu\end{smallmatrix}\right]}{k_B T}\right\} - 1\right) \left\langle \hat{R}^{\dagger}\left[\begin{smallmatrix}k\\ \nu\end{smallmatrix}\right] \hat{A}\left[\begin{smallmatrix}k\\ \nu\end{smallmatrix}\right]\right\rangle = \left\langle \hat{A}\left[\begin{smallmatrix}k\\ \nu\end{smallmatrix}\right] \hat{R}^{\dagger}\left[\begin{smallmatrix}k\\ \nu\end{smallmatrix}\right] - \hat{R}^{\dagger}\left[\begin{smallmatrix}k\\ \nu\end{smallmatrix}\right] \hat{A}\left[\begin{smallmatrix}k\\ \nu\end{smallmatrix}\right]\right\rangle \\ + O\left(\hat{R}^{\dagger}\left[\begin{smallmatrix}k\\ \nu\end{smallmatrix}\right] \hat{R}\left[\begin{smallmatrix}k\\ \nu\end{smallmatrix}\right]\right).\end{aligned} \tag{E.64}$$

Rearranging the terms in Eq. (E.64) results in

$$\left\langle \hat{R}^{\dagger}\left[\begin{smallmatrix}k\\ \nu\end{smallmatrix}\right] \hat{A}\left[\begin{smallmatrix}k\\ \nu\end{smallmatrix}\right]\right\rangle = \left(\exp\left\{\frac{\hbar\omega\left[\begin{smallmatrix}k\\ \nu\end{smallmatrix}\right]}{k_B T}\right\} - 1\right)^{-1} \left\langle \left[\hat{A}\left[\begin{smallmatrix}k\\ \nu\end{smallmatrix}\right], \hat{R}^{\dagger}\left[\begin{smallmatrix}k\\ \nu\end{smallmatrix}\right]\right]\right\rangle + O\left(\hat{R}^{\dagger}\left[\begin{smallmatrix}k\\ \nu\end{smallmatrix}\right] \hat{R}\left[\begin{smallmatrix}k\\ \nu\end{smallmatrix}\right]\right). \tag{E.65}$$

Using Eqs. (E.42) and (E.45), the zeroth order expression for $\hbar\delta\omega\left[\begin{smallmatrix}k\\ \nu\end{smallmatrix}\right]$ Eq. (E.61) can

be rewritten in terms of commutators as

$$\hbar\delta\omega\begin{bmatrix}k\\ \nu\end{bmatrix} = \frac{\left\langle\left[\hat{A}\begin{bmatrix}k\\ \nu\end{bmatrix}, \hat{R}^{\dagger}\begin{bmatrix}k\\ \nu\end{bmatrix}\right]\right\rangle}{\left\langle\left[\hat{A}\begin{bmatrix}k\\ \nu\end{bmatrix}, \hat{A}^{\dagger}\begin{bmatrix}k\\ \nu\end{bmatrix}\right]\right\rangle}. \tag{E.66}$$

The zeroth-order expression for $\left\langle \hat{A}^{\dagger}\begin{bmatrix}k\\ \nu\end{bmatrix} \hat{A}\begin{bmatrix}k\\ \nu\end{bmatrix}\right\rangle$ is obtained by setting $\widehat{\chi}^{\dagger} = \hat{A}^{\dagger}\begin{bmatrix}k\\ \nu\end{bmatrix}$ in Eq. (E.45) which gives

$$\left\langle \hat{A}^{\dagger}\begin{bmatrix}k\\ \nu\end{bmatrix} \hat{A}\begin{bmatrix}k\\ \nu\end{bmatrix}\right\rangle = \left(\exp\left\{\frac{\hbar\omega\begin{bmatrix}k\\ \nu\end{bmatrix}}{k_B T}\right\} - 1\right)^{-1} \left\langle\left[\hat{A}\begin{bmatrix}k\\ \nu\end{bmatrix}, \hat{A}^{\dagger}\begin{bmatrix}k\\ \nu\end{bmatrix}\right]\right\rangle + O\left(\hat{R}\begin{bmatrix}k\\ \nu\end{bmatrix}\right). \tag{E.67}$$

Substituting the zeroth-order expressions from Eqs. (E.65)–(E.67) in Eq. (E.60) results in

$$\begin{aligned}
&\left\langle \hat{R}^{\dagger}\begin{bmatrix}k\\ \nu\end{bmatrix} \hat{A}\begin{bmatrix}k\\ \nu\end{bmatrix}\right\rangle - \hbar\delta\omega\begin{bmatrix}k\\ \nu\end{bmatrix} \left\langle \hat{A}^{\dagger}\begin{bmatrix}k\\ \nu\end{bmatrix} \hat{A}\begin{bmatrix}k\\ \nu\end{bmatrix}\right\rangle \\
&= \left(\exp\left\{\frac{\hbar\omega\begin{bmatrix}k\\ \nu\end{bmatrix}}{k_B T}\right\} - 1\right)^{-1} \left\langle\left[\hat{A}\begin{bmatrix}k\\ \nu\end{bmatrix}, \hat{R}^{\dagger}\begin{bmatrix}k\\ \nu\end{bmatrix}\right]\right\rangle + O\left(\hat{R}^{\dagger}\begin{bmatrix}k\\ \nu\end{bmatrix} \hat{R}\begin{bmatrix}k\\ \nu\end{bmatrix}\right) \\
&- \frac{\left\langle\left[\hat{A}\begin{bmatrix}k\\ \nu\end{bmatrix}, \hat{R}^{\dagger}\begin{bmatrix}k\\ \nu\end{bmatrix}\right]\right\rangle}{\left\langle\left[\hat{A}\begin{bmatrix}k\\ \nu\end{bmatrix}, \hat{A}^{\dagger}\begin{bmatrix}k\\ \nu\end{bmatrix}\right]\right\rangle} \left\{\left(\exp\left\{\frac{\hbar\omega\begin{bmatrix}k\\ \nu\end{bmatrix}}{k_B T}\right\} - 1\right)^{-1} \left\langle\left[\hat{A}\begin{bmatrix}k\\ \nu\end{bmatrix}, \hat{A}^{\dagger}\begin{bmatrix}k\\ \nu\end{bmatrix}\right]\right\rangle + O\left(\hat{R}\begin{bmatrix}k\\ \nu\end{bmatrix}\right)\right\} \\
&= O\left(\hat{R}^{\dagger}\begin{bmatrix}k\\ \nu\end{bmatrix} \hat{R}\begin{bmatrix}k\\ \nu\end{bmatrix}\right).
\end{aligned} \tag{E.68}$$

From Eq. (E.68) it is clear that the evaluation of the energy shifts $\hbar\delta\omega\begin{bmatrix}k\\ \nu\end{bmatrix}$ in zeroth-order using Eq. (E.66) is consistent with the first-order calculations.

The first-order expressions derived in this section are useful in the derivation of the first-order SCA method using quantum mechanics developed in Section E.3.

E.3 First-order self-consistent approach

The first-order self-consistent approach involves the approximation of total potential energy with an effective harmonic potential energy such that the resultant effective harmonic hamiltonian can be used to study the effects of atomic vibrations. Here, the

coefficients of effective harmonic potential are calculated using the results from statistical perturbation method discussed in Section E.2. The first-order self-consistent equations are derived in Section E.3.1. Section E.3.2 explains the calculation of macroscopic quantities such as partition function and Helmholtz free energy using the first-order statistical averages. Finally, Section E.3.3 considers the self-consistent approach for the case of an ordinary perturbation problem and calculates the effective harmonic frequencies and corresponding Helmholtz free energy.

E.3.1 First-order self-consistent equations

The total hamiltonian operator of a chain of vibrating atoms about the configuration $\overset{o}{\mathbf{u}}$ is given by

$$\begin{aligned} \widehat{\mathcal{H}} &= \widehat{KE} + \widehat{\mathcal{E}}, \\ &= \widehat{KE} + \Phi_0 + \widehat{\Phi}_1 + \widehat{\Phi}_2 + \widehat{\Phi}_3 + \widehat{\Phi}_4 + \dots, \end{aligned} \tag{E.69}$$

where $\widehat{\mathcal{E}}$ is the total potential energy operator and $\widehat{\Phi}_1, \widehat{\Phi}_2, \widehat{\Phi}_3, \widehat{\Phi}_4, \dots$ are defined in Eq. (E.1).

The main idea of self-consistent approach is to introduce an effective harmonic potential operator $\widehat{\mathcal{E}}_{\text{eff}}$ such that

$$\begin{aligned} \widehat{\mathcal{H}} &= \widehat{KE} + \Phi_0 + \widehat{\mathcal{E}}_{\text{eff}} + \left(-\widehat{\mathcal{E}}_{\text{eff}} + \widehat{\Phi}_1 + \widehat{\Phi}_2 + \widehat{\Phi}_3 + \widehat{\Phi}_4 + \dots\right), \\ &= \widehat{\mathcal{H}}_{\text{eff}} + \left(-\widehat{\mathcal{E}}_{\text{eff}} + \widehat{\Phi}_1 + \widehat{\Phi}_2 + \widehat{\Phi}_3 + \widehat{\Phi}_4 + \dots\right), \\ &= \widehat{\mathcal{H}}_{\text{eff}} + \widehat{\mathcal{PT}}, \end{aligned} \tag{E.70}$$

where $\widehat{\mathcal{H}}_{\text{eff}}$ is the effective harmonic hamiltonian operator given by

$$\widehat{\mathcal{H}}_{\text{eff}} = \widehat{KE} + \Phi_0 + \widehat{\mathcal{E}}_{\text{eff}}, \tag{E.71}$$

and $\widehat{\mathcal{PT}} = \left(-\widehat{\mathcal{E}}_{\text{eff}} + \widehat{\Phi}_1 + \widehat{\Phi}_2 + \dots\right)$ is the perturbation operator. Here, $\widehat{\mathcal{E}}_{\text{eff}}$ has to be determined such that $\widehat{\mathcal{PT}}$ is small in the sense that it gives small contributions to the statistical averages. The kinetic and effective harmonic potential energy operators are

given by

$$\begin{aligned}\widehat{KE} &= \frac{1}{2}\sum_{\left[\begin{smallmatrix}\ell\\ \alpha\end{smallmatrix}\right]} m_\alpha \left(\delta\hat{u}\left[\begin{smallmatrix}\ell\\ \alpha\end{smallmatrix}\right]\right)^2, \\ \widehat{\mathcal{E}}_{\text{eff}} &= \frac{1}{2}\sum_{\left[\begin{smallmatrix}\ell\\ \alpha\end{smallmatrix}\right]}\sum_{\left[\begin{smallmatrix}\ell'\\ \alpha'\end{smallmatrix}\right]} \overset{o}{\Phi}_{\text{eff}}\left[\begin{smallmatrix}\ell\,\ell'\\ \alpha\alpha'\end{smallmatrix}\right] \delta\hat{u}\left[\begin{smallmatrix}\ell\\ \alpha\end{smallmatrix}\right] \delta\hat{u}\left[\begin{smallmatrix}\ell'\\ \alpha'\end{smallmatrix}\right].\end{aligned} \tag{E.72}$$

The position and momentum commutator relations are given by

$$\begin{aligned}\left[\delta\hat{u}\left[\begin{smallmatrix}\ell\\ \alpha\end{smallmatrix}\right], \delta\hat{u}\left[\begin{smallmatrix}\ell'\\ \alpha'\end{smallmatrix}\right]\right] &= \left(\frac{i\hbar}{m_\alpha}\right)\delta_{\ell\ell'}\delta_{\alpha\alpha'}, \\ \left[\delta\hat{u}\left[\begin{smallmatrix}\ell\\ \alpha\end{smallmatrix}\right], \delta\hat{u}\left[\begin{smallmatrix}\ell'\\ \alpha'\end{smallmatrix}\right]\right] &= \left[\delta\hat{u}\left[\begin{smallmatrix}\ell\\ \alpha\end{smallmatrix}\right], \delta\hat{u}\left[\begin{smallmatrix}\ell'\\ \alpha'\end{smallmatrix}\right]\right] = 0.\end{aligned} \tag{E.73}$$

Since total potential energy operator $\widehat{\mathcal{E}}$ is a general Taylor series in the atomic displacement operators $\delta\hat{u}\left[\begin{smallmatrix}\ell\\ \alpha\end{smallmatrix}\right]$, it follows that

$$\begin{aligned}\left[\widehat{\mathcal{E}}, \delta\hat{u}\left[\begin{smallmatrix}\ell\\ \alpha\end{smallmatrix}\right]\right] &= \left(\frac{i\hbar}{m_\alpha}\right)\frac{\partial\widehat{\mathcal{E}}}{\partial\left(\delta\hat{u}\left[\begin{smallmatrix}\ell\\ \alpha\end{smallmatrix}\right]\right)}, \\ \left[\widehat{\mathcal{E}}, \delta\hat{u}\left[\begin{smallmatrix}\ell\\ \alpha\end{smallmatrix}\right]\right] &= 0.\end{aligned} \tag{E.74}$$

Repeated application of Eq. (E.74) results in

$$\left[\left[\widehat{\mathcal{E}}, \delta\hat{u}\left[\begin{smallmatrix}\ell\\ \alpha\end{smallmatrix}\right]\right], \delta\hat{u}\left[\begin{smallmatrix}\ell'\\ \alpha'\end{smallmatrix}\right]\right] = \left(\frac{i\hbar}{m_\alpha}\right)^2 \frac{\partial^2\widehat{\mathcal{E}}}{\partial\left(\delta\hat{u}\left[\begin{smallmatrix}\ell\\ \alpha\end{smallmatrix}\right]\right)\partial\left(\delta\hat{u}\left[\begin{smallmatrix}\ell'\\ \alpha'\end{smallmatrix}\right]\right)}, \tag{E.75}$$

and so on.

Similar to Eq. (E.74), the effective harmonic potential operator $\widehat{\mathcal{E}}_{\text{eff}}$ defined by Eq. (E.72) satisfies

$$\begin{aligned}\left[\widehat{\mathcal{E}}_{\text{eff}}, \delta\hat{u}\left[\begin{smallmatrix}\ell\\ \alpha\end{smallmatrix}\right]\right] &= \left(\frac{i\hbar}{m_\alpha}\right)\frac{\partial\widehat{\mathcal{E}}_{\text{eff}}}{\partial\left(\delta\hat{u}\left[\begin{smallmatrix}\ell\\ \alpha\end{smallmatrix}\right]\right)}, \\ \left[\widehat{\mathcal{E}}_{\text{eff}}, \delta\hat{u}\left[\begin{smallmatrix}\ell\\ \alpha\end{smallmatrix}\right]\right] &= 0.\end{aligned} \tag{E.76}$$

Repeated application of Eq. (E.76) results in

$$\left[\left[\widehat{\mathcal{E}}_{\text{eff}}, \delta\hat{u}\left[\begin{smallmatrix}\ell\\ \alpha\end{smallmatrix}\right]\right], \delta\hat{u}\left[\begin{smallmatrix}\ell'\\ \alpha'\end{smallmatrix}\right]\right] = \left(\frac{i\hbar}{m_\alpha}\right)^2 \frac{\partial^2\widehat{\mathcal{E}}_{\text{eff}}}{\partial\left(\delta\hat{u}\left[\begin{smallmatrix}\ell\\ \alpha\end{smallmatrix}\right]\right)\partial\left(\delta\hat{u}\left[\begin{smallmatrix}\ell'\\ \alpha'\end{smallmatrix}\right]\right)}. \tag{E.77}$$

The effective harmonic hamiltonian operator $\widehat{\mathcal{H}}_{\text{eff}}$ is diagonalized by the transformation of atomic displacement operators $\delta\hat{u}\left[\begin{smallmatrix}\ell\\ \alpha\end{smallmatrix}\right]$ into normal coordinate operators

$$\begin{aligned}\delta\hat{u}\left[\begin{smallmatrix}\ell\\ \alpha\end{smallmatrix}\right] &= (nm_\alpha)^{-1/2}\sum_{\left[\begin{smallmatrix}k\\ \nu\end{smallmatrix}\right]}\hat{q}\left[\begin{smallmatrix}k\\ \nu\end{smallmatrix}\right]\mathrm{e}_{\text{eff}}\left[\begin{smallmatrix}\mathrm{k}\\ \nu\alpha\end{smallmatrix}\right]\exp\{\mathrm{ikX}[\ell]\},\\ \delta\hat{\dot{u}}\left[\begin{smallmatrix}\ell\\ \alpha\end{smallmatrix}\right] &= (nm_\alpha)^{-1/2}\sum_{\left[\begin{smallmatrix}k\\ \nu\end{smallmatrix}\right]}\hat{p}^*\left[\begin{smallmatrix}k\\ \nu\end{smallmatrix}\right]\mathrm{e}_{\text{eff}}\left[\begin{smallmatrix}\mathrm{k}\\ \nu\alpha\end{smallmatrix}\right]\exp\{\mathrm{ikX}[\ell]\},\end{aligned} \tag{E.78}$$

and by the transformation of normal mode operators into creation and annihilation operators

$$\begin{aligned}\hat{q}\left[\begin{smallmatrix}k\\ \nu\end{smallmatrix}\right] &= \left(\frac{\hbar}{2\omega_{\text{eff}}\left[\begin{smallmatrix}k\\ \nu\end{smallmatrix}\right]}\right)^{1/2}\left(\hat{A}\left[\begin{smallmatrix}k\\ \nu\end{smallmatrix}\right]+\hat{A}^\dagger\left[\begin{smallmatrix}-k\\ \nu\end{smallmatrix}\right]\right),\\ \hat{p}\left[\begin{smallmatrix}k\\ \nu\end{smallmatrix}\right] &= i\left(\frac{\hbar\omega_{\text{eff}}\left[\begin{smallmatrix}k\\ \nu\end{smallmatrix}\right]}{2}\right)^{1/2}\left(\hat{A}^\dagger\left[\begin{smallmatrix}k\\ \nu\end{smallmatrix}\right]-\hat{A}\left[\begin{smallmatrix}-k\\ \nu\end{smallmatrix}\right]\right),\end{aligned} \tag{E.79}$$

where $\omega^2_{\text{eff}}\left[\begin{smallmatrix}k\\ \nu\end{smallmatrix}\right]$ and $\mathbf{e}_{\text{eff}}\left[\begin{smallmatrix}k\\ \nu\end{smallmatrix}\right]$ are the eigenvalues and corresponding normalized eigenvectors of effective dynamical matrix given by

$$\mathbb{K}_{\text{eff}}\left[\begin{smallmatrix}k\\ \alpha\alpha'\end{smallmatrix}\right] = (m_\alpha m_{\alpha'})^{-1/2}\sum_{\ell'}\overset{o}{\Phi}_{\text{eff}}\left[\begin{smallmatrix}0\,\ell'\\ \alpha\alpha'\end{smallmatrix}\right]\exp\left\{ikX[\ell']\right\}. \tag{E.80}$$

Using the transformations in Eqs. (E.78) and (E.79), the effective harmonic hamiltonian operator $\widehat{\mathcal{H}}_{\text{eff}}$ is given by

$$\widehat{\mathcal{H}}_{\text{eff}} = \Phi_0 + \sum_{\left[\begin{smallmatrix}k\\ \nu\end{smallmatrix}\right]}\hbar\omega_{\text{eff}}\left[\begin{smallmatrix}k\\ \nu\end{smallmatrix}\right]\left(\frac{1}{2}+\hat{A}^\dagger\left[\begin{smallmatrix}k\\ \nu\end{smallmatrix}\right]\hat{A}\left[\begin{smallmatrix}k\\ \nu\end{smallmatrix}\right]\right), \tag{E.81}$$

where the phonon creation and annihilation operators satisfy the commutator relations

$$\begin{aligned}\left[\hat{A}\left[\begin{smallmatrix}k\\ \nu\end{smallmatrix}\right],\hat{A}^\dagger\left[\begin{smallmatrix}k'\\ \nu'\end{smallmatrix}\right]\right] &= \delta_{kk'}\delta_{\nu\nu'},\\ \left[\hat{A}\left[\begin{smallmatrix}k\\ \nu\end{smallmatrix}\right],\hat{A}\left[\begin{smallmatrix}k'\\ \nu'\end{smallmatrix}\right]\right] &= \left[\hat{A}^\dagger\left[\begin{smallmatrix}k\\ \nu\end{smallmatrix}\right],\hat{A}^\dagger\left[\begin{smallmatrix}k'\\ \nu'\end{smallmatrix}\right]\right] = 0.\end{aligned} \tag{E.82}$$

The total hamiltonian operator $\widehat{\mathcal{H}}$ is given by

$$\widehat{\mathcal{H}} = \Phi_0 + \sum_{\left[\begin{smallmatrix}k\\ \nu\end{smallmatrix}\right]}\hbar\omega_{\text{eff}}\left[\begin{smallmatrix}k\\ \nu\end{smallmatrix}\right]\left(\frac{1}{2}+\hat{A}^\dagger\left[\begin{smallmatrix}k\\ \nu\end{smallmatrix}\right]\hat{A}\left[\begin{smallmatrix}k\\ \nu\end{smallmatrix}\right]\right)+\widehat{\widehat{\mathcal{P}\mathcal{T}}}, \tag{E.83}$$

where $\widehat{\widetilde{\mathcal{PT}}} = \left(-\hat{\tilde{\mathcal{E}}}_{\text{eff}} + \hat{\tilde{\Phi}}_1 + \hat{\tilde{\Phi}}_2 + \dots\right)$ is the perturbation operator $\widehat{\mathcal{PT}}$ rewritten in terms of creation and annihilation operators.

From Eqs. (E.82) and (E.83), the hamiltonian commutator relations are given by

$$\left[\widehat{\mathcal{H}}, \hat{A}^\dagger\begin{bmatrix}k\\ \nu\end{bmatrix}\right] = \hbar\omega_{\text{eff}}\begin{bmatrix}k\\ \nu\end{bmatrix} \hat{A}^\dagger\begin{bmatrix}k\\ \nu\end{bmatrix} + \hat{R}^\dagger\begin{bmatrix}k\\ \nu\end{bmatrix}, \tag{E.84}$$

$$\left[\widehat{\mathcal{H}}, \hat{A}\begin{bmatrix}k\\ \nu\end{bmatrix}\right] = -\hbar\omega_{\text{eff}}\begin{bmatrix}k\\ \nu\end{bmatrix} \hat{A}\begin{bmatrix}k\\ \nu\end{bmatrix} - \hat{R}\begin{bmatrix}k\\ \nu\end{bmatrix}, \tag{E.85}$$

where

$$\hat{R}^\dagger\begin{bmatrix}k\\ \nu\end{bmatrix} = \left[\widehat{\widetilde{\mathcal{PT}}}, \hat{A}^\dagger\begin{bmatrix}k\\ \nu\end{bmatrix}\right], \tag{E.86}$$

$$\hat{R}\begin{bmatrix}k\\ \nu\end{bmatrix} = \left[\hat{A}^\dagger\begin{bmatrix}k\\ \nu\end{bmatrix}, \widehat{\widetilde{\mathcal{PT}}}\right]. \tag{E.87}$$

Based on Eq. (E.66), the phonon energy shifts $\hbar\delta\omega_{\text{eff}}\begin{bmatrix}k\\ \nu\end{bmatrix}$ corresponding to Eqs. (E.84)–(E.87) are given by

$$\hbar\delta\omega_{\text{eff}}\begin{bmatrix}k\\ \nu\end{bmatrix} = \frac{\left\langle\left[\hat{A}\begin{bmatrix}k\\ \nu\end{bmatrix}, \hat{R}^\dagger\begin{bmatrix}k\\ \nu\end{bmatrix}\right]\right\rangle}{\left\langle\left[\hat{A}[k]_\nu, \hat{A}^\dagger[k]_\nu\right]\right\rangle} = \left\langle\left[\hat{A}\begin{bmatrix}k\\ \nu\end{bmatrix}, \hat{R}^\dagger\begin{bmatrix}k\\ \nu\end{bmatrix}\right]\right\rangle, \tag{E.88}$$

where $\left\langle\left[\hat{A}\begin{bmatrix}k\\ \nu\end{bmatrix}, \hat{A}^\dagger\begin{bmatrix}k\\ \nu\end{bmatrix}\right]\right\rangle = 1$ by Eq. (E.82).

From Eq. (E.66), the statistical average $\left\langle\left[\hat{A}\begin{bmatrix}k\\ \nu\end{bmatrix}, \hat{R}^\dagger\begin{bmatrix}k\\ \nu\end{bmatrix}\right]\right\rangle$ is calculated using zeroth-order statistical perturbation method corresponding to Eqs. (E.84)–(E.87). The zeroth-order statistical perturbation method neglects the remainders in the hamiltonian commutator relations Eqs. (E.84) and (E.85). This implies that $\widehat{\mathcal{H}} \equiv \widehat{\mathcal{H}}_{\text{eff}}$ for calculating the statistical averages using zeroth-order statistical perturbation method. Hence, Eq. (E.88) becomes

$$\hbar\delta\omega_{\text{eff}}\begin{bmatrix}k\\ \nu\end{bmatrix} = \left\langle\left[\hat{A}\begin{bmatrix}k\\ \nu\end{bmatrix}, \hat{R}^\dagger\begin{bmatrix}k\\ \nu\end{bmatrix}\right]\right\rangle_{\widehat{\mathcal{H}}_{\text{eff}}}, \tag{E.89}$$

where

$$\langle\widehat{\chi}\rangle_{\widehat{\mathcal{H}}_{\text{eff}}} = \frac{\text{Tr}\left(\widehat{\chi}\exp\left\{-\frac{\widehat{\mathcal{H}}_{\text{eff}}}{k_B T}\right\}\right)}{\text{Tr}\left(\exp\left\{-\frac{\widehat{\mathcal{H}}_{\text{eff}}}{k_B T}\right\}\right)}. \tag{E.90}$$

The objective of the self-consistent approach is to choose effective harmonic potential

operator $\widehat{\mathcal{E}}_{\text{eff}}$ such that each energy shift $\hbar\delta\omega_{\text{eff}}\begin{bmatrix}k\\ \nu\end{bmatrix}$ vanishes

$$\hbar\delta\omega_{\text{eff}}\begin{bmatrix}k\\ \nu\end{bmatrix} = 0, \quad \text{for all } \begin{bmatrix}k\\ \nu\end{bmatrix}. \tag{E.91}$$

Substituting the expression for $\hat{R}^\dagger\begin{bmatrix}k\\ \nu\end{bmatrix}$ Eq. (E.86) into Eq. (E.89) results in

$$\begin{aligned}\hbar\delta\omega_{\text{eff}}\begin{bmatrix}k\\ \nu\end{bmatrix} &= \left\langle \left[\hat{A}\begin{bmatrix}k\\ \nu\end{bmatrix}, \left[\widehat{\widehat{\mathcal{PT}}}, \hat{A}^\dagger\begin{bmatrix}k\\ \nu\end{bmatrix}\right]\right]\right\rangle_{\widehat{\mathcal{H}}_{\text{eff}}} \\ &= -\left\langle \left[\left[\widehat{\widehat{\mathcal{PT}}}, \hat{A}^\dagger\begin{bmatrix}k\\ \nu\end{bmatrix}\right], \hat{A}\begin{bmatrix}k\\ \nu\end{bmatrix}\right]\right\rangle_{\widehat{\mathcal{H}}_{\text{eff}}} \\ &= 0, \quad \text{for all } \begin{bmatrix}k\\ \nu\end{bmatrix}.\end{aligned} \tag{E.92}$$

Inversion of Eq. (E.79) results in

$$\begin{aligned}\hat{A}^\dagger\begin{bmatrix}k\\ \nu\end{bmatrix} &= \left(2\hbar\omega_{\text{eff}}\begin{bmatrix}k\\ \nu\end{bmatrix}\right)^{-1/2}\left(\omega_{\text{eff}}\begin{bmatrix}k\\ \nu\end{bmatrix}\hat{q}\begin{bmatrix}-k\\ \nu\end{bmatrix} - i\hat{p}\begin{bmatrix}k\\ \nu\end{bmatrix}\right), \\ \hat{A}\begin{bmatrix}k\\ \nu\end{bmatrix} &= \left(2\hbar\omega_{\text{eff}}\begin{bmatrix}k\\ \nu\end{bmatrix}\right)^{-1/2}\left(\omega_{\text{eff}}\begin{bmatrix}k\\ \nu\end{bmatrix}\hat{q}\begin{bmatrix}k\\ \nu\end{bmatrix} + i\hat{p}\begin{bmatrix}-k\\ \nu\end{bmatrix}\right),\end{aligned} \tag{E.93}$$

and inversion of Eq. (E.78) results in

$$\begin{aligned}\hat{q}\begin{bmatrix}k\\ \nu\end{bmatrix} &= n^{-1/2}\sum_{\begin{bmatrix}\ell\\ \alpha\end{bmatrix}}(m_\alpha)^{1/2}\delta\hat{u}\begin{bmatrix}\ell\\ \alpha\end{bmatrix}\mathrm{e}\begin{bmatrix}-k\\ \nu\end{bmatrix}_\alpha\exp\{-ikX[\ell]\}, \\ \hat{p}\begin{bmatrix}k\\ \nu\end{bmatrix} &= n^{-1/2}\sum_{\begin{bmatrix}\ell\\ \alpha\end{bmatrix}}(m_\alpha)^{1/2}\delta\hat{u}\begin{bmatrix}\ell\\ \alpha\end{bmatrix}\mathrm{e}\begin{bmatrix}k\\ \nu\alpha\end{bmatrix}\exp\{ikX[\ell]\}.\end{aligned} \tag{E.94}$$

Substituting Eq. (E.93) into Eq. (E.92) and dropping all the terms in $\hat{q}\begin{bmatrix}k\\ \nu\end{bmatrix}$ since by Eq. (E.94) these operators are linear in $\delta\hat{u}\begin{bmatrix}\ell\\ \alpha\end{bmatrix}$ and hence they commute with $\widehat{\mathcal{PT}}$ which is given by Eqs. (E.74) and (E.76) results in

$$\left\langle \left[\left[\widehat{\mathcal{PT}}, \hat{p}\begin{bmatrix}k\\ \nu\end{bmatrix}\right], \hat{p}\begin{bmatrix}-k\\ \nu\end{bmatrix}\right]\right\rangle_{\widehat{\mathcal{H}}_{\text{eff}}} = 0, \quad \text{for all } \begin{bmatrix}k\\ \nu\end{bmatrix}. \tag{E.95}$$

Finally, replacing momentum operators $\hat{p}\begin{bmatrix}k\\ \nu\end{bmatrix}$ in Eq. (E.95) using Eq. (E.94) results

in

$$\begin{aligned}&\sum_{\left[\substack{\ell\\ \alpha}\right]}\sum_{\left[\substack{\ell'\\ \alpha'}\right]}(m_\alpha m_{\alpha'})^{-1/2}\left\langle\left[\left[\widehat{\mathcal{PT}},\delta\hat{u}\left[\substack{\ell\\ \alpha}\right]\right],\delta\hat{u}\left[\substack{\ell'\\ \alpha'}\right]\right]\right\rangle_{\widehat{\mathcal{H}}_{\text{eff}}}\\ &\times\exp\left\{ik\left(X[\ell]-X[\ell']\right)\right\}\mathrm{e}\left[\substack{\mathrm{k}\\ \nu\alpha}\right]\mathrm{e}\left[\substack{-\mathrm{k}\\ \nu\ \alpha'}\right]=0,\quad\text{for all }\left[\substack{\mathrm{k}\\ \nu}\right].\end{aligned}\tag{E.96}$$

Since Eq. (E.96) has to vanish for each and every $\left[\substack{k\\ \nu}\right]$, then each term in the sum over $\left[\substack{\ell\\ \alpha}\right]$ and $\left[\substack{\ell'\\ \alpha'}\right]$ must separately vanish, so

$$\left\langle\left[\left[\widehat{\mathcal{PT}},\delta\hat{u}\left[\substack{\ell\\ \alpha}\right]\right],\delta\hat{u}\left[\substack{\ell'\\ \alpha'}\right]\right]\right\rangle_{\widehat{\mathcal{H}}_{\text{eff}}}=0,\quad\text{for all }\left[\substack{\ell\\ \alpha}\right],\left[\substack{\ell'\\ \alpha'}\right].\tag{E.97}$$

Using Eqs. (E.75) and (E.77), the double commutator in Eq. (E.97) is converted such that

$$\left\langle\widehat{\mathcal{PT}}\right\rangle_{\widehat{\mathcal{H}}_{\text{eff}}}=0.\tag{E.98}$$

Rearranging the terms in Eq. (E.98), the coefficients of effective harmonic potential energy $\overset{o}{\Phi}_{\text{eff}}\left[\substack{\ell\,\ell'\\ \alpha\alpha'}\right]$ are determined as the statistical average of second derivatives of the total potential energy $\mathcal{E}$ with respect to atomic displacement operators $\delta u\left[\substack{\ell\\ \alpha}\right]$ given by

$$\overset{o}{\Phi}_{\text{eff}}\left[\substack{\ell\,\ell'\\ \alpha\alpha'}\right]=\left\langle\frac{\partial^2\left(\widehat{\Phi}_1+\widehat{\Phi}_2+\widehat{\Phi}_3+\widehat{\Phi}_4+\dots\right)}{\partial\left(\delta\hat{u}\left[\substack{\ell\\ \alpha}\right]\right)\partial\left(\delta\hat{u}\left[\substack{\ell'\\ \alpha'}\right]\right)}\right\rangle_{\widehat{\mathcal{H}}_{\text{eff}}}.\tag{E.99}$$

The coefficients of effective harmonic potential energy $\overset{o}{\Phi}_{\text{eff}}\left[\substack{\ell\,\ell'\\ \alpha\alpha'}\right]$ are temperature dependent due to the statistical average in Eq. (E.99). This implies that the effective harmonic frequencies $\omega^2_{\text{eff}}\left[\substack{k\\ \nu}\right]$ and corresponding normalized eigenvectors $\mathbf{e}_{\text{eff}}\left[\substack{k\\ \nu}\right]$ are all not only dependent on the configuration but also temperature.

Substituting $\widehat{\Phi}_1,\widehat{\Phi}_2,\widehat{\Phi}_3,\widehat{\Phi}_4,\dots$ defined in Eq. (E.1) and evaluating the statistical averages gives

$$\overset{o}{\Phi}_{\text{eff}}\left[\substack{\ell\,\ell'\\ \alpha\alpha'}\right]=\overset{o}{\Phi}\left[\substack{\ell\,\ell'\\ \alpha\alpha'}\right]+\frac{1}{2}\sum_{\left[\substack{\ell''\\ \alpha''}\right]}\sum_{\left[\substack{\ell'''\\ \alpha'''}\right]}\overset{o}{\Phi}\left[\substack{\ell\,\ell'\,\ell''\,\ell'''\\ \alpha\alpha'\alpha''\alpha'''}\right]\left\langle\delta\hat{u}\left[\substack{\ell''\\ \alpha''}\right]\delta\hat{u}\left[\substack{\ell'''\\ \alpha'''}\right]\right\rangle_{\widehat{\mathcal{H}}_{\text{eff}}}+\dots.\tag{E.100}$$

It is important to note that the series in Eq. (E.100) need not converge rapidly, as would be the case for an ordinary perturbation problem, but simply that the odd

terms in $\delta\hat{u}\begin{bmatrix}\ell\\ \alpha\end{bmatrix}$ average out and hence do not contribute to $\overset{o}{\Phi}_{\text{eff}}\begin{bmatrix}\ell\,\ell'\\ \alpha\alpha'\end{bmatrix}$. The effective harmonic frequencies $\omega^2_{\text{eff}}\begin{bmatrix}k\\ \nu\end{bmatrix}$ are calculated as the eigenvalues of effective dynamical matrix Eq. (E.80) and the coefficients of effective harmonic potential energy are calculated from Eq. (E.100). But Eq. (E.100) involves the statistical averages $\left\langle \delta\hat{u}\begin{bmatrix}\ell''\\ \alpha''\end{bmatrix}\delta\hat{u}\begin{bmatrix}\ell'''\\ \alpha'''\end{bmatrix}\right\rangle_{\widehat{\mathcal{H}}_{\text{eff}}}$ which are calculated in the effective harmonic representation. Hence, Eqs. (E.80) and (E.100) must be solved self-consistently.

E.3.2 First-order Helmholtz free energy

Once the coefficients of effective harmonic potential $\overset{o}{\Phi}_{\text{eff}}\begin{bmatrix}\ell\,\ell'\\ \alpha\alpha'\end{bmatrix}$ are determined from the self-consistent equations Eqs. (E.80) and (E.100), the macroscopic thermodynamic quantities such as partition function and Helmholtz free energy needs to be calculated.

The total partition function for a chain of vibrating atoms is given by

$$Z = \text{Tr}\left(\exp\left\{-\frac{\widehat{\mathcal{H}}}{k_B T}\right\}\right), \tag{E.101}$$

where $\widehat{\mathcal{H}}$ is the total hamiltonian operator Eq. (E.69). Using Eq. (E.70), the total partition function Eq. (E.101) can be written as

$$Z = \text{Tr}\left(\exp\left\{-\frac{\widehat{\mathcal{PT}}}{k_B T}\right\}\exp\left\{-\frac{\widehat{\mathcal{H}}_{\text{eff}}}{k_B T}\right\}\right). \tag{E.102}$$

Expanding the exponential term containing $\widehat{\mathcal{PT}}$ in Eq. (E.102) results in

$$Z = \text{Tr}\left(\left\{1 - \frac{\widehat{\mathcal{PT}}}{k_B T} + \ldots\right\}\exp\left\{-\frac{\widehat{\mathcal{H}}_{\text{eff}}}{k_B T}\right\}\right). \tag{E.103}$$

From Eq. (E.103), the total partition function correct to first-order in $\widehat{\mathcal{PT}}$ is given by

$$Z = Z_{\widehat{\mathcal{H}}_{\text{eff}}}\left(1 - (k_B T)^{-1}\left\langle\widehat{\mathcal{PT}}\right\rangle_{\widehat{\mathcal{H}}_{\text{eff}}} + O\left(\widehat{\mathcal{PT}}^2\right)\right), \tag{E.104}$$

where $Z_{\widehat{\mathcal{H}}_{\text{eff}}}$ is the effective partition function given by

$$Z_{\widehat{\mathcal{H}}_{\text{eff}}} = \text{Tr}\left(\exp\left\{-\frac{\widehat{\mathcal{H}}_{\text{eff}}}{k_B T}\right\}\right). \tag{E.105}$$

The total Helmholtz free energy is given by

$$\mathcal{F} = -k_B T \ln Z. \tag{E.106}$$

Substituting Eq. (E.104) into Eq. (E.106) results in

$$\begin{aligned}
\mathcal{F} &= -k_B T \ln\left(Z_{\widehat{\mathcal{H}}_{\text{eff}}}\left\{1 - (k_B T)^{-1}\left\langle\widehat{\mathcal{PT}}\right\rangle_{\widehat{\mathcal{H}}_{\text{eff}}}\right\} + O\left(\widehat{\mathcal{PT}}^2\right)\right), \\
&= -k_B T \ln Z_{\widehat{\mathcal{H}}_{\text{eff}}} - k_B T \ln\left\{1 - (k_B T)^{-1}\left\langle\widehat{\mathcal{PT}}\right\rangle_{\widehat{\mathcal{H}}_{\text{eff}}} + O\left(\widehat{\mathcal{PT}}^2\right)\right\}, \\
&= \mathcal{F}_{\widehat{\mathcal{H}}_{\text{eff}}} - k_B T \ln\left\{1 - (k_B T)^{-1}\left\langle\widehat{\mathcal{PT}}\right\rangle_{\widehat{\mathcal{H}}_{\text{eff}}} + O\left(\widehat{\mathcal{PT}}^2\right)\right\},
\end{aligned} \tag{E.107}$$

where effective free energy $\mathcal{F}_{\widehat{\mathcal{H}}_{\text{eff}}}$ is given by

$$\mathcal{F}_{\widehat{\mathcal{H}}_{\text{eff}}} = -k_B T \ln Z_{\widehat{\mathcal{H}}_{\text{eff}}}. \tag{E.108}$$

Expanding the logarithm in the last term of Eq. (E.107) and using Eq. (E.98) results in

$$\mathcal{F} = \mathcal{F}_{\widehat{\mathcal{H}}_{\text{eff}}} + O\left(\widehat{\mathcal{PT}}^2\right). \tag{E.109}$$

In principle, the effective harmonic frequencies $\omega^2_{\text{eff}}\left[{k \atop \nu}\right]$ can be computed from the self-consistent equations Eqs. (E.80) and (E.100) and hence the first-order Helmholtz free energy Eq. (E.109). But in practice, it is not possible to solve the self-consistent equations due to the infinite terms in Eq. (E.100). This practical limitation can be removed by considering an ordinary perturbation problem in which the series in Eq. (E.100) is assumed to converge rapidly.

E.3.3 Ordinary perturbation problem

The ordinary perturbation problem assumes that the series in Eq. (E.100) converges rapidly. In other words, the harmonic term $\widehat{\Phi}_2$ is considered to be significantly larger than the anharmonic terms $\widehat{\Phi}_4, \widehat{\Phi}_6, \ldots$. This implies that character of the phonons does not change significantly due to anharmonic terms and that only effect of the anharmonic terms is of change in the phonon frequency. With this the displacement operators $\delta\hat{u}\begin{bmatrix}\ell\\ \alpha\end{bmatrix}$ are transformed into normal mode coordinates using

$$\delta\hat{u}\begin{bmatrix}\ell\\ \alpha\end{bmatrix} = (nm_\alpha)^{-1/2}\sum_{\begin{bmatrix}k\\ \nu\end{bmatrix}} \hat{q}\begin{bmatrix}k\\ \nu\end{bmatrix} \mathrm{e}\begin{bmatrix}\mathrm{k}\\ \nu\alpha\end{bmatrix} \exp\{\mathrm{ikX}[\ell]\}, \tag{E.110}$$

and the normal mode coordinate operators $\hat{q}\begin{bmatrix}k\\ \nu\end{bmatrix}$ are transformed into creation and annihilation operators using

$$\hat{q}\begin{bmatrix}k\\ \nu\end{bmatrix} = \left(\frac{\hbar}{2\omega_{\mathrm{eff}}\begin{bmatrix}k\\ \nu\end{bmatrix}}\right)^{1/2}\left(\hat{A}\begin{bmatrix}k\\ \nu\end{bmatrix} + \hat{A}^\dagger\begin{bmatrix}-k\\ \nu\end{bmatrix}\right), \tag{E.111}$$

where $\mathbf{e}\begin{bmatrix}k\\ \nu\end{bmatrix}$ are the normalized eigenvectors of harmonic dynamical matrix Eq. (4.20) and the effective harmonic frequencies $\omega^2_{\mathrm{eff}}\begin{bmatrix}k\\ \nu\end{bmatrix}$ are to be calculated as shown below. Note that the eigenvectors $\mathbf{e}\begin{bmatrix}k\\ \nu\end{bmatrix}$ are considered in Eq. (E.110) instead of $\mathbf{e}_{\mathrm{eff}}\begin{bmatrix}k\\ \nu\end{bmatrix}$ due to the assumption of ordinary perturbation problem which implies that the character of the phonons is not changed but only the values of phonon frequencies are changed.

Considering that the series in Eq. (E.100) converges rapidly, the effective harmonic potential coefficients $\overset{o}{\Phi}_{\mathrm{eff}}\begin{bmatrix}\ell\,\ell'\\ \alpha\alpha'\end{bmatrix}$ can be considered as

$$\overset{o}{\Phi}_{\mathrm{eff}}\begin{bmatrix}\ell\,\ell'\\ \alpha\alpha'\end{bmatrix} = \overset{o}{\Phi}\begin{bmatrix}\ell\,\ell'\\ \alpha\alpha'\end{bmatrix} + \delta\overset{o}{\Phi}\begin{bmatrix}\ell\,\ell'\\ \alpha\alpha'\end{bmatrix}, \tag{E.112}$$

where

$$\delta\overset{o}{\Phi}\begin{bmatrix}\ell\,\ell'\\ \alpha\alpha'\end{bmatrix} = \frac{1}{2}\sum_{\begin{bmatrix}\ell''\\ \alpha''\end{bmatrix}}\sum_{\begin{bmatrix}\ell'''\\ \alpha'''\end{bmatrix}} \overset{o}{\Phi}\begin{bmatrix}\ell\,\ell'\,\ell''\,\ell'''\\ \alpha\alpha'\alpha''\alpha'''\end{bmatrix}\left\langle \delta\hat{u}\begin{bmatrix}\ell''\\ \alpha''\end{bmatrix}\delta\hat{u}\begin{bmatrix}\ell'''\\ \alpha'''\end{bmatrix}\right\rangle_{\widehat{\mathcal{H}}_{\mathrm{eff}}}. \tag{E.113}$$

The effective dynamical matrix Eq. (E.80) reduces to

$$\mathbb{K}_{\mathrm{eff}}\begin{bmatrix}k\\ \alpha\alpha'\end{bmatrix} = \mathbb{K}\begin{bmatrix}k\\ \alpha\alpha'\end{bmatrix} + \delta\mathbb{K}\begin{bmatrix}k\\ \alpha\alpha'\end{bmatrix}, \tag{E.114}$$

where $\mathbb{K}\left[\begin{smallmatrix} k \\ \alpha\alpha' \end{smallmatrix}\right]$ is the harmonic dynamical matrix Eq. (4.20) and

$$\delta\mathbb{K}\left[\begin{smallmatrix} k \\ \alpha\alpha' \end{smallmatrix}\right] = (m_\alpha m_{\alpha'})^{-1/2} \sum_{\ell'} \delta\overset{o}{\Phi}\left[\begin{smallmatrix} 0\,\ell' \\ \alpha\alpha' \end{smallmatrix}\right] \exp\left\{ikX[\ell']\right\}. \tag{E.115}$$

The diagonalization of Eq. (E.114) results in

$$\omega^2_{\text{eff}}\left[\begin{smallmatrix} k \\ \nu \end{smallmatrix}\right] = \omega^2\left[\begin{smallmatrix} k \\ \nu \end{smallmatrix}\right] + \sum_{\alpha\alpha'} \mathrm{e}\left[\begin{smallmatrix} -\mathrm{k} \\ \nu \quad \alpha \end{smallmatrix}\right] \delta\mathbb{K}\left[\begin{smallmatrix} \mathrm{k} \\ \alpha\alpha' \end{smallmatrix}\right] \mathrm{e}\left[\begin{smallmatrix} \mathrm{k} \\ \nu\alpha' \end{smallmatrix}\right], \tag{E.116}$$

where $\omega^2\left[\begin{smallmatrix} k \\ \nu \end{smallmatrix}\right]$ are the eigenvalues and $\mathbf{e}\left[\begin{smallmatrix} k \\ \nu \end{smallmatrix}\right]$ are the corresponding normalized eigenvectors of the harmonic dynamical matrix Eq. (4.20).

The last term in Eq. (E.116) is evaluated by substituting Eqs. (E.110) and (E.111) into Eq. (E.113) resulting in

$$\omega^2_{\text{eff}}\left[\begin{smallmatrix} k \\ \nu \end{smallmatrix}\right] = \omega^2\left[\begin{smallmatrix} k \\ \nu \end{smallmatrix}\right] + \frac{\hbar}{2} \sum_{\left[\begin{smallmatrix} k' \\ \nu' \end{smallmatrix}\right]} \left(\omega_{\text{eff}}\left[\begin{smallmatrix} k' \\ \nu' \end{smallmatrix}\right]\right)^{-1} V_4\left[\begin{smallmatrix} k & -k & k' & -k' \\ \nu & \nu & \nu' & \nu' \end{smallmatrix}\right] \left\langle \hat{A}^\dagger\left[\begin{smallmatrix} k \\ \nu \end{smallmatrix}\right] \hat{A}\left[\begin{smallmatrix} k \\ \nu \end{smallmatrix}\right] + \frac{1}{2} \right\rangle_{\widehat{\mathcal{H}}_{\text{eff}}}, \tag{E.117}$$

where $V_4\left[\begin{smallmatrix} k & -k & k' & -k' \\ \nu & \nu & \nu' & \nu' \end{smallmatrix}\right]$ is defined by Eq. (4.27). The statistical average $\left\langle \hat{A}^\dagger\left[\begin{smallmatrix} k \\ \nu \end{smallmatrix}\right] \hat{A}\left[\begin{smallmatrix} k \\ \nu \end{smallmatrix}\right] \right\rangle_{\widehat{\mathcal{H}}_{\text{eff}}}$ corresponding to the zeroth-order statistical perturbation method Eq. (E.47) is given by

$$\left\langle \hat{A}^\dagger\left[\begin{smallmatrix} k \\ \nu \end{smallmatrix}\right] \hat{A}\left[\begin{smallmatrix} k \\ \nu \end{smallmatrix}\right] \right\rangle_{\widehat{\mathcal{H}}_{\text{eff}}} = \left\langle n\left[\begin{smallmatrix} k \\ \nu \end{smallmatrix}\right] \right\rangle_{\widehat{\mathcal{H}}_{\text{eff}}} = \left(\exp\left\{ \frac{\hbar\omega_{\text{eff}}\left[\begin{smallmatrix} k \\ \nu \end{smallmatrix}\right]}{k_B T} \right\} - 1 \right)^{-1}. \tag{E.118}$$

Finally, using Eq. (E.118) the self-consistent equation to determine the effective harmonic frequencies $\omega^2_{\text{eff}}\left[\begin{smallmatrix} k \\ \nu \end{smallmatrix}\right]$ is given by

$$\omega^2_{\text{eff}}\left[\begin{smallmatrix} k \\ \nu \end{smallmatrix}\right] = \omega^2\left[\begin{smallmatrix} k \\ \nu \end{smallmatrix}\right] + \frac{\hbar}{2} \sum_{\left[\begin{smallmatrix} k' \\ \nu' \end{smallmatrix}\right]} \left(\omega_{\text{eff}}\left[\begin{smallmatrix} k' \\ \nu' \end{smallmatrix}\right]\right)^{-1} V_4\left[\begin{smallmatrix} k & -k & k' & -k' \\ \nu & \nu & \nu' & \nu' \end{smallmatrix}\right] \left(\left(\exp\left\{ \frac{\hbar\omega_{\text{eff}}\left[\begin{smallmatrix} k' \\ \nu' \end{smallmatrix}\right]}{k_B T} \right\} - 1 \right)^{-1} + \frac{1}{2} \right). \tag{E.119}$$

The Helmholtz free energy corresponding to Eq. (E.109) is given by

$$\mathcal{F} = \mathcal{F}_{\widehat{\mathcal{H}}_{\text{eff}}} + O\left(\widehat{\mathcal{P}\mathcal{T}}^2\right). \tag{E.120}$$

where $\mathcal{F}_{\widehat{\mathcal{H}}_{\text{eff}}}$ corresponding to Eqs. (E.108) and (E.105) is given by

$$\begin{aligned}\mathcal{F}_{\widehat{\mathcal{H}}_{\text{eff}}}(\overset{o}{\mathbf{u}};T) &= -k_BT\ln Z_{\widehat{\mathcal{H}}_{\text{eff}}},\\ &= \Phi_0(\overset{o}{\mathbf{u}}) + \frac{1}{2}\sum_{\left[\substack{k\\ \nu}\right]}\hbar\omega_{\text{eff}}\left[\substack{k\\ \nu}\right] + k_BT\sum_{\left[\substack{k\\ \nu}\right]}\ln\left[1-\exp\left\{-\frac{\hbar\omega_{\text{eff}}\left[\substack{k\\ \nu}\right]}{k_BT}\right\}\right].\end{aligned} \tag{E.121}$$

Therefore, the Helmholtz free energy correct to first-order is given by

$$\mathcal{F}(\overset{o}{\mathbf{u}};T) = \Phi_0(\overset{o}{\mathbf{u}}) + \frac{1}{2}\sum_{\left[\substack{k\\ \nu}\right]}\hbar\omega_{\text{eff}}\left[\substack{k\\ \nu}\right] + k_BT\sum_{\left[\substack{k\\ \nu}\right]}\ln\left[1-\exp\left\{-\frac{\hbar\omega_{\text{eff}}\left[\substack{k\\ \nu}\right]}{k_BT}\right\}\right], \tag{E.122}$$

where effective harmonic frequencies $\omega^2_{\text{eff}}\left[\substack{k\\ \nu}\right]$ are calculated from the self-consistent equation Eq. (E.119).

E.3.4 High temperature limit

The SCA method is developed in this chapter using quantum mechanical formulation. In the high temperature limit, defined as $k_BT \gg \hbar\omega_{\text{eff}}\left[\substack{k\\ \nu}\right]$, the self-consistent equation Eq. (E.119) and the free energy Eq. (E.122) can be compared to the corresponding results of SCA method within classical mechanics developed in Chapter 5.

Considering the temperature to be high such that $k_BT \gg \hbar\omega_{\text{eff}}\left[\substack{k\\ \nu}\right]$ results in

$$\left(\left\langle n\left[\substack{k'\\ \nu'}\right]\right\rangle_{\widehat{\mathcal{H}}_{\text{eff}}} + \frac{1}{2}\right) \cong \frac{k_BT}{\hbar\omega_{\text{eff}}\left[\substack{k\\ \nu}\right]} \gg 1. \tag{E.123}$$

Substituting Eq. (E.123) into Eq. (E.119) results in

$$\omega^2_{\text{eff}}\left[\substack{k\\ \nu}\right] = \omega^2\left[\substack{k\\ \nu}\right] + \frac{k_BT}{2}\sum_{\left[\substack{k'\\ \nu'}\right]} V_4\left[\substack{k-k\,k'-k'\\ \nu\nu\quad\nu'\nu'}\right]\frac{1}{\omega^2_{\text{eff}}\left[\substack{k'\\ \nu'}\right]}. \tag{E.124}$$

Eq. (E.124) is the self-consistent equation derived using quantum mechanical formulation of the SCA method at high temperature limit and it matches with the corresponding self-consistent equation Eq. (5.19) derived within classical mechanics.

Expanding the term $\exp\left\{-\frac{\hbar\omega_{\text{eff}}\left[\begin{smallmatrix}k\\ \nu\end{smallmatrix}\right]}{k_BT}\right\}$ in Eq. (E.122) results in

$$\begin{aligned}\mathcal{F}(\overset{o}{\mathbf{u}};T) &= \Phi_0(\overset{o}{\mathbf{u}}) + \frac{1}{2}\sum_{\left[\begin{smallmatrix}k\\ \nu\end{smallmatrix}\right]}\hbar\omega_{\text{eff}}\left[\begin{smallmatrix}k\\ \nu\end{smallmatrix}\right] + k_BT\sum_{\left[\begin{smallmatrix}k\\ \nu\end{smallmatrix}\right]}\ln\left[\frac{\hbar\omega_{\text{eff}}\left[\begin{smallmatrix}k\\ \nu\end{smallmatrix}\right]}{k_BT} - \frac{1}{2}\left(\frac{\hbar\omega_{\text{eff}}\left[\begin{smallmatrix}k\\ \nu\end{smallmatrix}\right]}{k_BT}\right)^2 + \dots\right], \\ &= \Phi_0(\overset{o}{\mathbf{u}}) + \frac{1}{2}\sum_{\left[\begin{smallmatrix}k\\ \nu\end{smallmatrix}\right]}\hbar\omega_{\text{eff}}\left[\begin{smallmatrix}k\\ \nu\end{smallmatrix}\right] + k_BT\sum_{\left[\begin{smallmatrix}k\\ \nu\end{smallmatrix}\right]}\ln\left(\frac{\hbar\omega_{\text{eff}}\left[\begin{smallmatrix}k\\ \nu\end{smallmatrix}\right]}{k_BT}\right) \\ &\quad + k_BT\sum_{\left[\begin{smallmatrix}k\\ \nu\end{smallmatrix}\right]}\ln\left[1 - \frac{1}{2}\left(\frac{\hbar\omega_{\text{eff}}\left[\begin{smallmatrix}k\\ \nu\end{smallmatrix}\right]}{k_BT}\right) + \dots\right].\end{aligned} \tag{E.125}$$

Considering the temperature to be high such that $k_BT \gg \hbar\omega_{\text{eff}}\left[\begin{smallmatrix}k\\ \nu\end{smallmatrix}\right]$ and expanding the last logarithm term in Eq. (E.125) results in

$$\begin{aligned}\mathcal{F}(\overset{o}{\mathbf{u}};T) &= \Phi_0(\overset{o}{\mathbf{u}}) + \frac{1}{2}\sum_{\left[\begin{smallmatrix}k\\ \nu\end{smallmatrix}\right]}\hbar\omega_{\text{eff}}\left[\begin{smallmatrix}k\\ \nu\end{smallmatrix}\right] + k_BT\sum_{\left[\begin{smallmatrix}k\\ \nu\end{smallmatrix}\right]}\ln\left[\frac{\hbar\omega_{\text{eff}}\left[\begin{smallmatrix}k\\ \nu\end{smallmatrix}\right]}{k_BT}\right] - \frac{1}{2}\sum_{\left[\begin{smallmatrix}k\\ \nu\end{smallmatrix}\right]}\hbar\omega_{\text{eff}}\left[\begin{smallmatrix}k\\ \nu\end{smallmatrix}\right], \\ &= \Phi_0(\overset{o}{\mathbf{u}}) - k_BT\sum_{\left[\begin{smallmatrix}k\\ \nu\end{smallmatrix}\right]}\ln\left[\frac{k_BT}{\hbar\omega_{\text{eff}}\left[\begin{smallmatrix}k\\ \nu\end{smallmatrix}\right]}\right].\end{aligned} \tag{E.126}$$

Eq. (E.126) is the Helmholtz free energy of the chain derived using quantum mechanical formulation of the SCA method at high temperature limit and it matches with the corresponding Helmholtz free energy Eq. (5.23) derived within classical mechanics.

Appendix F

Nelson's method

Nelson (*Nelson*, 1976) presented a powerful algorithm to determine the first- and second-order eigenvalue and normalized eigenvector derivatives of real matrices. Here, this method is discussed for the case of a hermitian matrix with real eigenvalues and normalized complex eigenvector such that the method can be applied to Eq. (6.22) discussed in Section 6.4.

Consider an eigenvalue problem

$$[\mathbf{A} - \lambda_i \mathbf{I}]\, \mathbf{e}_i = \mathbf{0}, \tag{F.1}$$

where $\mathbf{I}$ is an identity matrix, $\mathbf{A}$ is a hermitian matrix of dimension $M \times M$, λ_i is the real eigenvalue, and $\mathbf{e}_i$ is the normalized complex eigenvector of dimension $M \times 1$ such that

$$\mathbf{e}_i^* \mathbf{e}_i = 1. \tag{F.2}$$

where $\mathbf{e}_i^*$ is the complex conjugate of $\mathbf{e}_i$.

Now consider that matrix $\mathbf{A}$ is a function of parameters t and s. This implies that the eigenvalues λ_i and eigenvectors $\mathbf{e}_i$ are also functions of parameters t and s. The objective of this chapter is to determine derivatives $\frac{\partial \lambda_i}{\partial t}$, $\frac{\partial \mathbf{e}_i}{\partial t}$, $\frac{\partial^2 \lambda}{\partial t \partial s}$, and $\frac{\partial \mathbf{e}_i}{\partial t \partial s}$.

F.1 First-order derivatives

Differentiating Eq. (F.1) with respect to t results in

$$\left[\frac{\partial \mathbf{A}}{\partial t} - \frac{\partial \lambda_i}{\partial t}\mathbf{I}\right]\mathbf{e}_i + \left[\mathbf{A} - \lambda_i \mathbf{I}\right]\frac{\partial \mathbf{e}_i}{\partial t} = \mathbf{0}. \tag{F.3}$$

Multiplying Eq. (F.3) with $\mathbf{e}_i^*$ results in

$$\mathbf{e}_i^*\left[\frac{\partial \mathbf{A}}{\partial t} - \frac{\partial \lambda_i}{\partial t}\mathbf{I}\right]\mathbf{e}_i + \mathbf{e}_i^*\left[\mathbf{A} - \lambda_i \mathbf{I}\right]\frac{\partial \mathbf{e}_i}{\partial t} = \mathbf{0}. \tag{F.4}$$

Using Eqs. (F.3) and (F.2) it can be shown that

$$\mathbf{e}_i^*\left[\mathbf{A} - \lambda_i \mathbf{I}\right] = \mathbf{0}. \tag{F.5}$$

Substituting Eq. (F.5) into Eq. (F.4) gives an expression for the first-order derivative of eigenvalue given by

$$\frac{\partial \lambda_i}{\partial t} = \mathbf{e}_i^*\frac{\partial \mathbf{A}}{\partial t}\mathbf{e}_i. \tag{F.6}$$

Using Eq. (F.6), the eigenvector derivative $\frac{\partial \mathbf{e}_i}{\partial t}$ cannot be calculated directly from Eq. (F.3) since $[\mathbf{A} - \lambda_i \mathbf{I}]$ is singular as its rank is $M - 1$ when the matrix $\mathbf{A}$ contains distinct eigenvalues. Nelson (*Nelson*, 1976) proposed that the eigenvector derivative can be written as

$$\frac{\partial \mathbf{e}_i}{\partial t} = \mathbf{x}_i^t + c_i^t \mathbf{e}_i, \tag{F.7}$$

where $\mathbf{x}_i^t$ is some vector and c_i^t is a scalar constant which can be calculated. Substituting Eq. (F.7) into Eq. (F.3) and rearranging the terms result in

$$\left[\mathbf{A} - \lambda_i \mathbf{I}\right]\mathbf{x}_i^t = \mathbf{F}_i^t, \tag{F.8}$$

where $\mathbf{F}_i^t$ is given by

$$\mathbf{F}_i^t = -\left[\frac{\partial \mathbf{A}}{\partial t} - \frac{\partial \lambda_i}{\partial t}\mathbf{I}\right]\mathbf{e}_i. \tag{F.9}$$

The matrix $[\mathbf{A} - \lambda_i \mathbf{I}]$ on the left hand side of Eq. (F.8) is still singular. Nelson proposed that the p^{th} component of $\mathbf{x}_i^t$ be set to zero, where p is the location at which the eigenvector $\mathbf{e}_i$ has the maximum absolute value. This is achieved by replacing the p^{th}

row and column of $[\mathbf{A} - \lambda_i \mathbf{I}]$ matrix with zeros except for the diagonal term, which is set to one and setting the p^{th} component of the vector $\mathbf{F}_i^t$ to zero. The resulting partitioned form can be represented as

$$\mathbf{B}\mathbf{x}_i^t = \widetilde{\mathbf{F}}_i^t, \tag{F.10}$$

where

$$\mathbf{B} = \begin{bmatrix} [\mathbf{A} - \lambda_i \mathbf{I}]_{11} & \mathbf{0} & [\mathbf{A} - \lambda_i \mathbf{I}]_{13} \\ \mathbf{0} & 1 & \mathbf{0} \\ [\mathbf{A} - \lambda_i \mathbf{I}]_{31} & \mathbf{0} & [\mathbf{A} - \lambda_i \mathbf{I}]_{33} \end{bmatrix}, \quad \widetilde{\mathbf{F}}_i^t = \begin{Bmatrix} \left\{\widetilde{\mathbf{F}}_i^t\right\}_1 \\ 0 \\ \left\{\widetilde{\mathbf{F}}_i^t\right\}_3 \end{Bmatrix}. \tag{F.11}$$

The new matrix $\mathbf{B}$ is now non-singular and it is possible to calculate $\mathbf{x}_i^t$ using any numerical method to solve a system of linear equations. In this work, LU decomposition algorithm (*Press et al.*, 1992) which is available in BFBSymPac (*Elliott*, 2010) software package is used to determine $\mathbf{x}_i^t$ from Eq. (F.10). Once $\mathbf{x}_i^t$ is calculated, the value of scalar constant c_i^t is determined by differentiating the normalization condition Eq. (F.2) with respect to t which results in

$$\frac{\partial \mathbf{e}_i^*}{\partial t}\mathbf{e}_i + \mathbf{e}_i^* \frac{\partial \mathbf{e}_i}{\partial t} = 0. \tag{F.12}$$

Substituting Eq. (F.7) into Eq. (F.12) and rearranging the terms results in

$$c_i^t = -\frac{1}{2}\left[\left(\mathbf{x}_i^t\right)^* \mathbf{e}_i + \mathbf{e}_i^* \mathbf{x}_i^t\right]. \tag{F.13}$$

In conclusion, the eigenvalue derivative $\frac{\partial \lambda_i}{\partial t}$ is determined from Eq. (F.6) and eigenvector derivative $\frac{\partial \mathbf{e}_i}{\partial t}$ is obtained from Eqs. (F.7), (F.10), and (F.13).

F.2 Second-order derivatives

The second-order derivatives of eigenvalue $\frac{\partial^2 \lambda_i}{\partial t \partial s}$ and eigenvector $\frac{\partial^2 \mathbf{e}_i}{\partial t \partial s}$ can be determined following a similar procedure to that of Section F.1.

Differentiating Eq. (F.3) with respect to s results in

$$\left[\frac{\partial^2 \mathbf{A}}{\partial t \partial s} - \frac{\partial^2 \lambda_i}{\partial t \partial s}\mathbf{I}\right]\mathbf{e}_i + \left[\frac{\partial \mathbf{A}}{\partial t} - \frac{\partial \lambda_i}{\partial t}\mathbf{I}\right]\frac{\partial \mathbf{e}_i}{\partial s} + \left[\frac{\partial \mathbf{A}}{\partial s} - \frac{\partial \lambda_i}{\partial s}\mathbf{I}\right]\frac{\partial \mathbf{e}_i}{\partial t} + [\mathbf{A} - \lambda_i \mathbf{I}]\frac{\partial^2 \mathbf{e}_i}{\partial t \partial s} = \mathbf{0}. \tag{F.14}$$

Multiplying Eq. (F.14) with $\mathbf{e}_i^*$ and using Eq. (F.2) results in

$$\frac{\partial^2 \lambda_i}{\partial t \partial s} = \mathbf{e}_i^* \frac{\partial^2 \mathbf{A}}{\partial t \partial s} \mathbf{e}_i + \mathbf{e}_i^* \left[\frac{\partial \mathbf{A}}{\partial t} - \frac{\partial \lambda_i}{\partial t} \mathbf{I} \right] \frac{\partial \mathbf{e}_i}{\partial s} + \mathbf{e}_i^* \left[\frac{\partial \mathbf{A}}{\partial s} - \frac{\partial \lambda_i}{\partial s} \mathbf{I} \right] \frac{\partial \mathbf{e}_i}{\partial t}. \tag{F.15}$$

Similar to Eq. (F.7) consider that

$$\frac{\partial^2 \mathbf{e}_i}{\partial t \partial s} = \mathbf{x}_i^{ts} + c_i^{ts} \mathbf{e}_i, \tag{F.16}$$

where $\mathbf{x}_i^{ts}$ is some vector and c_i^{ts} is a scalar constant which can be calculated. Substituting Eq. (F.16) into Eq. (F.14) and rearranging the terms results in

$$\left[\mathbf{A} - \lambda_i \mathbf{I} \right] \mathbf{x}_i^{ts} = \mathbf{F}_i^{ts}, \tag{F.17}$$

where $\mathbf{F}_i^{ts}$ is given by

$$\mathbf{F}_i^{ts} = - \left\{ \left[\frac{\partial^2 \mathbf{A}}{\partial t \partial s} - \frac{\partial^2 \lambda_i}{\partial t \partial s} \mathbf{I} \right] \mathbf{e}_i + \left[\frac{\partial \mathbf{A}}{\partial t} - \frac{\partial \lambda_i}{\partial t} \mathbf{I} \right] \frac{\partial \mathbf{e}_i}{\partial s} + \left[\frac{\partial \mathbf{A}}{\partial s} - \frac{\partial \lambda_i}{\partial s} \mathbf{I} \right] \frac{\partial \mathbf{e}_i}{\partial t} \right\}. \tag{F.18}$$

Similar to the procedure in Section F.1, Eq. (F.17) is modified such that

$$\mathbf{B} \mathbf{x}_i^{ts} = \widetilde{\mathbf{F}}_i^{ts}, \tag{F.19}$$

where $\mathbf{B}$ is given by Eq. (F.11) and $\widetilde{\mathbf{F}}_i^{ts}$ is given by

$$\widetilde{\mathbf{F}}_i^{ts} = \left\{ \begin{array}{c} \left\{ \widetilde{\mathbf{F}}_i^{ts} \right\}_1 \\ 0 \\ \left\{ \widetilde{\mathbf{F}}_i^{ts} \right\}_3 \end{array} \right\}. \tag{F.20}$$

Once $\mathbf{x}_i^{ts}$ is determined from Eq. (F.19), the value of scalar constant c_i^{ts} is calculated by differentiating Eq. (F.12) with respect to s given by

$$\frac{\partial^2 \mathbf{e}_i^*}{\partial t \partial s} \mathbf{e}_i + \frac{\partial \mathbf{e}_i^*}{\partial t} \frac{\partial \mathbf{e}_i}{\partial s} + \frac{\partial \mathbf{e}_i^*}{\partial s} \frac{\partial \mathbf{e}_i}{\partial t} + \mathbf{e}_i^* \frac{\partial^2 \mathbf{e}_i}{\partial t \partial s} = 0. \tag{F.21}$$

Substituting Eq. (F.16) into Eq. (F.21) and rearranging the terms results in

$$c_i^{ts} = -\frac{1}{2}\left[\left(\mathbf{x}_i^{ts}\right)^* \mathbf{e}_i + \mathbf{e}_i^* \mathbf{x}_i^{ts} + \frac{\partial \mathbf{e}_i^*}{\partial t}\frac{\partial \mathbf{e}_i}{\partial s} + \frac{\partial \mathbf{e}_i^*}{\partial s}\frac{\partial \mathbf{e}_i}{\partial t}\right]. \tag{F.22}$$

In conclusion, the eigenvalue derivative $\frac{\partial^2 \lambda_i}{\partial t \partial s}$ is determined from Eq. (F.15) and eigenvector derivative $\frac{\partial^2 \mathbf{e}_i}{\partial t \partial s}$ is obtained from Eqs. (F.16), (F.19), and (F.22).